Role of Properdin in Tumour Growth and Cell Recruitment

Thesis submitted for the degree of Doctor of Philosophy
at the University of Leicester

By

Izzat Abdulsatar Mezher Al-Rayahi
(MSc.)

Department of Infection, Immunity and Inflammation
College of Medicine, Biological Sciences and Psychology
University of Leicester
Leicester, UK

2017

STATEMENT OF ORIGINALITY

This thesis submitted for the degree of PhD entitled “The role of properdin in tumour growth and cell recruitment” is based on the work accomplished by the author in the Department of Infection, Immunity and Inflammation at the University of Leicester (England, UK) during the period between January 2013 and December 2016.

To the best of my knowledge all the work recorded in this thesis is original unless otherwise acknowledged in the text or by references.

None of the work has been accepted for the award of any other degree or diploma in any university or other tertiary institution.

Signed Date:

Name: IZZAT ABDULSATAR MEZHER AL-RAYAHI

ABSTRACT

The role of Properdin in Tumour Development and Cell Recruitment

Izzat Al-Rayahi

Properdin, as the only positive regulator, amplifies complement activation and has been implicated in the tumour response in human lymphoma and carcinoma. This project investigated the role of properdin in a syngeneic orthotopic tumour model in mice engineered to be properdin deficient and their wildtype controls. The *in vitro* part of the project used macrophages differentiated from bone marrows of these mice and stimulated with conditioned medium of a syngeneic mouse melanoma cell line, B16F10. In comparison with macrophages from wildtype mice, macrophages from congenic properdin deficient mice showed skewing towards M2 profile, encompassing mRNA expression for genes involved in arginine metabolism, production of type 2 cytokines, and relatively lower surface expression of molecules needed for antigen presentation suggesting that properdin insufficiency promotes a tumour environment that helps the tumour evade the immune response.

The *in vivo* part of this project established the immune profile of tumour bearing mice. MDSCs, C5a, CCL2, TGF-β and mRNA FOXP3 were significantly less abundant in tumours of properdin deficient compared to wildtype mice. Protein levels for CCL2, a chemokine associated with tumour progression, was higher in wildtype tumour bearing mice. In spleen, MDSCs, regulatory T cells, M2 macrophages ($CD206^{+}F4/80^{+}$) and TGF-β were decreased significantly in properdin deficient compared with wildtype mice (control) after subcutaneous injection with B16F10 cells, indicating that properdin may contribute to the accumulation of MDSCs in spleen, as well as to the migration of these cells into tumours. $LDLR^{-/-}$ mice group were analysed in parallel because of their inherently greater M2 skewing. An advanced bioimaging technique was applied to some of the experimental animals.

Analysis of the level of serum properdin in response to treatment in a group of patients with pancreatic cancer showed high levels in this group.

In conclusion, this project identified complement properdin as significant in the macrophage response to conditioned melanoma cell medium, in the composition of the tumour microenvironment and systemic response to tumour *in vivo* and as an acute responder to chemotherapy in patients with pancreatic cancer.

ACKNOWLEDGEMENTS

I would like to express my greatest thanks to my creator (Allah) for blessing and help in my life. 'All praises and gratitude to the Almighty'

I would like to thank my supervisors Dr Cordula Stover for the excellent guidance and encouragement extended to me. I am extremely grateful and indebted to Dr Cordula Stover for sharing expertise and the experience I gained whilst working in her lab. No words would be enough to thank her for all her help which enabled me to develop better research skills. I could not have imagined having a better supervisor for my PhD study.

My sincere gratitude goes to my supervisor Dr Mike Browning for all his guidance and support. The feedback that he gave me during our lab meetings had a positive impact on my project. I have greatly benefited from his constructive comments.

I would also like to thank my third supervisor Dr Lee Mechado for his support through out my PhD. I am extremelly gratefull to him for his guidance and help with flow cytometry during my PhD project and also for his help in providing the B16F10- luc cell line.

Many thanks to the members of my progress review panel Professor Nigel Brunskill and Professor Jacqui Shaw for their input.

I would like to thank Dr Shiqiu Xiong from the department of biochemistry for his help and advice with Flow cytometry design and experiment analysis. My sincere thanks go to him for all the knowledge and experience that he kindly shared with me.

Furthermore, I wish to acknowledge the advice and continuous help with Flow cytometry design and experiment analysis that I received from Dr Vitor Silva Entrudo Fernandes.

I am grateful to Dr. Adam Wright for his help and advice with Flow cytometry design and experiment analysis.

Thanks, go to Dr Mike Kelly and DBS staff for their help with bioluminescence imaging.

I would also like to thank the Higher Committee for Education Development in Iraq for providing funding which allowed me to undertake this PhD.

Thank you to all members of lab 211b for their help and support, especially Dr Ramiar Kheder "special thanks for your friendship over the last years". I also

appreciate the proofreading and practical knowledge of Dr. Simon Byrne throughout my PhD.

I would like to thank Dr Franscois Robert (Leicester Royal Infirmary) for providing serum samples for patients with unresectable pancreatic carcinoma.

I am deeply indebted to my beloved mother and father who deserve all the credit for what I am today, their unwavering love and endless support are so important to me. I am also so grateful and thankful to my brothers, my Father in Law and my mother in Law for unforgettable support and encouragement during the period of my study and all family in Iraq. Special thanks to my uncle Ali who has always encouraged me to persue my postgraduate studies.

My sons, Mohammed, Mustafa and Abdullah, were a great inspiration throughout this period. To Mohammed and Mustafa, I would like to thank you so much for all the time you have spent waiting for mummy and daddy as you were always the last kids to be collected from nursery and the schools aftercare club.

My beloved wife Raghad provided an immense amount of support and encouragement throughout the course of my PhD, for which I will always be very thankful. We have started our PhD journeys together in hope of fulfilling one of our dreams, and at the end of my PhD I would like to dedicate this thesis to her.

TABLE OF CONTENTS

LIST OF TABLES

LIST OF FIGURES

LIST OF ABBREVIATIONS

%	Percent
(v/v)	By volume
(w/v)	Weight by volume
°C	Degree Celsius
°C	Degrees Centigrade
AP	Alternative pathway
APC	Antigen presenting cell or Allophycocyanin
APS	Ammonium persulphate
bFGF	basic fibroblast growth factor
BMDM	Bone Marrow Derived macrophage
bp	Base pairs
BSA	Bovine serum albumin
C4bp	C4 binding protein
C5aR	C5a receptors
CD	Cluster of Differentiation
cDNA	Complementary DNA
CFU	Colony Forming Units
CP	Classical Pathway
Crry	Complement-receptor 1–related gene/protein y
DAB	Diaminobenzidinetetrahydrochloride
DAMPs	Damage Associated Molecular Pattern Molecules
DC	Dendritic Cell
DEPC	Diethyl pyrocarbonate
dH_2O	Distilled water
DMEM	Dulbecco Modified Eagle's Medium
DMSO	Dimethylsulfoxide
DNA	Deoxyribonucleic acid
DNA	Deoxyribonucleic acid
$_d$NTP	Deoxynucleotide triphosphate
EDTA	Ethylene diaminetetraacetic acid
ELISA	Enzyme-Linked immunosorbent assay
FACS	Fluorescence Activated Cell Sorting
FBS	Fetal Bovine Serum
FC	Flow Cytometry
FCS	Fetal Calf Serum
FITC	Fluorescein isothiocyanate
FOXP3	forkhead box P3
g	g-force (RCF = Relative Centrifugal Force)
g	Grams
GM-CSF	Granulocyte/Macrophage Colony-Stimulating Factor
Hr	Hours
HRP	Horse reddish peroxidase
I.V	Intravenous injection
IFN-γ	Interferon gamma
Ig	Immunoglobulin
IL	Interleukin
IMS	Industrial Methylated Spirit
IN	Intranasal
IP	Intraperitoneal

IV	Intravenous
IVC	Individually Ventilated Caging
kb	Kilobases
L	Litres
$LDLR^{-/-}$ P^{KO}	LDL receptor knockout properdin knockout
$LDLR^{-/-}P^{WT}$	LDL receptor knockout properdin wildtype
LP	Lectin Pathway
LPS	Lipopolysaccharide
MAC	Membrane attack complex
MBL	Mannan binding lectin
MDSC	Myeloid derived suppressor cell
mg	Milligram
MHC	Major Histocompatability Complex
min	Minute
ml	Millilitre
mm:	millimetres.
mRNA	Messenger RNA
ng	nanogram
nH_2O	Nanopure water
NK	Natural Killer
OD	Optical Density
PBS	Phosphate buffered saline
PBS	Phosphate Buffered Saline
PCR	Polymerase Chain Reaction
PD	Partial Response
PE	Phycoerythrin
PE/Cy7	Phycoerythrin-Cy7 Tandem
PKO	properdin deficient mice
PMN	Polymorphonuclear leukocyte
PR	Progressive Disease
QTL	Quantitative Trait Locus
RNA	Ribonucleic acid
ROS:	Reactive oxygen species
rpm	Revolutions per minute
RPMI	Roswell Park Memorial Institute
RT	Room Temperature
S.C	Subcutaneous Injection
SD	Stable Disease
SD	Standard Deviation
SDS-PAGE	SDS-polyacrylamide gel electrophoresis
SEM	Standard Error of the Mean
TBS	Tris buffered saline
TCR T	cell receptor
TEMED	N, N, N', N'-tetramethyl ethylene diamine
TGF	Transforming Growth Factor
Th	T helper
TLR	Toll-like Receptor
TNF	Tumour Necrosis Factor
Treg	T regulatory
v/v	volume/volume

w/v	Weight/volume
WHO	World Health Organization
WT	Wildtype
α	Alpha
β	Beta
γ	Gamma
γδ T	Gamma delta T cells
δ	Delta
µg	Micrograms
µl	Microliter
µl	Microlitres
µm	Micrometer
µM	Micromolar

Chapter 1 Introduction

1.1 Cancer

Cancer is defined as an uncontrolled division of abnormal cells which can invade nearby tissue and spread systemically by metastasis (lymphatically or hematogenously). Tumour strictly describes a swelling, and as such may describe benign or malignant cell mass. The transformation of normal cells into malignant cells is a complex result of molecular, biochemical and genetic traits. A number of mutations have been identified that result in the activation of oncogenes coupled with the loss of function of tumour suppressor genes. Cancer cells arise when there is disruption in the circuits controlling normal cell proliferation. Hanahan and Weinberg managed to identify a number of traits "Hallmarks" shared by all types of cancer. These modifications to cell physiology dictate malignant growth. Self-sufficiency in growth signals, insensitivity to growth-inhibitory (antigrowth) signals, evasion of programmed cell death (apoptosis), limitless replicative potential, sustained angiogenesis, and tissue invasion and metastasis are described as being the hall marks of cancer (Hanahan and Weinberg, 2000). Cancer is one of the leading causes of death worldwide. In 2015, the WHO announced 8.8 million deaths as a result of cancer worldwide with the most common causes of cancer deaths being cancers of lung, liver, colorectal, stomach and breast. The majority of cancer deaths worldwide were in low and middle income countries with 25% of cancer deaths in those countries being attributed to cancer causing infections such as hepatitis and human papilloma virus. One third of deaths from cancer were due to behavioural and dietary risks such as high body mass index, low fruit and vegetable intake, lack of physical activity, tobacco use, and alcohol consumption (WHO, 2017). Following the primary transformation of normal cells to malignant cells, tumour cells migrate and invade the host stroma and acquire capability to induce angiogenesis. Tumour cells has the potential of spreading into the circulatory system and can reach the lymphatic channels (Talmadge and Fidler, 2010). The process of tumourgenesis involves two key stages. In the first stage, genetic and epigenetic changes required for the transformation of normal cells to tumour cells occur. While the second stage involves cell proliferation and cell turnover which determines the survival, reproduction and ultimately growth of cancer. Both

stages are inseparable and necessary for tumour initiation and survival (Gatenby and Brown, 2017).

1.1.1 Malignant melanoma

Skin is the most affected by cancer. Skin cancers can either be non-melanoma skin cancers such as squamous cell carcinoma and basal cell carcinoma, or malignant melanoma which is the is the most aggressive form of skin cancer. Malignant melanoma results from malignant transformation of melanocytes at the epidermal-dermal junction (Ellerhorst et al., 2010). The last 50 years has witnessed a constant increase in the incidence of melanoma. In the UK, melanoma of the skin was the 5th most common cancer in 2014 as shown in Figure1.

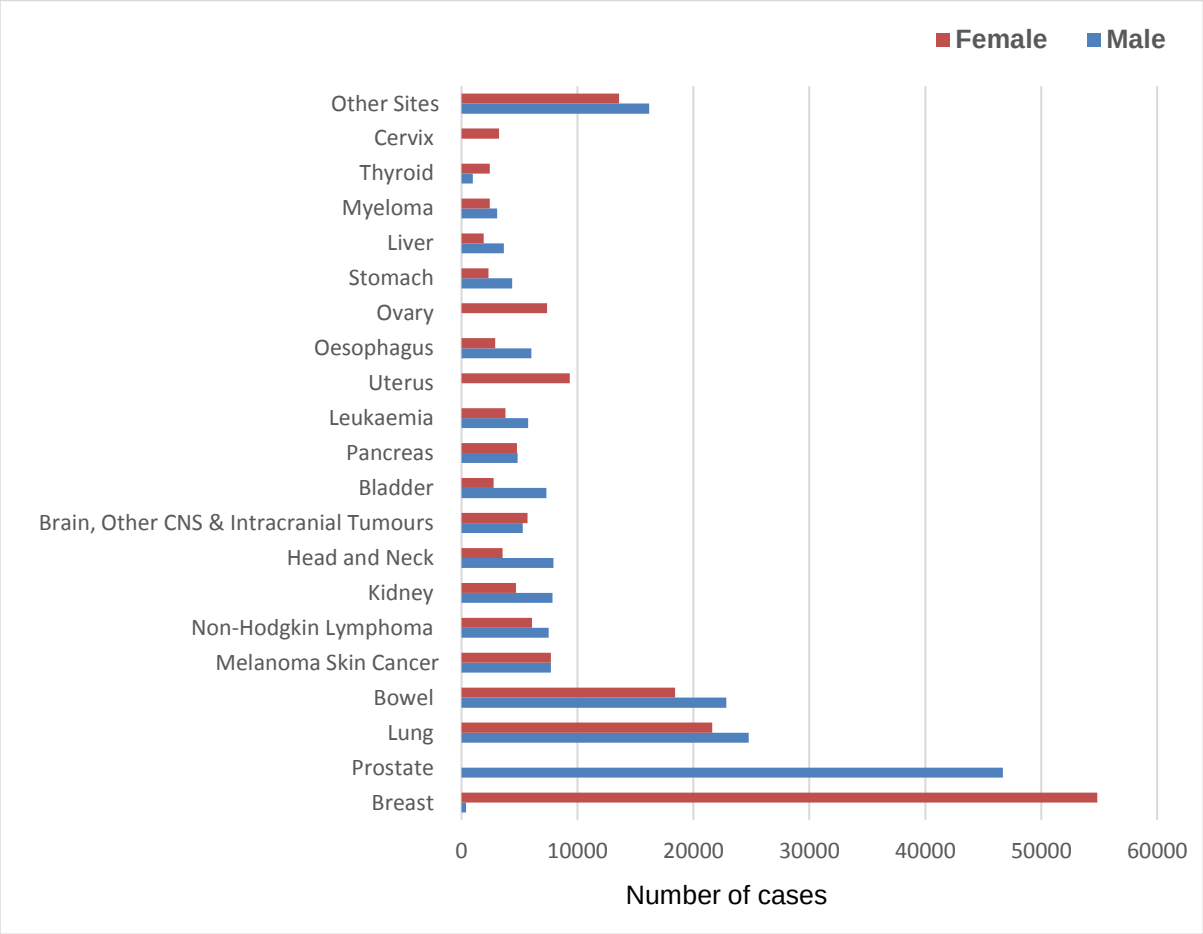

Figure 1: Ranking of 20 most common cancers in the UK in 2014 (Cancer Research UK, 2017).

During the last decade, the incidence rates of melanoma skin cancer has increased by 45% with the larger increase being in male rather than females (56 and 35% respectively). In 2014, melanoma skin cancer accounted for 4% of all new cancer cases in the UK. During the period between 2012 and 2014,50% of

skin cancer cases in the UK were diagnosed in people aged 65 and over (CANCER and RESEARCH UK, 2017). Survival from melanoma has been linked to tumour thickness highlighting the importance of early detection of this disease (Ellerhorst et al., 2010).

A recent study on the global burden of melanoma has revealed that Australia, New Zealand and North Europe have the highest incidence. Genetic predisposition, ultraviolet radiation (UVR) exposure, fair eye and hair colour are among the risk factors lying behind this high incidence (Karimkhani et al., 2017). Furthermore, gender, higher number of nevi, weakened immune system and history of severe sunburn are all risk factors that have been linked with melanoma (Cho et al., 2005). melanomagenesis can occur as a result of cellular damage from UVA induced reactive oxygen species as well as DNA damage from UVB exposure. Primary melanoma of the skin is characterised by a wide range of mutations which may be a result of the carcinogenic effects of ultraviolet light (Bastian, 2014). Estimates from the Global Burden of Disease 2015 study revealed that the greatest burden from melanoma falls on males (Karimkhani et al., 2017). A significant association between geographic UV index and cutaneous melanoma incidence which increased with age was found in males. No such association was found in females (Liu-Smith et al., 2017).

Studies into the genetic mechanisms underlying melanoma development have revealed that two proteins (namely RAS and BRAF) within the mitogen-activated protein kinase (MAPK) pathway frequently have mutations within the genes encoding them. Approximately 40-60% of patients with cutaneous melanomas were found to have mutations in the serine/threonine kinase BRAF (Samatar and Poulikakos, 2014). On the other hand, approximately 20% of melanomas harbour mutations in RAS which are almost exclusively present in melanomas without BRAF mutation (Curtin et al., 2005). Mutations in GNAQ and GNA11 are frequently found in uveal melanomas indicating that this type of melanoma harbour a genetic background that differs from cutaneous melanomas (Van Raamsdonk et al., 2010).

Aberrant DNA methylation has been considered as an epigenetic hallmark of melanoma and plays an important role in the formation and progression of melanoma. Among the aberrant methylation changes that have been described in melanoma is silencing of tumor suppressor genes such as PTEN, p16/14, and

RASSF1A. PTEN methylation has been linked with decreased immunohistological PTEN expression and increased risk of death, while the level of RASSF1A methylation is considered as a potential indicator of tumor progression. Besides tumour suppression genes, several other genes have been described as differentially methylated in melanoma relative to melanocytes. Among those are genes involved in pathways critical for cancer cell survival and growth, including cell cycle, DNA repair, apoptosis, metabolism, PI3K/mTOR signaling, immune response and metastasis (Reviewed in (Gatenby and Brown, 2017).

Early diagnosis is an important aspect in the management and successful treatment of melanoma. Complete surgical resection is used for the treatment of melanoma at early stages. This choice of treatment has proven to be successful in almost 95% of cases diagnosed at early stages (Garbe et al., 2008). Chemotherapy has shown minimal advantage in the treatment and management of late stage melanoma due to resistance to a wide range of chemotherapeutic agents. The minimal advantage of chemotherapeutic agents has prompted researchers to look for new possible treatments. The last couple of years has witnessed a dramatic improvement in the survival of patients with advanced or unresectable melanoma due to the introduction of two therapeutic strategies; targeted therapies and immunotherapy (Melis et al., 2017). Unfortunately, targeted therapies can only be used in patients with certain genetic aberrations. Notably, not all oncogenic mutations in melanoma are targetable. The European Medicines Agency (EMA) and The Food and Drug Administration (FDA) approved only two BRAF inhibitors (vemurafenib and dabrafenib) and two MEK inhibitors (trametinib and cobimetinib) for treatment of metastatic or unresectable melanoma (Ascierto et al., 2015).

Immunotherapy is used for the treatment of melanoma by enhancing the patient's immune system ability to eradicate tumour cells. This approach of treatment can theoretically be used in all patients with metastatic or unresectable melanoma regardless of mutation status. Augmentation of T-cell anti-tumour activity and enhancement of the patients' immune response is one the approaches employed in immunotherapeutic treatment of melanoma (Melis et al., 2017). Activation of T-cells is accomplished via the T cell receptor and a co-stimulatory interaction between CD28 and its ligand B7-1 or B7-2. The binding of molecules known as

immune checkpoints (cytotoxic T-lymphocyte-associated antigen-4 (CTLA4) or programmed death 1 (PD-1) to cognate ligands (CTLA-4 to dendritic cell B7.1 or B7.2; PD-1 to its ligands programmed death ligand 1 (PD-L1) and programmed death ligand 2 (PD-L2) on tumor cells and/or other cells of the microenvironment) results in negative signals and thus down regulates T cell activation. The use of immune checkpoints inhibitors results in reactivation of cytotoxicity and tumour regression. The blockade of immune checkpoints has the highest activity ever reported for metastatic is recommended as first-line therapy for most patients with advanced melanoma (Margolin, 2016).

Other immunotherapeutic approaches include vaccination strategies, adoptive transfer of autologous T cells directed against melanoma antigens, T cell engineering therapy and oncolytic virotherapy (Zhu et al., 2016). Among the first immunotherapeutic drugs used for the treatment of advanced melanoma was high-dose interleukin-2 (IL-2) which can be associated with sever toxicity. Nevertheless, this immunotherapeutic agent was the first to establish a role for immunotherapy in the treatment of advanced melanoma (Atkins et al., 1999). Interferon gamma is another immunotherapeutic agent employed in the treatment of melanoma. Improvement in disease free survival was noted in patients with high-risk cutaneous melanoma after treatment with IFNα adjuvant therapy (Mocellin et al., 2010).

1.2 Cancer Immunoediting

The immune system plays an important role in the prevention of tumours. If viral and bacterial infections are not successfully eliminated, protumourigenic conditions ensue. More directly, the immune system detects tumour-specific antigens leading to the elimination of tumour cells (Swann and Smyth, 2007). The process in which the immune system detects tumour cells and subsequently eliminates them is called immune surveillance. However, tumour cells can develop even if the immune system is competent.Tumour immunoediting describes a reciprocal interaction, which draws on cells of the innate and adaptive immune response (Swann and Smyth, 2007).

The tumour immunoediting concept or theory is divided into three distinct sequential phases; elimination, equilibrium and escape (Bhardwaj, 2007).The elimination phase is considered as an updated version of the previously known

concept of immune surveillance. In this phase both the innate and adaptive immunity detect any developing tumour cells and subsequently destroy them before establishment of cancer. There are parallel concepts for the mechanisms, which enable the immune system to detect a developing tumour. One proposed mechanism suggests the presence of classical “danger signals” such as type 1 Interferon (IFN) which activates dendritic cells and initiates an antitumour immune response. A second proposed mechanism is the release of molecules known as damage associated molecular pattern molecules (DAMPs) either directly from dying tumour cells or from damaged tissues. Another proposed mechanism involves the expression of what is known as stress ligands which bind to activating receptors on innate immune cells. As a result, pro-inflammatory cytokines are released which lead to the establishment of tumour specific adaptive immune response. Examples of such ligands include RAE-1 and H60 (in mouse) (Schreiber et al., 2011).

The elimination can either be complete when all tumour cells are destroyed or partial when a small portion of tumour cells persist indicating the initiation of the second phase which is termed equilibrium (Swann and Smyth, 2007). In the equilibrium phase the tumour cells are equilibrated by the immune system. The tumour cells are thought to be dormant in the equilibrium phase and may persist for decades. During this phase the immune system destroys susceptible tumour cells which result in the selection of tumour cells that are capable of avoiding the antitumour immune response leading to the next stage which is the escape phase. This phase starts when the immune system is no longer able to control the outgrowth of tumour cells, leading to the emergence of visibly growing tumour cells. One mechanism which may lead to the escape of tumour cells is loss of antigens resulting in reduced immune recognition. Another mechanism responsible for tumour escape is the resistance to the cytotoxic effects of immunity or relative immune suppression (old age, cytostatic drugs) (Schreiber et al., 2011).

1.3 Complement system

The complement system has a fundamental role in recognition and elimination of foreign antigens and pathogens. In addition, it exerts anti-immune regulatory role by enhancing humoral immunity, modifying T-cell immunity and influencing

tolerance to self-antigens (Thurman and Holers, 2006). There are three complement pathways: the classical, alternative and lectin pathways. The classical pathway activation is initiated by antigen-antibody complex formation, whereas the lectin pathway is activated by mannose containing polysaccharides. The alternative pathway is activated by a variety of microbial surfaces (Kemper et al., 2010). Under certain circumstances, complement activation may also be initiated by the binding of properdin to its target (Hourcade, 2006). All of these three complement pathways lead to the cleavage of C3 by C3 convertase forming C3a and C3b fragments. The C3b fragment can form a covalent bond with the surface of the target resulting in the generation of more C3 convertase. In addition, C3b fragment has the ability to form C5 convertase through binding to C3 convertase. Subsequently C5 convertase cleaves C5 producing C5a and C5b. The complement component C5b is bound by C6 and C7 leading to the formation C5b67 which in turn inserts itself to the microbial membrane, and binds to C8 and C9 forming the membrane attack complex (MAC); this initiates the destruction of the membrane and cell lysis (Merle et al., 2015b, Merle et al., 2015a).The alternative pathway was originally discovered in the mid-1950s as the properdin pathway. Before that, it was thought that complement can only be activated by the formation of antigen-antibody complex (Pillemer et al., 1954).

The alternative pathway can be auto activated in a process called “tickover” in which conformational changes happen in C3 which result in the formation of C3 (H_2O) molecule. This molecule in turn binds to factor B leading to the generation of conformational changes in factor B. This altered factor B can be cleaved by factor D generating Ba and Bb. The Bb component is capable of cleaving additional C3 molecules. Properdin, which is a trimeric serum protein, is responsible for the stabilisation of this process. In an attempt to study the interaction of properdin with C3b and factor B, Hourcade found that properdin has the ability to speed up convertase assembly through three mechanisms. Binding of properdin with C3b resulted in subsequent binding of C3b with factor B. In addition, properdin can bind to its target surface through C3b, iC3b and can utilise its other C3b binding sites to bind other nascent C3b, bystander C3b, or preformed C3bB and C3bBb complexes. Thus, the stabilising effect of properdin comes from its ability to bind to multiple ligands at the same time (Merle et al., 2015a, Hourcade, 2006).

The alternative pathway can also be trigged through the binding of fixed C3b formed either via the classical or lectin pathway activation to factor B in a process termed amplification loop (Thurman and Holers, 2006). These extra C3b molecules from either classical or alternative pathway which feed the amplification loop do not differ from those formed from the alternative C3 convertase in their ability to trigger amplification (Lutz et al., 2007). The alternative pathway has a unique role due to its activation by its own product which is C3b.Thus the alternative pathway has a central role in the activation of all three pathways due to the contribution of C3b molecules formed via the activation of both the classical and lectin pathways in the generation of alternative pathway C3 convertase (Grailer et al., 2012, Merle et al., 2015a). Selective monoclonal antibodies were used to investigate the role of the alternative pathway in classical pathway induced C5 activation and the results showed that this leads to the inhibition of a large quantity of the C5a and the terminal C5b-Ca complex (Harboe et al., 2004).

Properdin is a positively charged protein which exists as dimer (P2), trimer (P3) and tetramer (P4). It is responsible for stabilisation of the alternative complement pathway. It was first discovered by Louis Pillemer and colleagues in 1954. Properdin was described as a new plasma component which has the ability to activate complement (Pillemer et al., 1954).

Nevertheless, Pillemer's theory was the source of controversy and was not widely accepted at that time. Properdin increases the stability of the alternative pathway convertases 10-fold (Fearon and Austen, 1975, Medicus et al., 1976).

Properdin also known as factor P is a 53-kDa glycoprotein. It contains 7 thrombospondin repeat type I (TSR-0 to TSR-6) domains and an N-terminal domain. Properdin exsists as dimers (P2), trimers (P3) ,and tetramers (P4) in a ratio of 1:2:1. Unlike most complement proteins which are maily synthesised in the liver, Properdin is produced by a number of cells such as monocytes, neutrophils, primary Tcells,and shear-stressed endothelial cells (Cortes et al., 2012). In humans, plasma contains low levels of properdin (0.02 mg/mL). Properdin is the only known complement regulator that stabilises C3bBb convertase and the activity of the alternative pathway. The C3bBb complex is unstable and has a half-life of 90 s under physiological conditions (Pangburn and Muller-Eberhard, 1986). Properdin has the ability to bind and stabilise C3b.Bb

complex (C3 convertase) creating the more stable C3bBbP and thereby protects C3b in the complex from inactivation by Factor I with Factor H as co-factor.Binding of C3b to theC3b,Bb complex results in the formation of the alternative pathway C5 convertase (C3b)2−n,Bb, which is also stabilised by properdin (Cortes et al., 2012). In 2013, Alcorlo and co-workers used electron microscopy to investigate how properdin performs this function. This study managed to reveal that properdin associates with both the C345C domain in C3b and the VWF domain in Bb, thereby stabilising C3bBb convertase by linking together the two components of this enzymatic complex. It has been suggested that properdin interacts more efficiently when with these two fragments when Bb fragment is in the conformation found in C3bBb convertase than the closed conformation of the C3bB proconvertase. Furthermore, stabilisation of the C3bBb convertase was also accomplished by interference of properdin with the interaction of C3b with the complement regulators which effectively impacts their accelerated decay. Properdin interferes with C3bBb convertase decay by promoting a large displacement of the thioester-containing domain (TED) and complement protein subcomponents C1r/C1s, urchin embryonic growth factor and bone morphogenetic protein 1(CUB) domains of C3b. This interference probably impairs C3-convertase inactivation by regulatory proteins. The combined effect of molecular binding and structural reorganisation will increase the stability of C3 convertase and accelerate the recruitment of fluid-phase C3 convertase to the cell surfaces (Alcorlo et al., 2013). Besides stabilisation of alternative convertase, C3bBb, it has been suggested that properdin acts as a pattern recognition molecule via binding to negatively charged molecules on certain microbial surfaces, necrotic cells, apoptotic cells and cells undergoing malignant transformation. After binding to these surfaces, properdin directs C3b deposition and C3bBb assembly to provide a focal point for amplifying complement activation (Spitzer et al., 2007, Hourcade, 2006). Nevertheless, there has been a lot of controversy around the reports assigning the role of pattern recognition receptor to properdin. The studies were criticised due to the use of relatively artificial systems permitting either C3 activation with initial C3b deposition or in buffer systems with purified properdin. It has been suggested that in the presence of intact C3, it is was impossible to demonstrate whether properdin acts in a recognition manner or subsequently binds to C3b (Farries et

al., 1987). Furthermore, long term storage, freezing and thawing of properdin resulted in the appearance of properdin aggregates in certain purified preparations and thus may be considered as artifacts with different properties than serum properdin (Pangburn, 1989). Additionally, it is necessary to distinguish between passive binding of properdin to a surface and subsequent activation of the alternative pathway as a result of this binding. A recent study carried out by Harboe and co-workers looked into the controversy surrounding the role of properdin as a pattern recognition molecule noting that it lacks the structural homology shared by other pattern recognition molecules of the complement system. This study reported the inability of properdin to directly bind granulocyte myeloperoxidase, the surface of human umbilical vein endothelial cells (HUVECs), or to *Nisseria meningitidis* (Harboe et al., 2017). Furthermore, this study managed to show C3-dependent binding of properdin to granulocyte myeloperoxidase, HUVECs and *Nisseria meningitidis* contradicting a previous study which reported the initiation of the alternative complement pathway as a result of direct binding of properdin to granulocyte myeloperoxidase (O'Flynn et al., 2014).

A novel properdin defeciency (E244K) caused by a single point mutation resulting in a very low alternative pathway has recently been described. Experiments carried out with Recombinant FP E244K highlighted the important role of properdin oligomerization *in vivo* and gave detailed structural insights that could facilitate the emergence of novel modulators of complement. Additionally it has been suggested that the major binding of properdin to alternative pathway convertase is facilitated via a single properdin thrombospondin repeat and a small region in C3b. Monomeric properdin was able to bind C3b, C3MA, iC3b, C3c, the C3 proconvertase C3bB, and the convertase C3bBb. Interestingly, it seems that TSR5, and to some extent also TSR6 and TSR4 are principal modules for C3b-binding and stabilisation of C3bBb (Pedersen et al., 2017). Previous studies have shown that properdin oligomerisation was necessary for stimulation of hemolysis (a typical *in vitro* assay to assess alternative pathway activity), the formation of platelet/leukocyte aggregates *in vivo*, and binding to *Chlamydia pneumoniae* (Blatt et al., 2016, Pangburn, 1989).

Proteolytic activation of the central complement component C3 and subsequent formation of C5 convertase is where the three aforementioned complement

pathways meet. C5 convertase cleaves C5 at arginine 751 (R751) and thereby results in the release of the anaphylatoxin C5a and generation of C5b which initiates the formation of the membrane attack complex. Recent findings have reported the generation of biologically active cleavage products from C5 by phagocytic cells independent of the plasma complement system, suggesting the existence of a complement activation pathway in plasma other than the three already established pathways. Incubation of human blood neutrophils or rat alveolar macrophages with C5 resulted in the generation of C5a in a dose/time dependent manner. This C5 cleavage product was detected using anti-human C5a antibody. It has been proposed that activation of alveolar macrophages by a number of agonists such as bacterial products and tumour necrosis factor-α (TNF-α) lead to the expression of a serine protease with a C5-cleaving potential resulting in the production of C5a (Huber-Lang et al., 2002). Leakage of plasma C5 and production of C5 from lung macrophages, fibroblasts or alveolar epithelial macrophages are all possible sources of C5 (Strunk et al., 1988, Rothman et al., 1989). Activation of C5 in a C3 independent manner by several enzymes has been reported in a number of studies. Amongst those enzymes, is the central coagulation enzyme thrombin. During pathophysiologic conditions, both the complement and coagulation systems are activated in an effort to maintain homeostasis (Markiewski et al., 2007). A number of molecular links between the complement and coagulation systems have been identified highlighting the importance of the coordinated interplay between these two biochemical systems (Wetsel and Kolb, 1983, DiScipio et al., 1983, Polley and Nachman, 1978, Huber-Lang et al., 2006, Amara et al., 2010). The ability of thrombin to activate C5 and subsequent release of C5a has been identified as a new complement activation pathway. Although thrombin cannot efficiently cleave C5 at arginine 751 (R751), it has the ability to cleave C5 at a highly conserved thrombin-sensitive site which corresponds to R947. The cleavage of C5 by thrombin at R947 results in the formation of previously undescribed intermediates C5T and C5bT (Figure 2). Interestingly, C5bT forms a C5bT-9 membrane attack complex with more potent lytic activity than with C5b-9 (Krisinger et al., 2012). It has been suggested that any disturbance to the delicate balance between the complement and coagulation pathways (such as in the case of C3 knockout mice) results in a compensatory adaptive pathway characterised by increased production of

thrombin which in turn acts as a C5 convertase and subsequently generates authentic C5a (Huber-Lang et al., 2006).

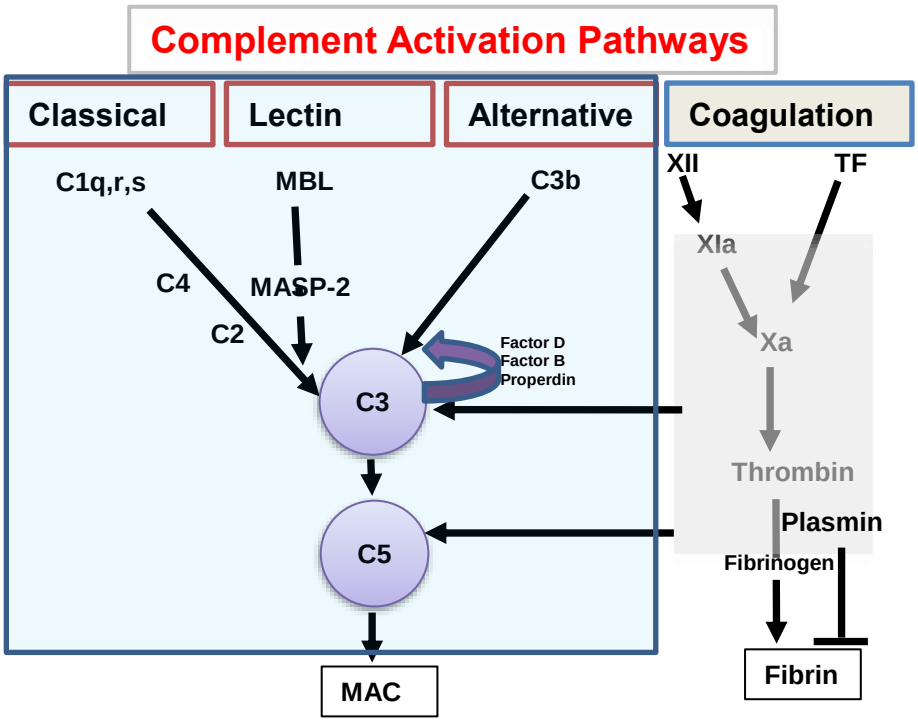

Figure 2: Interaction Between the Coagulation and Complement System.

Complement activation pathways (MAC membrane attack complex; MBL mannose binding lectin; MASP-2 mannose associated serine protease-2; TF tissue factor

1.4 The role of Complement in Tumour Growth.

Traditionally, activation of the complement system is thought of as an effector of innate immunity, which bridges the adaptive immunity but has its place in the acute immune response. This view has been challenged in models assessing its role in autoimmune disease such as rheumatoid arthritis, encephalomyelitis, myasthenia gravis and systemic lupus erythematosus (Ballanti et al., 2013, Vignesh et al., 2017) and recently, in models of cancer. The common denominator is, of course, inflammation, so it is entirely conceivable that complement activation, its products and its regulators have detectable modulatory functions. At the beginning of this research project, there are four key articles supporting the hypothesis that complement codetermines the outcome of cancer progression (in the immune escape stage of cancer), which are summarised as follows:

The ability of complement activation products (C5a in particular) to promote tumour growth was investigated in a syngeneic mouse model in which C57BL/6 mice were injected with a cervical cancer cell line by subcutaneous injection of TC-1.Complement activation was assessed by immunofluorescence and the results showed that C3 cleavage products were deposited in the tumour vasculature of the mice, however there was little C3 deposition in the benign tissue surrounding the tumour. Furthermore, subcutaneous injection of TC-1 cells in C3 deficient mice lead to significantly smaller tumours when compared to the wildtype. In addition, the role of C5a in tumour growth was investigated by blocking C5aR in tumour bearing wildtype mice using C5aR antagonist (hexapeptideAcF (OP (D)ChaWR). The results showed that tumour growth was retarded in those mice treated with C5aR antagonist after one week of injection of tumour cells compared to untreated mice. This study found that C5a promotes tumour growth by inhibition of $CD8^+$ T-cells response. The suppression of $CD8^+$ was accompanied by an increase in the number of myeloid derived suppressor cells (MDSCs) in the tumour microenvironment which subsequently produces reactive oxygen species (ROS) and reactive nitrogen species (Markiewski et al., 2008).

A further study carried out by Corrales et al (2012) addressed the role of C5a in creating an immune suppressive microenvironment for lung cancer. In this study,

Corrales and colleagues suggested that activation of complement may create a microenvironment favouring tumour growth and progression. A mouse syngeneic lung cancer model was used to show that C5a promotes tumour growth and progression. This model was obtained by subcutaneous injection of 3LL cells into the flank of C57BL/6J mice and subsequent blocking of C5a receptor by using C5aR antagonist. The ability of Mouse Lewis lung carcinoma (3LL) and human lung cancer lines to activate and release complement both in serum and serum free conditions was evaluated. Lung cancer cell lines have the ability to produce higher levels of C5a when compared with non-malignant epithelial cells (human bronchial epithelial cells). Furthermore, the ability of C5a to promote angiogenesis was investigated through treatment of mice with C5aR antagonist which led to less microvessel formation. Moreover, the level of angiogenic factor bFGF (basic fibroblast growth factor) was found to be lower in tumour bearing mice treated with C5aR antagonist. Analysis of splenocytes in tumour bearing mice treated with C5aR or the control peptide antagonist showed that the percentage of $CD8^+$ and $CD4^+$ T-cells were similar but the number of monocytic and granulocytic MDSCs were lower in mice treated with C5aR antagonist. The decrease in the number MDSCs due to the blockade of C5a receptors supports the previous conclusion that C5a creates a favourable environment for lung cancer cells growth and progression which may be linked to the induction of angiogenesis and immunosuppression (Corrales et al., 2012).

Further evidence of C5a being a key protumourigenic factor comes from a study in which murine lymphoma RMA and human ovarian carcinoma cells were transfected with secreting mouse C5a or empty vector plasmids. Tumour progression was increased in tumour bearing mice with high C5a producing syngeneic lymphoma. The effect of C5a on tumour progression in immunocompetent mice was investigated by implanting murine lymphoma RMA cells with or without C5a in WT C57BL/6. Comparison of tumour size between WT C57BL/6 with C5a expressing tumours and those without C5a expressing tumours showed a highly significant increase in tumour size in mice with C5a expressing tumours. In addition, the number of $CD11b^+$ MDSC was also increased in mice with C5a expressing tumours. On the other hand, tumour bearing mice with low C5a producing lymphoma cells had low tumour burden with an increase in both $CD4^+$ and $CD8^+$ T cells in spleen and tumour draining lymph

nodes. The human adenocarcinoma cell line (SKOV-3) was transfected with C5a or control plasmid. The cytotoxic activity of naïve innate leukocytes (NK and neutrophils) was evaluated in both SKOV-3CV (human ovarian carcinoma cells) and SKOV-3C5a tumour cells and the results show that NK cells are more active against SKOV-3V C5a tumour cells when compared with SKOV-3CV cells. In immunocompetent mice (WT C57BL/6) the growth of SKOV-3C5a was significantly faster than empty control vector transfected cells. This study reached the conclusion that the local concentration of C5a in the tumour is a contributor which determines tumour growth and stated that local C5a concentration determines the outcome of tumour cells. This study hypothesised that overactivation of the infiltrating cells due to high concentration of C5a may result in suppression of antitumour T cells, thus leading to progression of tumours. On the other hand, low concentration of C5a can lead to a powerful antitumour immune response (Gunn et al., 2012).

A study to investigate the role of complement during ovarian cancer progression crossed transgenic mice C57BL/6 TgMISIIR-Tag that can develop spontaneous epithelial ovarian cancer with two lines of mice with genetic complement deficiencies C3 (B6.129S4-C3^{tm1Crr}/J) or C5aR (C5ar1^{tm1Cge}/J). The resulting transgenes with deficiency in either C3 or C5aR either developed no ovarian tumours or a small and poorly vascularized tumour which implies that complement activation plays a critical role in the formation of ovarian tumours. The composition of tumour infiltration leucocytes was studied and the results showed no difference in tumour infiltrating leukocytes between the mice that had partial deficiency in C3 and the wildtype except in CD8+ (which was increased in mice with partial C3 deficiency) and CD4+ T cells (which was decreased in mice with partial C3 deficiency). This study concluded that activation of complement plays a major role in oncogene driven carcinogenesis (Nunez-Cruz et al., 2012).

Using a syngeneic model of melanoma developed in C57BL/6 WT and C1q-deficient (*C1qa-/-*) mice, Bulla et al. detected slower tumour growth in C1q-deficient (*C1qa-/-*) mice as compared to their wildtype counterparts. However, they failed to detect higher frequency of MDSCs in wildtype mice (Bulla et al., 2016).

In conclusion, complement activation and complement products have been found to have an important role in determining the extent of tumour growth. However,

no study to date has investigated the role of properdin in tumour growth. Hence one of the aims of this project was to determine the role of complement in tumour growth and cell recruitment.

1.5 Properdin and cancer

In 1957, Rottino and colleagues carried out a study to investigate properdin levels in the sera of patients with Hodgkin's disease. Initially, the main aim of this study was to investigate the behavior of properdin in the course of Hodgkin's disease and assess if variations in the level of properdin in those patient could have a role in determining its variable outcome. Blood samples were drawn from 56 patients with Hodgkin's disease, 25 with carcinoma (breast, mouth, larynx, colon, etc...) and 7 with lymphatic leukaemia, one with multiple myeloma, and one with tuberculosis adenitis). The study also included blood drawn from 100 normal blood donors. The results of this study demonstrated that serum properdin levels in normal adults varied from 2 to 12 units. The level of properdin in patients with Hodgkin's lymphoma was within the normal range. Interestingly, the level of properdin in almost half of the cancer patients included in this study was lower than 2 units per milliliter of serum (Rottino, 1957). On the other hand, this low level of properdin was only found in only 5% of normal control and 9 out of 70 patients with lymphoma (Rottino, 1957). Before the avenue of specific antibodies, the level of properdin was measured in unit/ml (U/ml). In the past, properdin used to be quantified as a haemolytic activity in comparison with a standard. The level of properdin in a test sample was obtained through determining the smallest volume of test sample which completely C3 in the presence of an optimal amount of zymosan (Rottino and Levy, 1957).

These surprising results tempted Rottino and his colleagues to carry out a more detailed study of the levels of properdin in sera of patients with malignant tumours. This study included 109 patients with carcinoma. In addition, 70 patients with Hodgkin's disease, 9 with chronic leukemia, 14 with lymphosarcoma, 5 with myeloma and 32 with non-neoplastic diseases. The aim of this study was to investigate if low level of properdin could be related to a drop in the total serum protein level. In addition, they wanted to investigate if properdin, an important component of the complement system had a role in the spread of cancer. The results of this study showed that 45% of cancer patients had properdin values

less than 2 U/ml. Whereas, this low level of properdin was found in approximately 22% of patients with lymphomatous disease, 5% of normal individuals and 47% of patients with noncancerous diseases. A significant relationship was found between low total serum protein and low properdin level. The results of this study confirmed the findings of the previous study. However, no correlation was found between this low level of properdin and metastasis (Rottino, 1957).

In an attempt to investigate a possible role for properdin in transplantable cancer, C3H mice bearing transplantable Gardner lymphosarcoma 6CH3HED were intravenously injected with various preparations of guinea pig sera (serum depleted of various components of complement, serum depleted in properdin, serum fractionated by centrifugation and serum heated at various temperatures). The results showed that treatment with normal sera, sera depleted in one of the complement components (C1, C3, C4 or properdin) and heated sera, supernatant from sera centrifuged at 35,000g at 2 ˚C for 3 hours lead to complete regression of tumour and a significant impairment of tumour growth. From these findings it was concluded that the tumor inhibitory factor previously found in guina pig sera is not complement, properdin or LPS. However, measurement of properdin level in the sera of mice treated with the preparations previously mentioned revealed that growing or large tumours were accompanied by a drop in properdin levels. In contrast, normal or increased properdin level was found in regressive tumour (Herbut et al., 1958).

Another study also reported a decrease in the level of properdin in tumour bearing mice when compared with normal non tumour bearing mice. This study reached conclusion that properdin levels decrease upon tumour growth and increase upon tumour regression (Herbut and Kraemer, 1958).

1.6 The tumour microenvironment

In 2000, Hanahan and Weinberg proposed that malignant growth is the result of six essential alterations. These alterations were later termed as the hallmarks of cancer, which include: self-sufficiency in growth signals, insensitivity to growth inhibitory (antigrowth) signals, evasion of programmed cell death (apoptosis), limitless replicative potential, sustained angiogenesis, and tissue invasion and metastasis. These hallmarks are acquired functional capabilities during the course of tumourigenesis, and thereby enable cancer cells to survive, grow and

disseminate (Hanahan and Weinberg, 2000). After 10 years, progress in cancer research lead to the addition of two enabling characteristics that complements the previously reported six hallmark capabilities; and two new emerging hallmark capabilities. The two enabling characteristics include genome instability and mutation; and the inflammatory state of malignant lesions which is governed by immune cells some of which may promote progression of tumour. Emerging hallmarks include reprogramming energy metabolism and evasion of immune eradication (Hanahan and Weinberg, 2011).

In addition to tumour cells, the tumour microenvironment consists of many components which impact the outcome of the disease. The tumour microenvironment contains diverse cell populations, structural molecules and signalling factors, and the collective interplay between these elements and tumour cells support the process of tumourigenesis. In general, elements of tumour microenvironment are classified into three categories which include; cells of haematopoietic origin, cells of mesenchymal origin and non-cellular components. Cells of haematopoietic origin include those that arise in the bone marrow (BM) and can either be of lymphoid lineage (including T-cells, B-cells and NK-cells) or of myeloid lineage such as macrophages, neutrophils and myeloid-derived suppressor cells (MDSC) (Pattabiraman and Weinberg, 2014). Tumour stroma contains inflammatory cells which can either be tumour promoting or tumour suppressive. Furthermore, a number of partially differentiated myeloid progenitors have been identified in tumours. These cells are intermediates between circulating bone marrow derived cells and fully differentiated immune cells present in inflamed tissue. Among those cells is a group of tumour infiltrating myeloid cells that co-express the macrophage marker CD11b and the neutrophil marker Gr1. These cells are termed myeloid derived suppressor cells and have been shown to have an antagonising effect on cytotoxic T cell (CTL) and Natural killer cells (NK). There have been suggestions that recruitment of these cells can be extremely helpful for developing tumours by promoting angiogenesis, tumour progression and contributing in the evasion of immune destruction (Qian and Pollard, 2010).

Two of the most important cell types that contribute to the biology of various tumours are the MDSCs and T-regulatory lymphocytes (T-regs), thus the following section will try to focus on these two cells in detail.

1.6.1 Myeloid suppressor cells (MDSCs)

MDSCs are a heterogenous population of cells that have the ability to suppress T-cell activity. A number of cytokines, chemokines and transcriptional factors are involved in the recruitment and expansion of MDSCs. One important chemokine receptor is CCR2, which plays a central role in regulating the recruitment and turnover of MDSCs to the tumour site (Sawanobori et al., 2008). Another pivotal player involved in the recruitment of MDSCs is the complement component C5a. Recruitment of MDSCs is mediated via the Interaction of this component with a G protein-coupled receptor (Markiewski et al., 2008). Depletion of amino acids arginine and cysteine, produOne ction of ROS, production of TGF-β and induction of T-regs are all mechanisms by which MDSCs suppress the immune response (Bronte et al., 2005, Huang et al., 2006, Movahedi et al., 2008, Nagaraj et al., 2007, Srivastava et al., 2010). During pathological conditions immature myeloid cells expand into MDSCs rather than differentiation into either macrophages, dendritic cells or mature granulocytes and have a pathogenic role in cancer, autoimmune disease and chronic infectious disease. Studies on tumour bearing mice have reported the accumulation of MDSCs within primary and metastatic tumours, BM, spleen as well as peripheral blood. Furthermore, increase of MDSCs has been described in blood of cancer patients (Zhang et al., 2013, Sun et al., 2012, Raychaudhuri et al., 2011). Based on morphology and expression of Ly6 family of glycoproteins two subsets of MDSCs were identified in mice. These subsets are: monocytic MDSCs (M-MDSCs) and granulocytic MDSCs (G-MDSCs). One important difference between these two subtypes is that M-MDSC-mediated immune suppression does not require cell-cell contact, but is characterised by up-regulation of two different enzymes of inducible nitric oxide synthase (iNOS) and arginase-1 (Arg1) as well as production of immunosuppressive cytokines. On the other hand, G-MDSCs-mediated immune suppression occurs via mechanisms which involve the release of ROS, a process that requires prolonged cell-cell contact between MDSC and T cell (Gabrilovich and Nagaraj, 2009). Nevertheless, it has been suggested that MDSCs mediated suppressive activity is a result of a group of phenotypically heterogeneous myeloid cells rather than a specific subset (Youn et al., 2008).

Tumour cells produce many factors involved in the differentiation of MDSCs. Among those factors are granulocyte monocytes-colony stimulating factor (GM-CSF), macrophage monocytes-colony stimulating factor (M-CSF), IL-6, IL-1β, VEGF and PGE2 (Marigo et al., 2010). The level of MDSCs expansion depends on the type of tumour model, with sarcomas having the lowest level of MDSCs expansion and breast carcinoma and colon carcinoma having the highest. One important determinant of the level of MDSCs expansion is the nature of soluble factors produced by tumours (Youn et al., 2008).

In melanoma, the tumour microenvironment is enriched with MDSCs and thereby results in suppression of antitumour immune response which leads to tumour progression. Melanoma cells have the ability to produce various inflammatory mediators (such as GM-CSF, VEGF, TGF-β), chemokines (CCL2, CCL4, CCL5), tumour necrosis factor (TNF)-α, IL-1β, IL-6 and IL-10) some of which have been implicated in the generation, expansion and migration of MDSCs (Gabrilovich et al., 2012, Filipazzi et al., 2012, Poschke and Kiessling, 2012, Condamine and Gabrilovich, 2011). During progression of melanomic tumours, it was noted that accumulation of various inflammatory mediators (including VEGF, IL-1β, IL-6, TNF-α, GM-CSF, IFN-γ, TGF-β, IL-10 and CCL2) in melanoma lesions coincided with increased accumulation of MDSCs in tumour microenvironment (Figure 3). Furthermore, these MDSCs were characterised by increased iNO production and ARG-1 expression; indicating their high level of activation and their strong T-cell suppressive ability. It has been suggested that melanoma immunotherapy should focus on inhibition of MDSC suppressive function (Umansky et al., 2014).One promising approach in cancer immunotherapy would be to inhibit MDSC pro-tumoural activity via enhancement of differentiation of MDSCs into mature cells (Sica et al., 2011, Najjar and Finke, 2013, de Haas et al., 2016).

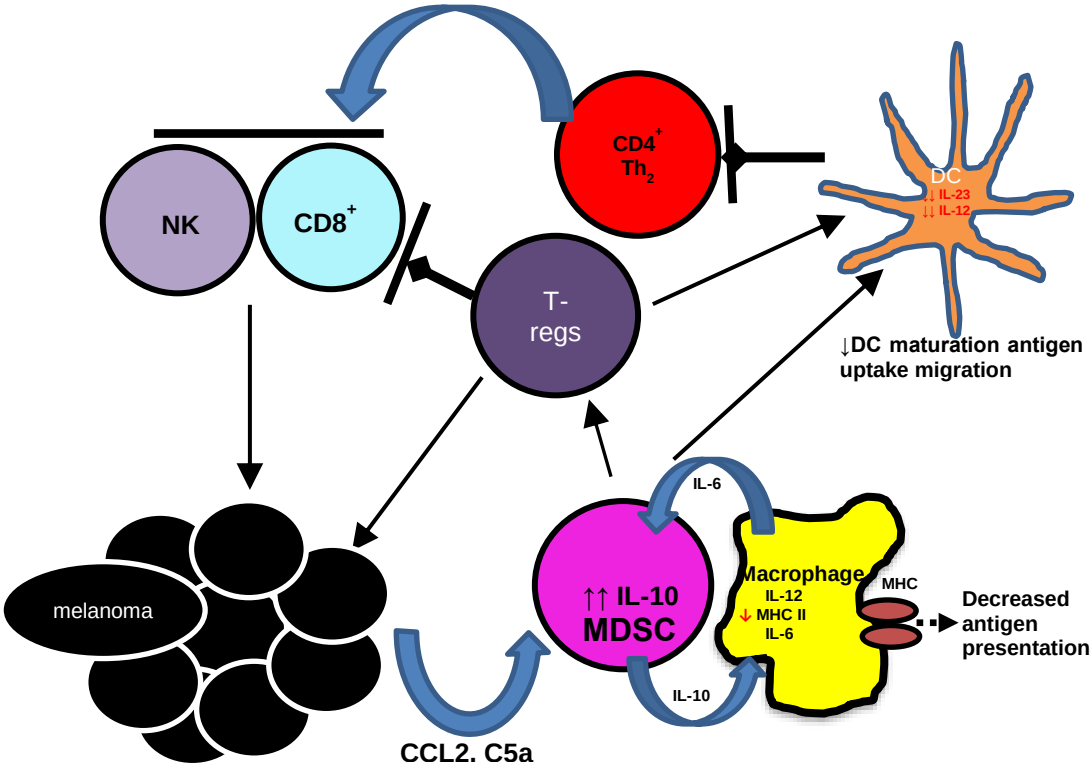

Figure 3: MDSCs suppress antitumour immunity through multiple different mechanisms.

Cross-talk between MDSC and macrophages polarizes immunity towards a type 2 response that promotes melanoma tumuor progression. MDSC, dendritic cells impairs DC function and macrophages interact with each other through a variety of soluble mediates and cell contact-dependent mechanisms that enhance the suppressive activity of each cell type. Cross-talk results in increased production of IL-10, decreased production of IL-12 and IL-6, and down-regulation of macrophage MHC II. The down-stream effects are the activation of $CD4^+$ Th_2 and T regulatory cells and decreased antigen presentation which impair cytotoxic $CD8^+$ T cell activity and impairment of NK cell cytotoxicity. Increased tumour burden facilitates the accumulation of MDSC which in turn decrease DC maturation, antigen uptake, migration, IL-23, IL-12 and T cell IFN production, thereby limiting the activation of CD8-mediated anti-tumour immunity.

1.6.2 Regulatory T cells (T-regs)

T-regs are characterised by the expression of CD4 antigen and the forkhead transcription factor, FOXP3 which regulates the expression of proteins that mediate T-regs suppressive function. T-regs modulate the expansion and activation of T and B cells, and NK cell cytotoxicity. T-regs play a prominent role in infection, allergy and autoreactivity. In cancer, a shifted balance towards increased T-regs contribute in hindering the body's ability to control the progression of tumour cells via supressing the anti-tumour immune response. Mechanisms by which T-regs weakens the anti-tumour immunity include suppression of cytotoxic cells, secretion of immunosuppressive cytokines and interference with tumour associated antigen presentation. Mouse models have shown that removal of T-regs results in rejection of tumour cell lines and thereby prevents the progression of these cells *in vivo* (Betts et al., 2007). Tumours are enriched with FOXP3 -expressing cells in humans and mice. Furthermore, cancer studies have shown the accumulation of T-regs in peripheral blood and spleen which implies that accumulation of these cells is a characteristic of cancer (Leong et al., 2006, Betts et al., 2007). There are two populations of T-regs; naturally occurring T-regs (nT-regs) which develop in the thymus and constitutively express CD25 and FOXP3 , and the other type is the induced T-regs (iT-regs) which develop in the periphery as $CD4^{+}CD25^{-}$ cells and subsequently acquire FOXP3 expression and suppressive activity (Gallimore and Simon, 2008). Tumours can be infiltrated with either or both of these cells via a number of mechanisms favoured by the tumour microenvironment (Adeegbe and Nishikawa, 2013). In melanoma, accumulation of T-regs in tumour tissue has been reported with the CD8+/T-regs value being frequently used to predict prognosis. Murine models of melanoma have shown that any temporary decrease in T-reg numbers augments antitumour immunity and improves survival, highlighting the functional significance of these cells in cancer. Similar observations were also noted in patients with metastatic melanomas in which T-regs were increased in peripheral blood when compared to healthy controls. In addition, estimation of T-reg numbers in primary and metastatic lesions, as well as affected lymph nodes revealed that the tumour microenvironment of melanoma patients is highly infiltrated with T-regs which are reported to be functionally immunosuppressive (reviewed in (Jacobs et al., 2012)). Although a

number of studies have linked the extent of T-reg expansion in tumour lesions and prognosis in melanoma patients, but others did not manage to find such correlation (Ladanyi et al., 2010, Miracco et al., 2007, Brody et al., 2009, Hillen et al., 2008). Vence and co-workers identified tumour-specific T-regs capable of recognising a broad range of melanoma-associated antigens circulating in melanoma patients (Vence et al., 2007). It has been suggested that each of nT-regs and iT-regs play independent roles in tumour specific tolerance. Mouse models of melanoma have revealed that tumour-infiltrating T-regs activated by one tumour-associated antigen suppress both naturally occurring and vaccine-induced antitumour immune responses against a broad range of tumour antigens. To date the factors which govern the migration of effector T cells and T-regs to tumour site is not fully understood. It has been suggested that production of the chemokine CCL22 by tumour-infiltrating macrophages results in migration of T-regs to tumour site (Zhou and Levitsky, 2007, Liu et al., 2007, Valzasina et al., 2006, Bui et al., 2006). Selective depletion of T-regs in an effort to overcome their suppressive activity represents a promising strategy to augment the effectiveness of tumour specific immunity (Gallimore and Simon, 2008).

1.7 Antimicrobial peptides and cancer

Chemotherapy and radiation in the treatment of cancer are associated with serious side effects like nonspecific toxicity and the emergence of multidrug resistance of tumour cells. These drawbacks have urged scientists to conduct an intensive search and propose new oncolytic therapies that are less toxic and more effective. One of the most widely studied oncolytic candidates is antimicrobial peptides (AMP), also known as host defence peptides (Papo and Shai, 2005). Antimicrobial peptides (AMPs) are regarded as part of the innate immune defence mechanism of several living organisms. Although these peptides were initially discovered due to their ability to kill bacteria subsequent studies have found that they can overcome the drawbacks of conventional cancer therapy via a unique mechanism of cancer killing (Papo et al., 2003, Leuschner and Hansel, 2004). Not all AMP possess an anticancer capability and those which have can be divided into two broad categories. The first includes those that are highly cytotoxic for bacteria and cancer cells but not against normal mammalian cells, while the second category include AMPs that can kill normal mammalian cells in addition to bacteria and cancer cells. The selectivity of AMP for tumour cells rather than normal cells is thought to arise due to the major differences between the cell membranes of these two cells. The selective killing of tumour cells by AMP is a consequence of the electrostatic interactions between cationic AMP and anionic cell membrane components (Hoskin and Ramamoorthy, 2008). Over the past 10 years, a considerable number of studies have been aimed at investigating the antitumour potential of some AMP. Among those peptides are members of the cationic antimicrobial peptide superfamily, defensins. It has been suggested that α and β defensins can act as immune modulators of the tumour microenvironment. Defencins induce T-lymphocyte and dendritic cell chemotaxis and thereby have the potential to restore antitumour immunity during cancer. A combination of immune system activators (such as Imiquimod) and defensins is another new promising potent anticancer treatment method (Suarez-Carmona et al., 2015). Several studies have found disrupted expression of defensins in malignant tissue linking these peptides with tumour initiation and progression (Rohrl et al., 2010, Donald et al., 2003). Nevertheless, there has been a debate about the role of defensins in tumour initiation and progression with some groups

reporting overexpression of some β defensins in certian types of cancer while others have reported diminished or suppressed expression in malignant tissue (reviewed in (Alrayahi and Sanyi, 2015)). Initiation of tumourgenesis and inflammation have also been linked to dysregulation of cathelicidin, a group of mammalian AMPs (Wu et al., 2014).

Investigations into the expression of CRAMP (cathelin related antimicrobial peptides) and β-defensins by measuring mRNA of these peptides in splenic tissue from wildtype and properdin deficient tumour bearing mice were carried out as part of this project. These investigations showed no significant difference in the expression of these two AMPs between both genotypes (see appendix).

1.8 Obesity and cancer

LDLR$^{-/-}$ mouse model combined with properdin-deficient mice was used to investigate the role of this complement component in our syngenic tumour model. The LDLR$^{-/-}$ is a mouse model in which the low-density lipoprotein (LDL) receptor had been knocked out. The LDL receptor is an important player in the clearance of apoB and apoE-containing lipoproteins (Kurano et al., 2015). The absence of the LDL receptor prolongs the plasma half-life of VLDL and LDL which results in the LDLR$^{-/-}$ mice being hypercholesterolemic (Ishibashi et al., 1993, Bieghs et al., 2012, Wouters et al., 2008). Published studies reported that tumour from high-cholesterol (hypercholesterolemic) mice had higher microvessel density, linking hypercholesterolemia with induction of angiogenesis and more tumour growth *in vivo* (Pelton et al., 2014).

A number of epidemiological studies have linked obesity with the incidence of many types of cancers including melanoma. Studies on the relationship between obesity and melanoma incidence revealed that obesity is a contributor in tumour growth. Furthermore, restrictions in dietary intake lead to a substantial decrease in tumour growth, supporting the role of obesity in promoting tumour growth (Brandon et al., 2009). Moreover, it was observed that leptin contributes to melanoma growth through an increase in nitric oxide production and circulating EPC (endothelial progenitor cell) leading to vasculogenesis (Amjadi et al., 2011). Adiponectin which is an adipocyte derived plasma protein involved in regulating fat and glucose metabolism has been linked to the development of many types of cancers. Recently, the role of adiponectin in promoting tumour growth was investigated by implanting B16F10 melanoma and Lewis lung carcinoma cells into adiponectin knockout and wildtype mice. It was found that adiponectin deficiency has a significant role in enhancing tumour growth. This observation was accompanied by a reduction in macrophage infiltration (macrophage infiltration within tumours from adiponectin knockout mice was 3 fold less than infiltration within tumours from wildtype mice). The increase in tumour growth which was observed in adiponectin null mice was reversed by injecting macrophages (Sun and Lodish, 2010). The upregulation of fatty acid synthase which was observed in human breast cancer lines, ovarian tumours, prostate tumours was considered as evidence for the utilisation of lipids by cancer cells

providing a source of structural lipids required for cell proliferation. Another interesting observation was the increase in lipolytic enzymes which results in mobilisation of lipid stores providing a source of pro-tumourgenic signalling lipids. *In vitro* studies showed that cancer cells have the ability to utilise lipids from surrounding tissues which provide a source of energy, leading to tumour growth. Thus the excess adipocyte mass found in obese individuals can be one of the factors influencing both prevalence and aggressiveness of cancer cells (Balaban et al., 2015, Louie et al., 2013, Karimi et al., 2016). $LDLR^{-/-}$ mice on a normal maintenance diet are a model for familial hypercholesterolemia. To what extent their elevated triglyceride levels promote tumour growth is not known.

It has been suggested that obesity is the causative agent lying behind approximately 20% of all cancer cases. Among the cancers that have been linked with obesity are colon, breast, endometrial, renal, oesophageal, thyroid and prostate cancer (Wolin et al., 2010). Notably, the association between melanoma and obesity as an etablished risk factor remained debatable. In 2015, Jiang and colleaugues decribed obesity as one of the environmental factors that increase the risk of melanoma (Jiang et al., 2015). A meta-analysis including case–control and cohort studies revealed increased risk of melanoma in overweight and obese men, whereas no such risk was found in females (Sergentanis et al., 2013). Probable reseaons for these contradictory findings is that overweight and obese females tend to self limit public sun exposure. Two mechanisms have been suggested to interpretate the positive link between melanoma and obesity. The first suggests that increased body weight means a large surface/number of cells are exposed to sunlight and thus more cells are at risk of malignant transformation. The second suggests that obesity acts via chronic insulin resistance, hyperinsulinaemia, downregulation of insulin-like growth factor (IGF) binding proteins 1 and 2 and increased activity of IGF-I (Renehan et al., 2006). Published data has referred to a link between obesity and melanoma due to common genetic susceptibilities, in both humans and mice. In mice, the introduction of function mutation in the agouti-signaling protein (ASIP) that regulates hair pigementation resulted in an obese phenotype with yellow fur. studies in humans, linked variants in the ASIP locus to obesity, hair pigmentation and melanoma susceptibility (Voisey and van Daal, 2002, Maccioni et al., 2013). Other genetic susuptibilties linking obesity to the risk of melanoma are the fat

mass and obesity-associated protein (encoded by the gene FTO), interferon regulatory factor 4, peroxisome proliferator-activated receptor-ɣ coactivator 1β and vitamin D receptor (Kostner et al., 2009, Li et al., 2013b, Granovetter, 2016, Shoag et al., 2013). Besides initiation of melanoma, modifications within obese adipose tissue is thought to enhance the growth of primary melanomas, support locally invasive tumuors and even drive melanoma progression (Reviewed in (Clement et al., 2017).

1.9 Aims and Objectives of this Study

The initial aim of the study was to establish a syngeneic tumour model in mice to allow testing of the following hypotheses:

The absence of properdin in the properdin-deficient mice impacts on tumour growth and cell recruitment via lower levels of C5a;

The use of $LDLR^{-/-}$ exacerbates the absence of properdin by providing an M2 skewed environment;

The absence of properdin in bone marrow derived macrophages from properdin-deficient mice impacts on their reaction towards tumour cell conditioned medium.

The objectives of the project:

The experimental model used is subcutaneous and intravenous injection of mouse melanoma cell line B16F10. Deficient and congenic wildtype mice were used in parallel.

1- Characterisation of cellular phenotype in bone marrow, spleen, tumour lysates. This was done using FACS with a wide range of CD markers in order to identify myeloid derived suppressor cells (MDSCs), T-regulatory cells, T-cytotoxic, natural Killer cells, macrophages, dendritic and myeloid cells. Immunochemistry was used to document angiogenesis and apoptosis.

2- Characterisation of tumour growth and metastasis. This was done by calliper measurements, weight, bioluminescence, and use of intravenous model.

3- Characterisation of candidate mRNA expression and complement proteins in mouse melanoma tumour cells by using reverse transcriptase polymerase chain reaction (RT-PCR)/ quantitative RT-PCR (qPCR) and Western blot, respectively.

4- Characterisation of cytokines and C5a released in melanoma tumour microenvironment using tumour homogenates, cytokines protein arrays, and ELISA, respectively.

5- Characterisation of complement component C3, C5a and C5b-9 as well as lectin pathway activation in sera of PWT and PKO tumour bearing mice.

6- Characterisation of the immune stimulatory effect of B16F10 conditioned medium on bone marrow derived macrophages using cell culture, qPCR, FACS, and ELISA.

7- Characterisation of the level of properdin in sera of pancreatic cancer patients undergoing chemotherapy with or without intravenous omega 3.

Chapter 2 Materials and Methods

2.1 Animals and cell line

2.1.1 Animals

The experiments were carried out using specific pathogen-free C57BL/6 wildtype and properdin deficient mice (from the properdin deficient mouse colony held at University of Leicester) after acquiring approval from the Ethical Committee of the University of Leicester and the Home Office (project license "The role of properdin in cancer", PPL80/2354). Properdin-deficient mice were generated at the University of Leicester and are unimpaired when kept in a specific pathogen free environment. The properdin gene of embryonic stem cells was targeted by homologous recombination. Selection and identification of the positive recombinant that was used for microinjection are described (Stover et al., 2008). Because the stem cells were from mice of 129/Ola background, the new transgenes were backcrossed to C57Bl/6 in excess of 12 generations. With relevance to this study, previous investigations of this transgenic line using infectious models have revealed that properdin deficient mice are impaired in their M1 response (Dupont et al., 2014). Crossing of properdin deficient mice with a commercially available $LDLR^{-/-}$ line (B6.129S7-*Ldlr*^{tm1Her}/J, strain 002207) gave rise to a new colony of $LDLR^{-/-}$ P^{KO} double knockouts and $LDLR^{-/-}$ P^{WT} mice maintained by intercrossing. Mice were genotyped by polymerase chain reaction. All mice were used in accordance with UK legislation (1986 Animals (Scientific Procedures) Act) and were housed in a controlled environment with a 12 h light/dark cycle at 22 ºC. All animal experiments were carried out in strict accordance with the recommendations in the guide for the Conduct of Animal Research, National Institutes of Health. The protocols were approved by the University of Leicester Ethical Review body and carried out under UK Home Office Project Licences. Importantly, wildtype control mice are matched and are always taken from the same colony. Figure 4 shows typical agarose gel electrophoresis of PCR products obtained from wildtype, homo- or hemizygous properdin-deficient and heterozygous mice by target specific amplification. Then heterozygous mice were backcrossed to C57BL/6 mice to obtain male wildtype and properdin-deficient littermates. These were used in the experiments wherever possible.

2.1.1.1 Genotyping of wildtype and properdin deficient mice.

The aim of this experiment was to confirm the genotype of the mice. This method involves the analysis of DNA extracted from tail snip biopsies using polymerase chain reaction.

For each sample to be tested, 120µl of 0.5M EDTA solution (pH 8.0) was added to 500µl of nuclear lysis solution in a centrifuge tube followed by chilling the mixture on ice. The next step was to add 0.5-1.0 cm of thawed mouse tail to a 1.5 ml microcentrifuge tube followed by adding 600 µl of EDTA/nuclei lysis solution previously prepared to the tube. Then 17.5µl of 20mg/ml proteinase K was added followed by overnight incubation at 55 ˚C with gentle shaking. In the next day the sample was allowed to reach room temperature for 5 minutes, then 3µl of RNaseA (4mg/ml) was added to the nuclear lysate followed by mixing the sample by inverting the tube 2-5 times. The mixture was incubated for 15-30 minutes at 37 ˚C. Then 200µl of protein precipitation solution was added followed by vortexing vigorously at high speed for 20 seconds. After that the samples were chilled on ice for 5 minutes and centrifuged at 13000-16000g for 4 minutes. The supernatant (containing the DNA) was removed carefully and transferred to a clean 1.5ml microcentrifuge tube containing 600µl of room temperature isopropanol. Then the mixture was incubated at room-temperature for 5 minutes. After incubation, the mixture was centrifuged at 15,500g for 4 minutes. After centrifugation, the supernatant was decanted and 200µl of 70% ethanol was added to the pellet, then the mixture was centrifuged as before. After centrifugation, the supernatant was decanted and the pellet left to dry, then 200µl of 0.2XTE performed (Tris EDTA buffer) was added. Polymerase chain reaction was done using the following primer pairs:

For the wildtype gene:

WT antiproperdin 5’-GGATTATCACATACTCGTTGACGG-3’

PCAS 5’-CTCTTGAGTGGCAGCTACAG-3’

For the targeted gene (KO specific):

OCP665’-CGTGCAATCCATCTTGTTCA-3’

Neoend anti5’-CAAGGCAGTCTGGAGCATGC-3’

A mixture containing 2µl of 25 mM $MgCl_2$, 0.5µl of genomic DNA (1/200 dilution), 2.5µl of 10X buffer, 4.0µl of dNTPs(1.25mM), 0.5µl of sense primers, 0.5µl of antisense primers and 0.2µl of Thermoprime Taq polymerase were added to a

nuclease free microcentrifuge tube. The reaction was made up to 24.5µl with sterile distilled water. The following cycling conditions were applied: initial denaturation at 94 ˚C for 2 minutes and 30 seconds, thirty cycles of denaturation at 94 ˚C 45 seconds, annealing at 59 ˚C for 30 seconds and extension at 72 ˚C for 1 minute and 30 seconds. The final extension was 72 ˚C for 10 minutes, finally the sample was held at 15 ˚C. The size of the PCR product was analysed using 1% agarose gel electrophoresis. The wildtype genotype should show a 1000bp band while the properdin deficient genotype should show a 500bp band.

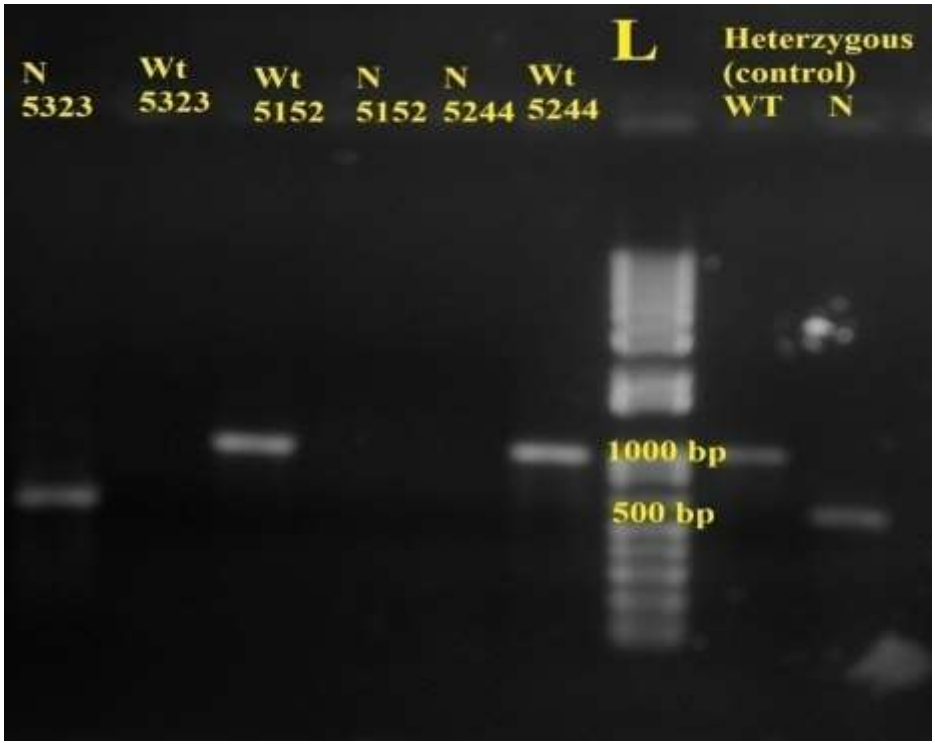

Figure 4: Genotyping of wildtype and properdin deficient mice by PCR.

Numbers indicate ID numbers of experimental mice. Products from PCR reaction were loaded in 1% agarose. Two PCR were done for each mouse: A 1000bp fragment was seen in the wildtype mice, while a 500bp fragment seen in the properdin deficient mice (representative image). (Wt= wildtype gene amplification; N=knockout specific gene amplification).

2.1.2 B16F10

B16F10 is a mouse (C57BL/6) melanoma cell line (kindly provided by Professor Steven Todryk from the University of Northumbria).The B16F10 line is a cell variant of B16 melanoma which has the tendency to generate a high number of pulmonary tumour foci when it is inoculated in the tail vein (de la Hoz and Baroja, 1993). These cells were maintained in DMEM (Gibco) supplemented with 10% (v/v) foetal calf serum (FCS) (Life Technologies, Ltd), 2mM L-glutamine, 100U/ml

penicillin, 100µg/ml streptomycin. They were incubated at 37°C with 5% CO_2. Every 2-3 days the cell medium was aspirated and the cells were detached using 0.25% (w/v) trypsin EDTA (SAFA Bioscience) followed splitting the cells at a 1:3 ratio. This cell line is a mixture of spindle-shaped and epithelial-like cells. They cause black discoloration of the medium due to the production of melanin. B16F10 is a well characterised subline of C57BL/6J melanoma (Hart, 1979, Danciu et al., 2013)

2.1.3 J774.1 cells

J774.1 is a semi adherent murine macrophage-like cell line. The cells were grown in RPMI 1640 (Sigma Aldrich) supplemented with 10% (v/v) FCS (Life Technologies, Ltd), 2mM L-glutamine, Penicillin 100U/ml and Streptomycin 100 µg/ml. The cells were sub-cultured twice a week by gently dislodging them from the flask with a cell scraper. Then a sample was taken for counting and viability assessment. After that the cells were split at a density of approximately 2-3 x 10^5 cells /ml by adding fresh media. The cells were incubated in a humidified incubator (5% CO_2) at 37°C.

2.1.4 Trypan blue counting and viability test

In a 0.6ml reaction tube, 10µl of cell suspension was mixed with an equal volume of trypan blue. Then, 10µl of the mixed suspension was loaded in a haemocytometer. After that the total number of cells and the number of dead blue cells were counted using 10X objective lens. Finally, the total number of cells and the percentage of viable cells were counted.

2.1.4.1 Trypan blue exclusion method

The aim of this method was to count the total number of cells and assess the viability of macrophages by using trypan blue exclusion. This was done by mixing 10µl of cell suspension with an equal volume of trypan blue. The total number of cells and the percentage of viable cells were calculated as following:

Number of cells/ml= number of cells counted per mm^2 X 2 dilute factor X 10^4

Viability of cells (%) = number of live cells / total number of cells X 100

2.1.5 Mycoplasma PCR test of B16F10 and B16F10 Luc

The principle of mycoplasma PCR test depends on the fact that prokaryotes, including mycoplasmas possess a well conserved rRNA gene sequence, whereas each species has a specific spacer region in the rRNA operon. In the

mycoplasma PCR test, both the conserved and mycoplasma specific 16S rRNA gene region are amplified. Agarose gel electrophoresis is used to detect the amplified region.

The EZ-PCR Mycoplasma Test Kit (Biological industries) was used. The test sample was prepared by transferring 1.0ml of cell culture supernatant of B16F10 and B16F10 Luc into a 1.5ml centrifuge tube. Then the samples were centrifuged briefly at 250 xg to pellet cellular debris. After that the supernatant was transferred into a fresh sterile tube and centrifuged at 16,000 xg for 10 minutes to sediment mycoplasma. Then the supernatant was carefully decanted and the pellet kept. The pellet was resuspended in 50µl of the buffer solution and subsequently heated at 95°C for 3 minutes. Then the reaction mixture was prepared in a PCR tube my mixing 10µl of reaction mix, 5µl of test sample and 35µl of H_2O. After that the PCR tubes were placed in a thermal cycler and the following cycling conditions were applied:

94°C 30 sec
94°C 30 sec
60°C 120 sec } 35 cycles
72°C 60 sec
94°C 30 sec
60°C 120 sec
72°C 5 min

At the end, 20µl of the PCR product was loaded into a 2% agarose gel and agarose gel electrophoresis was performed and the bands were visualised after ethidium bromide staining. The expected size of the amplified fragment using Mycoplasma specific primers is 270bp. A positive control was also included.

This was done to exclude contamination with mycoplasma, as a quality check before *in vivo* experiments.

2.2 Tumour implanatation in mice

2.2.1 Study intravenous subcutaneous syngeneic tumour implantation

To investigate the role of properdin in tumour metastasis, mice were injected intravenously with a suspension of B16F10 cells. In the beginning, a pilot experiment was carried on wildtype and properdin deficient female C57Bl/6 mice by intravenously injecting the lateral tail vein with a suspension of B16F10 mouse melanoma cell line (1.9 X 10^5 cell/100µl PBS). After 10 days, the mice were culled and lungs were removed. Macroscopic examination showed pigment aggregates less than 1mm on the lung surface in all lobes, which are indicative of lung metastasis, as shown in Figure 5.

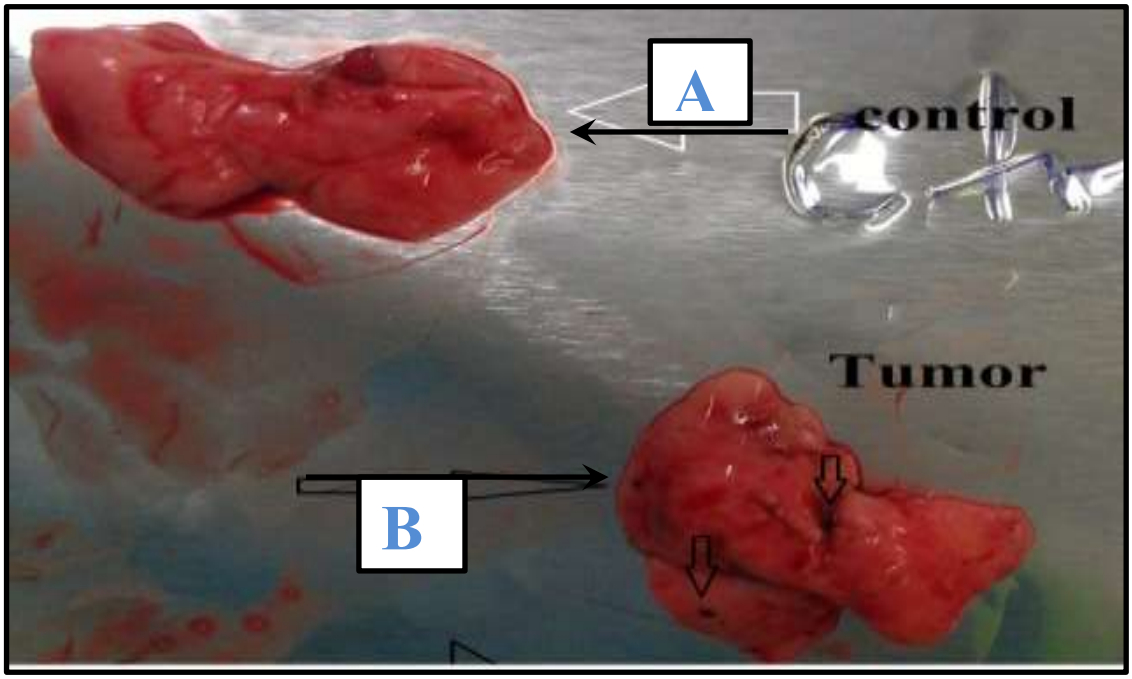

Figure 5: Macroscopic view of explanted lungs.

(A) Lungs of untreated, control mouse (wildtype female C57BL/6). (B) Lungs of intravenously injected female C57BL/6 mouse, 10 days p.i.(dose1.9x10^5 B16F10 mouse melanoma cell line in 100µl PBS). Circumscript pigmented aggregates (<1mm) on the lung surface in all lobes of the lungs are indicative of lung metastases. The mouse showed no signs of illness.

2.2.2 Analysis of pilot subcutaneous syngeneic tumour implantation.

A subcutaneous tumour model was established by injecting the flank of properdin deficient female mice with a suspension of B16F10 mouse melanoma cell line (1.9×10^5 cells in 100µl PBS). After 10 days, the mice were culled and dissected.

Macroscopic examination of the tissue in the site of injection showed a nodular pigmented non-infiltrative mass (about 3mm ×1.5mm) with lobulated contours, and no blood vessel formation was seen macroscopically. The surface was smooth and shiny as shown in Figure 6.

Tumour volume measurement by the use of external calipers is a standard method used in cancer studies. Calipers were used to measure baseline tumour width and length (in mm^3). The following formula was used to calculate tumour volume:

Tumour volume (mm^3) = (1/2) x (A) x $(B)^2$.

In which A refers to the long axis of the tumour and B refers to the short axis of the tumour in millimetres (Xu et al., 2013, Kretzer et al., 2012, Sumiyoshi et al., 2014, He et al., 2013).

Subcutaneous implantation of B16F10 will result in a palpable tumour in about 5 to 10 days. The tumours grow to 1 × 1 × 1–cm in size after about 14 to 21 days. If allowed to grow larger, the tumours usually become necrotic in the center and begin to ulcerate. Hence, it is recommended that mice are sacrificed before it reaches this stage. Typical dose for tumour implantation is 1-5 × 10^5 cells/mouse. A consistent injection technique is vital for subcutaneous tumour implantation, as any difference in site/depth of injection may result in variation. Prior to injection, the fur on the area of interest was shaved to facilitate monitoring of injection and tumour. Upon injection, each mouse should show a clear visible bleb. The absence of a clear bleb after injection may indicate delay in tumour growth or absence of tumour. After tumour implantation, mice should be monitored daily for the appearance of visible nodule.

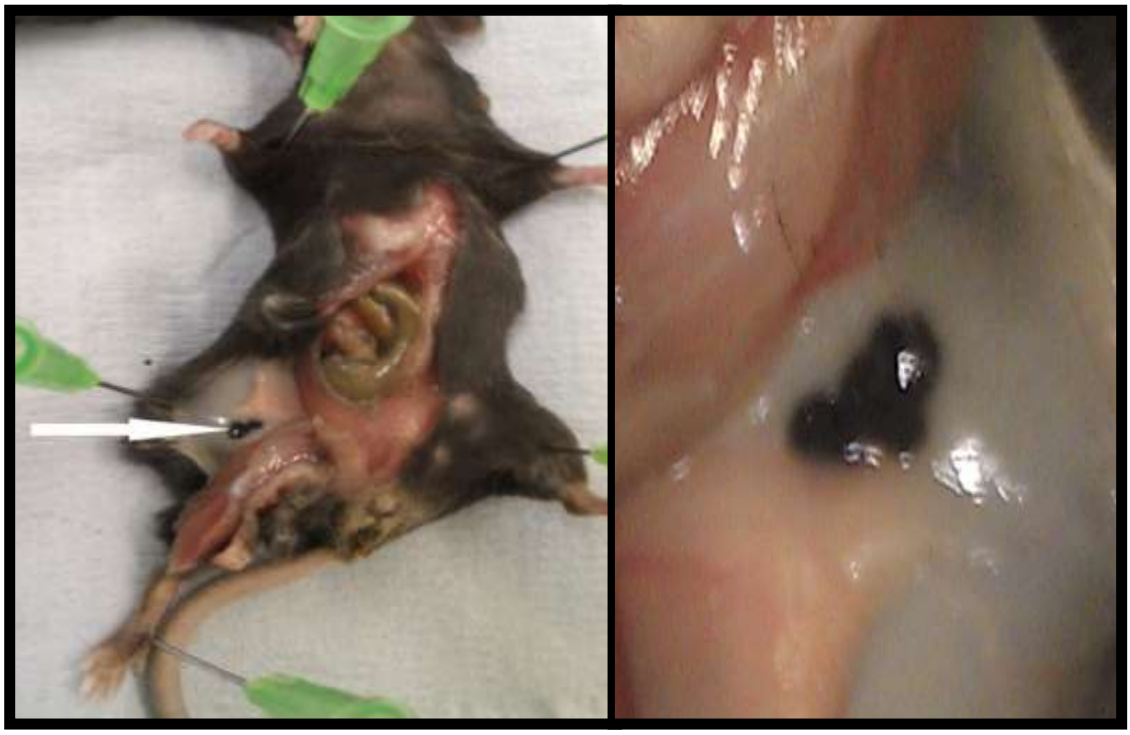

Figure 6: In situ aspect of subcutaneous tumours in the flank of a properdin-deficient female mouse.

Mice were culled 10 days after subcutaneous injection with a suspension of 1.9x10 ^{5} B16F10 mouse melanoma cell line (in100µl PBS). In the sub-cutis, a pigmented, non-infiltrative mass is seen, which measured about 3mmx1.5mm. Its contours were lobulated. The mouse showed no signs of impairment. The tumour appear as a dark (pigmented) nodule (indicated by arrow in left hand photograph; higher powered photograph of the tumour in right hand photograph).

2.2.3 Tumour harvesting and tissues collected for different types of analyses

Mice usually reached the endpoint within 13-14 days, after which the mice were sacrificed, and macroscopically examined for tumour formation. Tumour size (volume) was measured by calipers. Tumour tissue and spleens were collected for analysis using autoclaved forceps and scissors. Tumour tissue was either cut into small pieces for fixation with formaldehyde (10%) and subsequent embedding in paraffin (used for immunohistochemistry), used to prepare single cell suspension for FACs or used for RNA preparation for gene expression (qPCR). Spleens were either used to prepare single cell suspension for FACS analysis or used to prepare RNA for gene expression exeriments (qPCR). Bone marrow cells were isolated from tibias and femurs of both properdin deficient and

wildtype mice and FACS was done to analyse cell phenotype. Mouse sera was also collected for ELISA as shown in Figure 7.

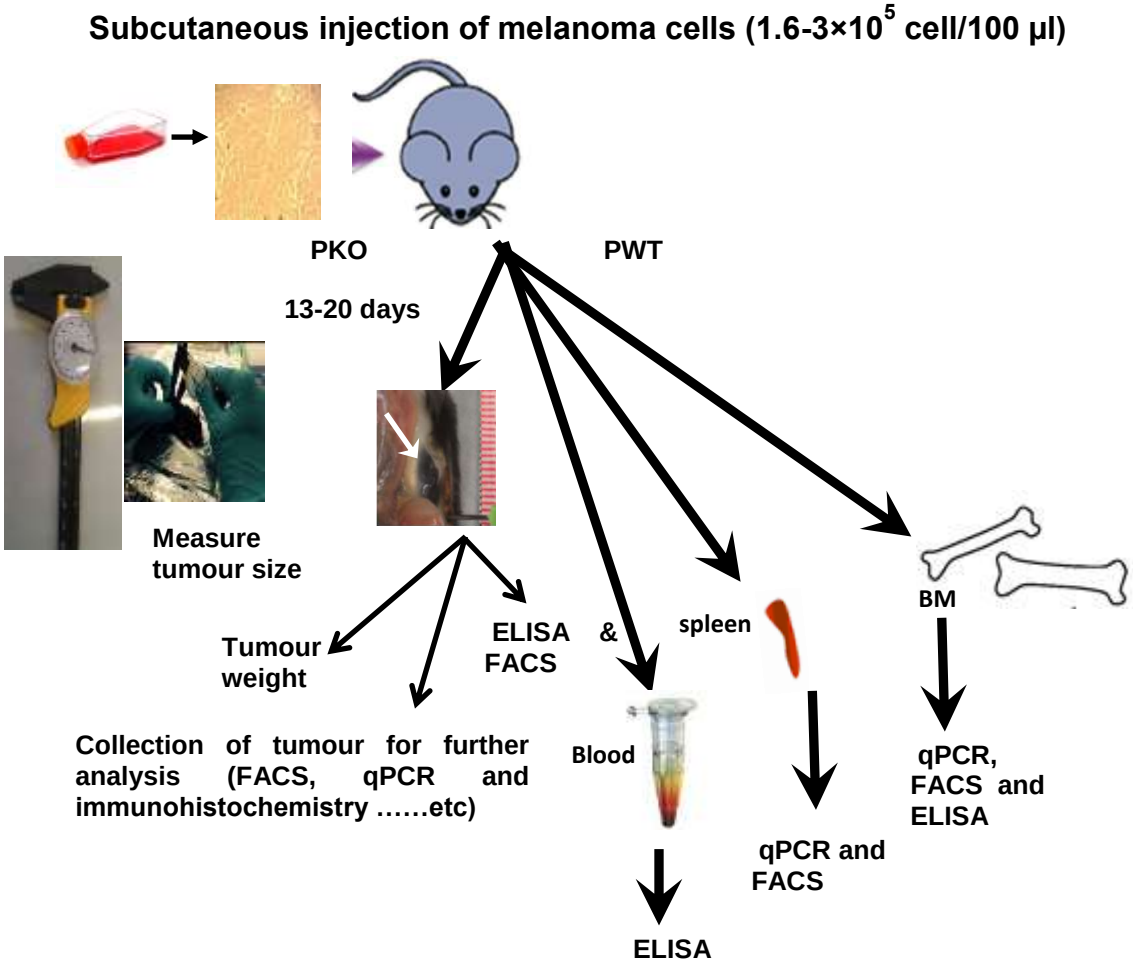

Figure 7: Schematic representation of experiment protocol (subcutaneous model).

2.3 RNA Extraction

2.3.1 RNA Extraction from Tissue

Trizol reagent (Invitrogen, Paisley, UK) was used to extract total RNA from mouse tissue. This was done by placing the tissue in a tube containing trizol. Then the sample was homogenised using a glass homogenisor. After that the supernatant was left to stand at room temperature for 10 minutes. Chloroform was added with mixing. Then, centrifugation was done at 12,000g for 15 minutes and centrifugation of the sample allowed a good separation of the pink organic phase

(bottom) from the aqueous phase (top) containing the RNA. The aqueous phase was transferred to a new tube. Isopropanol was added to precipitate the RNA. After washing with 75% ethanol (7500 g for 8 minutes) and drying, the pellet was resuspended in Diethylpyrocarbonate DEPC-treated water. After that the RNA preparation was diluted using (DEPC)-treated water. Finally, 1µl was placed in the nanodrop to measure the concentration of RNA (absorbance at 260 nm).

2.3.2 RNA Extraction from cells

1ml of Trizol reagent (Invitrogen, Paisley, UK) was added to a 25 cm^2 flask containing of growing cells after removal of medium. Then, the suspension was collected in a reaction tube. The next steps were the same steps as those done in RNA Extraction from Tissue.

2.3.3 Reduction of genomic DNA

DNase digestion of Trizol-based Nucleic Acid isolation was carried out to eliminate genomic DNA (gDNA) contamination. Briefly, the following components were assembled on ice in a centrifuged DNase-free reaction tube for each RNA sample to yield a final volume of 100µl:

Table 1: Reduction of genomic DNA mixing reaction reagents.

Reagent and concentration	volume
10x DNase I buffer	10µl
DNase I (2 unit/ µl)	1µl
RNA (10 µg)	*x µl
DEPC H_2O	Up to 100 µl

*The volume of total RNA suspension used in the reaction varied on a per sample basis; however, a concentration of 10µg of the total RNA was used and the rest of the volume made up with water.

All the components were mixed well and incubated at 37ºC for 10 min. Thereafter, another RNA extraction was carried out to remove any trace of proteins and to inactivate DNase present in the samples. For this RNA purification, only 500µl of TRI regent and half of the other reagents previously used for the RNA extraction were used.

2.3.4 RNA Extraction and Quantitative Real-Time PCR

Total RNA was extracted from cells stimulated with LPS and IFNɣ, IL-4 and B16F10 conditioned medium using RNeasy Mini Kit (Qiagen). Contaminating genomic DNA was removed from RNA samples using the RNase-Free DNase Set (Qiagen). 2 µg total RNA was reverse-transcribed into cDNA using first strand

synthesis kit (Thermoscientific). Gene-specific amplification using SensiMix SYBR kit (Bioline Reagents Ltd., London) was analysed with Rotor-Gene 6000 (Corbett Life Science) for IL-6, IL-1β, iNOS, TNF-α, IL-10, arginase-1 and MCP-1 in comparison with GAPDH. Sequences of priming oligonucleotides are given in Table 2. ΔΔCT values were used (Livak and Schmittgen, 2001), the mRNA expression corrected for GAPDH and compared with unstimulated BMDM. Amplifications were set up in duplicates.

Table 2: Sequences of oligonucleotides used in this study.

Primers , mouse	**Sequence**	**Size (bp)**	**T_A (°C)**	**Reference sequence accession number NCBI**
GAPDH	5'-CCTGGAGAAACCTGCCAAGTATG-3' 5'-AGAGTGGGAGTTGCTGTTGAAGTC-3'	132	55	NM_0080848
IL-10	5'-CCCTGGGTGAGAAGCTGAAG-3' 5'-CACTGCCTTGCTCTTATTTTCACA-3'	84	58	NM_010548
TNF-α	5'- GGCAGGTCTACTTTGGAGTCATTGC-3' 5'- ACATTCGAGGCTCCAGTGAATTCGG-3'	333	55	NM_0013693
iNOS	5'-TAAAGATAATGGTGAGGGG-3' 5'-GTGCTTCAGTCAGGAGGTT-3'	270	60	NM_010927
Arginase-1	5'-AGGAACTGGCTGAAGTGGT-3' 5'-GATGAGAAAGGAAAGTGGC-3'	220	60	NM_007482
IL-6	5'-GACAACTTTGGCATTGTGC-3' 5'-ATGCAGGGATGATGTTCTG-3'	160	53	NM_031168.1
MCP-1	5'- CACTCACCTGCTGCTACTCATTCAC-3' 5'-GGATTCACAGAGAGCGAAAAATGG-3'	490	57	NM_0011333
IL-1β	5-' TTGACGGACCCCAAAAGATG-3' 5'- AGAAGGTGCTCATGTCCTCA-3'	200	55	NM_008361

2.4 Reverse transcriptase polymerase chain reaction (RT-PCR):

cDNA was synthesised using first strand synthesis kit (Thermoscientific) according to the manufacturer's instructions. Briefly, a 20ul reaction was set up on ice in nuclease free 0.2ml tube by firstly mixing up to 5µg of total RNA, oligo(dT) primers and nuclease free water to a total volume of 12ul. Then the reaction was mixed followed by incubation at 65 ˚C for 5 minutes. After that the tubes were chilled on ice and the following components were added; 4ul of 5X reaction buffer, 1µl of RiboLockRnase inhibitor (20 U/µl), 2ul of 10mM dNTP mix and 1µl of M-MuLV reverse transcriptase. Then the reaction was mixed and centrifuged briefly. After that, the mixture was incubated at 42 ˚C for 60 minutes followed by heating at 70 ˚C for 5 minutes. Then the samples were stored at -20 ˚C.

2.5 Polymerase chain reaction(PCR)

PCR was carried out to examine gene expression. Occasionally, optimisation of annealing temperatures was needed. The reaction was performed by mixing the following reagents in 0.5ml PCR reaction tube on ice:

Table 3: PCR mixing reaction reagents.

Reagent and concentration	Volume
Reaction buffer IV (10x)	2.5µl
5mM MgCl2 (1.5mM)	1.5µl
2.5mM dNTPs (0.2mM)	2µl
dH_2O	12.75µl
Forward primer (5µM)	2µl
Reverse primer (5µM)	2µl
Thermoprime plus DNA polymerase (Taq 5Units/(µl)	0.2µl

Thereafter, 2µl of each cDNA was added into each PCR reaction, giving the final volume of 25µl. The tubes were then pulse-centrifuged and placed into a thermocycler and the following programme was applied to the machine:

Table 4: PCR amplification cycle.

Step	Temp. (ºC)	Time (min)	Number of cycles	Function
1	94	2	1	Initial denaturation
2	94	1	30	Denaturation
	55*	1		Annealing
	72	1		Extension
3	72	10	1	Final extension
	14			Hold

***The annealing temperature varied for each primer pair (Table 6)**

2.6 Quantitative polymerase chain reaction (qPCR):

The expression of the gene of interest can be measured by using quantitative polymerase chain reaction. In this method, the production of amplification product during each cycle is monitored by a fluorescent molecule which means that the DNA is amplified and detected in a single assay. The intensity of fluorescence is proportional to the increase in amplification product of target gene resulting in an amplification curve during each PCR cycle. The threshold cycle (CT) is detected when the amount of fluorescence reaches a signal beyond background level. In quantitative PCR, the results are reported as either absolute numbers or relative amounts which are normalised using a normalising gene (housekeeping gene).

2.6.1 Quantitative analysis of mRNA expression by Real-Time RT-PCR (qPCR) in Tumour tissue

Tumour tissue from wildtype and properdin deficient tumour bearing mice were collected and stored at -80 ˚C. Then the tissue was homogenised as described before and RNA was extracted.

A qPCR reaction was set up in 0.2ml PCR tubes by mixing 3µl of diluted cDNA (1:4 in RNase free water) and 10µl of 2X SensiMix^{TM}SYBRgreen mix (BIOLINE). In addition, 2µl of each of gene-specific forward and reverse primers (5µM) were added to the mixture. 3µl of H_2O, were added to make a total volume of 20µl. Reaction which contained distilled water instead of cDNA templates served as negative control. All qPCRs were run in duplicates; the average standard deviation within duplicates of all samples studied was 0.15 cycle.

qPCR efficiencies in the exponential phase were calculated for each primer pair by standard curves (5point 5-fold dilution series of pooled cDNA), the mean quantification cycle (Cq) values for each serial dilution were plotted against the logarithm of the cDNA dilution factor and calculated according to the equation E= 10[-1/slope]

A standard curve was obtained by using gene specific primers and a ten fold serially diluted pooled cDNA samples. The qPCR was carried out using a Rotor gene 6000 (Corbett). The following amplification cycle was used in the PCR run:

Table 5: qPCR amplification cycle .

Step	Temp. (ºC)	Times (sec)	Number of cycles	Function
1	95	600	1	Hold
2	95	15		Denaturation
	51-60*	15	X40	Annealing
	72	15		Extension
3	Ramp from 50-99		Rising by 1	Melt

*The annealing temperature varied for each primer pair (see Table 6).

Reverse-transcribed cDNA sample reaction, no template control and no reverse transcriptase (RT) control reactions were run in duplicate or triplicate. For quality control, an efficiency test (standard curve) was carried out using 10-fold dilutions from 1:4 diluted cDNA samples for each primer. The cDNA standards included in each run were: 10^0, 10^1 ,10^2 ,10^3, 10^4 and 10^5 X genome copy numbers per microliter. The standard curve was constructed by plotting the threshold cycle (C_1) corresponding to each standard versus the value of their corresponding number of genome copies (genome copies/µl) as shown in Figure 8. This process was automated by Rotor-Gene 6000 (Corbett) software and the data were analysed as stated in below.

2.6.2 Data and software analysis

Rotor-Gene 6000 software series 1.7 (Corbett Research) was used to assign C_T values to each sample and analyse the efficiencies of the qPCRs through the direct analysis of the fluorescence application curve and analysis of a dilution series.

Microsoft Excel was used for the calculation of relative gene expression, standard deviations and co-efficients of variation. All other statistics were performed using Graph pad Prism 7 (Graph pad software).

The data was calculated by using the levac method or $2^{-\Delta\Delta C_T}$ in which the expression of target gene is normalised with the reference to a housekeeping gene. By this we assume that both genes are amplified with an efficiency of almost 100% and that the efficiency difference between them is no more than 5% (Livak and Schmittgen, 2001).

The result obtained was the fold increase (or decrease) of the target gene in the test sample relative to the calibrator (control) sample and was normalized to the expression reference gene (housekeeping gene). A high $\Delta\Delta C_T$ value, whether negative or positive, indicates significant changes in the expression levels of mRNA of the target gene. A positive $\Delta\Delta C_T$ indicates an up-regulation in expression levels of the target gene's mRNA.

2.6.3 Agarose gel electrophoresis

Agarose gel electrophoresis was used to assess purity and estimate the molecular weight of the PCR products. For this, a 1% (w/v) agarose gel was dissolved into 1x TBE buffer (89mM Tris base,89mM boric acid, 2mM EDTA, pH 8) and heated up for 2 min at moderate power in a microwave oven. The solution was left to cool down for approximately 5 min, and then 5µl of 10mg/ml ethidium bromide (EtBr) (Sigma-Aldrich, Gillingham,UK) was added. The mixture was then immediately poured into a casting apparatus and a comb was inserted to form wells. The gel was left for 20-30 min at RT; thereafter, the gel was transferred to the running tank and immersed with 1x TBE buffer. The DNA samples were mixed with 6x DNA gel loading dye. The mixed samples were then loaded into the agarose gel wells. The gel electrophoresis was then performed at a constant voltage of 90 V. Electrophoresis was stopped when the line of bromophenol blue dye had migrated through $^3/_4$ of the gel. The DNA fragments on the gel were then visualised using a UV transilluminator (UVP Dual Intensity Transilluminator) and the images were recorded using an Olympus camera connected with Image Quant 100 capture software (GE Healthcare, UK). A 1Kb plus DNA Ladder (Invitrogen, UK) was run alongside the samples to determine fragment size.

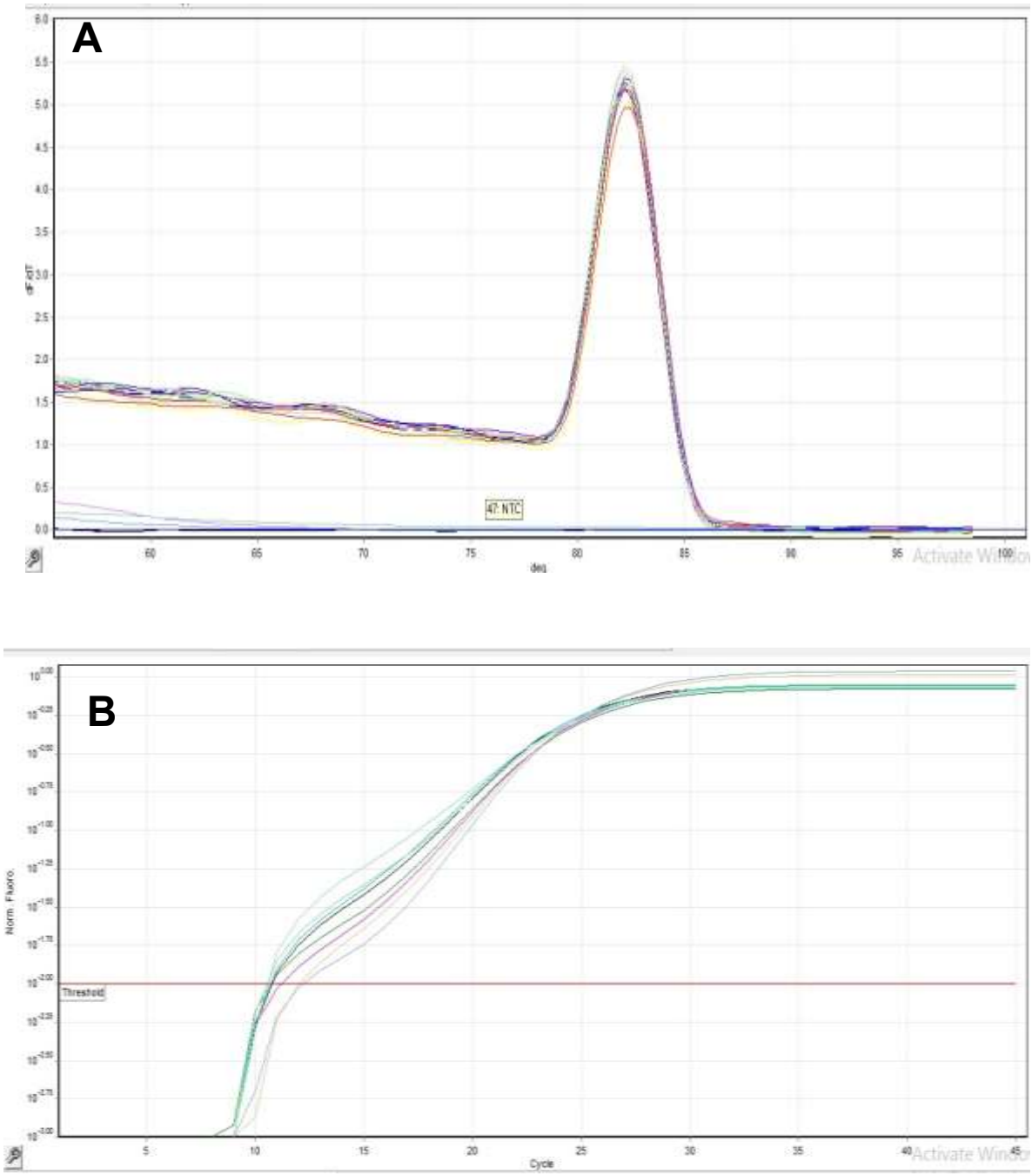

Figure 8: Example of the melting curve and amplification curves from the qPCR analysis. (A) example of the melting curve analysis of the mouse melanoma expression of target gene. Temperature was plotted against dF/dT [rate of change of fluorescence (F) in the reaction with time (T)]. (B) The graph shows the amplification curves from the qPCR analysis; each assay target is represented by a different colour.

Table 6: Primer sequences, annealing temperatures and the expected size generated in this study.

Primer	Sequence 5' 3'	Size (bp)	Temperature °C (TA)
IL-10	FW: CCCTGGGTGAGAAGCTGAAG Rev: CACTGCCTTGCTCTTATTTTCACA	360	61 NM_010548
Mouse GAPDH	For: CCTGGAGAAACCTGCCAAGTATG Rev: AGAGTGGGAGTTGCTGTTGAAGTC	132	55 NM_0080848
mVEGF-A	GGCTGACCCCTAAGAAACC CTGAAAATCAATAGCACGAAC	500	55
TNF-α	For: GGCAGGTCTACTTTGGAGTCATTGC Rev: ACATTCGAGGCTCCAGTGAATTCGG	333	55
L-17A	For: GGCTGACCCCTAAGAAACC Rev: CTGAAAATCAATAGCACGAAC	79	95 NM_010552.3
C3	GAATACGTGCTGCCCAGTTT TGAGTGACCACCAGCACTTT	500	55 NM_009778
Mouse C5	For: CAAA GGA TCC AGA AAA GAA GCC TGT AAA CC Rev: CCT TAA GCT TCG TGCA GCA ACT TTT CAT TC	400	(Bolger et al,2007) 60
Mouse Crry	CCA GCA GTG TGC ATT GTC AGT CC CCC CTT CTG GAA TCC ACT CAT CTC		60 (Yang et al., 2009)
Mouse cathelin	TCGGAAGCTAATCTCTAC GGAACCATGCAGTTCCAGAGGGA CTGGACCAGCCGCCCAAG TTTGCGGAGAAGTCCAGC	310	55 (Gallo et al., 1997)
mouse β-defensin 14	GTA TTC CTC ATC TTG TTC TTG G AAG TAC AGC ACA CCG GCC AC	104	63.5 (Rohrl et al., 2008)
Properdin	TTCACCCAGTATGAGGAGTCC GCTGACCATTGTGGAGACCT	149	62 NM_008823.3
FOXP3	CTAGTCATGGTGGCACCGTC GATGATCTGCTTGGCAGTGCTTGA GAAACTCTTCTGGCTCCTCGAAG	-	60

2.7 Bioluminescence imaging (BLI)

2.7.1 Animals and cell line:

B16F10-luc cells (mouse melanoma cells labelled with luciferase gene) kindly provided by Dr Victoria Brentville (University of Nottingham). Three wildtype C57BL/6 mice aged 8-12 weeks were used in the pilot BLI experiment. B16F10-luc cells were maintained as previously described in (2.1.2). The cells were prepared for injection by detaching them from the flask as mentioned above and washing them twice. Then the cells were counted and resuspended in PBS at a concentration of $4x10^5$ cell/100µl.

2.7.2 Tumour implantation:

A pilot experiment for *in vivo* imaging was performed to determine the optimal kinetics for further studies. The *in vivo* experiment was carrying out after amendant of the project license "The role of properdin in cancer", PPL80/2354). Three wildtype C57BL/6 mice were humanely restrained by scruffing, fur clipped, swabbed, and injected subcutaneously into the flank with 100µl ($4x10^5$cells) of freshly prepared B16F10-luc cell suspension using a 29 guage needle.

2.7.3 Preparation of the mice prior to imaging:

After 8 and 12 days of tumour implantation the mice were prepared for *in vivo* imaging. Prior to imaging, the mice were administered D-luciferin firefly in PBS (purchased from Xenogen Corporation USA) at a concentration of 150mg/kg through subcutaneous injection and then the mice were anesthetized using isoflurane (1–3%). The mice were shaved over the tumour site to minimize the amount of light absorbed. The mice were placed in a light tight chamber. BLI was done using the xenogen *In Vivo* Imaging System (IVIS, Caliper life science). This system consists of a highly sensitive cooled CCD camera apparatus placed in light tight chamber which was used to detect photon emission from tumour bearing mice with acquisition times ranging from 1 s to 2 min until the peak signal was observed. Regions of interest were drawn and quantified using the Living Image software version 2.5. Bioluminescence signal was reported as total light emission within the region of interest (photon/s). Specific signal was calculated as the ratio of bioluminescent signal in the region of interest to the bioluminescent signal in a background region containing no cells or tumours. A signal was

defined as positive when it was greater than the sum of the mean background signal plus 2 standard deviations of the background signal.(Lim et al., 2009).

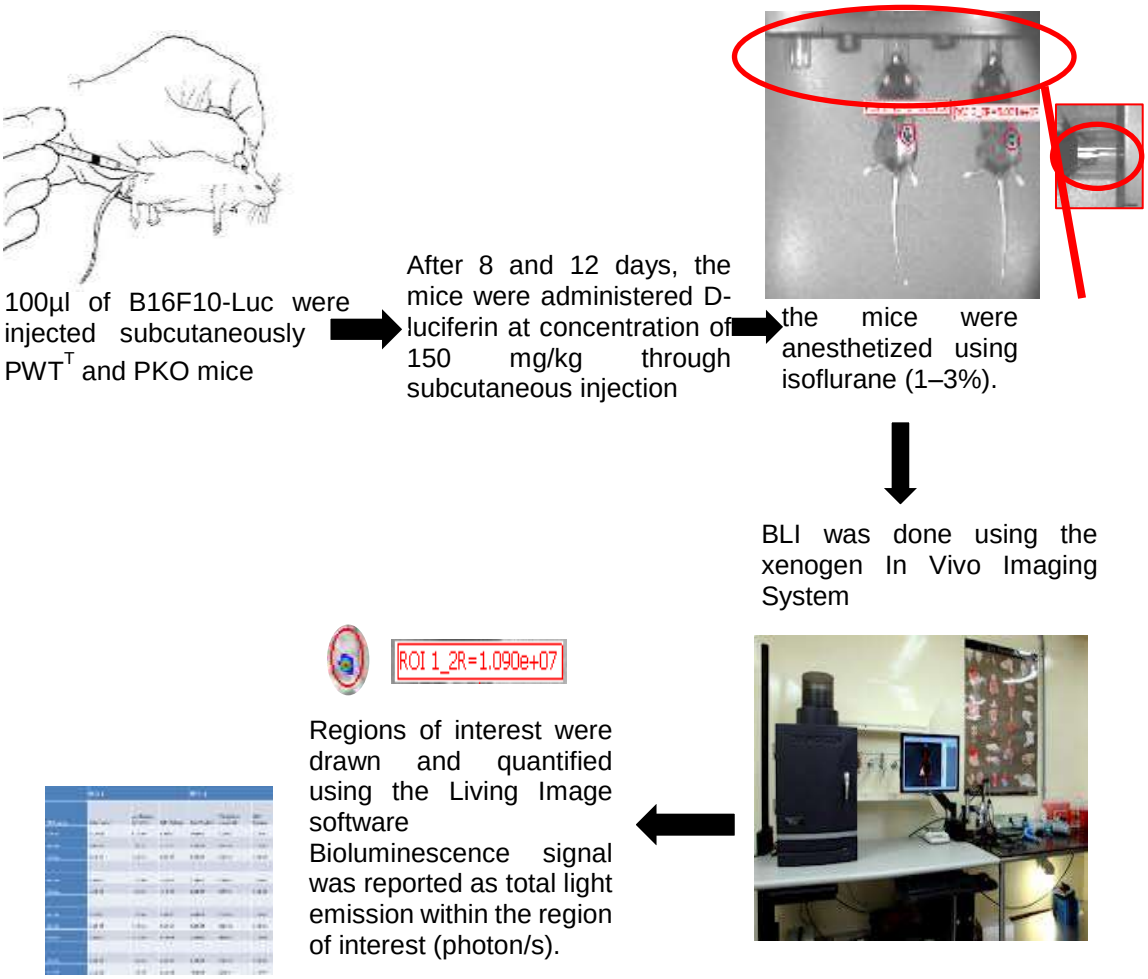

Figure 9: Schematic representation of bioluminescence protocol.

monitoring of tumour growth in a subcutaneous syngeneic mouse model by bioluminescence imaging. B16-F10-Luc cells were subcutaneously injected into C57BL\6 mice. BLI of animals imaged after 8 and 12 days from injection. A representative quantification of bioluminescence intensity as total flux (photons/second).

2.7.4 *In vivo* bioluminescent image quantification

To measure photon radiance, regions of interest (ROI) were selected on the surface of the mice using the automatic ROI. Bioluminescence was measured quantitatively by the Living Image® software, which gave the total flux of photons or radiance (photons/second from the surface) in each pixel, summed or integrated over the ROI area, in a square centimeter (cm^2) of the tissue. These data were multiplied by one steradian (sr). The photon radiance is displayed as the average radiance, which is the sum of the radiance from each pixel inside the

ROI/number of pixels or superpixels (photons/sec/cm2/sr) and the standard deviation of the pixel radiance inside the ROI. Bioluminescence, acquired by the CCD camera, was quantified by the Living Image® software using three types of ROI: (1) the automatic ROI measurement tool, which identifies bioluminescent emission automatically, considering a threshold of 20 to 28%; (2) the average background ROI, which measures the background signal in the area specified by the user and corrects the bioluminescent emission by subtraction; and (3) the subject ROI, which identifies each animal in an image. Whenever necessary, individual bioluminescent spots (foci) were summed to get the photon radiance measurements (photons/sec/cm^2/sr) of each tumour. Photon flux from the tumour is proportional to the number of live cells expressing luciferase so bioluminescence correlates directly with tumour size.

2.8 Western blot

Western blot was used to separate and identify proteins of interest. Separation was done through gel electrophoresis based on molecular weight. This was followed by transferring to a membrane to produce a band corresponding to each protein. The membrane was then incubated in the presence of labelled antibodies specific to the protein of interest. The first step was preparing a 12% separating polyacrylamide gel as following:

Table 7: Components Stacking gel resolving gel (12%).

Components	Stacking gel	Resolving gel (12%)
dH_2O	0.68	1.6
Acrylamide 30% (v/v)	0.17	2.0
1.5M Tris HCl pH 8.8	---	1.3
1.0M Tris HCl pH 6.8	0.13	---
10% (w/v) SDS	0.01	0.05
10% (w/v) APS	0.01	0.05
TEMED	0.001	0.002

Prior to polymerisation, the separating gel was placed into the gel casting apparatus followed by adding 0.3-0.4ml of water on top and leaving the gel to set. After this, the water was removed using a 3M filter paper avoiding touching the surface of the gel. Then the sample comb was partially placed in the gel sandwich. Next, the stacking gel was prepared as described above and the gel was slowly poured on top of the separating gel followed by gently pushing the comb down and topping with stacking gel to fill any spaces in the comb. Once the stacking gel had set, the comb was carefully removed and the gel was transferred to the electrophoresis apparatus. The tank was filled with 1x running buffer. The samples were prepared by mixing cell lysates with 2X Laemmli sample buffer followed by heating at 95ºC for 5 minutes. Afterwards, 20 µl of sample was loaded in each well and gels were run at 150 V for 70 minutes. Then the separated proteins were transferred onto nitrocellulose membrane (Bio-Rad laboratories, UK), at 300 mA for 1 hour on ice, using cold transfer buffer (25mM Tris, 192mM glycine, and 20% v/v methanol; pH 8.3). After transfer, the membranes were washed once with 1x tris-buffered saline (TBS)-0.1% Tween-20 (TBS-T), on an orbital shaker, for 5 minutes at room temperature. Then non-specific binding sites were blocked by placing the membrane in 5% (w/v) skimmed milk and PBS solution for 1 hour. Afterwards the membranes were extensively washed four

times with TBS-T (each time for 5 minutes). The membranes were then probed overnight, with a primary antibody specific for the protein of interest, at the appropriate concentration, with constant agitation at 4°C. Primary antibody (e.g. Goat anti-C3 polyclonal 1:1000 Ab biorbyt) solutions were prepared in 10 ml of 5% (w/v) skimmed milk and PBS solution. The next day, the membrane was washed three times with TBS-T (as mentioned above), then the membrane was incubated with horseradish peroxidase conjugated secondary antibody (Donkey anti-goat 1:4000 Santa Cruz Biotechnology) 5% (w/v) skimmed milk and PBS solution for 1 hour. Afterwards, the membrane was developed using ECL kit (Pierce kit) (Pierce ECL western Blotting Substrate Cat# 32209). In a plastic foil the membrane was exposed to ECL by mixing equal volume of detection reagent 1 (Peroxide solution) and detection reagent 2 (Luminol enhancer solution) to yield a final volume sufficient to cover the membrane for a minute. After that the membrane was exposed to X-ray film (autoradiography). By using the developer solution and fix solution, for 10 seconds each solution, then washed with water.

Table 8: Lysis buffer for extraction of phosphoproteins from cultured mammalian cells. This buffer should be prepared on ice and mixed well before usage.

Stock solutions	For 5ml	Final concentration
1M Beta glycerophosphate (PH 7.4)	50µl	10mM
0.5M EDTA (PH 8)	10µl	1mM
40mM EGTA (PH 7.5)	125µl	1mM
1M Tris-HCl (PH 7.5)	250µl	50mM
100mM Na Orthovanadate	50µl	1mM
1M Benzamidine	5µl	1mM
100mM PMSF	10µl	0.2mM
Protease Inhibitor Cocktail (Sigma, P830)	20µl	N/A
Beta-Mercaptoethanol	5µl	0.1%
10% Triton X-100	500µl	1%
500mM Na Fluoride	500µl	50mM
MilliQ water	2.81ml	xxxx

2.9 Flow cytometry

The compensation bead set (Becton and Dickinson™) is ideal to optimise the fluorescence settings for the multicolour flow cytometric assay without using precious cell suspension. This set includes two types of polystyrene microparticles beads; the first are anti-mouse Immunoglobulin kappa coupled particles which can bind any mouse kappa light chain, while the second has no binding capacity, serving as a negative control. These beads are usually mixed with the same fluorochrome labelled mouse antibody which is going to be used in the experiment providing positive and negative populations which are used to adjust the settings.

The compensation beads were prepared according to manufacturer's instructions. Briefly, the beads were vortexed. Then three separate 12 X 75mm sample tubes were labelled with the name of the flurochrome labelled Rat anti-mouse antibodies used (Gr-1 Clone: RB6-8C5, CD11b Clone M1/70and CD45 Clone: 30-F11 eBioscience). 100µl of staining buffer (BD Pharmingen stain) was added to each tube followed by adding 60µl of BD™compBeads negative control and 60µl of BD™compBeads anti-mouse Ig kappa to each tube. Then 20µl of each prediluted antibody to the appropriate tube followed by vortexing. The tubes were protected from direct light and incubated at room temperature for 15-30 minutes. After incubation, 2ml of staining buffer was added to each tube followed by centrifugation at 200xg for 10 minutes. After centrifugation, the supernatant was aspirated and discarded then the pellet was resuspended in 0.5ml of staining buffer followed by vortexing. Finally, each tube was run separately on the flow cytometer.

2.9.1 Tumour cell preparation

The mice were sacrificed and tumour tissue was collected using autoclaved forceps and scissors. Then the tumour tissue was cut into small pieces followed by incubation in 1ml MACs buffer with collagenase (100µg/ml) for 30 minutes at 37 ºC. During the incubation period the mixture was pipetted up and down every 10 minutes. After that the mixture was filtered through a 70micron cell strainer (BD) using a plunger from a disposable 5ml syringe with MACs buffer. Then the suspension was centrifuged at 400xg for 10 minutes followed by rinsing the pellet with 10 ml of MACs buffer. The remaining cells in the cell strainer were flushed

into a Falcon tube. Then the suspension was centrifuged as before. The supernatant was discarded and the pellet resuspended in 0.5-1ml of MACs buffer with 3% of FBS (depending on the size of the tumour). (Stephanie et al., 2012).

2.9.1.1 Preparation of MDSC from bone marrow of naïve and tumour bearing mice for FACS.

Bone marrow cells were prepared as mentioned in (Dupont et al., 2014). Single cell suspension from bone marrow cells was prepared after red blood cell lysis using ammonium chloride (0.87% Tris-NH_4Cl (pH 7). Then the cells were counted using a Neubauer chamber and the number was adjusted to $1X10^6$ cell/ml in PBS with 1% FBS. Then the cells were stained with 50 µl of purified anti-Fc receptor blocking antibody (anti-CD16/CD32 from Biolegend) diluted 1:200 to avoid non-specific binding and background fluorescence. Cells were incubated on ice for 30 minutes , covered with foil and 500µl of cells was added to each tube followed by adding 2µl of FITC Gr-1,2 µl of PE CD11b, 2µl of APC CD45, 2µl of each of the previously mentioned antibodies, 2µl of Gr-1 isotype , 2µl of CD11b isotype, 2µl of CD45 isotype and 2µl of each of the previously mentioned isotypes was added to the first, second, third, fourth, fifth , sixth, seventh and eighth tube respectively, while the ninth tube was left unstained as a control. After the addition of antibodies, the tubes were vortexed and incubated on ice for 15-30 minutes. Then 1.5-2ml of PBS-FBS was added to each tube followed by centrifugation at 300g for 5 minutes. After centrifugation, the supernatant was aspirated without disturbing the pellet and the pellet was resuspended in 500µl of paraformaldehyde (1%) and maintained at 4 ˚C in the dark until acquisition.

2.9.2 Preparation of suspension from mouse spleen for FACS.

Spleens of mice were harvested and single cell suspensions were prepared by passing through a 70µM cell strainer followed by centrifugation for 5 minutes at 270g. After centrifugation, the supernatant was aspirated and the pellet was resuspended in 2ml of hypotonic 0.87% Tris-NH_4Cl (pH7) followed by incubation for 2-3 minutes at room temperature to lyse the red blood cells. 10ml of PBS-1%FBS was added to neutralise the hypotonic solution followed by incubation for 2-3 minutes at room temperature to allow large pieces to sediment to the bottom of the tube. Then the suspension was aspirated and placed in a clean tube followed by centrifugation at 270g for 5 minutes. After centrifugation the

supernatant was aspirated and the cells were counted and the number was adjusted to $1X10^6$ cell/ml. Then 9 tubes were appropriately labelled and 500µl of cell suspension was added to each tube. The cells were stained for FACS analysis as above.

2.9.3 Preparation of cells for flow cytometric staining.

Tumour, spleen and bone marrow were collected, tissue weight was checked in order to quantify the number of positive cells per mg of tissue (Neill et al., 2012) and prepared for flow cytometric analysis as mention previously.

Following centrifugation, cells were resuspended in 1x PBS 3% (v/v FCS), to a concentration no more than 1×10^7/ml. The volume of 1x PBS 3% (v/v FCS) added to the cell suspension was done either defined by using a hemocytometer or using an approximation guide according to the tissue sample: Bone marrow cells in 2ml; spleen cells in 2ml; tumour cells in 0.5-1ml. Cells were then stained as described in section (2.9.4 and 2.9.5) or cryopreserved for further analysis Cell cryopreservation

Polycarbonate freezing box was used to preserve tissue from tumour, spleen and bone marrow for later analysis. This box has ability to gradually decrease temperature, which minimize the loss of cell viability. The cold-preserved tissue samples were resuspended in storing solution After the preparation of cells, (as described in section 2.9.1 and 2.9.2), instead of resuspending cells in the final buffer (1x PBS 3% v/v FCS), the cell pellet was resuspended in 1ml of storing solution (10% v/v DMSO, 80% v/v FBS and 10% v/v RPMI), the vials were labelled and subjected to a -1°C/min cooling in a polycarbonate cryogenic container (Nalgene) and stored at -80°C.

2.9.4 Surface marker analysis.

Extracellular antibody staining was carried out to determine the phenotype of the different immune cell populations present in tumour tissue, spleen and bone marrow. Cell suspensions prepared from different mouse tissue were stained for cell surface markers using either one or a combination of the following antibodies; FITC-, PE-, PE-Cy7-, APC and PE conjugated monoclonal antibodies (Table 9). The appropriate combination of fluorochromes was chosen to ensure optimal results from flow cytometric multidimensional analysis. FACS buffer (1x PBS supplemented with 3% v/v FCS) was used throughout the procedure for preparation of cell suspension, as a wash buffer and for the dilution of the

antibodies. The appropriate isotype control monoclonal antibodies were also included. The cells from each tissue were harvested and numbers were adjusted to a concentration of $5x10^5$ - $1x10^6$ cells. A method was developed using 96 well plates to obtain more accurate results and to save antibody usage. The cells were stained in a 96-well round-bottomed microtiter plates 100µl of cell suspension from each sample were added to each well. Then the cells were stained with 50µl of purified anti-Fc receptor blocking antibody (anti-CD16/CD32 from Biolegend) diluted 1:200 to avoid non-specific binding and background fluorescence. Subsequently, the plate was incubated on ice for 30 minutes. Cells were washed and then stained by adding 50µl /well of the appropriate antibody or antibodies (Table 9). The manufacturer's instructions were followed for all the antibodies used for extracellular staining. Then the plate was covered with aluminium foil and incubated on ice for 30 minutes. Then, the plate was centrifuge at 300 g for 5 minutes. Finally, cells were washed and resuspended in a total volume of 400µl of 1x PBS 3% (v/v) FCS. FACs analysis was done with a FACSCalibur (BD) and Canto (Becton-Dickinson, UK) according to the manufacturer's instructions. The compensation and fluorescence intensity for each tissue were adjusted before running samples. Then the cell populations were gated for analysis. A scatter gate was set to exclude any residual red blood cells, platelets, or debris. Flow cytometry data acquisition was done using either CellQuest or FACSDiva 6.3 software (BD) and analysed using FlowJo software (version 8.8.3, Tree Star). Further statistical analysis was done using Prism GraphPad software (version 7). Compensation for tumour cell suspension has proven to be a challenge due to differences between cells within individual tumours (intratumour heterogeneity) especially when using more than three fluorochromes.

2.9.5 Intracellular staining

Intracellular flow cytometry staining is an important tool used to analyse the signalling and functional responses within a cell population. This technique is carried out to quantify cytokines in the cellular matrix. The first step was to block cellular secretion of cytokines by incubating the cells (2-5 x 10^5 cells per well) in a 96 well round bottom plate in RPMI medium supplemented with 1% (v/v) GolgiPlug (BD Biosciences) or Brefeldin (eBiosciences). Induction of cytokine-producing cells was done by adding phorbol 12-myristate 13-acetate (PMA) at a concentration of 50 ng/ml and ionomycin (500 ng/ml). The plate was incubated

at 37ºC for 6 hours. Following incubation, the cells were washed and stained with antibodies against extracellular markers as described previously. After that 100μl of Fix/Perm solution (1:4 dilution; BD Biosciences) was added and the cells were further incubated for 20 minutes. Then the cells were washed with 100μl Perm/Wash buffer (1:10 diluted in nanopure water) (BD Biosciences). Subsequently staining with antibodies (previously diluted in Perm/Wash buffer) against intracellular cytokines was carried out. Then the cells were washed and resuspended in 400μl 1x PBS 3% (v/v) FCS. FACs analysis was done with a FACSCalibur (BD) and Canto (Becton-Dickinson, UK) according to the manufacturer's instructions. The compensation and fluorescence intensity for each tissue were adjusted before running samples. Then the cell populations were gated for analysis. Flow cytometry data acquisition was done using either CellQuest or FACSDiva 6.0 software (BD) and analysed using FlowJo software (version 8.8.3, Tree Star). Further statistical analysis was done using Prism GraphPad software (version 7).

Table 9: Surface cell markers (Abs) used in the study.

Ab	Fluorophore	Clone	dilution	company
CD45	APC, PE	30-F11	1:400	Biolegend, ebioscience
CD4	FITC,PE	GK 1.5	1:300	Biolegend
CD11b	PE	M1/70	1:300	Biolegend, ebioscience
CD11c	PE,FITC	N418	1:250	Biolegend
CD8a	PE-Cy7	53-6.7	1:300	Biolegend
Gr-1	FITC	RB6-8C5	1:300	Biolegend, ebioscience
C5aR	APC	20/70	1:350	Biolegend
CD25	PE-Cy7	PC61	1:350	Biolegend
F4/80	APC,FITC	BM8	1:250	Biolegend
TCRγδ	FITC	GL3	1:250	Biolegend
NKP46	FITC	29A1.4	1:300	Biolegend
CD3	FITC	17A2	1:300	Biolegend
CD40	FITC		1:250	BD Bioscience
CD80 (B7-1)	FITC	(16-10A1)	1:250	BD Bioscience
CD86(B7-2)	FITC	(GL-1)	1:250	BD Bioscience
CD16/32	FITC	2.4G2	1:250	BD Bioscience
MHC-II (I-A/I-E)	FITC	2G9	1:250	BD Bioscience
CD11c	PE	HL3	1:250	BD Bioscience
F4/80	FITC	BM8	1:250	Biolegend
CD205	PerCP-Cy5-5	NLDC-145	1:250	Biolegend
CD206	APC	C068C2	1:250	Biolegend
CD3	PerCP-Cy5-5 FITC	145-2C11 17A2	1:250 1:300	Biolegend Biolegend
CD45	APC, PE	30-F11	1:400	Biolegend, ebioscience
Rat anti-mouse CD45/B220	PE	RA3-6B2	1:250	BD pharmingen

Table 10: Intracellular Abs used in the study.

Ab	**Fluorophore**	**Clone**	**dilution**	**company**
IL-10	APC	JEs5-16E3	1:400	Biolegend
IL-17	APC	TC11-18H10.1	1:400	Biolegend
TGF-β	APC	TW7-16B4	1:400	Biolegend
FOXP3	PE	FJK-16S	1:300	ebioscience

2.9.6 Flow cytometry for BMDMs

BMDMs were differentiated for 48 hours in M1 or M2 conditions cell suspensions were stained for cell surface markers using either one or a combination of the following antibodies; FITC-, PE-, PE-Cy7-, APC and PE- conjugated monoclonal antibodies (Table 11). The appropriate combination of fluorochromes was chosen to ensure optimal results from flow cytometric multidimensional analysis. FACS buffer (1x PBS supplemented with 3% v/v FCS) was used throughout the procedure for preparation, as a wash buffer and for the dilution of the antibodies. The appropriate isotype control monoclonal antibodies were also included. A method was developed using 96 well plates to obtain more accurate results and to save antibody usage. The cells were stained in 96-well round-bottomed microtiter plates. 100µl of cell suspension from each sample were added to each well. Then the cells were stained with 50µl of purified anti-Fc receptor blocking antibody (anti-CD16/CD32 from Biolegend) diluted 1:200 to minimise non-specific binding and background fluorescence. Subsequently, the plate was incubated on ice for 30 minutes. Cells were washed and then stained by adding 50µl/well of the appropriate antibody or antibodies (Table 11). The manufacturer's instructions were followed for all the antibodies used for extracellular staining. Then the plate was covered with aluminium foil and incubated on ice for 30 minutes. Then, the plate was centrifuged at 300 g for 5 minutes. Finally, cells were washed and resuspended in a total volume of 400µl of 1x PBS 3% (v/v) FCS. FACs analysis was done with Canto II (Becton Dickinson, UK) according to

the manufacturer's instructions. The compensation and fluorescence intensity for each BMDM cells were adjusted before running samples for intracellular staining. Intracellular flow cytometry staining is an important tool used analyse signalling and functional responses within a cell population. This technique is carried out to quantify cytokines in the cellular matrix. The first step was to block cellular secretion of cytokines by incubating the cells (2,5 x 10^5 cells per well) in a 96 well round bottom plate in RPMI medium supplemented with 1% (v/v) Golgi Plug (BD Biosciences) or Brefeldin A (eBiosciences). Induction of cytokine-producing cells was done by adding phorbol 12-myristate 13-acetate (PMA) at a concentration of 50ng/ml and ionomycin (500ng/ml). The plate was incubated at 37ºC for 6 hours. Following incubation, the cells were washed and stained with antibodies against extracellular markers as described previously. After that 100μl of Fix/Perm solution (1:4 dilution; BD Biosciences) was added and the cells were further incubated for 20 minutes. Then the cells were washed with 100μl Perm/Wash buffer (1:10 diluted in nanopure water) (BD Biosciences). Subsequently staining with antibodies (previously diluted in Perm/Wash buffer) against intracellular cytokines was carried out. Then the cells were washed and resuspended in 400μl 1x PBS 3% (v/v) FCS. FACs analysis was done with and Canto II (BD) according to the manufacturer's instructions. The compensation and fluorescence intensity for each tissue were adjusted before running samples. Then the cell populations were gated for analysis. Flow cytometry data acquisition was done using Canto II (Becton Dickinson, UK) and analysed using FlowJo software (version 8.8.3, Tree Star). Further statistical analysis was done using Prism GraphPad software (version7.0).

Table 11: Antibodies used in this study.

Ab	Fluorophore	Clone	dilution	company
CD11b	PE	M1/70	1:300	Biolegend, ebioscience
CD11c	PE,FITC	N418	1:250	Biolegend
Gr-1	FITC	RB6-8C5	1:300	Biolegend, ebioscience
F4/80	APC,FITC	BM8	1:250	Biolegend
CD80 (B7-1)	FITC	(16-10A1)	1:250	BD Bioscience
CD86(B7-2)	FITC	(GL-1)	1:250	BD Bioscience
CD16/32	FITC	2.4G2	1:250	BD Bioscience
MHC-II (I-A/I-E)	FITC	2G9	1:250	BD Bioscience
CD11c	PE	HL3	1:250	BD Bioscience
F4/80	FITC	BM8	1:250	Biolegend
CD205	PerCP-Cy5-5	NLDC-145	1:250	Biolegend
CD206	APC	C068C2	1:250	Biolegend
IL-12/IL-23	APC	C15.6	1:250	Biolegend
IL-10	APC	JES5-16E3	1:250	Biolegend

2.10 Mouse Cytokine Array:

The mouse Cytokine Array allows detection and measurement of a number of cytokines simultaneously. It involves the use of carefully selected capture antibodies which have been spotted on nitrocellulose membranes. The principle of this assay depends on the reaction between these capture antibodies and the corresponding cytokines present in the sample which could be sera, cell lysates or tissue homogenates. The sample is usually diluted and subsequently mixed with a cocktail of biotinylated detection antibodies. Then this mixture is incubated with the Mouse Cytokine Array membrane. The immobilised capture antibody on the membrane will bind its cognate cytokine-detection antibody complex present in the sample. Any unbound elements are removed by washing, then

Streptavidin-HRP and chemiluminescent detection reagents are added. The amount of light produced in each spot reflects the concentration of cytokine bound.

Preparation of tissue lysates: tissue lysates are prepared by homogenising the excised tissue in PBS in the presence of 10 µg/ml protease inhibitors cocktail (Sigma,UK). Then triton X-100 is added at a final concentration of 1%, and homogenates are frozen at ≤ -70 °C and subsequently thawed. Then cellular debris is removed by centrifugation at 10,000 x g for 5 minutes. The protein concentration of the sample is measured using a total protein assay and the samples are immediately stored at -80 °C.

Procedure:

The Proteome Profiler^{TM} Array (R&D systems) was the kit used for parallel determination of the relative levels of selected mouse cytokines and chemokines. The membrane was blocked by incubating the membranes in the presence of array buffer 6 (blocking buffer). This was done by adding 2ml of array buffer 6 into each well on the 4-Well Multi-dish to be used. Then each membrane was carefully removed from the protective sheets using flat tip tweezers and placed in a well of the 4-Well Multi-dish with the number of the membrane facing upwards. The membranes were incubated for 1 hour with gentle agitation. During the incubation step the samples were prepared by adding 300µg of each sample (tumour homogenate) to 0.5ml of array buffer 4, and then the final volume was adjusted to 1.5ml by adding buffer 6. This was followed by adding 15µL of Mouse Cytokine Array Panel A Detection Antibody Cocktail to each prepared sample. Then the sample-detection antibody mixture was mixed and incubated at room temperature for 1 hour. Following incubation, array buffer 6 was aspirated from the 4-well multi dish and the previously prepared sample-detection antibody mixture was added. Then the 4-Well Multi-dish was sealed and incubated overnight on a rocking platform shaker at 2-8 °C. The next day, membranes were removed and each placed in a separate plastic container containing 20ml of 1X wash buffer. Each membrane was washed by placing the container on a rocking platform shaker for 10 minutes. The washing step was repeated three times. Following washing, the Streptavidin-HRP was diluted in array buffer 6 and 2ml was added into each well of the 4-well multi dish. Then each membrane was carefully removed from the wash container and excess buffer was drained. After

that the membrane was placed in the 4-well multi dish containing the diluted Streptavidin-HRP. The wells were covered with the lid and subsequently incubated at room temperature for 30 minutes on a rocking platform. After incubation each membrane was placed in a separate container containing 20ml of 1X wash buffer and washed as previously mentioned above. Following washing, excess buffer was drained from the membrane by blotting the lower edge of the membrane on a paper towel. Then each membrane was placed on the bottom sheet of the plastic sheet protector with the identification number facing up. Then each membrane was completely covered by adding 1ml of Chemi Reagent Mix. The membranes were carefully covered with the top sheet of the plastic sheet protector and any air bubbles were carefully removed. Then the membranes were incubated for 1 minutes, excess Chemi Reagent Mix was squeezed out by carefully placing paper towels on the top and sides of the plastic sheet protector containing the membranes. Then the top plastic sheet protector was removed and an absorbent lab wipe was carefully placed on top of the membranes to blot off any remaining Chemi Reagent Mix. With the membranes left on the bottom of the plastic sheet protector, the membranes were covered with a plastic wrap. Any air bubbles were gently removed and the sheet protector was completely covered by wrapping excess plastic around the back. Then the membranes were placed in an autoradiography film cassette and membranes are exposed to X-ray film for 2 minutes. The positive signals on the developed film are identified by placing the transparency overlay template on the array image and aligning it with the pairs of reference spots in three corners of each array. Pixel densities on developed X-ray film were analysed using a transmission mode scanner and image analysis software. A template was created to analyse pixel density in each spot of the array. Then signal values were exported to a spread sheet of an excel file. The average signal of the pair of duplicate spots representing each cytokine was determined. The signal from a clear area of the array or negative control spots was used as a background value and the background signal was subtracted from each spot.

2.11 clinical trial and Pancreatic Adenocarcinoma patients

The full clinical trial design has been previously described in a previous study (Arshad et al., 2014). In summary: Patients presenting to a tertiary hepatobiliary

unit with histologically confirmed locally advanced or metastatic pancreatic adenocarcinoma unsuitable for surgical resection but suitable for gemcitabine chemotherapy were recruited. Following informed consent they were treated on an outpatient basis with weekly gemcitabine chemotherapy (Gemzar, Lilly: 1000mg/m3 over 30 minutes by peripheral intravenous infusion) immediately followed by an n-3 fatty acid-rich lipid infusion (Lipidem: 200mg/ml 50% MCT, 40% LCT, 10% Fish oil, BBraun, Melsungen: 50g by peripheral intravenous infusion). This regimen was given weekly for 3 weeks, followed by a rest week from all treatment: this constitutes one treatment cycle. This was continued until death, withdrawal by investigator or participant or tumour progression on CT for a maximum of 6 cycles in total. 29 patients who achieved at least 2 cycles of treatment and up to 6 cycles with varying degrees of response to treatment (Either partial response, stable disease or progressive disease) were selected. Patients were followed up until death in all cases.

Primary outcome measure was objective response rate on CT evaluated using Response Evaluation Criteria in Solid Tumours (RECIST) version 1.1 criteria by an experienced independent clinical trials radiologist. Tumour progression was defined by a >20% increase in target lesion dimensions or any new lesion occurrence since baseline CT. Evaluation by CT was carried out every 2 cycles of treatment (8 weeks). Secondary outcome measures included Overall Survival (OS), which was defined as the interval between first treatment and death, Progression free survival (PFS) which is defined as the interval between first treatment and progression of the disease and measurement of properdin levels. Plasma samples were taken immediately prior to treatment each week, frozen and stored prior to analysis.

A control arm of n-3 fatty acid naïve patients was subsequently recruited. These consisted of a similar cohort to the above: histologically confirmed unresectable pancreatic adenocarcinoma who only receive gemcitabine, without intravenous n-3 fatty acid, act as a control group for comparison. These patients were matched to the intervention group and have tumour assessments as per normal clinical protocol to the above. Informed consent for the analysis of plasma samples was obtained prior to commencing into the study. Ethical approval was obtained from the regional ethics board (REC Reference number 12/EE/0425). 5 patients were recruited.

A control arm of healthy Dutch volunteers was also obtained from a previous study, with their baseline properdin levels available for comparison. These consisted of 30 volunteers, without pancreatic adenocarcinoma or receiving parenteral n-3 fatty acid infusion.

2.12 Enzyme-linked immunosorbent assays (ELISA)

ELISA was used to detect CCL2, C5a, C3, C5b9, Lectin pathway in mouse sera, Properdin, αM(ITG/CD11b) in human sera and IFN-ɣ, IL-10, IL12 and IL-6 secretion into culture supernatants of BMDM cells.

2.12.1 Quantification of Mouse CCL2 (MCP-1) by ELISA

Measurement of mouse CCL2 protein levels in serum was carried out using the mouse CCL2 (MCP-1) ELISA Ready-SET-Go kit (Affymetrix eBioscience, 88-7391) according to manufacturer's instructions. Corning costar ELISA plates were coated with 100µL/well of capture antibody in 1X Coating Buffer, followed by sealing the plate and incubation at 2-8°C overnight. The next day, the wells were aspirated and washed 3 times with wash buffer followed by blotting the plate on absorbent paper to remove any remaining buffer. Then each well was blocked by adding 200µl of diluted ELISA/ELISPOT diluent followed by 1hour incubation at room temperature. Then, 100µL of each standard and diluted sample (1/10) were added into pre-designated wells in duplicate followed by incubation at room temperature for 2 hours. Following incubation, the wells were washed 4 times as described earlier before adding 100µl/well of detection antibody diluted in 1X ELISA/ELISPOT diluent and incubation at room temperature for 1 hour in the dark. Then the wells were washed as described earlier and 100µl of Avidin-HRP diluted in 1X ELISA/ELISPOT diluent was added to each well. After that the plate was incubated at room temperature for 30 minutes in the dark. Then the wells were aspirated and washed by soaking in wash buffer for 2 minutes followed by aspiration. This washing step was repeated 5 times, and followed by adding 100 of 1X TMB solution to each well. Then the plate was incubated at room temperature for 15 minutes. Finally, 50µl of stop solution was added to each well and the optical density at 450 nm, with correction at 570nm, was determined using a plate reader using a Multiskan FC microplate photometer and SaknIt software version 2.5 (Thermo scientific, UK). Optical density values were corrected to the blank and CCL2 concentrations, in serum samples, were

determined through the linear equation of the standard curve and multiplication by the dilution factor.

2.12.2 Quantification of C5a in tumour lysates of wildtype and Properdin deficient mice.

This experiment was to measure the quantity of mouse C5a using a commercially available ELISA kit (sandwich ELISA).

Preparation of tumour lysates for ELISA: Mechanical homogenization in liquid nitrogen was used to prepare tumour lysates as previously described by Weigand and colleagues with modification. Briefly, excised tumours were homogenized using mortar and pestle with adding liquid nitrogen. After that the powdered tissue for each sample was weighed and normalized by adding 90% of lysis buffer (100 mM Tris, pH 7.4, 150 mM NaCl, 1 mM EGTA, 1 mM EDTA, 1% Triton X-100 and 0.5% Sodium deoxycholate) to the powdered tissue (for each/mg tissue, 9µl lysis buffer was added) followed by transferring the lysates to an eppendorf tube and centrifugation at 20000g for 15 minutes at 4 ˚C. After centrifugation, the supernatant was isolated and stored at -80 ˚C until further analysis (Weigand *et al.,* 2012).

C5a was measured in tumour lysates and sera of tumour bearing wildtype and Properdin deficient mice. The protocol was carried out according to manufacturer's instructions. The capture antibody was purified rat anti-mouse C5a (cat:558027 BD Pharmingen,UK) at a concentration of 10µg/ml. Recombinant mouse C5a; (BD Pharmingen,UK) was used as a standard. Individual levels (means) were obtained and multiplied with the dilution factor and expressed as ng/ml.

2.12.3 Quantification of mouse Complement Component C5a by ELISA

The DuoSet ELISA kit (R&D Systems, DY2150) was used to measure mouse complement component C5a according to manufacturer's instructions. This kit employs a sandwich ELISA to measure natural and recombinant mouse complement component C5a. The microtiter plate was prepared for the assay by diluting the capture antibody to the working concentration in PBS and adding 100 µl to each plate followed by overnight incubation at room temperature. In the next day, the wells were aspirated and washed 3 times with wash buffer. After the last

wash, any remaining wash buffer was removed by aspirating and inverting the plate and blotting it. The plate was then blocked by adding 300µl of reagent diluent to each well followed by Incubation at room temperature for a minimum of 1 hour. 100 µl of sample (diluted 1/200) or standards in reagent diluent were added into pre designated wells in duplicate. Next, the microtiter plate was incubated at room temperature for 2 hours with the plate covered. Following incubation, the wells were washed as previously described and 100µl of the detection antibody, diluted in reagent diluent was added to each well. Then the plate was covered and incubated at room temperature for 2 hours followed by washing as described earlier. Then, 100µl of the working dilution of Streptavidin-HRP was added to each well and the plate was incubated in the dark for 20 minutes at room temperature. Then the wells were washed for 3 times and 100µl of substrate solution was added to each well before incubation for 20 minutes at room temperature in the dark. Finally, the resulting colorimetric reaction was stopped by adding 50 µl of stop solution to each well and mixing by gentle taping. The optical density at 450 nm, with correction at 570 nm, was immediately determined using a plate reader using a Multiskan FC microplate photometer and SaknIt software version 2.5 (Thermo scientific, UK).

Optical density values were corrected to the blank and C5a concentrations, in the test samples, were determined through the linear equation of the standard curve.

2.12.4 Quantification of C5a in sera of wildtype and Properdin deficient tumour bearing mice.

The protocol was carried out according to manufacturer's instructions. Briefly, 100µl of diluted capture antibody (purified rat anti-mouse C5a (152-1486 BD Pharmingen) at a concentration of 10µg/ml was added to a 96-well Maxisorp-plate. After that the plate was sealed and incubated overnight at room temperature. The next day, the wells were aspirated and washed 5 times using 200µl of washing buffer. After each washing step the plate was inverted forcefully and blotted to a paper towel to remove any excess liquid. After the last washing step, 200µl of blocking buffer (1% bovine serum albumin in PBS) was added to each well followed by incubation for 1 hour at room temperature. Then the plate was washed 5 times as previously mentioned. The standard (purified recombinant mouse C5a; BD Pharmingen) was diluted to 60, 30, 15, 7.5, 3.7, 1.87, 0.935, 0.467 and 0 ng/ml in dilutes (0.05(v/v) % tween 20, 1% (W/v) BSA

in PBS). One hundred microliter of sample (diluted 1:20) or standard was added to triplicate wells. Then the plate was incubated for 2 hours at room temperature. After that the plate was washed as above and 100µl of detection antibody (biotin rat anti-mouse C5a BD Pharmingen) at a concentration of 2µg/ml was added to each well followed by incubation at room temperature for two hours. Then the plate was again washed 5 times. One hundred microliters of Streptavidin-peroxidase conjugate (from Sigma-Aldrich) diluted 1:100 was added to each well followed by incubation for 30 minutes at room temperature. The plate was aspirated and washed 5 times. Then 100µl of substrate solution (TNB from R&D systems, USA) was added to each well. The plate was incubated at room temperature for color development. After that, stop solution was added and the results were obtained by reading absorbance at 450nm. The absorbances were plotted against the standards. Individual levels (means) were obtained multiplied with the dilution factor and expressed as µg/ml.

2.12.5 Quantification of mouse terminal complement complex C5b-9 (TCC C5b-9) by ELISA

Quantitative determination of mouse terminal complement complex C5b-9 (TCC C5b-9) in serum was carried out by sandwich enzyme immunoassay technique (MyBiosource, MBS703522). As recommended by the manufacturer, serum samples were diluted 1/200 prior to the assay. Similarly, the standard was reconstituted in 1ml of sample diluent, followed by a 2-fold dilution series to yield a range that covers C5b-9 level in the different samples. 100µl of standard and sample were added per well in duplicate followed by incubation for 2 hours at 37°C in the dark. Then the contents of each well was aspirated and 100µl of Biotin-antibody (1X) was added to each well followed by incubation for 1 hour at 37°C in the dark. After incubation, the wells were aspirated and washed 3 times with wash buffer. After the last washing step, any remaining wash buffer was removed by decanting the plate and blotting against clean paper towels. Next, 100µl of HRP-avidin (1x) was added to each well and the microtiter plate was incubated for 1 hour at 37°C in the dark. Then the wells were aspirated and washed 5 times as described above. After washing and removing any remaining wash buffer, 90µl of TMB Substrate was added to each well followed by incubation for 15-30 minutes at 37°C in the dark. After incubation, the colorimetric reaction was stopped by the addition of 50µl of Stop Solution to each well

followed by gentle tapping to ensure thorough mixing. Finally, the optical density of each well was determined within 5 minutes using a microplate reader using a Multiskan FC microplate photometer and SaknIt software version 2.5 (Thermo scientific, UK). Set to 450 nm with correction at 570nm. The absorbances were plotted against the standards. Individual levels (means) were obtained multiplied with the dilution factor and expressed as µg/ml.

2.12.6 Quantification of complement C3 by ELISA

Quantitative measurement of Complement C3 in mouse serum was carried out using complement C3 mouse ELISA kit (Abcam-ab157711) according to the manufacturer's instructions. The mouse complement C3 calibrator was diluted to a range that covers C3 levels in the different samples, while samples were diluted to 1/50,000 via 2 steps. 100µL of each standard and diluted sample were added into pre designated wells in duplicate. Then the microtiter plate was incubated at room temperature for 20 minutes to allow the binding of complement C3 to the anti-complement C3 immobilised antibodies. Following incubation, Wells were aspirated and washed 4 times with 1x wash buffer, to remove unbound substances, before incubation with 100µL/well of 1X Enzyme-Antibody conjugate at room temperature for 20 minutes with the plate covered. Then the wells were washed as previously described before adding TMB substrate solution into each well. Next, the microtiter plate was incubated in the dark at room temperature. After 10 minutes, stop solution was added to each well and the absorbance (450 nm) of each well was determined using a plate reader using a Multiskan FC microplate photometer and SaknIt software version 2.5 (Thermo scientific, UK) within 20 minutes with correction at 570nm. Optical density values were corrected to the blank and C5a concentrations, in the test samples, were determined through the linear equation of the standard curve.

2.12.7 C9 functional complement ELISA for lectin pathway

ELISA was optimised based on published work on mouse assays which is considered a new assay to investigate functional complement activities (Kotimaa et al., 2014). Briefly, 10µg/ml mannan (M7504, Sigma-Aldrich) was coated in CB buffer (diluted 1:1000) for the final volume 100µl per well and for 16 h RT on Nunc Maxisorp plates (Thermo Fisher Scientific). Then, the wells were washed with 200µl of PT buffer (3 times, 5minutes). LP was blocked with 150µl of PB buffer per well for 90 minutes at 37°C. Afterwards, the wells were washed with 200µl of

PT (PBS/0.05% Tween 20) buffer per well (3 times for 5 minutes). The serum samples, normal mouse serum (NMS) and heated inactivated serum (HIS, prepared by heating the NMS for 30 minutes at 56°C in hot blot) were diluted (1 to 5) into BVB++ buffer (Veronal buffered saline/ 0.5mM $MgCl_2$/ 2mM $CaCl_2$/ 0.05% Tween 20/ 1% BSA, pH 7.5). Afterwards, 100µl of each sample was added in each well on the Maxisorp plates and incubated for 1h at 37°C. Then, the wells were washed with 200µl of PT buffer per well (3 times, 5 minutes). After washing, 100µl of polyclonal Polyclonal rabbit complement component 9 antibody anti-mouse rC9 (0.2 mg/ml, MyBioSource) was added per well and incubated at 37°C for 1h. The wells were then washed with 200µl of PT buffer per well (3times, 5minutes). After washing, 100µl of polyclonal 1mg/ml swine anti-rabbit HRP antibody (diluted 1:200 with 1xPBS) (Dako) was added per well and incubated at 37°C for 1h. Then, the wells were washed with 200µl of PT buffer per well (3 times, 5 minutes). Later, 100µl of the coloured substrate TMB (sigma) was added per well and left at room temperature for 10-15 minutes, followed by adding 50µl of the stop solution to each well to stop the over reaction. Finally, the result was read immediately using ELISA reader TECAN Magellan for F50.

2.12.8 Quantitative measurement of mouse IFN-γ secreted from BMDM

Sandwich ELISA (Peprotech) was used for quantification of Murine IFN-γ within the range of 15-2000pg/ml according to manufacturer's instructions. Briefly, 100µl of diluted capture antibody (1µg/ml) was added to a 96 well ELISA microplate. After that the plate was sealed and incubated overnight at room temperature. The next day, the wells were aspirated and washed 5 times using 200µl of washing buffer. After each washing step the plate was inverted and blotted to a paper towel to remove any excess liquid. After the last washing step, 200 µl of blocking buffer (1% bovine serum albumin in PBS) was added to each well followed by incubation for 1 hour at room temperature. Then the plate was washed 5 times. The standard (murine IFN-γ) was diluted to 2, 1, 0.5, 0.25, 0.125, 0.0625, 0.0315 and 0 ng/ml in diluents (0.05% tween 20, 0.1% BSA in PBS). One hundred microliter of sample or standard was added to triplicate wells. Then the plate was incubated for 2 hours at room temperature. After that the tube was washed. Then 100µl of detection antibody (0.25µg/ml) was added to each well followed by incubation at room temperature for two hours. Then the plate was washed 5 times. Avidin-HRP conjugate was diluted 1:2000 by adding 5.5µl to

11ml of diluents, and then 100µl was added to each well followed by incubation for 30 minutes at room temperature. The plate was aspirated and washed 5 times. Then 100µl of substrate solution (ABTS 2,2) was added to each well. The plate was incubated at room temperature for color development. The absorbance was obtained by using an ELISA plate reader at 450 nm.

2.12.9 Quantitative measurement of mouse IL-10 secreted from BMDM

Murine IL-10 ELISA kit (Peprotech) was used according to manufacturer's instructions. The protocol used was similar to the one mentioned above with the exception that the detection range was 39-5000 pg/ml and the concentration of capture antibody was 2µg. The upper limit for concentration of standard was 5ng/ml.

2.12.10 Quantitative measurement of mouse IL-12 secreted from BMDM

Murine IL-12 was quantified using ELISA kit (Peprotech) which had a detection range of 16-1000pg/ml. The manufacturer's instructions were followed which were similar to 2.12.8 with the exception that concentration of capture antibody was 0.5 µg/ml and concentration of standard was 1ng/ml.

2.12.11 Quantitative measurement of mouse IL-6 secreted from BMDM

Murine IL-6 ELISA kit (Peprotech) was used according to manufacturer's instructions. The protocol used was similar to 2.12.9 with the exception that the detection range was 63-4000 pg/ml and the concentration of capture antibody which was 2µg. The upper limit for concentration of standard was 4ng/ml.

2.12.12 Quantification of Human Properdin by ELISA

Properdin was determined from 1/5000 plasma sample dilutions using commercial kits (HK334 Human Properdin, Hycult Biotech, Uden, The Netherlands) following the manufacturer's protocol. This kit is a ready to use solid phase enzyme immune sorbent assay based on the sandwich principle. Serum samples and standard were diluted 1:5000 and 100µl was added in triplicate to a microtiter plate coated with an antibody recognizing human properdin. After 1 hour of incubation at room temperature, the wells were washed 4 times. Then 100 µl of biotinylated antibody was added, followed by incubation at room temperature for 1 hour. Then the wells were washed 4 times and 100 µl of streptavidin peroxidase conjugate was added followed by incubation for 1 hour at room temperature. After incubation, 100 µl of TMB solution was added to the wells, followed by an incubation step for 30 minutes at room temperature. After that, stop solution was added and the results were obtained by reading absorbance at 450nm. The absorbances were plotted against the standards. Individual levels (means) were obtained multiplied with the dilution factor and expressed as µg/ml.

Concentrations from duplicate measurements were calculated from a standard curve set up in duplicate. Properdin levels were measured at baseline/week 0 (prior to any intervention or treatment), week 7 (after 2 cycles of either intravenous gemcitabine with n-3 fatty acid infusion or without n-3 fatty acid infusion), week 15 (after 4 cycles of either intravenous gemcitabine with n-3 fatty acid infusion or without n-3 fatty acid infusion) and week 23 (after 6 cycles of either intravenous gemcitabine with n-3 fatty acid infusion or without n-3 fatty acid infusion).

2.12.13 Quantification of Human integrin αM (ITG/CD11b) by ELISA

To quantify human ITG/CD11b concentrations in serum and plasma, a sandwich ELISA was performed using Human Integrin αM,ITG/CD11b ELISA Kit (CSBCSB -E11638h ,CUSABIO, UK), according to manufacturer's instructions. The minimum detectable dose for ITG/CD11b is typically less than 0.195ng/ml.

100µl of standard and sample were added per well in duplicates followed by incubation for 2 hours at 37°C in the dark. Then the contents of each well was aspirated and 100µl of Biotin-antibody (1X) was added to each well followed by incubation for 1 hour at 37°C in the dark. After incubation, the wells were

aspirated and washed 3 times with wash buffer. After the last washing step, any remaining wash buffer was removed by decanting the plate and blotting against clean paper towels. Next, 100µl of HRP-avidin (1x) was added to each well and the microtiter plate was incubated for 1 hour at 37°C in the dark. Then the wells were aspirated and washed 5 times. After washing and removing any remaining wash buffer, 90µl of TMB Substrate was added to each well followed by incubation for 15-30 minutes at 37°C in the dark. After incubation, the colorimetric reaction was stopped by the addition of 50µl of Stop Solution to each well followed by gentle tapping to ensure thorough mixing. Finally, the optical density of each well was determined within 5 minutes using a microplate reader (Multiskan FC microplate photometer and SaknIt software version 2.5 ,Thermo scientific, UK) Set to 450 nm with correction at 570nm. The absorbances were plotted against the standards. Individual levels (means) were obtained expressed as ng/ml.

2.13 Immunohistochemical and Histology staining melanoma tumour

2.13.1 CD88 immunohistochemistry

C5a is an anaphylatoxin which works after binding to the high affinity C5a receptor (CD88). Expression of C5aR was found on peripheral blood leukocytes (neutrophils, eosinophils, monocytes and macrophages). Furthermore, recent studies have demonstrated that C5aR expression can also be found in liver and lung cells (Havoiland et al., 1995). Studies on the role of C5a in tumour growth have concluded that C5a concentration plays an important role in determining tumour progression (Gunn et al., 2012). The aim of the current experiment was to study the expression of C5aR (CD88) in lung tissue sections from tumour bearing mice (PWT and PKO), *S.pneumoniae* infected and healthy mice (as controls, from a past project, Dupont et al.,). CD88 was detected in lung tissue sections using a rabbit polyclonal antibody (Santa Cruz Biotechnology) raised against amino acids 251-350 of CD88. Tissue sections were deparaffinised by immersion in two changes of xylene for 5 minutes followed by soaking in two changes of 100% IMS for 3 minutes each time. Then the slides were soaked in a solution containing 90% of absolute methanol and 10ml 30% of H_2O_2 for 10

minutes. The sections were rehydrated by soaking in descending grades of alcohol (90% and 70% of IMS). The second step was antigen retrieval which was done by a 20 minutes treatment in 10mM citrate buffer (pH 6.0) at 95 ˚C followed by another 20 minute in room temperature 10mM citrate buffer. Antigen retrieval was followed by blocking non-specific protein binding sites by treating each slide with 100µl of DAKO chemamate peroxidase blocking solution for 5 minutes at room temperature followed by draining the slides. Then the sections were blocked in 3% BSA and 0.1% Tween for 20 minutes at room temperature followed by washing three times in PBS-Tween. Then 100 µl of different dilutions (1:50, 1:100, 1:200 and 1:400) of primary antibody (rabbit polyclonal CD88 antibody) was added to each slide followed by overnight incubation at 4˚C. The next day, the slides were washed five times with a solution of PBS-tween. Then 100µl of secondary antibody (DAKO peroxidase-DAP, rabbit-mouse) was added to each slide followed by a 30 minutes incubation period at room temperature. After incubation, the slides were washed 5 times with PBS-tween. The next step was adding the chromogen substrate for 3 minutes followed by washing the slides with distilled water. Then the slides were soaked in PBS for 5 minutes followed by washing with tap water for 5 minutes and rinsing with distilled water. The next step was to add carazzi ‘s hematoxylin stain for 5 minutes followed by washing with tap water. Then the sections were dehydrated with ascending grades of alcohol (70% and 90% of IMS) followed by adding a drop of xylene. The last step was adding mounting media (DPX) to the slides. The slides were examined and the results showed that CD88 reactivity was in consistent, therefore a different approach was used by quantification of C5a by ELISA.

2.13.2 C3 Immunohistochemistry

The aim of this experiment was to recognize target proteins (C3) in the tissue sections using specific antibodies that bind only to the protein of interest.

The first step is fixation of the tissue to allow preparation of thin tissue sections. Fixation was done by placing pieces of mouse liver in 10% formal saline for 6-7 days. Then the tissue was embedded in paraffin wax according to standard histological procedures. After that 5µm tissue sections were cut from this paraffin embedded tissues using a microtome, followed by floating these sections on water (52˚C) on charged glass slides. The next step was deparaffinising, which was done by placing the slides in two changes of xylene for 2 minutes. Then the

sections were rehydrated by treatment with descending grades of alcohol (100%, 90% and 70% IMS). After that antigen retrieval was done by using 10mM sodium citrate, 0.05% tween-20 PH 6.0 (20 minutes at 95˚C followed by 20 minutes in fresh buffer at room temperature). The next step was blocking non-specific protein binding sites by a 20 minutes treatment with 1% bovine serum albumin in TBS-tween (tris buffered saline with 0.1% (v/v) tween 20). The primary antibody (rat monoclonal antihuman C3) at an initial concentration of 0.05mg/ml was diluted 1/75 in blocking buffer. Then 100µl was added to each section, followed by overnight incubation at 4-6 ˚C in a humified chamber. In the next day, the slides were washed five times in TBS-Tween. The secondary antibody (peroxidase labelled swine anti rat IgG- Serotec) was diluted 1:200 in blocking buffer and added to the sections as mentioned above. Then the sections were incubated at 4-6 ˚C in a humified chamber for 1 hour and 30 minutes followed by washing 5 times. The substrate was prepared by adding 5ml of 0.2M Tris/HCL (pH 7.5) into two tubes. Then 32 gm of ammonium nickel sulphate hexahydrate (Sigma-Aldrich) was added to the first tube and 10mg of 3, 3` -diaminobenzide (Sigma-Aldrich) was added to the second tube. Then the two tubes were combined together in a universal tube followed by the addition of 30% H_2O_2. The substrate was filtered through a 0.2µm syringe filter and dropped on the top of sections and left for 2-10 minutes. Then the slides were placed in a jar containing distilled water followed by placing the slides in a jar containing nuclear fast red stain for 5 minutes. After that the slides were washed with tap water. Then dehydration was done through an ascending grades of alcohol (70%, 90% and 100% of IMS) followed by clearing in two changes of xylene. After that, one drop of mountant was applied followed by covering the sections with a coverslip.

2.13.3 Toluidine blue staining:

Four wildtype and four Properdin deficient C57BL/6 mice were subcutaneously injected with 4 $\times 10^5$ cell/100µl of B16F10 cell suspension. After 13 days the mice were sacrificed and dissected for collection of tumour tissue. Tissues were fixed with formaldehyde (10%) and subsequently embedded in paraffin. Then the sections were deparaffinized and dehydrated. The sections brought to water and stained in toluidine blue, which stains acid mucopolysaccharides metachromatically such as mast cells. Tissue sections brought to water and stained in 0.5% toluidine blue (aq.) for 3-4 minutes. The slides were then rinsed

in tap water followed by Wright's stain for 1-2 minutes. Then the slides were rinsed in water and blotted on filter paper to dry. The next step was dehydrating in butan-1-ol followed by clearing in xylene and adding mounting in DPX.

2.13.4 Martius yellow staining

The aim of this stain is to identify the red blood cells in the tumour which indicate the location of blood vessels which are formed due to angiogenesis.

Four wildtype and four Properdin deficient C57BL/6 mice were subcutaneously injected with 4 $\times 10^5$ cell/100µl of B16F10 cell suspension. After 13 days the mice were sacrified and dissected for collection of tumour tissue. Tissues were fixed with formaldehyde (10%) and subsequently embedded in paraffin. Then the sections were deparaffinized and dehydrated. Then the sections stained with Martius yellow (1% in100% methanol) for 30 seconds followed by rinsing in 100% IMS, then the slides were blotted on filter paper. Then the slides were counterstained by dipping in a jar containing Wright's stain for 1-2 minutes. Then the slides were rinsed in water and blotted on filter paper to dry. Dehydrated in butan-1-ol followed by clearing in xylene and adding mounting in DPX.

2.13.5 Schmorl's stain

This stain is used to visualise melanin in histological tissue sections by employing the chemical reducing properties of melanin. In this reaction, melanin reduces ferric ions (Fe^{3+}) to ferrous ions (Fe^{2+}), which is followed by the ferrous ions combining with ferricyanide. This leads to the production of ferrous ferricyanide, which is a blue to dark blue pigment. This stain was used to stain the melanin produced by B16F10 as an indication of the extent of pigmentation in the tissue. The protocol described by Disbery and Rack 1976, was followed. Briefly tissue sections were deparaffinised in two changes of xylene, then they were hydrated through graded alcohols (100%, 100% and 70% IMS) to distilled water. A working ferricyanide solution was made by mixing 3 parts of freshly made ferric chloride, (1% aqueous solution) with 1 part of freshly made potassium ferricyanide (1% Aqueous Solution). The slides were immersed in working ferricyanide solution for 3 minutes followed by immersing in 1% acetic acid for 2-3 minutes. Then the slides were rinsed with distilled water. The slides were counter stained in nuclear fast red stain solution for 3 minutes followed by rinsing in distilled water. Then the sections were dehydrated with graded alcohol followed by clearing in xylene and

coverslip with mounting media. This stain should show the melanin blue, nucleus red and the cytoplasm pink (Disbrey & Rack, 1976).

2.13.6 Peroxidase staining:

The aim of this experiment was to stain for peroxidase activity, as would be present in neutrophils, which may associate with tumours as so-called tumour-associated neutrophils.

Lung tissue sections from wildtype and properdin deficient mice (after 13 days of intravenous injection with $3X10^5$cells of B16F10) were fixed and embedded in paraffin as previously described. Staining of hydrogen peroxidase was done by incubating the slides in a jar of diaminobenzidinetetrahydrochloride (DAB) solution (prepared by adding 10 mg of diamino-benzidine tetrahydrochloride (Sigma-Aldrich) to 10 ml pH 7.5 Tris/Hcl 200mM) at room temperature until a brown colour developed (about 5 minutes). After that the slides were washed in distilled water to stop the reaction. Then 8µl of H_2O_2 (30%) was added followed by adding 0.5% of toluidine blue. After the slide were quickly immersed in a jar containing butan-1-ol followed by drying using filter paper. Then the sections were air dried and cleared in xylene and coverslip with mounting media.

2.14 of mouse Bone Marrow Derived Macrophages (BMDMs).

2.14.1 Scheme for the isolation, formation and stimulation of mouse Bone Marrow Derived Macrophages (BMDMs).

To maintain sterility, the process of isolation, formation and stimulation of mouse BMDM was performed in a BioSafety Level 2 (BSL2) cabinet. The steps required for mouse BMDM isolation, formation and stimulation are outlines in Figure 10

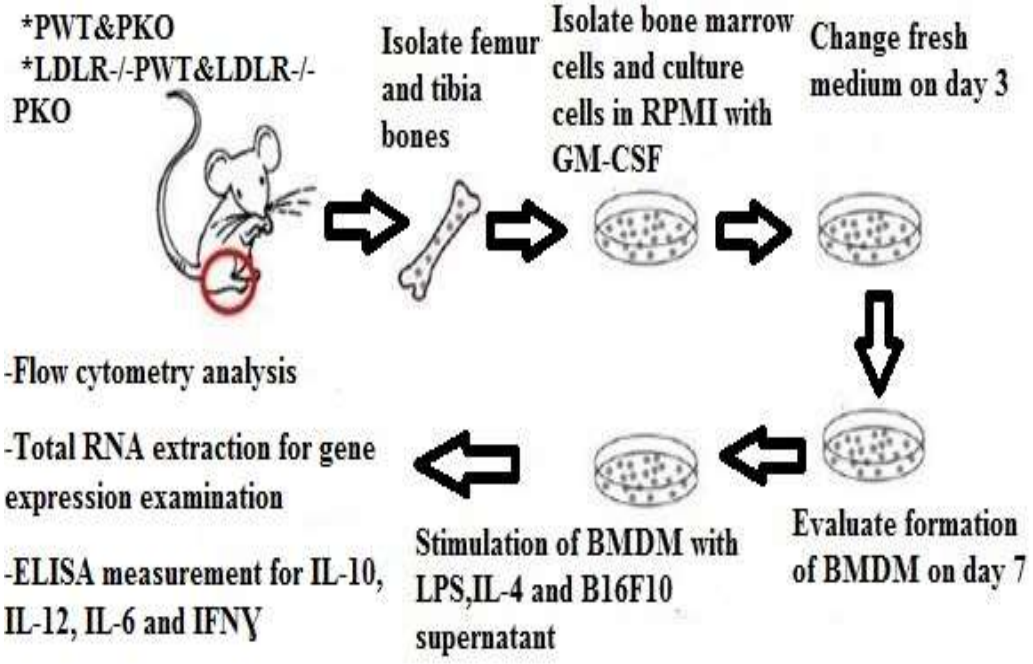

Figure 10: Scheme for the isolation, formation and stimulation of mouse BMDMs.

Scheme for the isolation, formation and stimulation of mouse BMDMs. Step by step procedures are described in the text. In brief, femur and tibia bones are collected from matched genotypes and bone marrow cells flushed out using PBS supplemented with 2% heat inactivated FBS. After that red blood cells are lysed with NH_4Cl solution, cells are cultured in BMDM growth medium for 7 days followed by maturation and analysis for purity of the cell population. For analysis of macrophage polarisation, cells were stimulated with LPS or LPS+IFNγ for M1, or IL-4 for M2 activation. surface marker presentation and cytokine production were investigated.

2.14.2 Bone marrow preparation (BMDM)

Bone marrow cells were isolated from tibias and femurs of mice of both properdin deficient and wildtype genotypes (Dupont et al., 2014). This preparation was done with modification according to the protocols described by Inaba and Westcott (Inaba et al., 1992, Westcott et al., 2007). First of all, mice were sacrificed and sprayed with 70% industrial methylated spirit (IMS). Then they were dissected and both bones were removed after purification from surrounding tissues. Then the bones were put in 100% IMS for a few minutes and subsequently washed with PBS. The bones were then cut from both sides and flushed with PBS in a 15 ml falcon tube using a 1 ml syringe which has a 0.45 mm diameter needle. The tube was then vigorously shaken to prevent clustering of cells. After waiting for a few minutes the supernatant was transferred to a new tube then centrifuged at 277g for 5 minutes. The supernatant was discarded and 2ml of hypotonic 0.87% Tris-NH_4CL (pH 7) was added to the pellet for a few

minutes to lyse RBCs. Then 10ml of PBS was added followed by centrifugation at 277g for five minutes. After that the supernatant was discarded and the pellet suspended in an appropriate volume of RPMI supplemented with 10% of foetal calf serum (FCS) to obtain a cell count of $1x10^6$ cell/ml and transferred into a tissue culture plate. Then the cells were treated either with 20ng/ml of GM-CSF (Granulocyte/Macrophage Colony-Stimulating Factor) or M-CSF (10ng/ml) (Peprotech) for 7 days. The cells were differentiated either into M1 or M2 cells by stimulation with LPS (100ng/ml)+ IFN-γ (20ng/mL, eBioscience, San Diego, CA) or IL-4 (20ng/ml) respectively, in addition to stimulation of untreated cells with B16F10 supernatant for seven days incubation at 37°C. During this period the old medium was replaced by new medium every two days. After 7 days of incubation, the medium was aspirated and fresh medium was added to the flask which contained attached cells (bone marrow macrophages). Then the cells were differentiated either into M1 or M2 cells by stimulation with LPS (100 ng/ml)+ IFN-γ (20ng/mL, eBioscience, San Diego, CA), or IL-4 (20ng/ml) respectively, in addition to stimulation of untreated cells with B16F10 supernatant.

2.14.3 The Effect of B16F10 supernatant on macrophage secretion of cytokines indicative of a certain polarisation (M1/M2).

Briefly, mouse bone marrow derived macrophages from wildtype and properdin deficient mice were cultured with B16F10 supernatant, followed by measurement of levels of IFN-γ-,IL-6, IL-12 and IL-10.The protocol described by Jackaman et al 2013, was followed with modification (Jackaman et al., 2013).

Bone marrow derived macrophages from wildtype and properdin deficient mice were prepared as previously described in 2.14.2. After preparation, macrophages were counted and the number adjusted to $5×10^5$ cell/ml. For each of the wildtype and the properdin deficient BMDM, a 6 well tissue culture plate was prepared by seeding 2 ml of cells into 4 wells. In order to differentiate these cells, either 20 ng/ml of GM-CSF or 10 ng/ml of M-CSF was added to each well, then the cells were incubated at 37 ˚C for seven days. At day 3 and 5 the media was changed. After 7 days of incubation most of the macrophages were adherent. The media was then discarded. Two millilitres of RPMI was added to well number1 (control) , 2 ml of B16F10 supernatant was added to well number 2 and 2ml of RPMI with either100ng/ml of LPS+ 20 ng/ml of interferon gamma (INF-ɣ) was added to well

number 3. (100 ng/ml) LPS+IFNɣ was used as a control to stimulate polarisation towards M1 macrophages. Two milliliters of RPMI with 20ng/ml of IL-4 were added to well number 4. IL-4 was used as a control to stimulate polarisation towards M2 macrophages. After that the two 6 well plates were incubated at 37 ˚C overnight. In the next day, the supernatant was collected from each well and aliquoted in reaction tubes, then stored at -80˚C for quantification of IFN-γ, IL-6, IL-12 and IL-10.

2.14.4 Preparation of B16F10 tumour cell conditioned medium

B16F10 cells, a pigmented mouse melanoma cell line, were cultured in DMEM supplemented with 10% (v/v) fetal calf serum, 2mM L-glutamine, 100U/ml penicillin, 100 µg/ml streptomycin. When cells reached about 70% confluence, the medium was collected and centrifuged at 350g. The supernatant was filtered (0.2µm) to serve as the conditioned medium and was used fresh.

2.14.5 Perls' Prussian blue staining

Spleens from PWT/PKO and $LDLR^{-/-}$ mice were harvested and single cell suspensions were prepared by passing through a 70µM cell strainer followed by centrifugation for 5 minutes at 270g. After centrifugation, the supernatant was aspirated and the pellet was resuspended in 2ml of hypotonic 0.87% Tris-NH_4Cl (pH 7) followed by incubation for 2-3 minutes at room temperature to lyse the red blood cells. 10ml of PBS-1%FBS was added to neutralise the hypotonic solution followed by incubation for 2-3 minutes at room temperature to allow large pieces to sediment at the bottom of the tube. Then the suspension was aspirated and placed in a clean tube followed by centrifugation at 270g for 5 minutes. After that the supernatant was aspirated and the cells were transferred into a tissue culture plate for overnight incubation at 37 °C. The following day, the supernatant was discarded and cover slips with attached cells were washed with PBS two times. Then the coverslips were fixed with 4% formalin (w/v) followed by washing with PBS. After that the covers were immersed in a solution of 10% (w/v) of potassium ferrocyanide in water for 10 minutes followed by immersion in 10% HCL for 20 minutes and washing with PBS. The coverslips were counterstained with nuclear fast red for 10 minutes, followed by rinsing in distilled water. The cells were put in 95% alcohol and 2 changes of 100% alcohol followed by Xylene, 2 changes, 3 minutes each. Finally, slides were put in DPX with cover slips.

2.15 Detection of apoptotic cells in mouse melanoma

A commercial *in situ* apoptosis kit (ApopTag peroxidase kit, (S7100, Chemicon International, Inc., MA, USA) was used to detect apoptotic cells in tumour tissue sections. The procedure was carried out according to manufacturer's instructions with modification. This kit is a mixed molecular biological-histochemical system that allows sensitive and specific staining of very high concentrations of 3'-OH ends localised in apoptotic bodies unlike normal or proliferative nuclei, which have relatively insignificant numbers of DNA 3'-OH ends. DNA fragmentation results in the formation of new DNA ends typically localised in morphologically identifiable nuclei and apoptotic bodies. These DNA strand breaks in apoptotic cells are detected by reacting the free 3'-OH termini with modified nucleotides, whereas normal nuclei do not stain due to insignificant numbers of DNA 3'-OH ends. All incubation steps were carried out at room temperature unless otherwise indicated. In the beginning sections were dewaxed 2 times in xylene (2 minutes each), soaked 2 times in IMS (2 minutes each) and brought to water followed by washing in PBS. Afterwards sections were treated for 15 min with proteinase K (Sigma; St Louis,MO) (20pg/ml) to allow partial digestion of proteins from the nuclei followed by rinsing four times (2 min each) with deionized distilled water (DDW). Then the equilibration buffer was added directly on the section for 10 min followed by incubation for 1 hr at 37°C in the presence of TdT and digoxigenin-11 dATP. Next termination of the reaction was done by transferring the slides for 30 min at 37°C into the prewarmed stop/wash buffer. After washing in PBS containing 0.1% (w/v), chemically modified bovine serum albumin (BSA), then sections were incubated for 2 hr in the Fab fragment of sheep antidigoxigenin labeled with ultrasmall gold (Aurion) and diluted 1:30 in PBS. After washing in PBS and rinsing in PBS, the sections were post fixed for 10 min in 2% (v/v) glutaraldehyde in PBS. The nq"3 sections were thoroughly washed in DDW and the immunoreactivity was revealed by the Aurion R-Gent gold signal enhancement system. Then sections were washed in DDW and then flooded in AEC substrate until colour development (3-6 minutes). Afterwards the sections were rinsed 3 times in DDW (1 minute each) and counterstained with Methyl green for 3 minutes. After washing sections were washed with running tap water and cover slipped in pre-warmed glycerol jelly. The procedure included the use

of negative control in which proteinase K, the immunogold conjugate, or the mixture of nucleotides and TdT were omitted, these sections were counterstained with 0.5% (w/v) aqueous solution of Methyl Green Counterstain for Nuclei.

2.16 Statistical analyses

Statistical analyses and significance tests were performed using Prism 7 (GraphPad Software, Inc.) statistical software, whereas calculations were carried out using Excel 2013 (Microsoft Corp.). Two tailed, unpaired students T- test was used to determine the P value unless otherwise stated. Appropriate tests were used to calculate p values, with a significance level set at <0.05. Kaplan-Meier tests were used for survival curves.The statistical significance between results was denoted by either * ($P < 0.05$), ** ($P < 0.01$) or *** ($P < 0.001$).

Chapter 3 Characterisation of Bone Marrow Derived Macrophages (BMDM) from properdin-deficient and wildtype mice in their response to B16F10 *in vitro*

3.1 Introduction

The aim of this chapter is to characterise the macrophage response to conditioned medium from B16F10 cells. The hypothesis is that soluble products from B16F10 are able to influence the phenotype of macrophages and this response is modulated by complement properdin. For this reason, BM from PWT and PKO cultured in the presence of GM-CSF or MCSF with IL-4 will be incubated with medium prepared from B16F10 cultures. These *in vitro* experiments are expected to give insight into the changes that could occur in tumour microenvironment *in vivo.*

3.1.1 Macrophage expression markers

Macrophages (and their precursors, monocytes) are some of the major sentinels in the immune response. The diverse function of macrophages is mediated through cytokine receptors which are expressed on the surface, as well as inside the cell. It has been reported that the various macrophage functions are dictated by the type of receptor interaction on the macrophage and the presence of cytokines (Taylor et al. 2005). Both cell markers and functional activities contribute in defining the macrophage subpopulation. As with other mediators, the type of cytokines dictate whether macrophages will exhibit a proinflammatory or anti-inflammatory function (Arango Duque and Descoteaux, 2014).

One of the available murine macrophage expression markers is the antigen F4/80 which is an excellent marker for macrophage infiltration (Hume and Gordon, 1983). Mouse monocytes can be defined by the expression of the cell surface receptors Ly6C (known as Gr-1), CD43, CD11b and chemokine receptors CCR2 (Ziegler-Heitbrock et al., 2010, Tsou et al., 2007). High level of CD115 (M-CSF) expression aids in differentiation of blood monocytes from granulocytes and lymphocytes which also express CD11b (Mac-1). Another macrophage marker is CD11c which is expressed on many monocytic-derived cells, including macrophages.

Macrophages sense the different environmental cues and respond to activation stimuli by either the M1 or classical, and the M2 or alternative activation. Intracellular pathogens, lipoproteins, bacterial cell wall components, cytokines such as interferon gamma (IFN-γ) induce M1 activation. On the other hand, parasites, fungal cells, complement, macrophage colony stimulating factor

(MCSF), interleukin-4 (IL-4), IL-13, IL-10, tumour growth factor beta (TGF-β) induce M2 activation (Lin and Zhao, 2015, Roszer, 2015). Monocyte differentiation into macrophages involve the presence of granulocyte macrophage colony stimulating factor (GM-CSF) and macrophage colony stimulating factor (M-CSF) (Jaguin et al., 2013).

The classically activated (M1) macrophages are the effector cells in TH1 immune response. Both LPS and IFN-ɣ drive macrophages to polarise towards the M1 phenotype, resulting in large amounts of TNF, IL-12, and IL-23 and subsequently escalate the antigen specific cell inflammatory response. The effective pathogen elimination potential of M1 macrophages is characterised by up-regulation of enzymes, such as inducible nitric oxide synthase (iNOS) that generate nitric oxide from L-arginine (MacMicking et al., 1997). M1 macrophages can be characterised by the expression of high levels of inducible nitric oxide. Furthermore, secretion of the proinflammatory and T cell polarising cytokines (IL-1β,TNF-α, IL-12 and IL-23) and chemokines (CXCL9 and CXCL10) is a distinguishing signature of M1 macrophages following activation (Mosser and Edwards, 2008).

On the other hand, TH2 cytokines such as IL-4 drive macrophages to polarise towards the M2 phenotype resulting in high levels of IL-10 and IL-1RA, and low expression of IL-12. M2 macrophages dampen the immune response, clear parasitic infection and promote tumour progression. M2 macrophages express high levels of scavenger mannose and galactose receptors.

Arginase-1 is a prototypic M2 marker in mice. The murine Arginase-1 encoding gene contains elements that respond to the IL-4 induced transcription factor signal transducer and activator of transcription-6 (STAT-6) upstream of its promoter region, the transcription of which is amplified by IL-4, IL-13, and TGF-β. Another murine M2 marker is the Chitinase-3-Like Protein 3 or Ym1. This marker is expressed in alveolar, splenic and bone marrow macrophages, and microglia of the mouse. CD206 (C-Type Mannose Receptor 1) and CD163 (Hemoglobin-Haptoglobin Scavenger Receptor) are M2 macrophage markers. CD206, also known as MRC1 (C-type mannose receptor 1) is a M2 macrophage marker of both mice and humans. CD206 is proposed to have a role in the resolution of inflammation by clearing inflammatory molecules from the blood. CD163 is not restricted to M2 macrophages and hence should not solely be used as an identification marker for M2 macrophages. M2 macrophages also function

as antigen presenting cells and thus also express major histocompatibility complex-II (MHC-II).In this thesis, the function driven categorisation of M1 and M2 put forward by CH Mills is followed (Mills, 2015). Studies have proposed a number of maturation and activation regimens. One of the most widely used regimen involves the use of granulocyte macrophage colony-stimulating factor (GM-CSF) as a maturation factor, and IFN-γ, LPS, or a combination of these two mediators as activation factors for M1 induction. On the other hand, macrophage colony-stimulating factor (M-CSF) is used as a maturation factor and IL-4, IL-10, IL-13, or a mixture of these mediators are used as activation factors for M2 induction.

Another well-established protocol involves the use of GM-CSF/M-CSF for generation of classical (M1) and alternative (M2) macrophages followed by priming with LPS for both phenotypes (Fleetwood et al., 2007).

3.1.2 Melanoma tumour cells

Isolated from C57BL/6J mouse melanocytes, B16F10 is a widely used model in cancer research. It is thought that the poorly immunogenic nature of B16F10 is attributed to low basal expression of the surface molecules MHC Class I, B7-1 and Intercellular Adhesion Molecule 1 (ICAM-1), regard which are important for Cytotoxic T lymphocytes recognition (CTL). In this, B16F10 resemble human melanoma cells which are weak immunogens and have low/undetectable expression of receptors required for activation of naïve CTL.Their expression of complement components is not known.

3.2 Results

3.2.1 characterisation of B16F10 tumour cells

The first step in this project was to characterise the cell line used for tumour implantation which is B16F10.

3.2.1.1 Production of complement components

The aim of this experiment was to characterise B16F10 cell line regarding the expression of C3, C5 and properdin prior to start of *in vivo* experiments. This was carried out by PCR and the results showed that B16F10 cells express C3 and C5 mRNA (as shown in Figure 11 A i and ii). However, no expression for properdin was detected (3.2.1.1 A iiii). To test production at the protein level, B16F10 cells were analysed for properdin and Factor B by Western blot. The membrane was probed with goat anti human/mouse/rat Factor B, sc-34888, and detected with Donkey anti goat Fab, HRP conjugated, sc-3851 and the result was negative. B16F10 were also negative for properdin using rabbit anti human properdin antiserum (Gift Prof B Sim), while human serum gave the expected 53kDa band (data not shown). Furthermore, this Western blot was repeated by loading higher concentration of B16F10 lysate (25μg) and the result also showed no expression of properdin (data not shown). The expression of properdin by B16F10 was re-investigated using PCR and the results showed no expression (data not shown). The aforementioned data indicate either that properdin was below the limit of detection under our experimental conditions or that B16F10 tumour cells do not synthesize properdin.

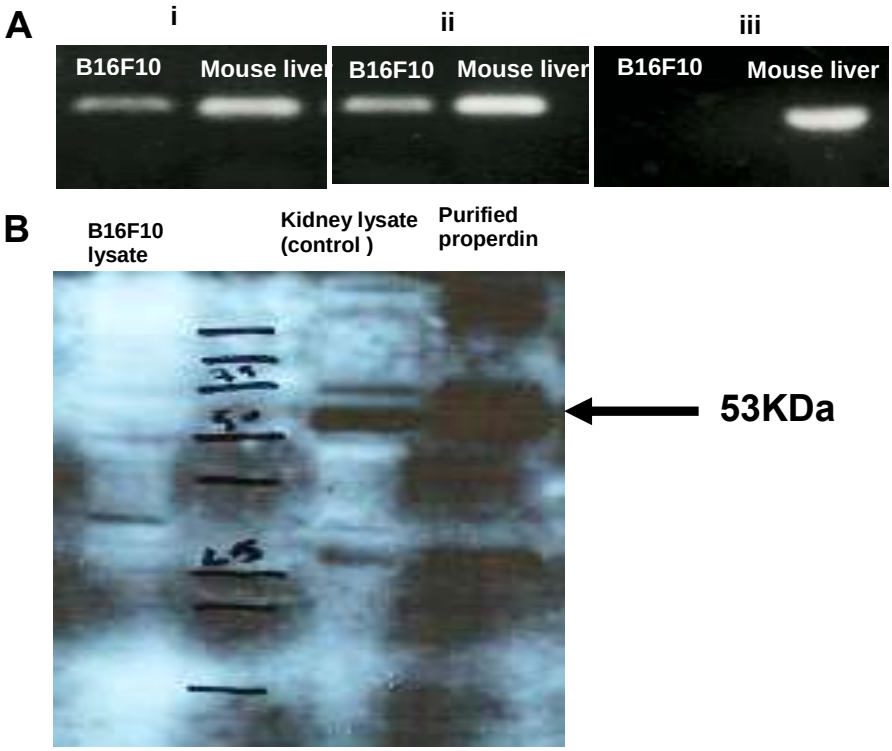

Figure 11: Expression of C3, C5 and properdin in B16F10 cells by PCR

A-Gel image of RT-PCR product using mouse liver, liver/WT. RT-PCR products obtained using B16F10 cell line and mouse PWT Liver cells, (i) C5 (ii) C3, (iii) properdin Lane1: B16F10, Lane:2. Sizes were as expected for C5, 540 bp, C3 gene, 500 bp,and properdin 360bp. Mouse Liver from PWT was used as a control. The experiment was repeated two times.

B-Western blot analysis of properdin was performed by loading 20µg of B16F10 and kidney lysate (control) per well onto a SDS-PAGE gel and 20ug of tumour cell lysate per well onto a SDS-PAGE gel. Proteins were transferred to a PVDF membrane and blocked with 5% non-fat milk in TBST for 1 hour at room temperature. Proteins were transferred to a PVDF membrane and blocked with 5% non-fat milk in TBST for 1 hour at room temperature. The membrane was probed with monoclonal anti-human properdin Ab at a dilution of 1:200 overnight at 4°C, washed in TBST, and probed with an HRP-conjugated goat anti-mouse IgG secondary (DAKO) at a dilution of 1: 5,000 for 1 hour at room temperature. Chemiluminescent detection was performed using ECL substrate. Films were exposed for 1min.

3.2.2 Cytochemical screen of B16F10-mediated effect on macrophage phenotype Perl's Prussian Blue.

During the last few years, the importance of macrophages in tissue iron homeostasis has been recognised (Gaetano et al., 2010). Polarisation of macrophages leads to differential iron management: M1 macrophages possess an iron storage phenotype (coinciding with their antibacterial activity), while M2 macrophages increase iron availability to tissues and can be characterised by low iron content (Gaetano et al., 2010). Thus, assessing iron deposition in splenocytes isolated from wildtype and properdin deficient mice was used to give a preliminary indication whether the genotypes were differently skewed towards M1or M2 type cells. Splenocytes from wildtype and properdin deficient mice were cultured in the presence and absence of B16F10 supernatant. Iron deposition in stimulated and unstimulated splenocytes from both genotypes was assessed by Perls' Prussian blue staining. This stain involved treatment of splenocytes in acid solution of ferrocyanides. Ferric ion (+3) in splenocytes combines with the ferrocyanide and subsequently forms a bright blue pigment called 'Prussian blue'' or ferric ferrocyanide. Figure 12 shows the percentage of Perls' Prussian blue Stained splenocytes. No comparative difference was found between splenic macrophages from wildtype and properdin deficient mice. On the other hand, a statistically significant difference was found between B16F10 stimulated and unstimulated splenocytes from both genotypes. There were iron positive cells within the adherent fraction when cells were incubated with B16F10 conditioned medium.

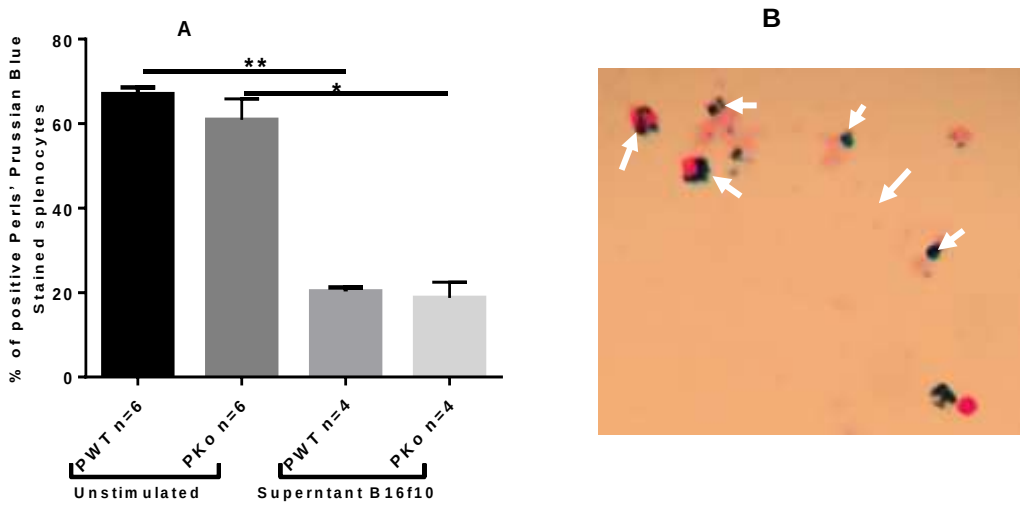

Figure 12 : Percent of positive Perls' Prussian blue stained splenocytes.

Splenocytes from wildtype and properdin deficient mice were harvested. Then the splenocytes were placed on a coverslip (one coverslip/mice) and each coverslip was cultured on a seperate well of a 6 well plate. Then the cells were stimulated with B16F10 supernatant for 24 hrs. After that attached cells were stained with Prussian blue and examined under the microscope. Then coverslips were blindly selected and 400-500 cells were manually counted in each coverslip. The percentage of positive cells was calculated (A): the percentage of Prussian blue stained cells (B) Representative image under the microscope (100X) showing positive (Blue) and negative (red) cells. Data are expressed as mean±SEM, n= number of mice used from each genotype, * ($P < 0.05$), ** ($P < 0.01$).

3.2.3 mRNA expression study for mouse BMDM

BMDM were used as an *in vitro* model to investigate polarisation of activated macrophages in the tumour microenvironment because of the greater numbers that can be obtained compared to spleen. Culturing of mouse BMDM in the presence of GM-CSF/M-CSF leads to differentiation of these cells which can be followed for M1 or M2 skewing on stimulation. LPS stimulates macrophages towards M1 phenotype, while M2 polarisation is favoured by IL-4. In addition, B16F10 supernatant was used to stimulate BMDM from both genotypes in an attempt to investigate whether this stimulation would skew BMDM towards M1 or M2 phenotype. Quantitative RT-PCR was used to measure changes in cytokine production (and cell signalling pathways) associated with macrophage polarisation. M1 and M2 macrophages exhibit a distinct biomarker profile and some of these markers can be used to define M1 and M2 polarisation. M1 produce high levels of pro-inflammatory cytokines (IL-6, IL-1β, and TNF-α),

whereas M2 macrophages can be characterised by an anti-inflammatory cytokine signature such as IL-10. In addition, Arg-1 and MCP-1 are regarded as M2 markers, while iNOS is associated with M1 macrophages (MacMicking et al., 1997).

3.2.3.1 Analysis of B16F10- mediated skewing of BMDM from naïve mice by qPCR.

Cytokine production and pro-inflammatory/inhibitory molecule expression in BMDM were used to investigate macrophage polarisation in wildtype and properdin deficient naïve mice. For evaluation of BMDM phenotype, qPCR was used to measure mRNA expression of IL-6, IL-1β, iNOS and TNF-α as markers for M1 macrophages(Mosser and Edwards, 2008), while IL-10, Arginase-1 and MCP-1 were used as markers for M2 macrophages. The results represented by Figure 13 showed that stimulation of BMDM with GM-CSF and LPS, M-CSF and IL-4 or B16F10 supernatant did not result in any significant difference in expression of IL-6 between both genotypes. B16F10 supernatant resulted in low expression of IL-6 in both genotypes. On the other hand, wildtype cells showed upregulation of IL-1β in all three stimuli, but only reached statistical difference compared with PKO mice in B16F10 supernatant stimulated cells (P=0.0159). Figure 13 also demonstrated that GM-CSF and LPS stimulation resulted in significant upregulation of iNOS in wildtype cells when compared to properdin deficient cells (P=0.0328). Surprisingly, stimulation with B16F10 supernatant did not result in any upregulation of iNOS in both genotypes. No significant difference between PWT and PKO was seen in TNF-α expression in any of the stimulations, though LPS and B16F10 conditioned medium were able to upregulate TNFα mRNA. No difference was seen in IL-10 expression between both genotypes, but B16F10 conditioned medium increased IL-10 mRNA expression considerably. Expression of Arginase-1 was significantly higher in properdin deficient cells when compared to PWT cells when stimulated with B16F10 conditioned medium (P=0.0328). In addition, MCP-1 expression was upregulated in properdin deficient cells compared to PWT cells after stimulation with GM-CSF and LPS or B16F10 supernatant, with a statistical significant difference between genotypes (P=0.0172). Based on the results of the *in vitro* analyses of mRNA gene expression in BMDM after stimulation, which showed that PWT cells had high

level of IL-1β post B16F10 stimulation and high level of iNOS post LPS stimulation, it would be reasonable to conclude that PWT cells show a more M1 skewed immune response. In contrast to PWT, PKO cells showed more arginase and MCP-1 mRNA expression upon B16F10 stimulation. Comparison between stimulation with LPS, IL-4 and B16F10 supernatant revealed that stimulation with the latter gave results mostly similar to when cells were stimulated with IL-4 indicating that B16F10 supernatant skews the immune response towards an M2 macrophage phenotype.

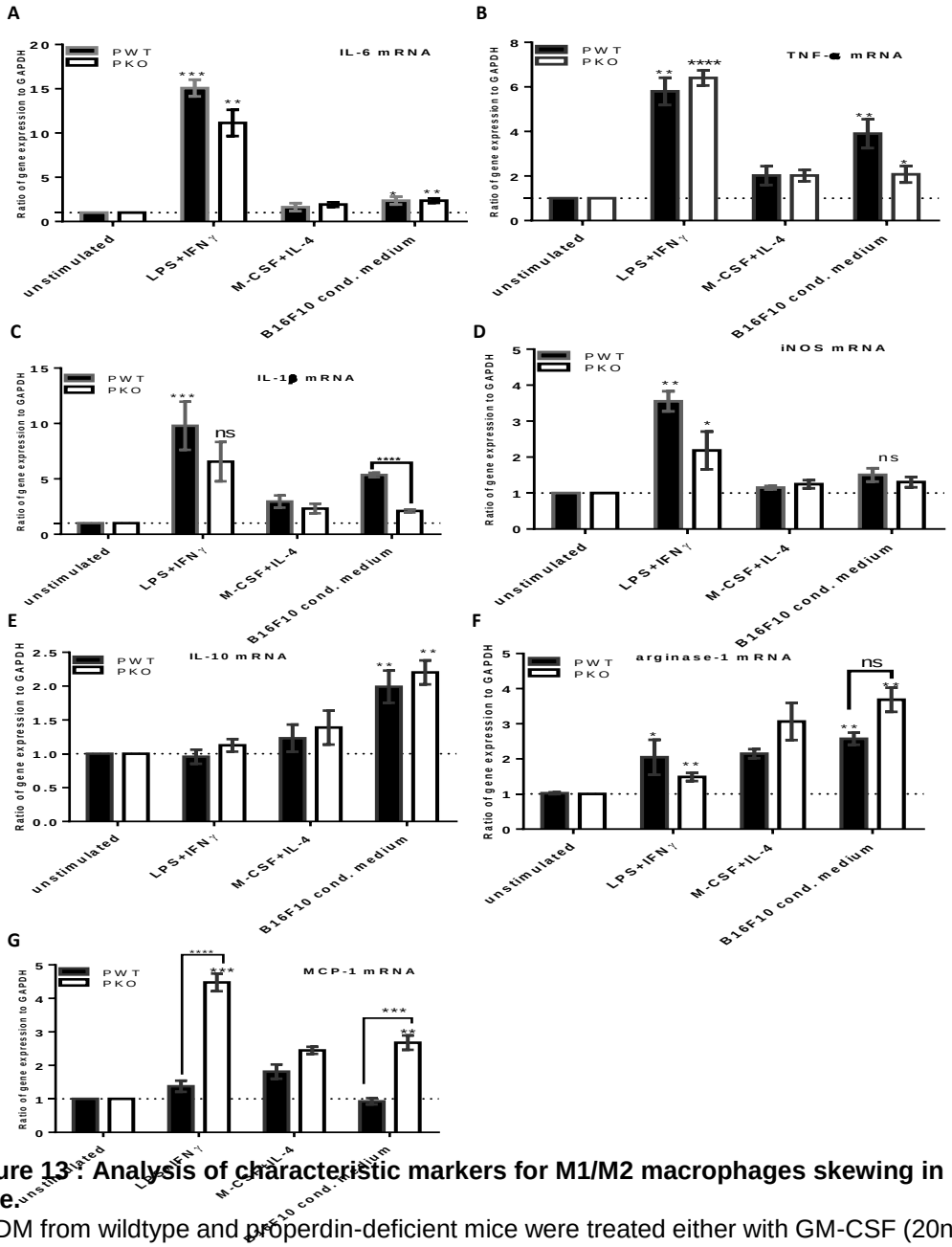

Figure 13 : Analysis of characteristic markers for M1/M2 macrophages skewing in naïve mice.

BMDM from wildtype and properdin-deficient mice were treated either with GM-CSF (20ng/ml) or M-CSF (10 ng/ml) for 7 days. The cells were then stimulated with LPS (100ng/ml +IFN-γ (20ng/mL) or IL-4 (20ng/ml), or with B16F10 supernatant respectively. mRNA was prepared for quantitative real time PCR (RT-qPCR) to quantify gene expression of IL-6, IL-1β, iNOS, TNF-α, IL-10, arginase-1 and MCP-1 in comparison with GAPDH gene expression. ΔΔCT value were used, the mRNA expression corrected for GAPDH and compared with unstimulated BMDM. The QPCR results represent at least three experiments, each set up in duplicate. The data are presented as means ±SEM. Statistical analysis was performed by using ANOVA and Student t-test (significances on top of columns compare to the respective unstimulated controls). * ($p < 0.05$).

3.2.3.2 Analysis of B16F10- mediated skewing of BMDM from wildtype and properdin deficient tumour bearing mice by qPCR.

Due to the distinctive difference between PWT and PKO cells in their response to stimulation seen in 3.2.3.1, mRNA expression in BMDM of tumour bearing mice from both genotypes was carried out. It was assumed that macrophage

phenotype would adapt to the tumour within 14 days of injection with B16F10, and therefore both genotypes would have similar macrophage phenotype, reflecting the results of tumour size measurement which showed no significant difference in tumour burden between genotypes. Because of the absence of significant difference between genotypes when stimulated with IL-4 (as shown in 3.2.3.1), the present experiment was set up to compare between stimulated and unstimulated B16F10 cells without the inclusion of LPS or IL-4 stimulation as with 3.2.3.1.

The phenotype of BMDM from wildtype and properdin deficient tumour bearing mice was investigated using qPCR. This was done by stimulating the cells with B16F10 supernatant and measuring mRNA expression of IL-6 and TNF-α as markers for M1 macrophages, while IL-10 and Arginase-1 as markers for M2 macrophages. The aim of this experiment was to investigate whether the tumour microenvironment was proinflammatory or anti-inflammatory. The results presented in Figure 14 showed no significant difference in expression of IL-6 between both genotypes. Expression of TNF-α and iNOS was higher in wildtype mice when compared to properdin deficient mice (P=0.0047 and 0.0223 respectively). On the other hand, cells of properdin deficient mice had significant upregulation of Arg-1 when compared to cells from wildtype mice (P=0.0101). Altogether, stimulation with B16F10 supernatant resulted in increased expression of the investigated markers when compared to unstimulated cells. Surprisingly, stimulation resulted in higher expression of TNF-α and iNOS in cells from PWT tumour bearing mice, indicating of more M1 macrophage phenotype. Furthermore, arginase was higher in PKO tumour bearing mice, indicating M2 phenotype. This apparent discrepancy between tumour size, which had a tendency towards larger size PWT, and macrophage polarisation might be attributed to the fact that *in vitro* stimulation may not necessary modulate the *in vivo* environment. *In vivo* experimentation of maximum 14 days is relatively short and may only allow macrophages to manifest themselves in tumour before an adaptive immune response to this low immunogenic tumour can be innocent. BMDM from PKO mice clearly showed a M2 phenotype, whilst PWT mice showed a M1 phenotype.

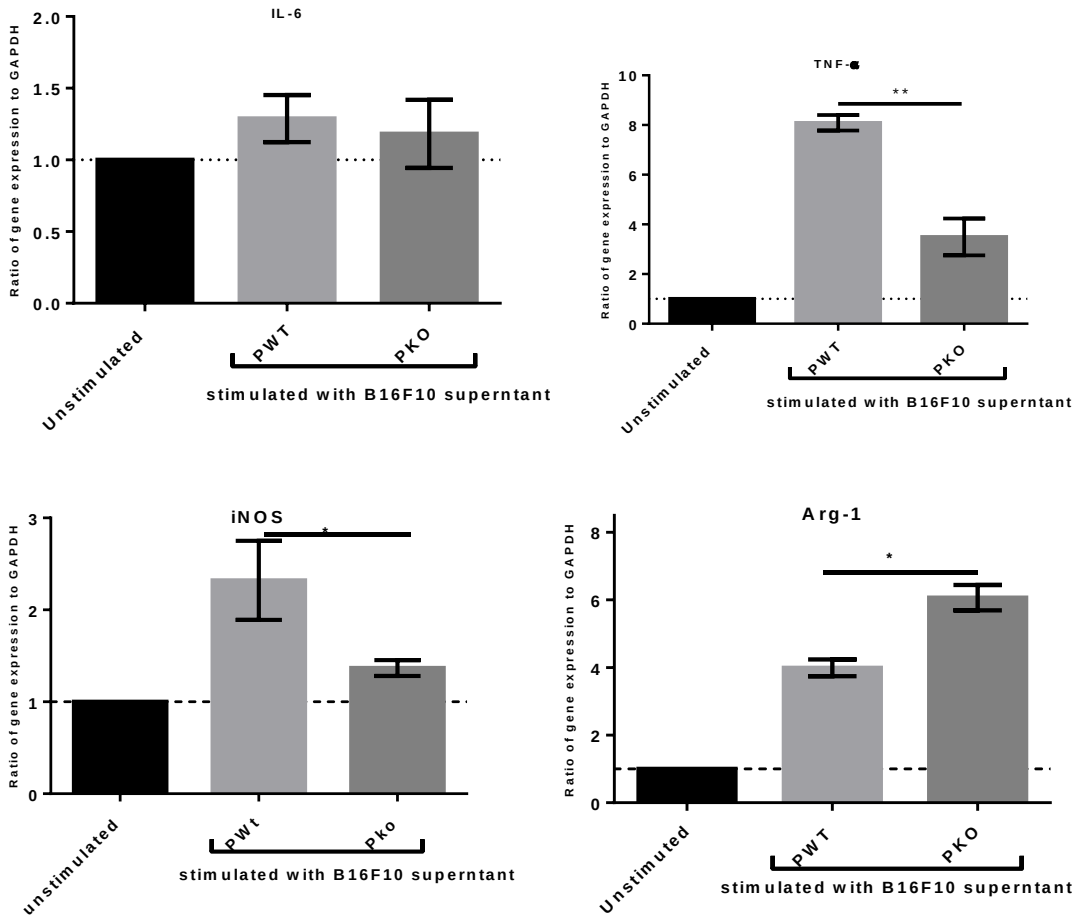

Figure 14 : Analysis of characteristic markers for M1/M2 macrophage in tumour bearing mice.

BMDM from tumour bearing wildtype and properdin-deficient mice were differentiated with M-CSF (10ng/ml) for 7 days. Then the cells were stimulated with B16F10 supernatant, unstimulated cells were used as a control. Quantitative real time PCR (RT-qPCR) was used to quantify gene expression of IL-6, TNF-α, iNOS and arginase-1 compared with GAPDH gene expression. ΔΔCT value were used, the mRNA expression corrected for GAPDH and compared with unstimulated BMDM. The QPCR results represent at least three experiments, each set up in duplicate. The data are presented as means ±SEM. Statistical analysis was performed by one-tailed Mann-Whitney U test. * ($p < 0.05$).

3.2.4 Quantitative measurement of Cytokines from stimulated BMDM of wildtype and properdin deficient mice.

Studying *in vitro* stimulation of macrophages helps in understanding how macrophages respond to different stimuli such as infection, injury or tumour, and measuring cytokine profile during stimulation is helpful in this regard. In order to investigate the level of cytokines, BMDM cells were prepared from wildtype and properdin-deficient mice and cultured with GM-CSF for 48hrs and then cells were stimulated with conditional medium which includes B16F10 supernatant, LPS (100ng/ml) or IL-4 (20ng/ml). Measurement of cytokines was carried out by ELISA to investigate whether the cytokine signature is shaped in a properdin dependent manner after stimulation, and to confirm the previous results of mRNA expression studies which showed that PWT cells seems to polarise towards a more M1 phenotype, and B16F10 stimulation resulted in a more M2 polarisation, with the PKO cells being more M2 phenotype.

IFN-γ and IL-12 were chosen to evaluate further the profile of inflammatory reaction observed in BMDM by qPCR (3.2.3.1). IFN-γ is atypical (type 2 cytokine) and IL-12 is a C5a enhance of macrophage activity. The role of properdin on the level of pro-inflammatory mediators IFN-γ and IL-12 was investigated in supernatant of BMDM. This was done in LPS, IL-4 and B16F10 stimulated cells. Figure 15 shows that release of IFN-γ in supernatant of BMDM from properdin deficient mice stimulated with B16F10 supernatant was lower compared to wildtype mice (P=0.0235). No significant difference between genotypes was seen in IFN-γ release when cells were stimulated either with LPS or IL-4. Stimulation with LPS resulted in the highest secretion of IFN-γ in both genotypes.

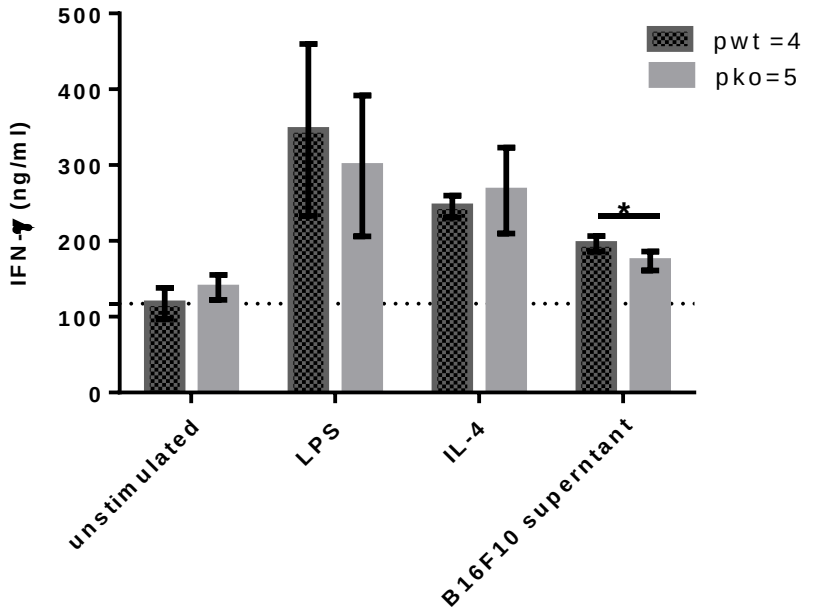

Figure 15: Level of mouse IFN-γ in supernatant of BMDM after stimulation

BMDM from wildtype and properdin-deficient mice were treated with GM-CSF (20ng/ml) for 7 days. Then the cells were stimulated either with LPS (100ng/ml), IL-4 (20ng/ml) or B16F10 supernatant. Unstimulated cells were used as controls. Supernatant was used for measurement IFN-γ by ELISA. Results represent at least four experiments each set up in duplicate. The data are presented as means ±SEM. Statistical analysis was performed by one-tailed Mann-Whitney U test. * $(\mathrm{p} < 0.05)$.

Figure 16 shows that stimulation with either IL-4 or B16F10 supernatant resulted in comparable levels of IL-12 between both genotypes, but compared to properdin deficient mice, cells from wildtype secreted more IL-12 upon stimulation with LPS (P=0.0041).

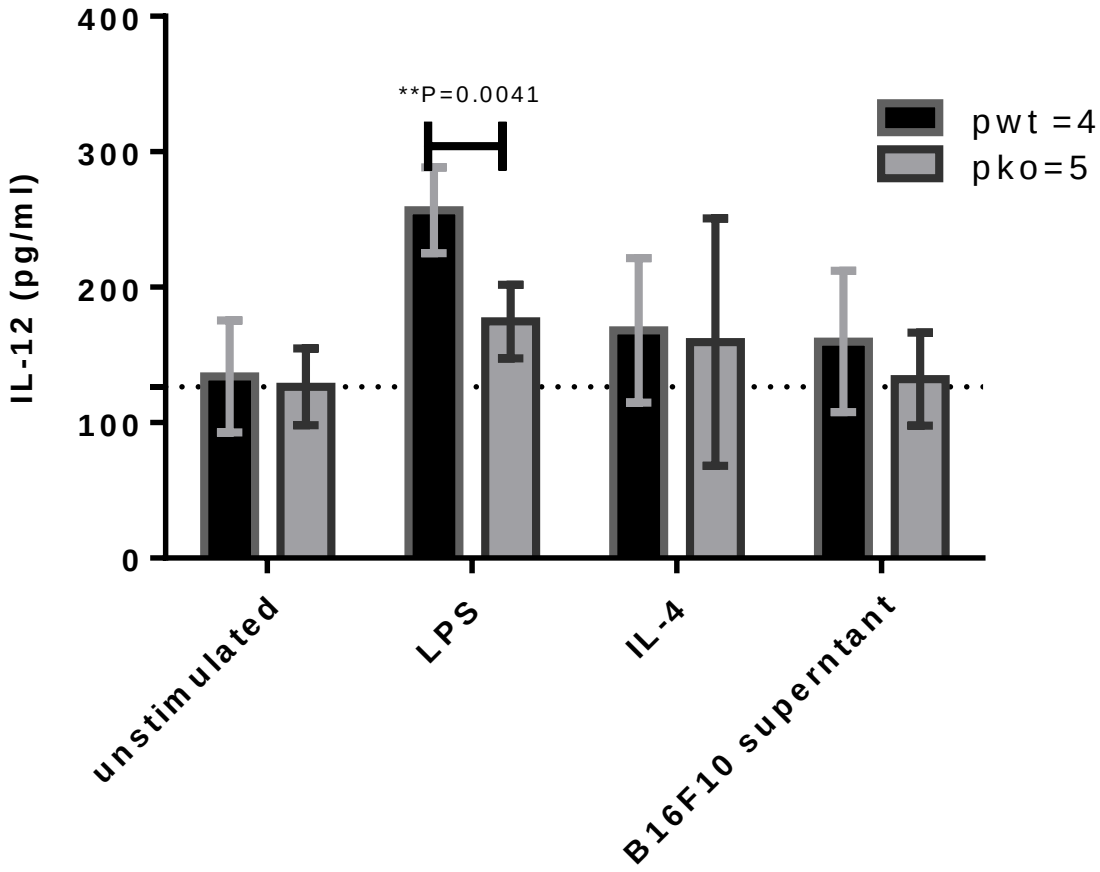

Figure 16: Level of mouse IL-12 in supernatant of BMDM after stimulation.

BMDM from wildtype and properdin-deficient mice were treated with GM-CSF (20ng/ml) for 7 days. Then the cells were stimulated either with LPS (100ng/ml)+ 20ng/ml of INF-ɣ), IL-4 (20ng/ml) or B16F10 supernatant. Unstimulated cells were used as control. Supernatant was used for measurement IL-12 by ELISA. Results represent at least four experiments each set up in duplicate. The data are presented as means ±SEM. Statistical analysis was performed by one-tailed Mann-Whitney U test. * ($p < 0.05$).

The role of properdin on level of IL-10 secreted from BMDM isolated from properdin wildtype and deficient mice after stimulation was investigated and the results are presented in Figure 17. This experiment shows that cells from properdin deficient mice secreted a significantly higher level of the anti-inflammatory cytokine IL-10 after stimulation with B16F10 supernatant when compared to wildtype (P=0.0220). Stimulation with either LPS or IL-4 did not result in any difference in level of IL-10 between genotypes.

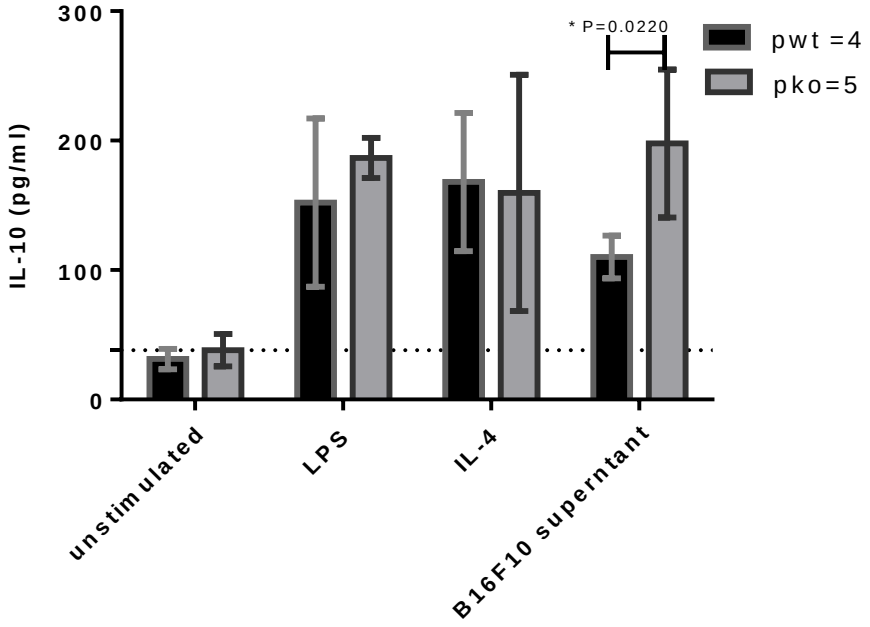

Figure 17: Level of IL-10 in supernatant of GM-CSF differentiated BMDM.

BMDM from wildtype and properdin-deficient tumour bearing mice were differentiated with GM-CSF (20ng/ml) for 7 days. Then the cells were stimulated either with LPS (100ng/ml)+ 20ng/ml of INF-ɣ, IL-4 (20ng/ml) or B16F10 supernatant respectively. Unstimulated cells were used as controls. Supernatant was used for measurement of IL-10 by ELISA. Results represent at least four experiments each set up in duplicate. The data are presented as means ±SEM. Statistical analysis was performed by one-tailed Mann-Whitney U test. * $(p < 0.05)$.

3.2.4.1 Quantitative measurement of IL-10 in BMDM supernatant after stimulation of Naïve PWT and PKO Mice with GM-CSF or M-CSF.

The level of IL-10, after differentiation of bone marrow cells into macrophages in the presence of GM-CSF or M-CSF, and following stimulation was investigated. This experiment was also aimed to validate the current protocol of using GM-CSF and M-CSF which lead to polarisation of BMDM. The results presented in Figure 18 revealed that stimulation resulted in higher levels of IL-10 in M-CSF differentiated cells when compared to GM-CSF differentiated cells. Furthermore, IL-10 was significantly higher in M-CSF differentiated and B16F10 stimulated cells from PKO mice when compared to wildtype cells (P=0.0286). Surprisingly, no significant difference was found between wildtype and properdin deficient mice when cells were M-CSF differentiated and stimulated either with LPS or IL-4. LPS stimulation of GM-CSF differentiated bone marrow cells seems to result

in a marginal increase in level of IL-10 in properdin deficient mice when compared to wildtype.

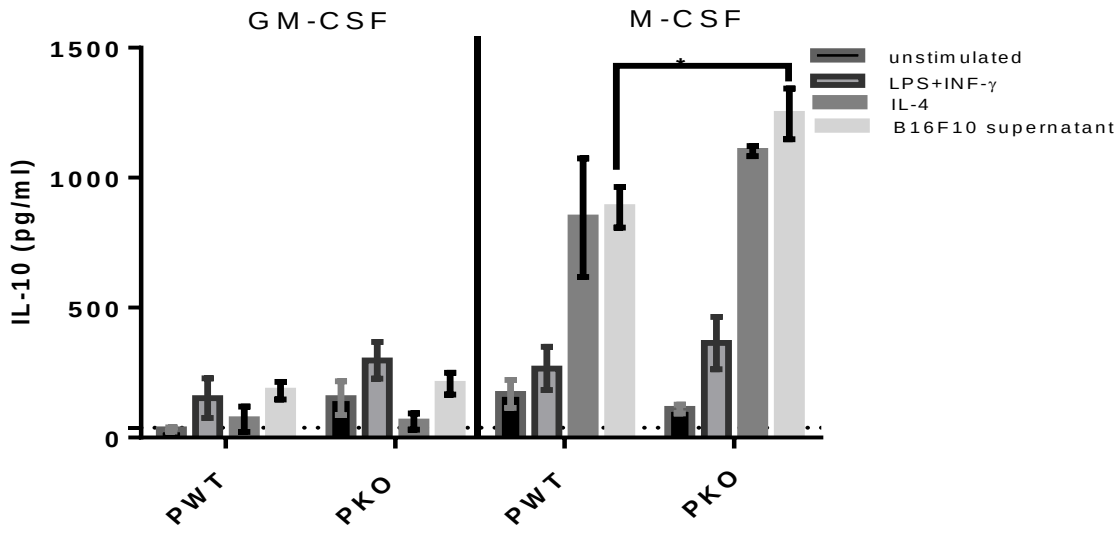

Figure 18 : Level of IL-10 in supernatant of BMDM cultured with GM-CSF/M-CSF after stimulation.

BMDM from wildtype (n=5) and properdin-deficient (n=4) male mice were differentiated either with GM-CSF (20ng/ml) or M-CSF (10ng/ml) for 7 days. Then the cells were stimulated either with LPS (100ng/ml)+ 20ng/ml of INF-ɣ, IL-4 (20ng/ml) or B16F10 supernatant respectively, unstimulated cells were used as controls. Supernatant was used for measurement of IL-10 by ELISA. Results represent at least four experiments each set up in duplicate. The data are presented as means ±SEM. Statistical analysis was performed by one-tailed Mann-Whitney *U* test. * ($p < 0.05$).

3.2.5 Characterisation stimulated BMDM by Flow cytometry.

3.2.5.1 Surface markers in BMDM of wildtype and properdin deficient tumour bearing mice.

Surface markers were studied to further characterise the cells which showed increase in mRNA expression and cytokine levels after B16F10 stimulation. Additionally, the influence of properdin on surface markers signature of BMDM in tumour bearing mice was investigated. These investigations were done to assess if stimulation with B16F10 supernatant exerted any change in surface markers of BMDM with GM-CSF in tumour bearing mice.

3.2.5.1.1 CD11b and Gr-1 from BMDM from tumour bearing mice

CD11b together with CD18 makes up CR3 on macrophage which bind iC3b and C3dg (Bajic et al., 2013). CD11b is commonly expressed on granulocytes and monocytes/macrophages. Gr-1 is a glycosylphosphatidylinositol (GPI)-linked protein expressed on granulocytes and macrophages. Granulocyte differentiation and maturation in bone marrow correlates with the level of Gr-1 expression. Transient expression of Gr-1 is found in the monocyte lineage of the bone marrow and these Immature Myeloid Gr-1+ cells were linked with the development of antitumour immunity (Chen et al., 2001).

The expression of surface markers CD11b and Gr-1 was investigated in BMDM of tumour bearing mice from both genotypes after stimulation, and the results are shown in Figure 19. This figure show that in both genotypes, stimulation did not result in a comparable difference in expression of CD11b. Notably, the percent of $CD11b^+$ cells was around 60-70% when M-CSF was used for differentiation of BMDM from tumour bearing mice (data not shown). On the other hand, the percent of BMDM from tumour bearing mice expressing CD11b was around 90% when GM-CSF was used for differentiation. B16F10 stimulation led to higher percent of Gr-1 in properdin deficient mice when compared to wildtype (10.5 and 2.8% respectively).

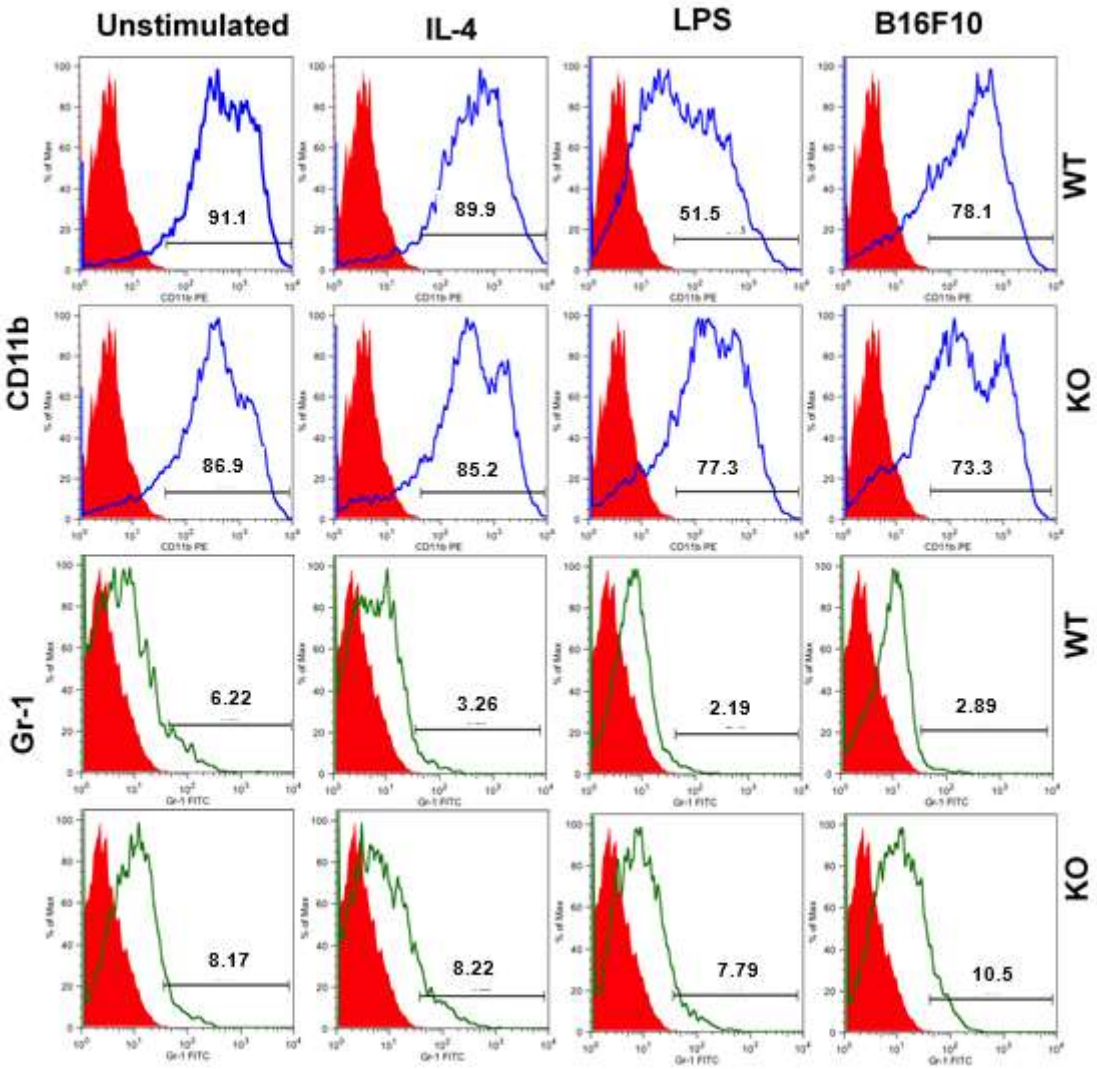

Marker (MFI)		Unstimulated	IL-4	LPS	B16F10 supernatant
CD11b	PWT	462	437	44	225
	KO	342	345	173	216
Gr-1	PWT	8.89	3.7	6.05	6.17
	KO	9.02	3.92	9.49	9.55

Figure 19: Expression of CD11b and Gr-1 in BMDM of tumour bearing wildtype and properdin deficient mice after stimulation.

Macrophages from wildtype and deficient tumour bearing mice were differentiated *in vitro* with GM-CSF for eight days and then stimulated either with LPS (100ng/ml), IL-4 (20ng/ml) or B16F10 supernatant for 24 hours. Unstimulated cells were used as controls. Samples were stained for the expression of Gr-1 FITC and CD11b PE. The above results represent pooled BMDM sample where n= 4 in Wildtype and n=5 in properdin deficient mice. The filled histogram is the isotype control. Table show mean fluorescence intensity for CD11b and Gr-1.

3.2.5.1.2 CD11c and F4/80 BMDM Cells from tumour bearing mice

CD11c is part of the CD11c/CD18 leukocyte integrin CR4 which binds iC3b and ICAM-1. F4/80 belongs to adhesion G protein coupled receptor family and is a marker of murine macrophages. Expression of cell surface markers CD11c and F4/80 BMDM was also investigated. The first is expressed in dendritic cells and monocytes/macrophages, while F4/80 is widely used as a murine macrophage marker. The aim of the experiment was to evaluate levels of expression of BMDM from tumour bearing mice in response to different stimuli. The results represented by Figure 20 show that stimulation with B16F10 supernatant did not change expression of CD11c. Furthermore, no difference in CD11c expression was found between genotypes. On the other hand, stimulation with IL-4 or B16F10 supernatant resulted in down regulation in expression of F4/80 in both genotypes.

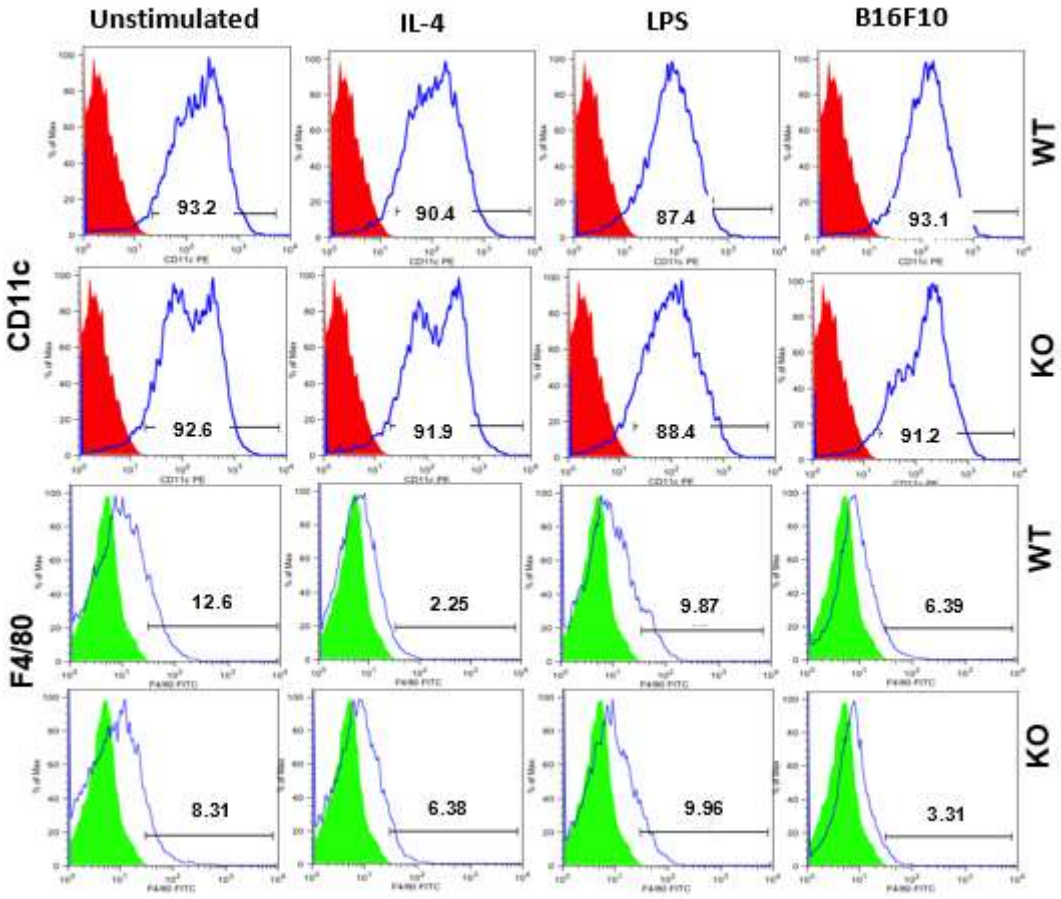

Marker (MFI)		Unstimulated	IL-4	LPS	B16F10 supernatant
CD11c	PWT	171	107	78.6	128
	KO	125	139	92.4	150
F4/80	PWT	7.51	5.33	6.71	7.45
	KO	6.12	5.7	7.08	6.94

Figure 20: Expression of CD11c and F4/80 in BMDM of tumour bearing wildtype and properdin deficient mice after stimulation.
Macrophages from wildtype and properdin deficient tumour bearing mice were *in vitro* differentiated with GM-CSF for eight days and then stimulated either with LPS (100ng/ml), IL-4 (20ng/ml) or B16F10 supernatant for 24 hours. Unstimulated cells were used as controls. Samples were stained for the expression of F4/80 FITC and CD11c PE. The above results represent pooled BMDM sample where n= 4 in wildtype and n=5 in properdin deficient mice. Table show mean fluorescence intensity for CD11c and F4/80.

3.2.5.1.3 Percentage of Gr-1+CD11b+ cell in BMDM of Wildtype and properdin deficient tumour bearing mice.

The aim of this experiment was to investigate the percentage of $CD11b^{+}Gr\text{-}1^{+}$ cells in BMDM of wildtype and properdin deficient tumour bearing mice after stimulation with B16F10 supernatant as an indicator of MDSCs. Previous *in vivo* results had shown that wildtype mice have high percentage of MDSCs ($CD45^{+}CD11b^{+}Gr\text{-}1^{+}$) in spleen compared to propedin deficient tumour bearing mice (see Chapter 4). Figure 21A shows that the percentage was 12.5 in properdin deficient mice and 6.9 in wildtype mice after stimulation with B16F10.

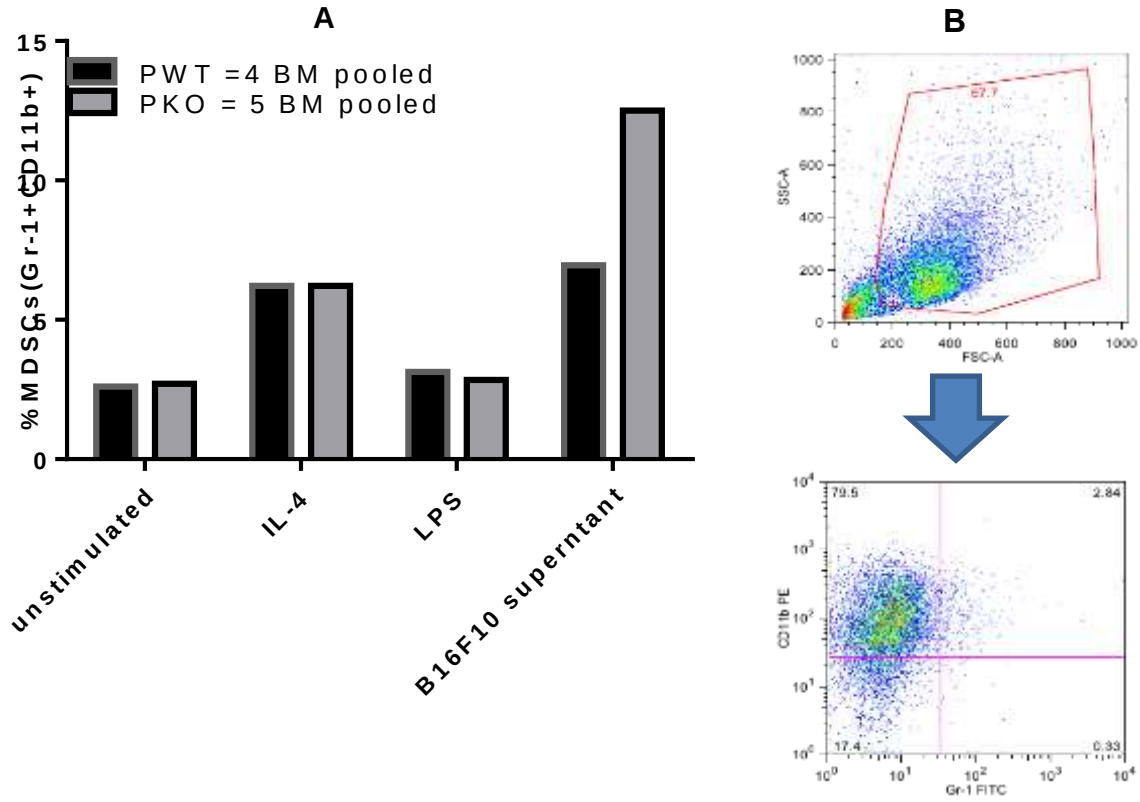

Figure 21: A-Expression of MDSCs(CD11b+Gr-1+) in BMDM of tumour bearing PWT and PKO mice after stimulation. B-repesentive dot plot of CD11b+Gr-1 after gating on main population.

Macrophages from wildtype and deficient Tumour bearing mice were differentiated *in vitro* with GM-CSF for eight days and then stimulated either with LPS (100ng/ml), IL-4 (20ng/ml) or B16F10 supernatant for 24 hours. Unstimulated cells were used as controls. Samples were stained for the expression of Gr-1 FITC and CD11b PE. The above results represent pooled BMDM sample where n= 4 in Wildtype and n=5 in properdin deficient mice.

3.2.5.1.4 CD80, MHC-II and CD86 from tumour bearing mice

The expression of surface markers, CD80, CD86 and MHC-II was investigated. CD80 is constitutively expressed non-dendritic cells and monocytes/macrophages, while CD86 and MHC-II are expressed on antigen presenting cells. Both CD80 and CD86 are co-stimulatory molecules that result in enhanced cell activation, proliferation, and cytokine production of T cells upon ligation with CD28. As with others, the expression of these molecules was used as an indication of M1 macrophages. Figure 22 showed that B16F10 stimulation resulted in lower expression of CD80 in both wildtype and properdin deficient mice (9.7 and 6.4% respectively). On the other hand, LPS stimulation lead to increased expression of CD80. Comparable expression of MHC-II was found in both stimulated and unstimulated BMDM from both genotypes. Nevertheless, BMDM from tumour bearing wildtype mice seems to show higher expression of MHC-II when compared to properdin deficient mice. Expression of CD86 was similar in both genotypes, however B16F10 stimulation seems to result in down regulation of CD86 expression.

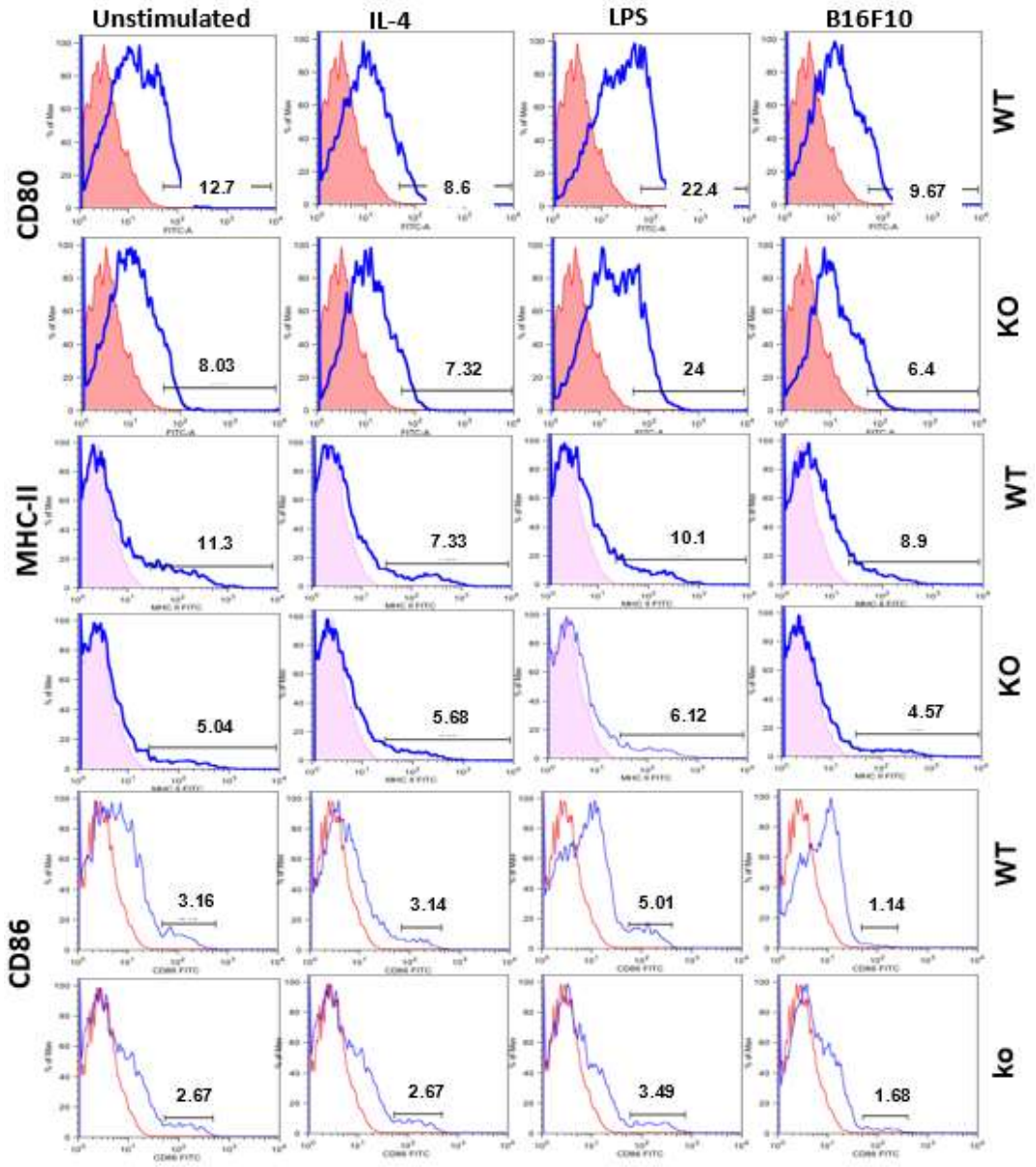

Marker (MFI)		Unstimulated	IL-4	LPS	B16F10 supernatant
CD80	PWT	7.35	5.31	9.76	6.96
	KO	5.33	6.29	8.18	6.35
MHC-II	PWT	10.53	7.43	9.73	9.17
	KO	6.44	6.22	8.55	3.22
CD86	PWT	126	131	143	75.7
	PKO	75	117	174	119

Figure 22: Surface receptor expression (CD80, MHC-II and CD86) of polarised macrophages.

Macrophages from wildtype and deficient Tumour bearing mice were *in vitro* differentiated with GM-CSF for eight days and then stimulated either with LPS (100ng/ml), IL-4 (20ng/ml) or B16F10 supernatant for 24 hours. Unstimulated cells were used as controls. Samples were stained for the expression of MHC-II FITC and CD80 deficient mice. Table show mean fluorescence intensity for CD80, MHC-II and CD86.

3.2.5.2 Surface and Intracellular markers in BMDM of naïve mice

The aim of these experiments was to characterise BMDM cells from naïve mice of the two genotypes in their ability to adapt their expression of cell surface markers and products to the stimulation of B16F10 conditioned medium, and whether one genotype is able to do this more or less than the other.

3.2.5.2.1 CD80, MHC-II and CD86 from naïve mice

In this section cells from BM PWT/PKO and LDLR$^{-/-}$ were investigated in parallel. CD80, CD86 and MHC II are important costimulatory molecules for T cell stimulation. Flow cytometry analysis was carried out to investigate the percent of CD80, CD86 and MHC-II in BMDM cells of PWT and PKO naïve mice after stimulation. These investigations were done on a pooled sample of BM cells to give preliminary data on the level of expression of CD80, CD86 and MHC-II after stimulation with LPS, IL-4 and B16F10 supernatant. Figure 23 demonstrate that expression of these markers was upregulated after stimulation with LPS in both genotypes. Additionally, stimulation with IL-4 showed no difference between genotypes in expression of CD80, CD86 and MHC-II. Interestingly, BMDM cells from PKO mice showed less expression of the aforementioned markers after B16F10 stimulation compared to BMDM cells from PWT mice after B16F10 stimulation. Therefore, further investigations into the expression of CD80, CD86 and MHC-II after B16F10 stimulation were carried out using BM cells from individual naïve mice from PWT and PKO, as well as LDLR$^{-/-}$ mice. These investigation demonstrated that BMDM cells from PWT cells showed frequent expression of CD80, CD86 and MHC-II (25.33± 1.56%, 23.03±1.398 % and 22.97±2.643% respectively) when compared to PKO (16.29±2.268%, 13.76±2.723% and 8.660 ±1.389%), whereas, BMs cells from LDLR$^{-/-}$ group showed similar levels of expression (Figure 24). Notably, comparison between PWT cells from PWT/PKO group with its respective counterpart in LDLR group showed that both had similar expression of the aforementioned markers.

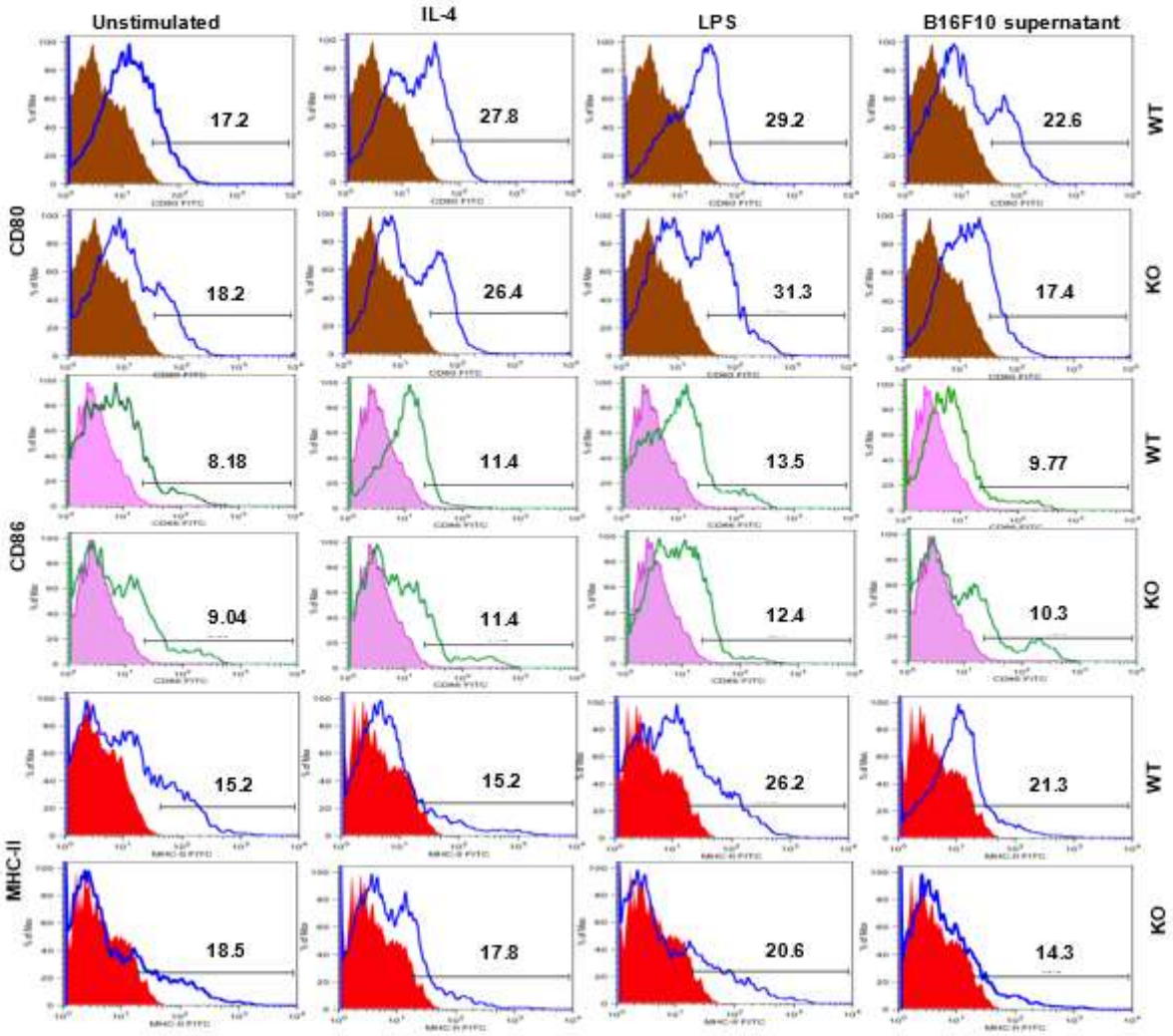

Marker (MFI)		Unstimulated	IL-4	LPS	B16F10 supernatant
CD80	PWT	11.1	17.8	19.9	12.6
	KO	7.38	18.1	20.4	11.7
MHC-II	PWT	2.42	3.41	8.58	7.11
	KO	3.01	4.49	7.33	6.93
CD86	PWT	4.61	4.39	9.57	8.31
	PKO	2.58	4.99	6.19	5.51

Figure 23 : Surface receptor expression (CD80, MHC-II and CD86) of macrophages.
BMDM from wildtype and properdin deficient mice. Cells were differentiated with GM-CSF for eight days and then stimulated either with LPS (100ng/ml), IL-4 (20ng/ml) or B16F10 supernatant for 24 hours. Unstimulated cells were used as controls. Samples were stained for the expression of MHC-II FITC and CD80 FITC. The above results represent pooled BMDM sample where n= 3 in Wildtype and n=3 in properdin deficient mice. Table show mean fluorescence intensity for CD80, MHC-II and CD86.

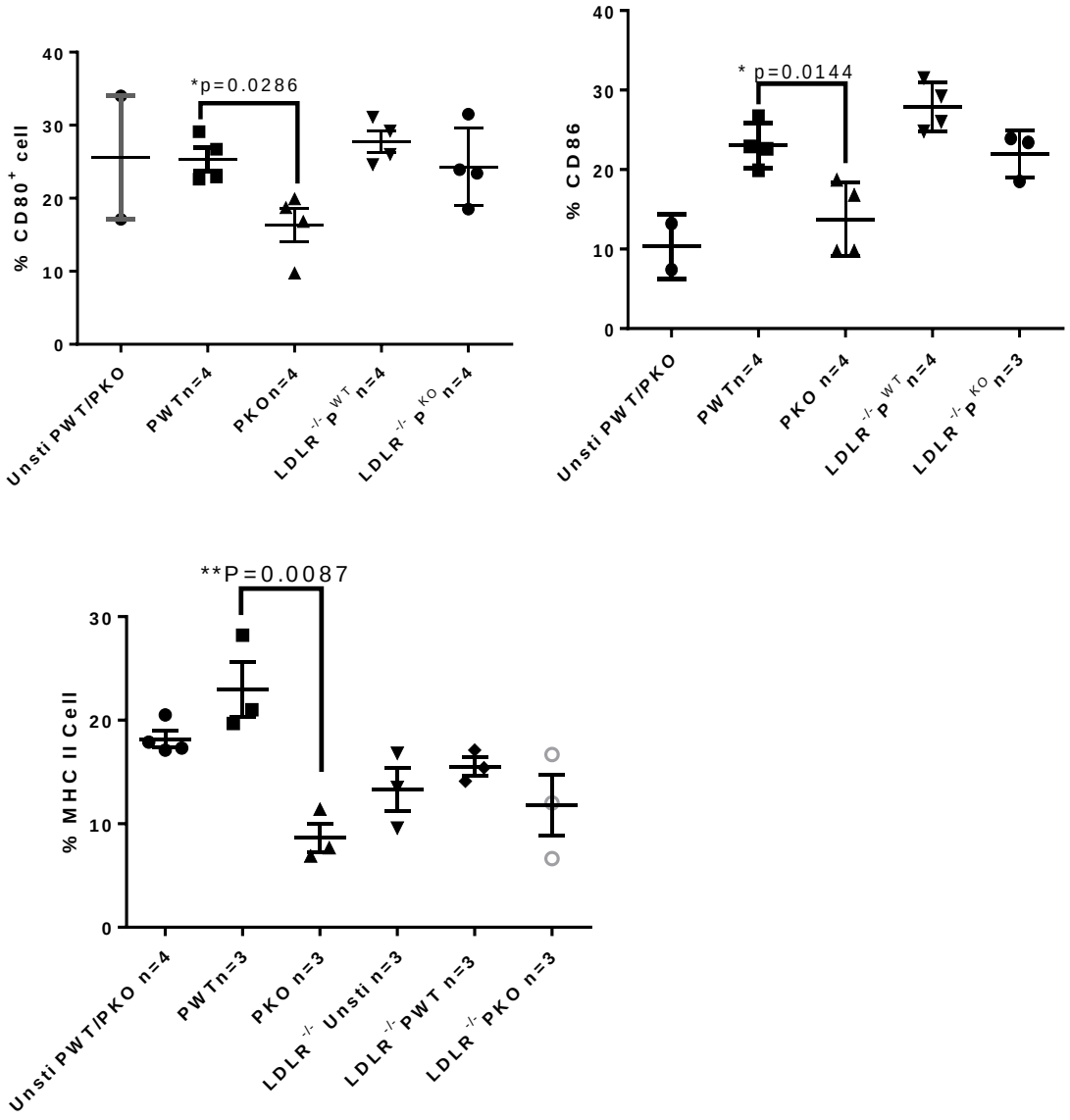

Figure 24: Surface receptor expression (CD80, MHC-II and CD86) of macrophages from naïve mice.

BMDM from PWT/PKO and LDLR$^{-/-}$ mice were differentiated with GM-CSF for eight days and then stimulated with B16F10 supernatant for 24 hours. Unstimulated cells were used as controls. Samples were stained for the expression of MHC-II FITC and CD80 FITC.

3.2.5.2.2 FACS analysis of CD11b+F4/80

3.2.5.2.3 BMDM from PWT and PKO with M-CSF.

The F4/80 antigen is expressed by a majority of mature macrophages and is the best marker for this population of cells. Expression of F4/80 commences during early myeloid development and is upregulated on all BM cells stimulated *in vitro* with M-CSF. One of the most important antigens used to identify murine macrophages is the F4/80 pan–macrophage marker. The results presented in Figure 25 showed no difference between B16F10 supernatant stimulated and unstimulated cells in expression of F4/80 expression. Additionally, no significant difference was found between genotypes.

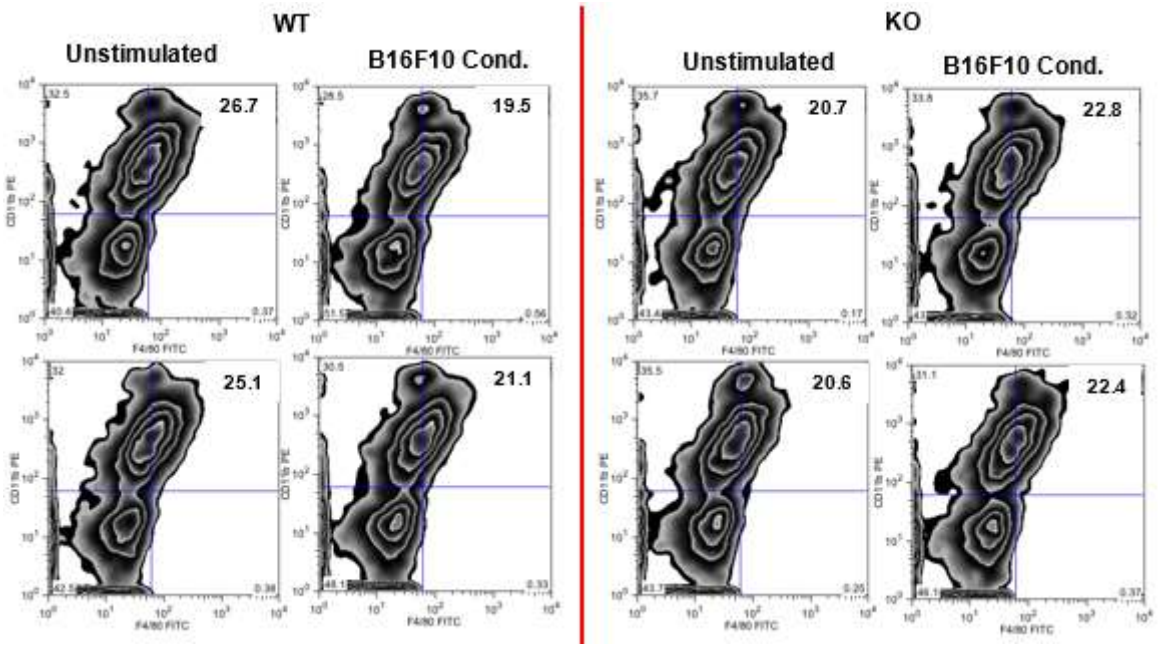

Figure 25: Expression of CD11b+F4/80 in BMDM of wildtype and properdin deficient mice after stimulation with B16F10 supernatant.

Macrophages from wildtype and properdin deficient Tumour bearing mice were *in vitro* differentiated with M-CSF for 7 days and then stimulated with B16F10 supernatant for 24 hours. Unstimulated cells were used as controls. Samples were stained for the expression of F4/80 FITC and CD11b PE. The results represent a pooled BMDM sample in which n= 3 for each genotypes. The above and the bottom panels represent dublicates of the same pooled sample which have been stimulated independently.

3.2.5.2.4 BMDM from LDLR-/-PWT and LDLR-/-PKO with GM-CSF.

The aim of this experiment was to investigate the effect of B16F10 supernatant on BMDM polarisation from both genotypes. Data illustrated by Figure 26 shows that BMDM in the presence of B16F10 supernatant are skewed towards M2 in $LDLR^{-/-}P^{WT}$ mice. FACS analysis of unstimulated BMDM showed that 11.9% were $CD11b^{+}$ F4/80+. In contrast to 6.44% in cells stimulated with B16F10 supernatant. On the other hand, this effect was not seen in $LDLR^{-/-}P^{KO}$.

It was noted that the ratio between M1/M2 was 2.5 in $LDLR^{-/-}P^{WT}$. In contrast to 5 in $LDLR^{-/-}P^{KO}$. The aforementioned results provide two pieces of evidence that M2 phenotype in BMDM was high in $LDLR^{-/-}P^{WT}$ when compared to $LDLR^{-/-}P^{KO}$.

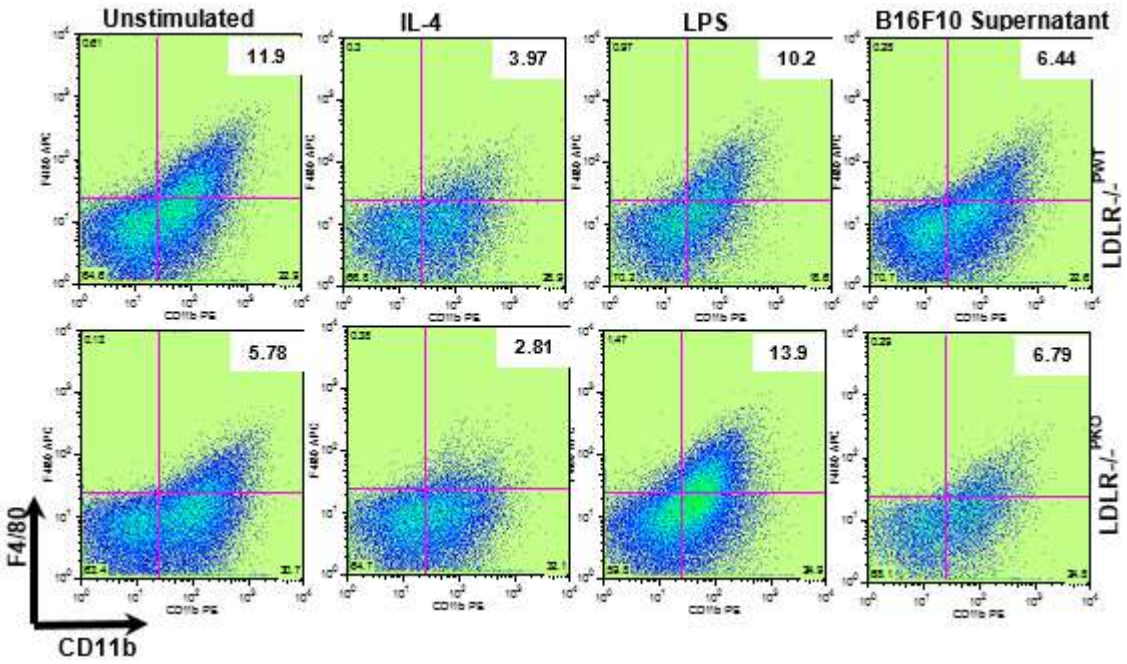

Figure 26: FACS analysis (CD11b+F4/80+) of BMDM derived from $LDLR^{-/-}P^{WT}$ and $LDLR^{-/-}P^{KO}$ mice in response to different stimuli.

Bone marrow derived macrophages prepared from $LDLR^{-/-}$ wildtype and properdin deficient mice were cultured with GM-CSF for 24hrs with LPS (100ng/ml), IL-4 (20ng/ml) or B16F10 supernatant. BMDM were analysed CD11b +F4/80.

3.2.5.2.5 Expression of CD206 and CD11b in differentiated BM cells of naïve mice after stimulation.

In addition to cytokine release, distinct macrophage phenotypes can also be characterised by differential expression of key surface markers.

$CD206^+CD11b^+$ have been previously used as an indication of M2 polarised macrophages. Hence, the percentage of $CD206^+CD11b^+$ cells was investigated after GM-CSF differentiation and stimulation. Figure 27C show the percentage of $CD206^+CD11b^+$cells in PWT/PKO group of mice which revealed that B16F10 stimulation resulted in a significantly higher percentage of $CD206^+CD11b^+$ cells in properdin deficient mice when compared to wildtype (P=0.0228). Figure 27D show the percentage of $CD206^+$CD11b positive cells in $LDLR^{-/-}$ group after stimulation with IFN-ɣ, LPS and B16F10 supernatant. In addition to LPS stimulation, IFN-ɣ was used as another option for M1 stimuli. This was done as stimulation with IL-4 did not show difference between genotypes in PWT/PKO group. Similar to PWT/PKO mice, B16F10 stimulation resulted in higher percentage of $CD206^+CD11b^+$ cells in properdin deficient mice when compared to wildtype. Interestingly, unstimulated cells from $LDLR^{-/-}$ group showed higher percentage of $CD206^+CD11b^+$ cells than those of PWT/PKO group (mean 7.5 vs 3.2% respectively) mostly indicating that $LDLR^{-/-}$ group possess more $CD206^+$ cells.

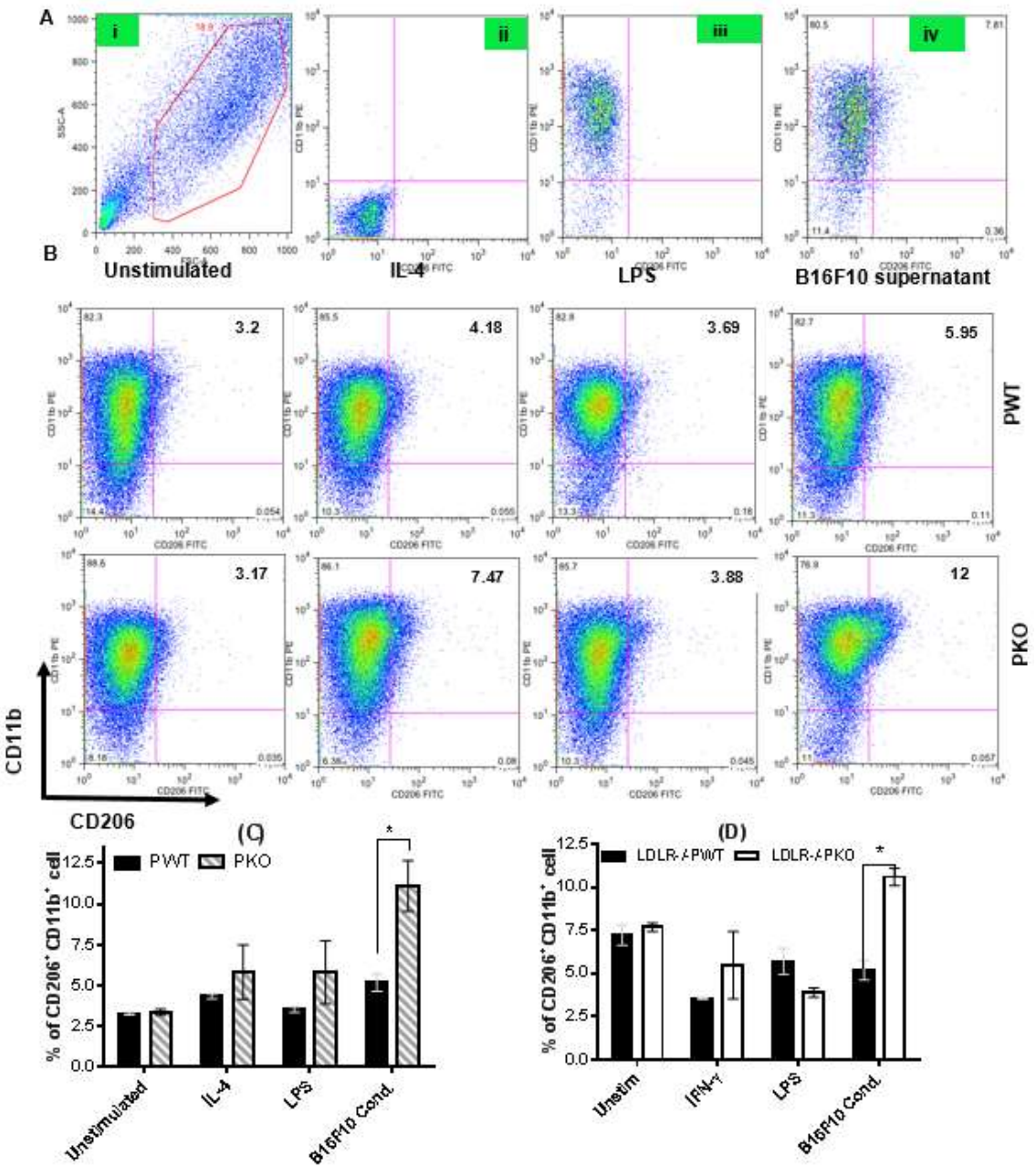

Figure 27: Expression of CD206 and CD11b in GM-CSF differentiated BMDM cells of naïve mice after stimulation.

A-Strategy of FACS analysis of $CD11b^{+}CD206^{+}$ cell i-gating on the main macrophage population, ii-unstained cells. iii-Single stain for only CD11b+ cell labelled with PE fluorochrome iv-double positive cell CD11b+CD206. B. representive dot plot for $CD11b^{+}CD206^{+}$ in different conditioned medium. (C) BMDM from wildtype and properdin-deficient mice cells, and (D) $LDLR^{-/-}$ group were differentiated with GM-CSF (20ng/ml) for 7 days. Then the cells were stimulated either with LPS (100ng/ml), IL-4 (20ng/ml) or B16F10 supernatant. Unstimulated cells were used as controls. After that cells were stained with CD206 FITC and CD11b PE and then FACS was done. Results represent three independent experiments. The data are presented as means ±SEM. Statistical analysis was performed by one-tailed Mann-Whitney U test. * ($P < 0.05$).

Expression of CD206 and CD11b was also investigated in M-CSF differentiated BM cells from wildtype and properdin deficient naïve mice following stimulation with B16F10 supernatant. The aim of this experiment was to investigate the percentage of these cells in the presence of M-CSF which is traditionally used to differentiate macrophages into an M2 phenotype. The results represented by Figure 28 showed that the percentage of $CD206^+$ and $CD11b^+$ cells is about 15. Notably, stimulation with B16F10 resulted in upregulation of this surface marker. However, no difference was found between the two genotypes probably due to shifting of cells towards M2 macrophage phenotype. Interestingly, differentiation with M-CSF resulted in higher percentage of CD206 and $CD11b^+$ cells as opposed to the numbers reported when GM-CSF was used for differentiation (15 % and 3.2 % respectively).

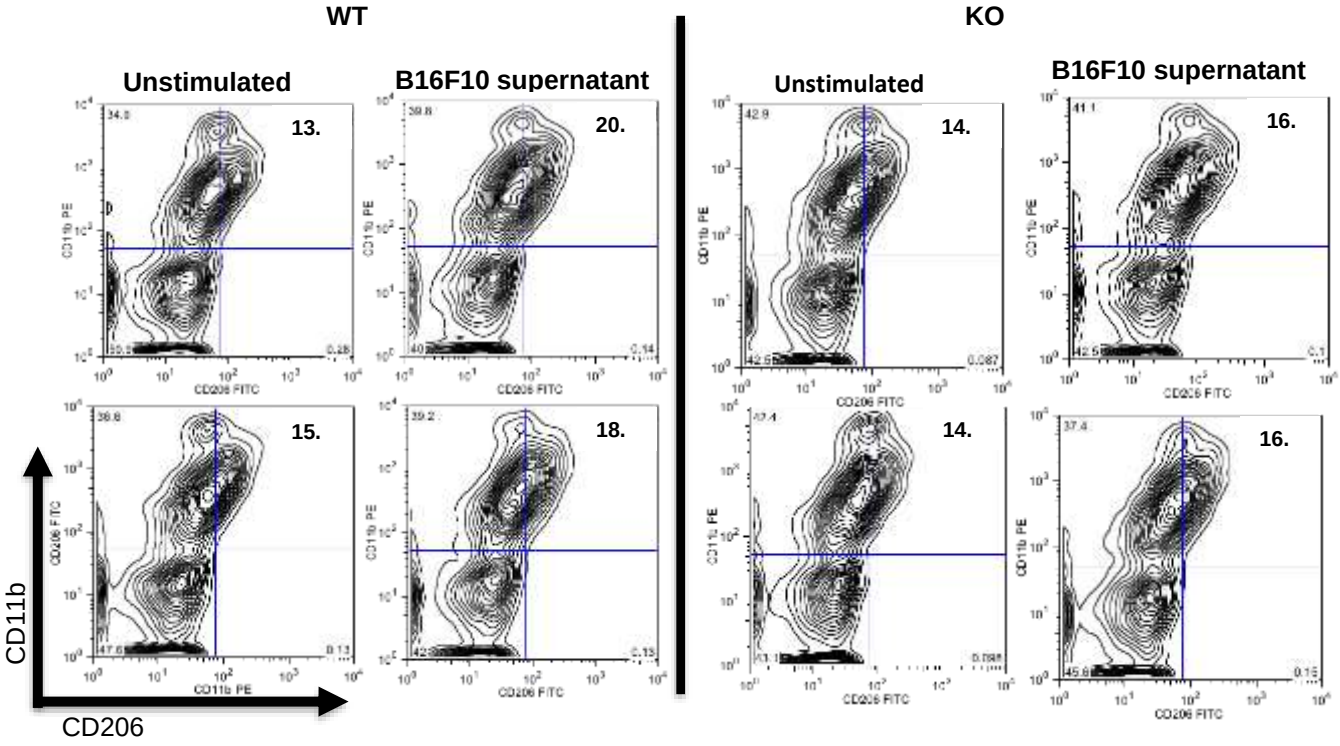

Figure 28: Expression of CD206 and CD11b in M-CSF differentiated BMDM cells of naïve mice after stimulation.

BMDM from PWT and PKO (n=2) mice were treated with M-CSF (20ng/ml) for 7 days. Then the cells were stimulated with B16F10 supernatant. Unstimulated cells were used as controls. FACS samples were collected without or with stimulation and samples were stained for the expression of $CD11b^+CD206$. Pooled samples were used in this experiment n= 3 for each genotype.

In addition to GM-CSF and M-CSF, supernatant of L929 cells producing M-CSF (Weischenfeldt and Porse, 2008) was also used to differentiate BM cells followed by flow cytometry analysis of CD206 and $CD11b^+$ cells. It has been previously reported that supernatant of L929 cells is a rich source of M-CSF (Weischenfeldt and Porse, 2008), hence this supernatant was used to provide a source of M-

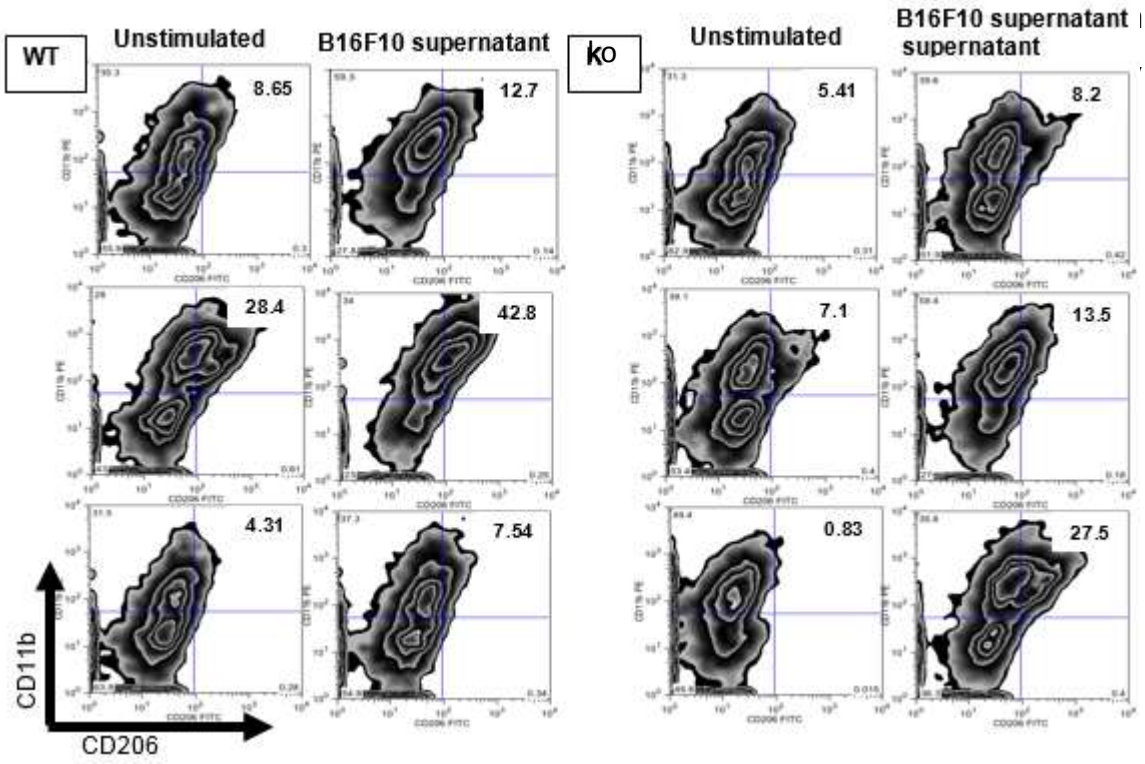

Figure 29: Expression of CD206 and CD11b in 20% L929 supernatant differentiated BMDM cells of naïve mice after stimulation.

BMDM from PWT and PKO mice were grown in culture dishes in the presence of M-CSF for 7 days, which is secreted by L929 cells and is used in the form of L929-conditioned medium (20%). Then the cells were stimulated with B16F10 supernatant. Unstimulated cells were used as controls. Samples were collected before and after stimulation and Samples were stained for the expression of $CD11b^+CD206$.

3.2.5.2.6 Change of intracellular cytokines (IL-12 and IL-10) in GM-CSF differentiated BMDM of naïve mice.

IL-12 is a pro-inflammatory cytokine secreted mainly by monocytes, macrophages, and dendritic cells. This cytokine is produced as a response to bacterial products such as LPS, intracellular pathogens, or upon interaction with activated T cells, and subsequently results in proliferation, differentiation and maintenance of T helper 1 (Th1) responses that lead to IFN-ɣ and IL-2 production. Both of IFN-ɣ and IL-2 mediate macrophage activation and T cell response.

As shown in Figure 30 stimulation with LPS and B16F10 supernatant resulted in higher percentage of $CD11b^{+}IL\text{-}12^{+}$ cells in PWT (5.69% and 6.72% respectively) compared to PKO mice (1.97% and 1.37% respectively). The unexpected finding of high $CD11b^{+}IL\text{-}12^{+}$ cells in BMDM of wildtype upon B16F10 stimulation may be indicative of mixed population of BMDM after differentiation with GM-CSF. Thus it seems that the M1 phenotype macrophages predominate in wildtype cells even after stimulation with B16F10 supernatant, which is expected to elicit a M2 phenotype.

Percentage of $CD11b^{+}IL\text{-}12$ was detectable in wildtype and properdin deficient mice. However, percentage of $CD11b^{+}IL\text{-}12^{+}$ cells $LDLR^{-/-}P^{WT}$ and $LDLR^{-/-}P^{KO}$ was low and no difference was seen between the genotypes after stimulation with B16F10 supernatant. On the other hand, stimulation with LPS resulted in high percentage of $CD11b^{+}IL\text{-}12^{+}$ cells in $LDLR^{-/-}P^{WT}$ compared to PKO mice (3.45% and 0.87% respectively).

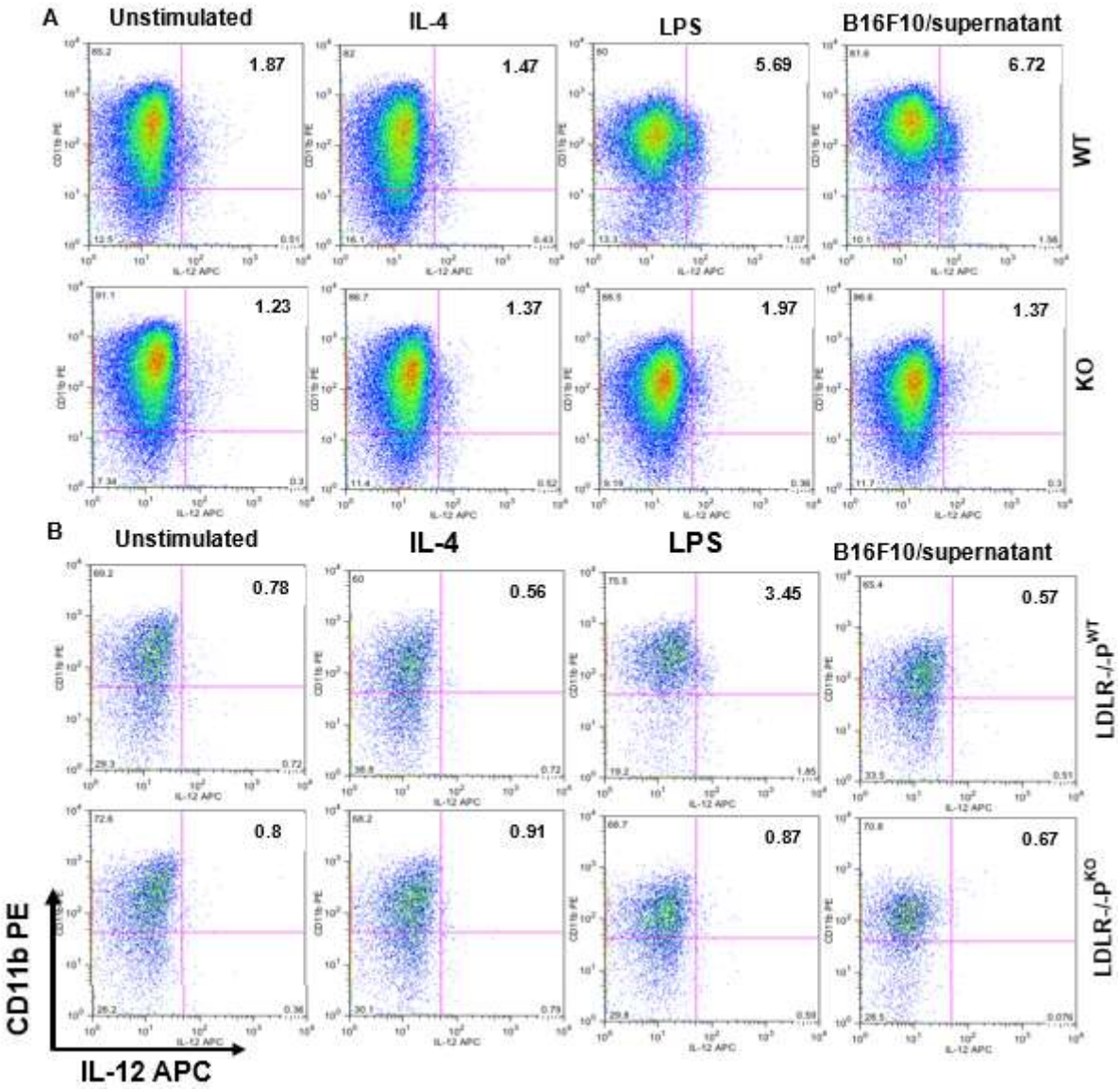

Figure 30: Surface receptor expression of polarised macrophages and intracellular IL-12 staining.

A-BMDM of PWT and PKO. B-BMDM of LDLR$^{-/-}$P^{WT} and LDLR$^{-/-}$P^{KO}. BMDM from wildtype and properdin-deficient mice were treated with GM-CSF (20ng/ml) for 7 days. Then the cells were stimulated either with LPS (100ng/ml), IL-4 (20ng/ml) or B16F10 supernatant. Unstimulated cells were used as controls. Samples were collected before and after stimulation and samples were stained for the expression of CD11b+IL-12.

IL-10 is produced by activated immune cells, it is one of the key anti-inflammatory cytokines. IL-10 exerts its action via a transmembrane receptor complex which is composed of IL-10R1 and IL-10R2. Activation of macrophages by various endogenous as well as exogenous mediators such as bacterial lipopolysaccharide lead to the secretion of IL-10 which in turn result in

suppression of the inflammatory immune response. The important role of IL-10 lies in its ability to restrict the specific and unspecific immune reactions and induction of tolerance.

Stimulation with B16F10 supernatant resulted in high percentage of $CD11b^{+}IL\text{-}10^{+}$ cells PKO in compared to PWT mice. Percentage of $CD11b^{+}IL\text{-}12^{+}$ cells PWT and PKO was low and no difference was seen between the genotypes.

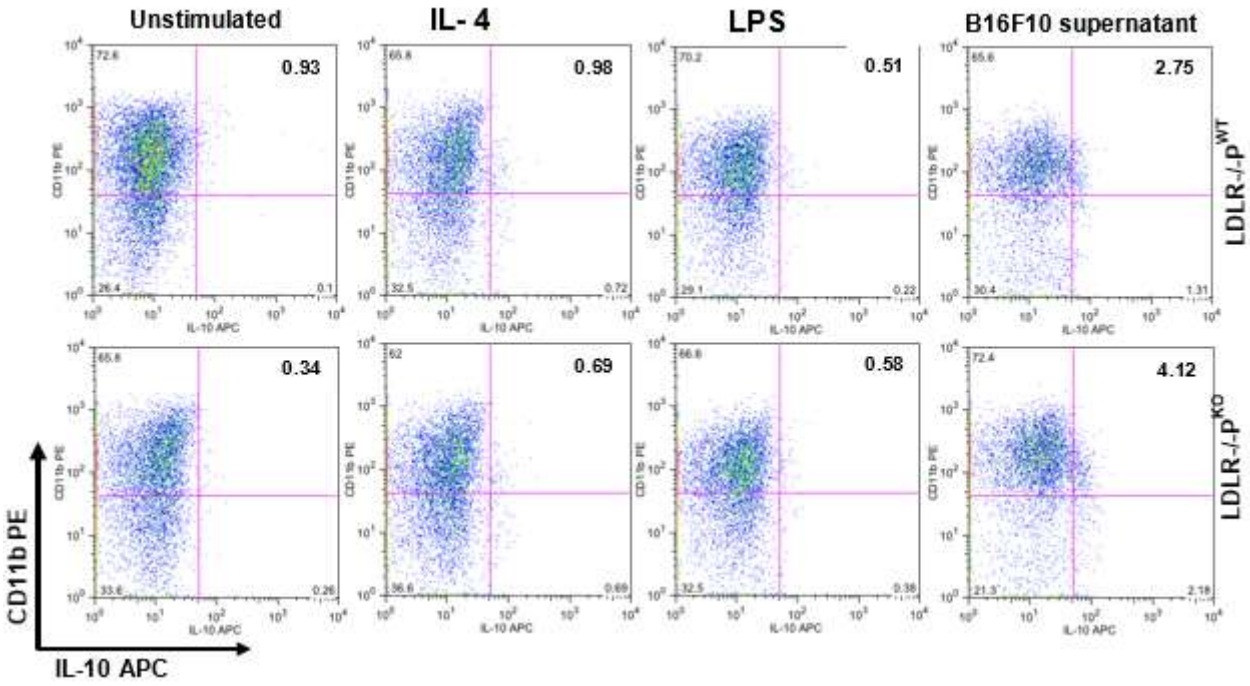

Figure 31: Surface receptor expression of polarised macrophages and intracellular IL-10 staining.

BMDM from $LDLR^{-/-}P^{WT}$ and $LDLR^{-/-}P^{KO}$ mice were treated with GM-CSF (20 ng/ml) for 7 days. Then the cells were stimulated either with LPS (100ng/ml), IL-4 (20ng/ml) or B16F10 supernatant. Unstimulated cells were used as controls. Samples were collected before and after stimulation and samples were stained for the expression of $CD11b^{+}IL\text{-}10$.

3.3 Discussion and conclusions

3.3.1 Discussion

The majority of studies have agreed that differentiation of macrophages by GM-CSF and priming with LPS would result in M1-polarised macrophages which were weak producers of IL-10 (Fleetwood et al., 2007). Although the ELISA assay showed high levels of IL-10 following differentiation of BMDM with GM-CSF and priming with LPS, it did not reach the level of IL-10 attained when macrophages were differentiated and primed with classical M2 macrophage stimuli, M-CSF and IL-4. It has been reported that LPS stimulation of M-CSF pre-incubated mouse BMDM results in induction of IL-10 in which activation of TLR4 by LPS induces the expression of IL-10 through the sequential induction of type I IFNs followed by induction and signalling through IL-27 (Iyer et al., 2010).

Previous work on a model of acute bacterial infection had revealed that complement protein properdin is an influential factor on the humoral and cellular immune responses. In this model, splenocytes and bone marrow-derived myeloid cells from wildtype and properdin deficient mice managed to show that properdin-deficient mice polarise macrophages to an M2 phenotype and thereby contributes to determining the outcome of infection. These findings supported the role of complement components in determining a cellular phenotype. Properdin deficient mice infected with *S. pneumoniae* had a more favourable clinical outcome when compared to wildtype. This finding was attributed to reduced activation of macrophages and decrease in release of proinflammatory cytokines (Dupont et al., 2014).

This chapter utilises an *in vitro* model of bone marrow derived macrophage polarisation to characterise the nature of an influence exerted by medium obtained from B16F10 in culture (so-called conditioned medium) and to investigate whether activities are modulated differently in cells from properdin wildtype and properdin deficient mice. This *in vitro* model involves the differentiation of hematopoietic stem/progenitor cells from mouse bone marrow in the presence of GM-CSF/M-CSF, followed by either M1 or M2 typical stimulation. Interferon-ɣ and LPS stimulation is used to prime macrophages toward M1 phenotype (Murray et al., 2014), while IL-4 or IL-13 yields macrophages with M2 phenotype (Ying et al., 2013).

In this chapter, GM-CSF was used to drive BMDM towards an M1 macrophage phenotype. Classical M1 macrophages develop in tissue in the presence of high levels of GM-CSF and IFN-ɣ (Murray and Wynn, 2011). *In vitro* studies have widely used GM-CSF and LPS to generate M1 macrophage phenotype. On the other hand, M-CSF and IL-4 have been used to generate macrophages with typical M2 phenotype (Lawrence and Natoli, 2011, Zheng et al., 2013). Upon stimulation, macrophage activation is directed either towards classic M1 or alternative M2 phenotype. M1 macrophage activation depends on Toll-like receptors (TLRs) and activation of nuclear factor kappa B (NFκB)/c-Jun N-terminal kinase 1(JNK1). M1 macrophages are characterised by the production of high levels of inflammatory cytokines such as IL-12, IL-6 and IL-1β (Martinez and Gordon, 2014, Murray et al., 2014). In addition, activation of iNOS, results in increased generation of reactive oxygen species such as nitric oxide (NO). On the other hand, M2 macrophage activation depends on PPARγ, PPARδ, or IL-4-STAT6 pathways, resulting in an anti-inflammatory response that is accompanied by upregulation of mannose receptor CD206, and arginase 1(Arg1)(Mills, 2012).

3.3.1.1 B16F10 supernatant stimulation leads to a significant increase in the level of IL-10 gene expression in both genotypes

Previously it has been demonstrated that B16F10 cell line produces IL-10 *in vitro.* Furthermore, implantation of B16F10 in mice result in the production of IL-10 in the tumour microenvironment (Miranda-Hernández et al., 2013). IL-10 simulated macrophages have been shown to possess an enhanced M2 macrophage-related gene expression (Makita et al., 2015). It might be reasonable to speculate that IL-10 in B16F10 conditioned media would stimulate macrophages towards an M2 phenotype. This would explain increased IL-10 mRNA expression which is one of the distinctive M2 macrophage markers after stimulation of BMDM with B16F10 supernatant.

The results presented in this chapter showed that stimulation with B16F10 supernatant resulted in a significant increase in the level of IL-10 gene expression in both genotypes when compared to unstimulated cells, exceeding the activity of M-CSF and IL-4 to stimulate IL-10. IL-10 is a major anti-inflammatory cytokine secreted by activated macrophages and T cells. IL-10 inhibits cytokine production by macrophages and plays a central role in shaping the outcome of the immune

response. This is mainly achieved via the ability of IL-10 to decrease expression of pro-inflammatory cytokines, inhibiting T helper cell type 1 effector cell development.

3.3.1.2 Analysis of BMDM by cytokines IL-10 and IL-12

Results of ELISA assay showed that stimulation with B16F10 lead to higher levels of IL-10 in PKO cells when compared to wildtype cells. Surprisingly, measurement of IL-10 by ELISA showed high levels in both genotypes when cells were stimulated with LPS as compared to unstimulated cells. Simultaneous production of IL-10 and TNF-a has been described. Agbanoma and co-workers (Agbanoma et al., 2012) have described prolonged production of TNF-α from macrophages stimulated with autologous anti-CD3–activated T cells or synovial rheumatoid T cells. This excessive pro-inflammatory response is thought to be due to lack of responsiveness to IL-10 by stimulated macrophages and thus may explain the skewed pro-inflammatory cytokine profile which characterise chronic inflammatory autoimmune diseases. Furthermore, it has been shown that IL-10 regulation of TNF production is dependent upon the stimulus used to activate the macrophage, as LPS stimulation seems to generate a different response than stimulation with autologous anti-CD3–activated T cells or synovial rheumatoid T cells (Agbanoma et al., 2012).

BMDM from $LDLR^{-/-}$ were analysed as well, in order to evaluate qualitatively the cell responsiveness compared to PKO/WT (which are $LDLR^{+/+}$). Investigation of $CD11b^{+}IL\text{-}10^{+}$ cells by FACS in PKO/PWT and $LDLR^{-/-}$ groups revealed low expression in PKO/PWT group and good expression in $LDLR^{-/-}$. In $LDLR^{-/-}$ group, stimulation with B16F10 resulted in higher expression of $CD11b^{+}IL\text{-}10^{+}$ cells in $LDLR^{-/-}$ cells.

Measurement of the pro-inflammatory cytokine IL-12 by ELISA showed that stimulation with either IL-4 or B16F10 supernatant did not result in a significant increase in the level of IL-12 in both genotypes. As expected, LPS stimulation resulted in increased level of IL-12 which was significant in the wildtype. Flow cytometric analysis of $CD11b^{+}IL\text{-}12^{+}$ cells in PWT/PKO group of mice revealed that wildtype mice had increased expression after LPS and B16F10 stimulation. Based on this result B16F10 stimulation would be classified as a stimulus that generates a more M1 macrophage phenotype. However, previous work has

shown that myeloid cells derived from murine bone marrow using GM-CSF pass through an immature stage in which they are able to produce much higher amounts of IL-12 than more mature cells. During this immature stage cells usually lose surface markers characteristic of immature myeloid cells and acquire markers distinctive of mature macrophages (Oliveira et al., 2003). Although flow cytometric analysis showed low expression in LDLR group, LPS stimulation resulted in increased expression in wildtype after LPS stimulation.

3.3.1.3 Analysis of mRNA (IL-6, IL-1β, iNOS, MCP-1,TNF-α, IL-10 and arginase-1) B16F10-mediated skewing of BMDM by qPCR

Investigations into mRNA expression of selected genes (IL-6, IL-1β, iNOS, MCP-1, TNF-α, IL-10 and arginase-1) reported in this chapter revealed that PWT cells had high levels of IL-1β post B16F10 stimulation, and high levels of iNOS post LPS stimulation. In contrast to WT, PKO cells showed more arginase and MCP-1 mRNA expression upon B16F10 stimulation (Al-Rayahi et al., 2016). An increasing body of evidence have indicated that IL-6, IL-1, iNOS and TNF-α are typical markers of M1 (classically activated) macrophages. On the other hand, IL-10 and arginase-1 are markers for M2 markers. Ying and co-workers have shown that LPS stimulation results in increased expression of pro-inflammatory cytokines IL-1β and TNFα. In contrast, IL-4 stimulation lead to increased expression of IL-10 and arginase-1.These findings were attained by flow cytometry analysis and quantitative RT-PCR (Weisser et al., 2013, Ying et al., 2013).

The mannose receptor CD206, as a marker of M2 profile, was also analysed by flow cytometry to further investigate the inflammatory properties of BMDM stimulated with B16F10 supernatant. This analysis revealed that B16F10 stimulation resulted in a significantly higher percentage of CD206+ CD11b+ cells in properdin deficient mice when compared to wildtype (P=0.0228). Stimulation with either LPS or IL-4 resulted in no comparative difference between genotypes. In unstimulated cells, the percentage of $CD206^{+}CD11b^{+}$ cells was higher in $LDLR^{-/-}$ group compared to PWT/PKO group (mean 7.5 vs 3.2%). CD206 is a known cell surface receptor marker indicative of M2 macrophages. (Weisser et al., 2013), demonstrating that the $LDLR^{-/-}$ line is indeed more M2 skewed than in the presence of LDLR.

3.3.1.4 lack of upregulated expression of MHC II, CD80 and CD86 of BMDM from properdin deficient mice compared to wildtype mice

Expression of CD80, CD86 and MHC-II was less in BMDM of PKO mice than that of PWT following stimulation with B16F10 conditioned medium (Al-Rayahi et al., 2016), possibly indicating M2 macrophages, as down regulation of these co-stimulatory molecules are consistent of M2 macrophage phenotype (Lawrence and Natoli, 2011, Yamaguchi et al., 2016).

As expected, the level of IL-10 secreted in the presence of M-CSF as mediator for differentiation of BM cells was higher than when GM-CSF was used. These findings validate our protocol and confirm previous reports which have demonstrated that different phenotypic changes arise in macrophage lineage populations when GM-CSF and M-CSF are used for differentiation. Based on cytokine profile, treatment with GM-CSF induces M1 macrophages (classical), while M-CSF treatment induce M2 macrophages which are characterised by an anti-inflammatory cytokine signature (Lacey et al., 2012). Additionally, B16F10 stimulation resulted in a significant increase in PKO BM cells IL-10 when compared to the wildtype indicating, that PKO mice have more M2 macrophages.

Flow cytometry analysis of surface marker $CD11b^{+}$ cell in BMDM of wildtype and Properdin deficient mice as well as $LDLR^{-/-}P^{WT}$ and $LDLR^{-/-}P^{WT}$ showed no difference between the genotypes. However, $LDLR^{-/-}P^{WT}$ and $LDLR^{-/-}P^{WT}$ have fewer $CD11b^{+}$ cells (reduced by about 25%) compared to PWT and PKO. However, this results need to be more narrowly defined in future work.

Pooled samples were used when studying tumour bearing mice for reasons of the sheer volume of work when tissues from a group size of for example 8-10 mice was harvested at their endpoints of reaching 1 cm in one dimension of tumour growth. Therefore, the results obtained are averages of the mice analysed. Naïve mice, where tissues except of course tumour were analysed, required less time and therefore could be studied singly.

Cytokine screening array of B16F10 cell lysates was done to investigate 18 different cytokines. However, this array failed to detect any of the investigated cytokines. The array was able to detect the positive control, hence the lack of detection in B16F10 sample is probably due to the detection limit of the assay.

Possible proteins responsible for this pattern of macrophage polarisation in WT and PKO is the effect of two members of Suppressor of cytokine signalling

proteins (SOCS1 and SOCS3) which are implicated in shaping M1 and M2 polarisation. Previous results have demonstrated that subcutaneous implantation of melanoma cells in mice with a macrophage-specific deletion of SOCS3, did not show a difference in tumour size although the number of metastasis increased in these mice (Hiwatashi et al., 2011). A positive link was found between macrophage polarisation and SOCS when macrophages from SOCS3-deficient mice were found to produce less IL-6 and TNF-α after stimulation with tumour lysates, most likely due to aberrant STAT3 activity. Additionally, SOCS1 regulation of M1-macrophage activation was described. This activation is mainly via inhibiting the IFN-ɣ induced JAK2/STAT1 pathway and TLR/NF-κB signalling. Some studies propose SOCS3 is associated with M1 macrophages and pro-inflammatory response. Linking any effect of SOCS1 and SOCS3 with the pattern of macrophage polarisation in PWT and PKO reported in this chapter would require measurement of these two protein in BM cell from both genotypes (Wilson, 2014).

3.3.1.5 Conclusions

One of the aims of this chapter was to investigate the influence of B16F10 conditioned medium on the phenotype of BMDM compared to unstimulated BM cells. In both genotypes, qPCR results revealed that stimulation with B16F10 supernatant resulted in increased mRNA expression of IL-1β, IL-10, Arginase and TNF-α. In contrast to PWT, PKO cells showed more MCP-1 upon stimulation with B16F10.conditioned medium Measurement of selected cytokines by ELISA show increased levels of IFN-ɣ and IL-12 in both genotypes under these conditions. Nevertheless, flow cytometry analysis of surface markers demonstrated that the percent of $CD206^{+}CD11b$ cells was only increased in PKO cells after B16F10 stimulation. To conclude, B16F10 supernatant has the ability to activate BM cells and polarise macrophages most probably towards M2 phenotype cells (see Table 12). Comparison between wildtype and properdin deficient mice, shows that stimulation with B16F10 condition medium results in higher expression of IL-1β, iNOS and TNF-α and lower expression of MCP-1 and Arginase in wildtype mice. Furthermore, levels of IFNɣ and IL-12 were more in PWT cells indicating that PWT cells show a more M1 skewed immune response (as shown in Table 13). Finally, unstimulated BMDM from $LDLR^{-/-}P^{WT}$ and $LDLR^{-/-}P^{WT}$ show more of the

M2 surface marker $CD206^{+}$ than BMDM of wildtype and properdin deficient mice (Al-Rayahi et al., 2016).

Table 12: summary of the significantly different abundances elicited by B16F10 conditioned medium for BMDM compared to unstimulated BM cells as characterised in this chapter

	PWT	PKO
qPCR	IL-1β,IL-10,Arginase and TNF-α	IL-1β,IL-10,Arginase,TNF-α and MCP-1
ELISA	IFN-ɣ and IL-12	IFN-ɣ and IL-12
FACS		CD206+CD11b

Table 13: BMDM from PWT show more M1 skewing than pKO.

	PWT
qPCR	↑↑ IL-1β, ↑↑iNOS ↓↓ MCP-1, ↓Arginase and ↑TNF-α
ELISA	↓↓IL-10 and ↑ IFNɣ
FACS	↑ MHC-II, CD80 and CD86, ↑ IL-12, ↓↓ CD206+CD11b

Arrows indicate relative expression compared to PKO.

Chapter 4 Analysis of properdin deficient mice and their congenic controls in a syngeneic tumour model

4.1 Analysis of physical dimensions of Tumour

In order to investigate the role of properdin in tumour growth, wildtype and properdin deficient mice (on C57BL/6 background sex and age matched) were injected subcutaneously in the flank with 100µl of freshly prepared B16F10 cell suspension. Other than the pilot experiment, more than five independent subcutaneous experiments were carried out using an injection dose that ranged from 1 x10^5 to 5x10^5 cells. After 7-24 days, mice were culled and dissected. Their flanks were macroscopically examined for tumour formation. Tumour was not invasive and there was no evidence of melanotic lymph nodes and no necrosis. Tumour size was measured by using dial calipers and tumour weight was recorded (as shown in Figure 32).

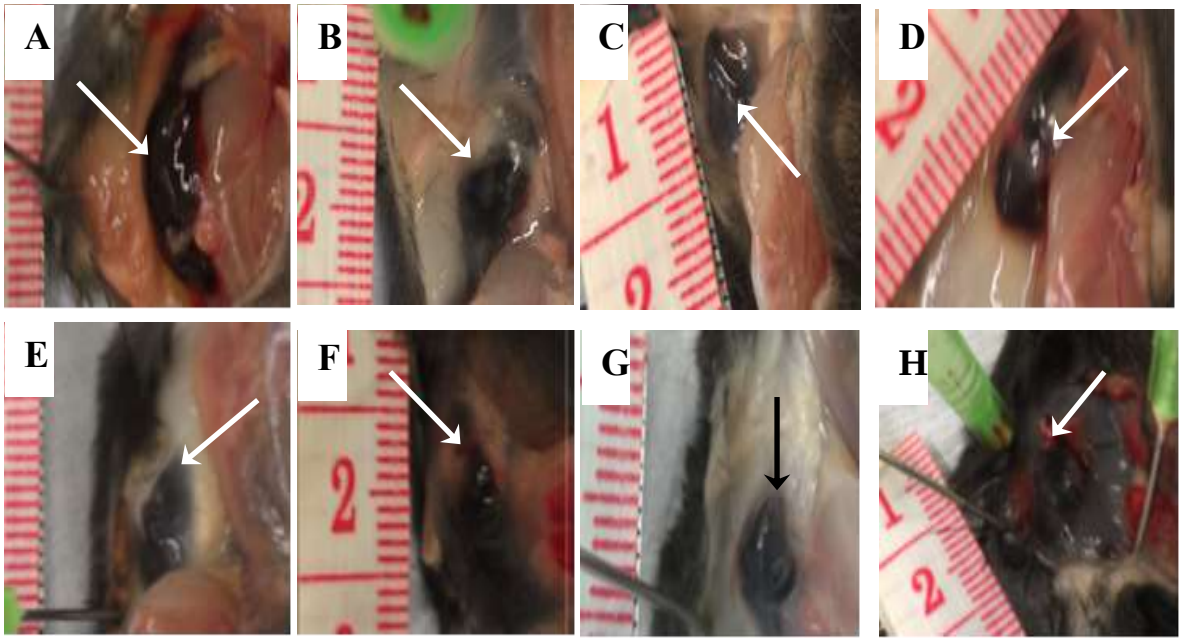

Figure 32: Subcutaneous implantation of B16F10 in wildtype and Properdin deficient C57BL/6 mice

Wildtype and Properdin deficient C57BL/6 male mice were injected subcutaneously with 3.6x10^5 cell/100µl of B16F10. After 14 days the mice were sacrificed, the mice were macroscopically examined for tumour formation and tumour size was recorded. Representative images showing A-D properdin deficient C57BL/6 mice, E-H wildtype C57BL/6 mice. The arrows indicate the melanotic tumours in the subcutis after exteriorisation of the abdominal skin, leaving the peritoneal cavity intact. The surface of the tumours was shiny. Tumours were circumscript/nodular (A and D), lobulated (B, C, E and G), show signs of hemorrhagia (F and H). No vascularisation was seen under gross examination.

Mice were sacrificed and dissected. Tumours were removed and visually checked for infiltration of tumour and vessel formation around the site of injection.

4.1.1 Tumour size determination by caliper.

Tumour volume measurement by the use of external calipers is a standard method used in cancer studies. Calipers were used to measure baseline tumour width and length (in mm^3). The following formula was used to calculate tumour volume:

Tumour volume (mm^3) = (1/2) x (A) x $(B)^2$.

In which A refers to the long axis of the tumour and B refers to the short axis of the tumour in millimetres (Xu et al., 2013); (Kretzer et al., 2012); (Sumiyoshi et al., 2014); (He et al., 2013).

The results generated by the subcutaneous tumour model showed no difference in tumour size between the wildtype and the properdin deficient mice, however, there was large variation in wildtype tumour bearing mice as shown in Figure 33.

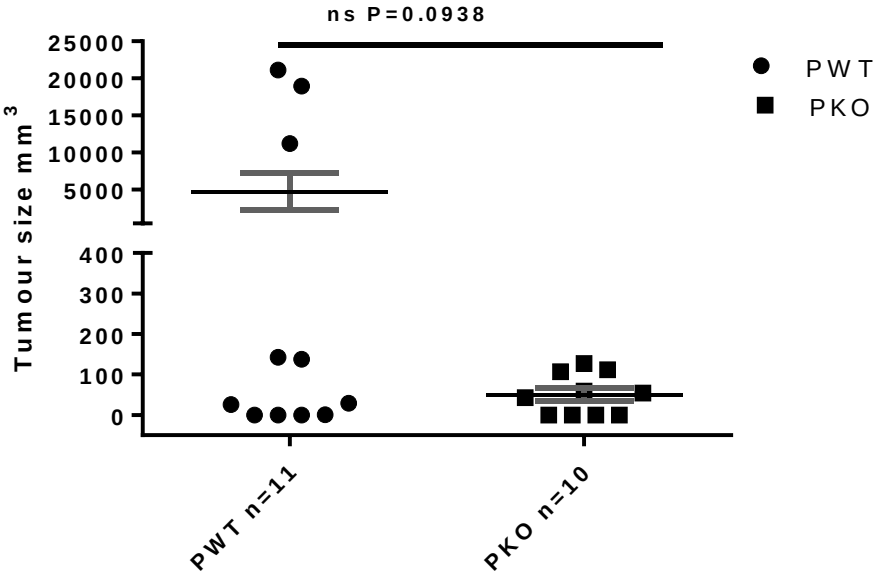

Figure 33: Tumour size of subcutaneous tumours.

Wildtype and properdin deficient C57BL/6 male mice were injected subcutaneously with $1.6x10^5$ cell of B16F10. After 14 days the mice were sacrificed and tumour size was measured by calipers. Values are expressed as mean ± SEM from two independent experiments.

The results presented here showed no difference in tumour size between genotypes. Due to ethical reasons to avoid animal suffering, animal license restricts that mice should be culled when tumours reach 1cm at maximum

(usually after 13-14 days of tumour challenge). Hence, it is not known whether leaving tumour to grow any larger would result in difference between genotypes. It is possible that this method for tumour size measurement may generate measurement with an error value which increases with tumour volume. One reason for this inaccuracy is the assumption that all tumours have the same shape. Jensen and colleagues have reported that tumour size measured by external calipers did not correlate well with true tumour size (Jensen et al., 2008).

4.1.2 Tumour weights in Wildtype and properdin deficient mice

As mentioned previously, tumour weight was recorded as an additional parameter to evaluate any difference between genotypes. Similar to tumour size by calipers, measurement of tumour weight showed no difference between the genotypes as demonstrated in Figure 34.

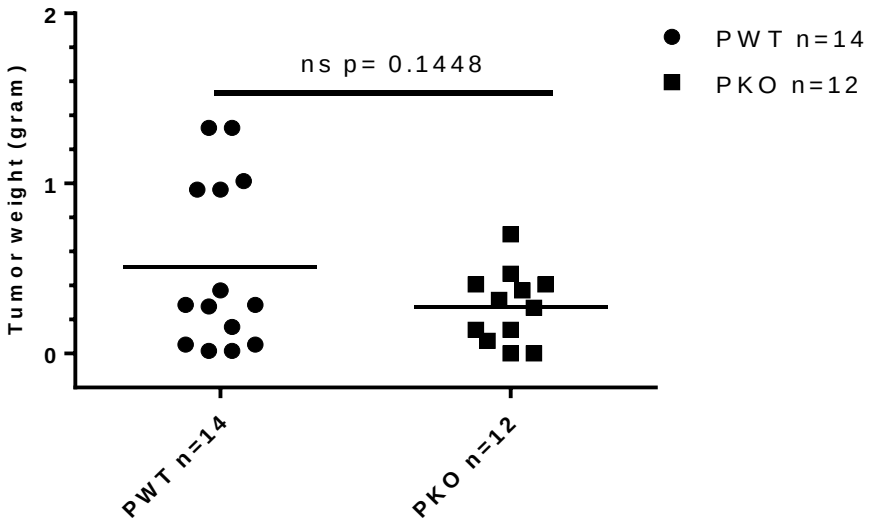

Figure 34: Tumour weight of subcutaneous tumours.

Properdin deficient and wildtype C57BL/6 male mice were injected subcutaneously with 1.6 x10^5 cell of B16F10. After 14 days the mice were sacrificed and tumour mass was measured using calipers. Values are expressed as mean ± SEM. Statistical analysis did not show any significance between the groups.

As for Figure 34, there again is large variation among tumour bearing PWT compared to PKO, when analysing tumour weights. There is no statistical difference between the genotypes.

4.1.3 Bioluminescence imaging (BLI) of luciferase expressing tumour masses

Analysis of physical dimensions of tumour stressed the need to employ a more accurate method for tumour size measurement. A number of imaging techniques for monitoring tumour progression and metastasis have recently become available. Of those techniques, bioluminescence imaging has demonstrated an ability to detect microscopic tumours with high accuracy (Puaux et al., 2011). BLI is a sensitive non-invasive imaging technique which enables monitoring of the tumour burden and progression in the animal body in a timely manner without the need to sacrifice the animal. Tumour growth can be quantified by counting the number of photons emitted from the animals (O'Neill et al., 2010). This method reduces the number of animals used in each experiment, as each animal serves as its own control over the period of the experiment. However, it has recently been recognised that tracking across longer intervals (weeks) provides a more accurate measure of tumour growth and development (Dr M.Kelly, personal communication).

This experiment aimed to demonstrate that BLI could be used to estimate and monitor tumour growth in our model of mouse melanoma. The results of the pilot BLI experiment represented by Figure 35 demonstrated that light emission could be detected from the regions of interest, which confirms that BLI was able to detect melanomic tumours. The bioluminescent signal is represented in a colour scale with yellow the most intense signal and purple the weakest signal.Figure 35 shows that the optimal imaging time is about 35 minutes.

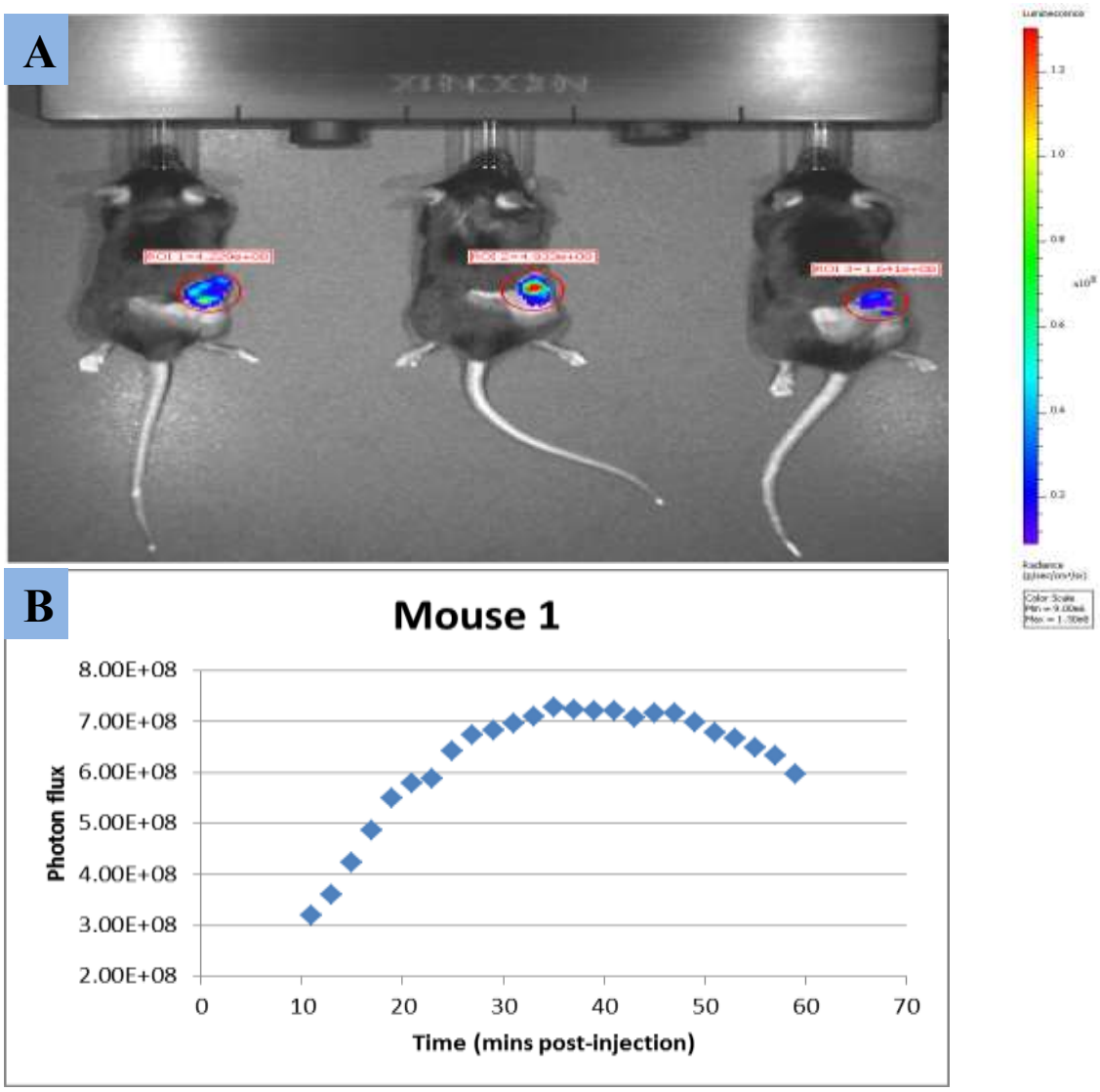

Figure 35: monitoring of tumour growth in a subcutaneous syngeneic mouse model by bioluminescence imaging.

B16-F10-Luc cells were injected subcutaneously into C57 BL\6 male mice (n = 3) for PWT and PKO. (a) BLI of animals imaged after 8 days from injection. (b) A representative quantification of bioluminescence intensity as total flux (photons/second).

Based on the results of this experiment and recommendations from the manufacturing company, the protocol was modified by using subcutaneous injection of luciferin instead of intraperitoneal injection. Subsequently, this modification led to another modification of the animal licence.

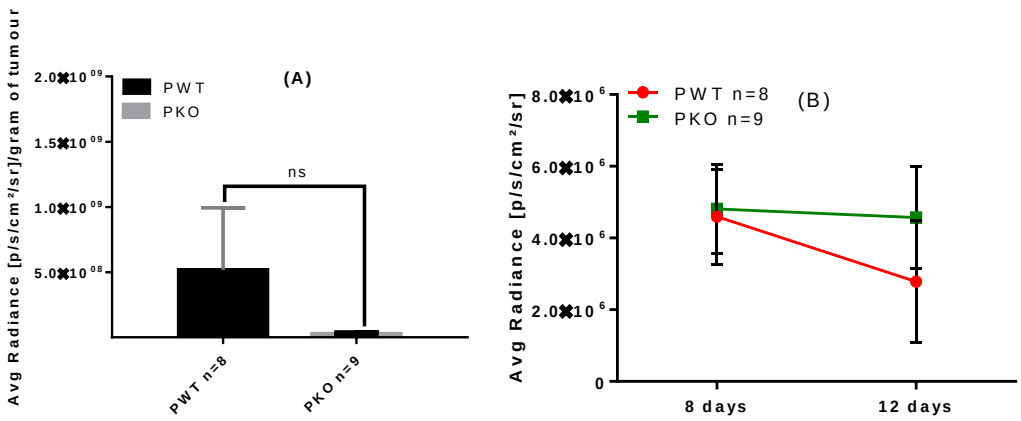

Figure 36: Bioluminescent signal in wildtype and properdin deficient tumour bearing mice.

A-Standardisation of quantitative analysis of the luciferase signal (Avg Radiance [p/s/cm²/sr])/ weight according to genotype at day 12. B-quantitative analysis of the luciferase signal (Avg Radiance [p/s/cm²/sr]) according to genotype on day 8 and 12.tumour development following subcutaneous injection of $1.6x10^5$ -B16F10 cells was monitored *in vivo* by measuring the bioluminescence emitted by melanoma cells 5 minutes after the injection of 150µg/kg luciferin. Light emission was measured at day 8 and 12 (10 minutes), after cell injection (n=17 male mice). The photon counts and pictures illustrating tumour progression in a representative mouse are shown.

The results in Figure 36 and Figure 37 show the average of photon emissions at day 8 and 12 as an indicator of tumour size. Average radiance signal at day 8 showed no significant difference between genotypes. In contrast, the average radiance signal seems to decrease in the wildtype at 12 days post injection. It is possible that tumours in wildtype mice exhibited necrotic areas subsequently leading to a decrease in bioluminescent signal at later stage.

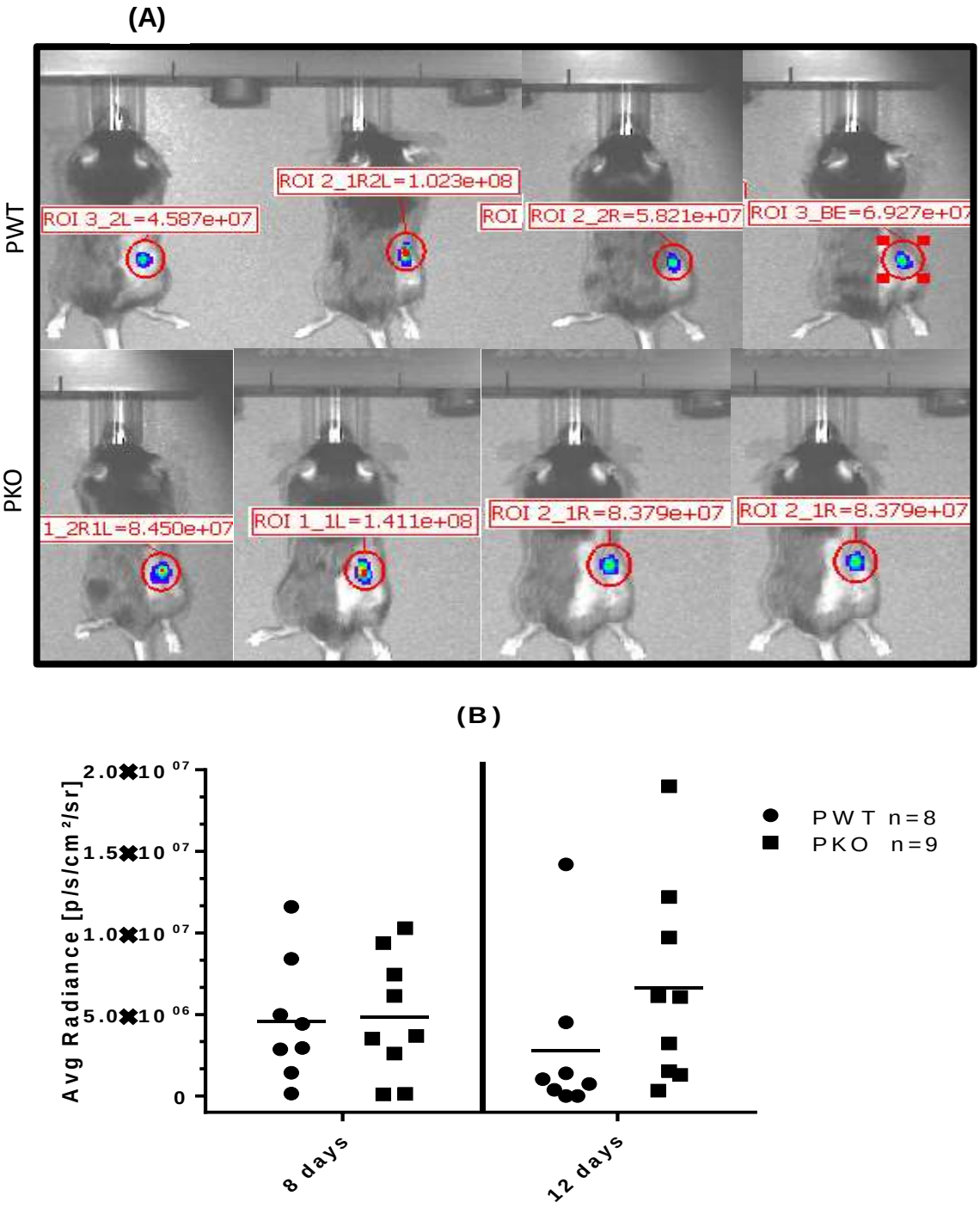

Figure 37: Longitudinal monitoring of tumour growth by bioluminescence imaging.

B16F10-Luc cells were injected subcutaneously into wildtype and properdin deficient male mice. BLI of a representative animal imaged weekly for 8 days. (b) Average radiance signal in wildtype and properdin deficient tumour bearing mice at day 8 and 12 post tumour implantation for all 17 animals.

4.2 Description of the model and justification (3R consideration).

Murine tumour models have been an essential tool in cancer research. Different numbers of B16F10 cells were injected in the four subcutaneous experiments which were done, the reason for this was to establish which dose manages to catch the reaction of the immune system before entering the escape phase. The duration of each experiment was carefully selected after searching the literature (Eberting et al., 2004, Baird et al., 2013, Takeda et al., 2011, Lv et al., 2009).

This study has employed this model to investigate the immune response of the organism to the development of tumourous growth. In particular, the role of part of the innate immune response in attracting cells to tumour or altering their abundance in system circulation. Calipers have been traditionally used to monitor tumour growth through direct measurement. However, recent promising approaches have utilised non-invasive imaging for assessing tumour burden in host animals. This study has used an imaging technique using luciferase-modified tumour cells to achieve refinement and reduction. Bioimaging reduces the number of mice used and offers the best combination of sensitivity and accuracy because luciferase-modified tumour cells allow highly sensitive monitoring of tumour growth in vivo. Moreover, using lower numbers of injected tumour cells means smaller tumour size in mice, tumour growth monitoring over a longer period of time, and less distress to mice. A further way to refine the use of experimental animals is to advance the analyses of data generated from *in vivo* experimentation. Freezing containers are available to generate a maximum number of analyses per experimental animal. These containers provide the opportunity for more efficient freezing of cells and material obtained at the end of the 14-day experimental duration and thus contribute to refine and reduce experimentation. The principle of the 3Rs (replacement, refinement and reduction) is an important concept which governs or reduce the use of animals for the purpose of research and testing. Originally proposed by Professor William Russell and Rex Burch, the aim is to improve animal welfare and limit the use of animals in research where appropriate. These principles aim firstly to replace the use of animals in research, when the use of animals is unavoidable, the second aim, selects scientific technologies which limit actual or potential pain leading to

improved animal welfare. Lastly, this principle encourages the improvement of experimental design, statistical analysis and use of techniques such as imaging which will eventually lead to the use of fewer animals. Application of these principles has been an important priority in this study but also a limitation when trying to compare data with the literature.

4.3 Specifics of the tumour model in properdin deficient mice

Syngeneic tumours are tumours that arise after implantation of a tumour cell line into mice, where both recipient mice and cell line are from the same genetic background. This type of tumour model uses immune competent hosts and ensures intra-species interactions between cancer cells and their microenvironment, while other models such as xenogeneic model require the use of immune compromised mice, which limits the assessment of host immune response (Pearson and Pouliot, 2000). Syngeneic tumours have made use of the widely available cell lines which represent different tumour types. One of the available tumour cell lines is the well-established and widely used B16 melanoma cell line. The B16 melanoma cell line is a tumour of spontaneous origin in C57BL/6 mice. This cell line has been quite popular because it can be implanted in the skin and monitored using non-imaging techniques. One of the distinguishing features of B16 melanoma is the ability to produce a black pigment (melanin). This feature is broadly utilised to study metastases in syngeneic C57BL/6 mice due to the ability of B16F10 to produce pulmonary tumour nodules which can be macroscopically counted on the surface of the lungs. B16F10 is also characterised by low expression of MHC-I which appears to be a feature of normal C57BL/6 mouse melanocytes that is retained after transformation to melanoma (Li et al., 1998).

Subcutaneous implantation of B16F10 will result in a palpable tumour in about 5 to 10 days. The tumours grow to 1 × 1 × 1–cm in size after about 14 to 21 days. If allowed to grow larger, the tumours usually become necrotic in the center and begin to ulcerate. Hence, it is recommended that mice are sacrificed before it reaches this stage. Typical dose for tumour implantation is 1-5 × 10^5 cells/mouse. A consistent injection technique is vital for subcutaneous tumour implantation, as any difference in site/depth of injection may result in variation. Prior to injection, the fur on the area of interest was shaved to facilitate monitoring of injection and

tumour. Upon injection, each mouse should show a clear visible bleb. The absence of a clear bleb after injection may indicate delay in tumour growth or absence of tumour. After tumour implantation, mice should be monitored daily for the appearance of visible nodule. Notably, monitoring tumours may be difficult as tumours growing subcutaneously may appear larger due to attachment of B16F10 cells to the skin. In addition, growing tumours take different shapes, such as nodular and flat.

In my study tumour, spleen and bone marrow were collected for further analysis. Bone marrow is a key lymphoid organ which plays an important role in the body's immune response. Bone marrow contains a number of immune cells such as T-cells, $CD11c^+$ dendritic cells, B cells, myeloid derived cells and NK cells. It has been shown that bone marrow can serve as a site of primary immune response. Immune regulation in bone marrow microenvironment is achieved as a result of cell to cell contact and through the action of cytokines and other soluble factors. Elucidating the factors contributing to immune regulation in the bone microenvironment is an important element to gain further insights into the host immunity during disease, including cancer (Zhao et al., 2012).

Of the immune cells in the bone marrow are the myeloid derived cells which include myeloid progenitors, immature cells and macrophages. During pathological conditions, such as tumours, immature myeloid cells generated in the bone marrow proliferate into myeloid-derived suppressor cells (MDSCs). These cells are capable of producing immune suppressive factors such as arginase-1, iNOS or TGF-β (Condamine and Gabrilovich, 2011).

Besides the conventional role of spleen in filtering blood born microbes and antigens, mouse spleens exhibits both immune and hematopoietic functions. Animal models have reported splenic hematopoiesis in a number of diseases including atherosclerosis, cancer and myocardial infarction, suggesting that hematopoietic stem and progenitor cells may accumulate in spleens of diseased animals. These cells proliferate and produce progeny locally in a process which is skewed toward myelopoiesis rather than erythropoiesis and lymphopoiesis. Furthermore, research has shown that the resulting myeloid progenitors are capable of *in vitro* proliferation similar to their bone marrow counterparts (Bronte and Pittet, 2013).

Cortez-Retamozo and co-workers have reported recruitment of tumour associated macrophages (TAM) and tumour associated neutrophils (TAN) progenitors from spleen to tumour tissue, highlighting the importance of spleen as an extramedullary site supplying tumours with TAM and TAN (Cortez-Retamozo et al., 2012).

4.4 Histology of melanoma tumour in PWT and PKO.

Histological examination using different antibodies and stains was carried out to study the distinctive features of melanoma tumour in PWT and PKO mice.

4.4.1 Immunohistochemical staining of tumour

Different melanomic tumours may exhibit different panels of angiogenic factors. To assess the level of angiogenesis, tumour sections were stained for with CD31, VEGF (data not shown) and Von Willebrand Factor (VWF). The endothelial cell marker, CD31 was used to determine the blood vessel lumen area and blood vessel density in tumour sections of B16F10. Paraffin sections were stained with monoclonal rat-antimouse platelet endothelial cell adhesion molecule-1(CD31 purchased from BD PharMingen (San Diego, CA). This antibody was found to give results only with frozen sections, thus paraffin embedded sections were not suitable. For VWF staining, Anti-Von Willebrand Factor (ab6994 Abcam) sheep polyclonal antibody was used. The control (mouse kidney section) gave positive results, however tumour sections stained with this antibody gave inconsistent results (see appendix). Previously, this antibody worked well with mouse tissue but the manufacturing company (Abcam) has lately reported that recent batches seem to generate inconsistent results in mice. VEGF immunohistochemistry of tumour paraffin sections was performed using polycloncal rabbit anti-VEGF (biorbyt) mouse Antibody and anti-rabbit/mouse IgG (DAKO). For unknown reasons, VEGF expression using this antibody was not detected in our tumour tissue.

4.4.2 Hematoxylin and eosin stain staining

For decades, Hematoxylin and eosin (H&E) stains have been used to distinguish various tissue types and the morphologic changes during disease such as cancer. This stain has the ability to display a broad range of cytoplasmic, nuclear, and extracellular matrix features (Fischer et al., 2008). H&E staining was performed on tumour tissue sections from PWT and PKO mice and the results

are presented in Figure 38. No apparent difference was found between the genotypes.

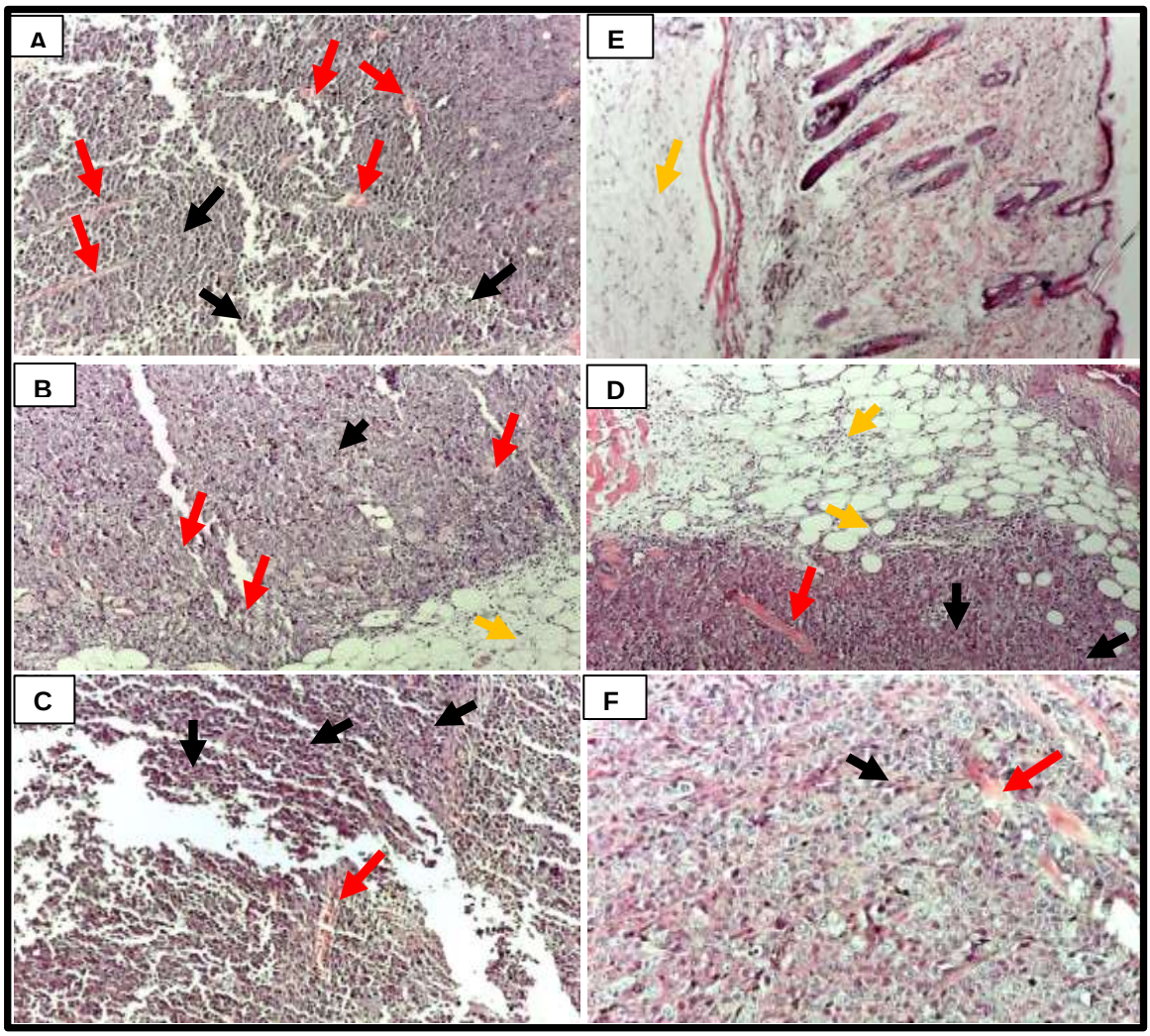

Figure 38: Tumour sections from both genotypes were examined by H&E staining.
Wildtype and Properdin deficient C57BL/6 male mice were injected subcutaneously with 4×10^5 cell/100µl of B16F10 cell suspension. Fourteen days after injection, tumour mass was isolated from mice and fixed. Tumour tissue was sectioned and examined by H&E staining. Representative images of PWT (A, B and C) and PKO (D, E, F) mice. Area of necrosis (Black arrows), blood vessels (red arrows) and fat vacuoles (yellow arrows) are indicated. Compact tumour mass can also be seen. All images were taken at 10x magnification.

4.4.3 Martius yellow staining

Martius yellow ($C_{10}H_6N_2O_5$) is sometimes used in staining due to its ability to stain red blood cells yellow. Due to the dependence of tumour growth and metastasis on angiogenesis, Martius yellow staining was carried out to identify red blood cells in tumour tissue to indicate the presence of blood vessels formed due to

angiogenesis. Tumour tissue from both genotypes were stained with Martius yellow and the results are presented in Figure 39. The results revealed rather quickly growing tumours considering the new formation of vessels and reaching the end point at 14 days.

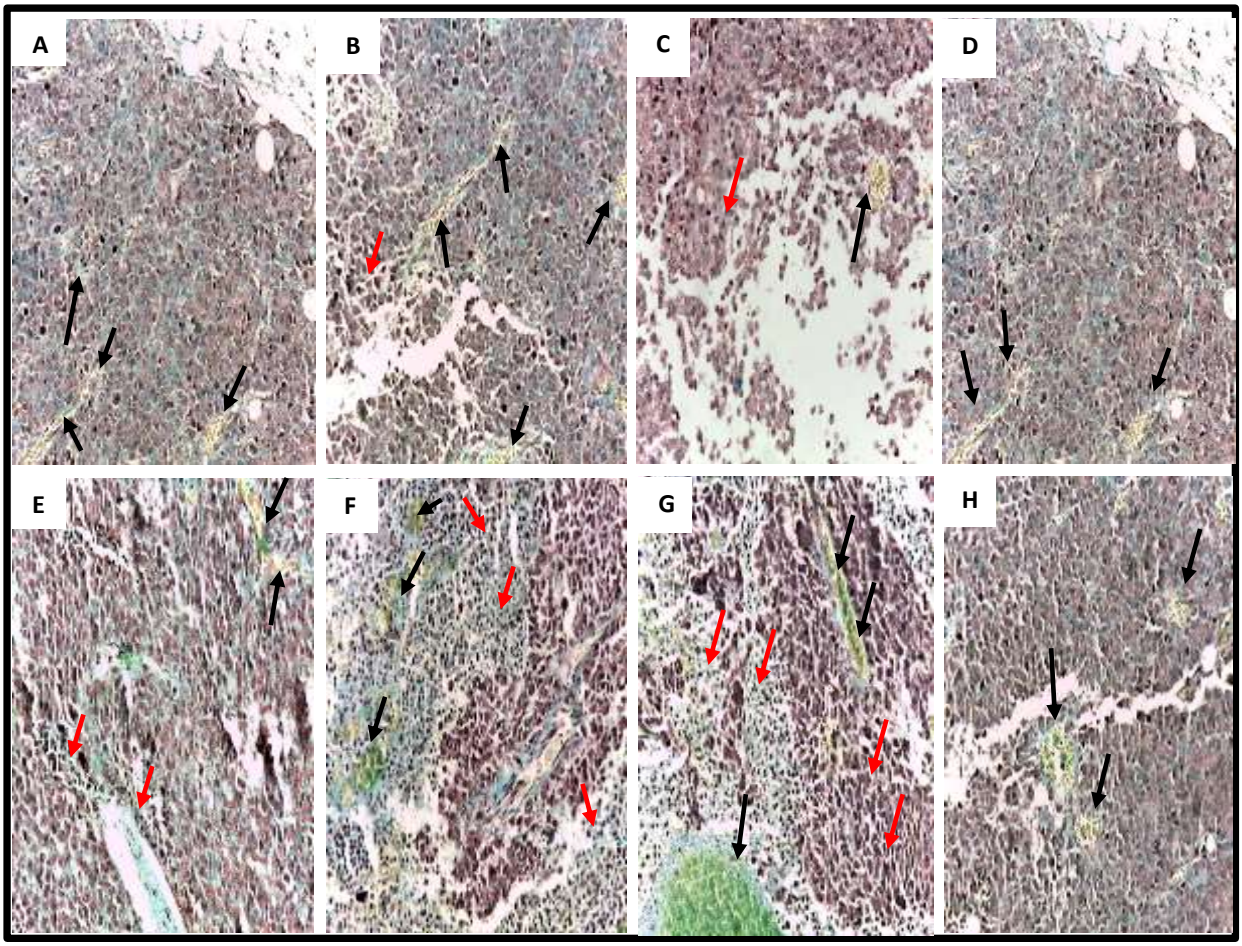

Figure 39:Martius yellow staining of tumour tissue from wildtype and properdin deficient mice.

Four wildtype and four Properdin deficient C57BL/6 mice were injected subcutaneously with 4 $\times 10^5$ cell/100µl of B16F10 cell suspension. After 14 days, the mice were sacrificed and dissected for collection of tumour tissue. Tissue section from both genotypes were stained with Martuis yellow to stain erythrocytes (yellow), in addition to Celestine blue-haemalum to stain nuclei (black), Alcian green to stain connective tissue(blue) and brilliant crystal scarlet to stain fibrin (red). Black arrows refer to red blood cells inductive of blood vessels, red arrows indicate necrosis. There are areas of compact tumour tissue and others that are necrotic. Lymphatic infiltration was seen.

4.4.4 Apoptotic cells in mouse melanoma

Detection of apoptotic cells was carried out on tumour tissue sections from wildtype and properdin deficient mice using a commercially available kit based on a mixed molecular biological-histochemical system that allows sensitive and specific staining of very high concentrations of 3'-OH ends that are localised in apoptotic bodies. This experiment was done to investigate the degree of apoptosis in tumour sections from each genotype as the results of bioluminescence imaging in tumour bearing mice (which will be presented later) showed a decrease in the signal in wildtype tumour bearing mice at 12 days time point, possibly indicating that wildtype mice undergoes apoptosis earlier than their properdin deficient counterparts. Investigations into apoptotic cells in tumour tissue were inconclusive due to the uneven distribution of apoptotic cells as some regions of the tumour tissue had intense accumulation of apoptotic cells while other regions showed the absence of apoptotic cells as shown in Figure 40.

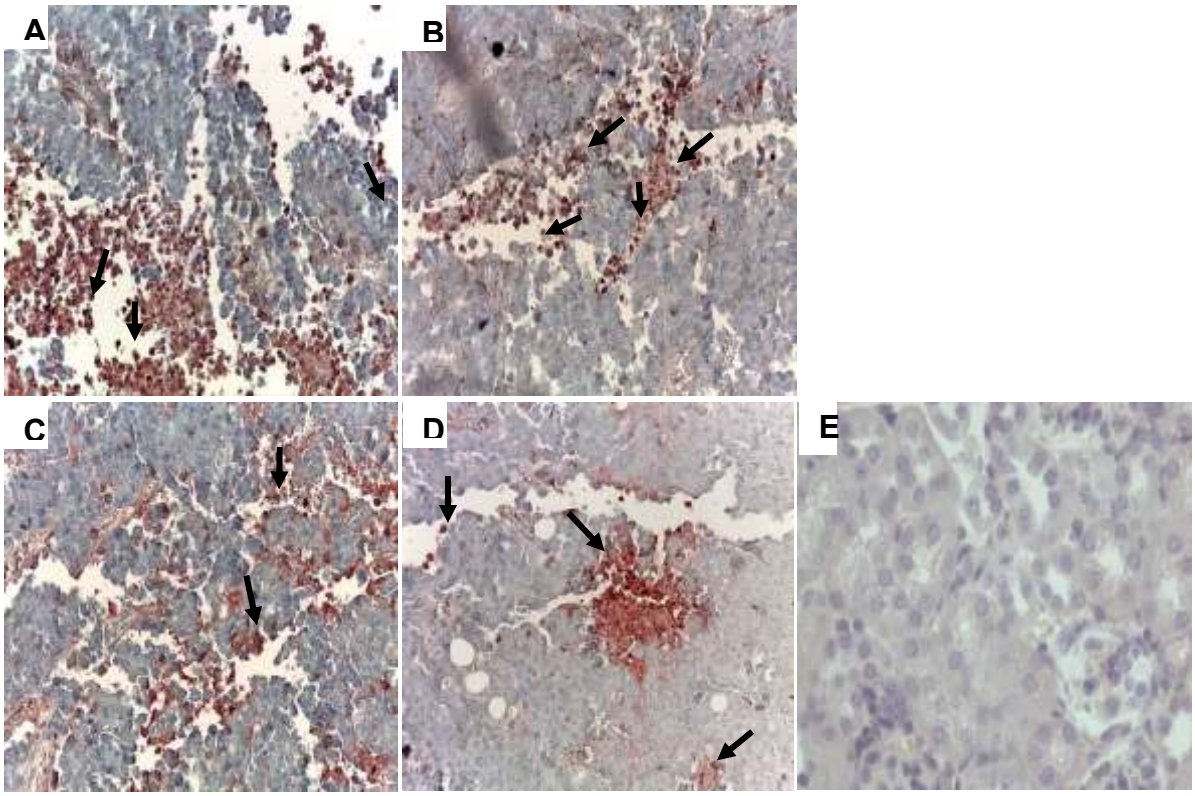

Figure 40: Apoptotic cells in tumour sections from both genotypes were examined.

PWT and PKO mice were injected subcutaneously with 1.6×10^5 cell/100µl of B16F10 cell suspension. Fourteen days after injection, tumour mass was isolated from mice and fixed. Tumour tissue was sectioned and staining using ApopTag peroxidase kit to detect apoptotic cells. Representative images of PWT (A and B) and PKO (C and D) mice. Red colour indicates apoptotic cells. E, control tissue (kidney) as negative. All images were taken at 20x magnification, while negative control under light microscope (40X).

4.5 Intravenous syngeneic tumour implantation

Experimental metastasis is one of the widely used models to study cancer. This model of metastasis involves the injection of tumour cells directly into the circulatory system of mice. Of the commonly used sites for experimental metastasis is intravenous injection into the lateral tail vein of mice, which subsequently results in lung metastasis. Direct implantation of tumour cells was first found to be influenced by the fact that clonal variant differs in their metastatic potential. To avoid possible variation in the metastatic ability, scientists managed to develop cell lines with higher metastatic ability. B16F10 is one of the most characterised models capable of resulting in experimental metastasis. One of the advantages of experimental metastasis is the short duration, as metastasis is usually rapid (10-14 days). Furthermore, scientists can control the type and number of cells introduced (Khanna and Hunter, 2005).

The fact that B16F10 is pigmented (due to the production of melanin) makes it a widely used cell line to study the metastasis in the lungs, by counting the number of black pigmented colonies after injecting the mice with these cells(Burghoff et al., 2014). It has been reported that these malignant cells migrate from the tumour through its blood vessels and attach to the vessel wall of the affected organ. Then they migrate to the parenchyma leading to the formation of new tumours (Geiger and Peeper, 2009).

4.5.1 Histology of melanoma in lung Schmorl's stain

Lung tissue sections from tumour bearing wildtype and properdin deficient mice were stained with Schmorl's stain. This stain was used to stain the melanin produced by B16F10 as an indication of the extent of pigmentation in the tissue. Microscopic examination of stained lung tissue sections showed more intense and abundant melanin pigment in tumour cells from wildtype mice than those seen in properdin deficient mice

The difference in numbers of tumour cells between wildtype and properdin deficient mice was investigated by calculating the percentage of tumour cells in lung sections on Schmorl's stained slides. This was done by microscopically counting the number of 1mm^2 fields which show tumour cells in a total area of 100 mm^2 and calculating the percentage in each genotype as shown in Figure 42. The results show that tumour bearing wildtype mice have a tendency to higher

percentage of tumour cells in a given area when compared with properdin deficient tumour bearing mice.

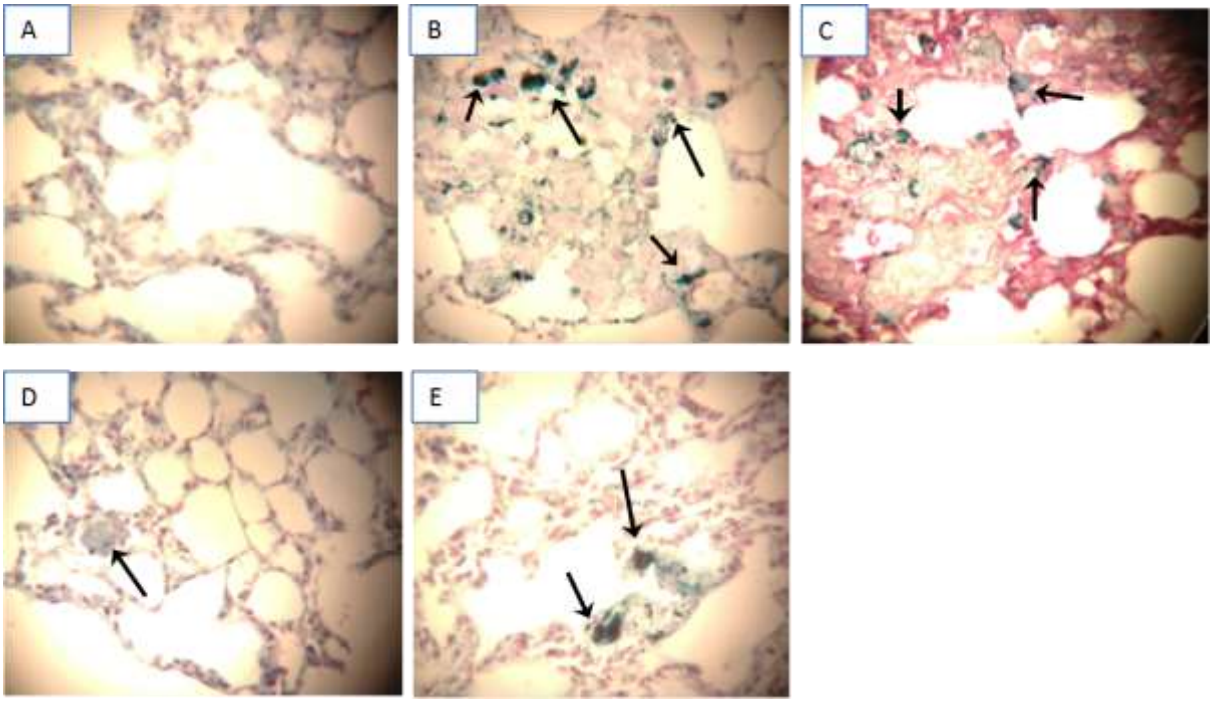

Figure 41: lung tissue sections stained with Schmorl's stain.

(magnification 40X oil immersion, picture was taken using iPhone camera with Magnify TM adaptor) A: lung of healthy mouse (control). Alveoli and parenchymal interalveolar spaces can be seen; B&C: lung tissue from PWT mice showing tight accumulation of tumour cells with abundant melanin pigment and marked cellular infiltration of interalveolar spaces, D&E: lung tissue from properdin deficient mice showing tumour cells with some melanin pigment.

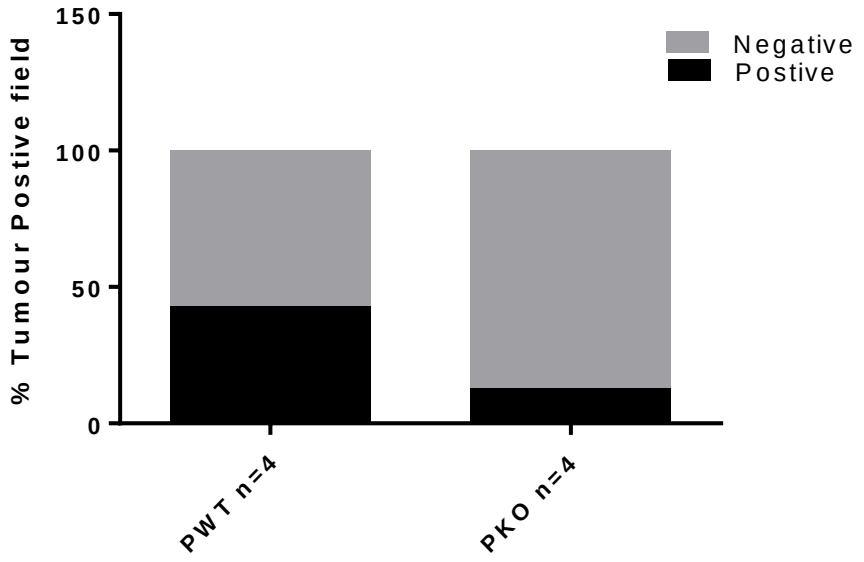

Figure 42: Percent of tumour cells in lung tissue sections from tumour bearing wildtype and properdin deficient mice.

Lung tissue sections from tumour bearing wildtype and properdin deficient mice were stained with Schmorl's stain, then an area of 100 mm^2 was examined microscopically and the number of 1mm fields showing tumour cells as visualised by Schmorl's stain was counted manually. The Percent of positive fields in each genotype was calculated. The percentage of positive cells expressed as Means± SEM in the PWT and PKO were 43 ±7.89 and 13 ±2.17 repectively, while the percentage of negative cells in the PWT and PKO was 57 ±7.8 and 84.75 ±1.8 respectively.

Intravenous instillation of tumour cells was not very successful. Only out of the16 injected mice, only 4 received the full dose due to technical reasons (tail veins hard to visualise in black mice). Realising that this model does not truly capture a metastatic growth, rather seeding of a bolus of tumour cells into the first capillary network after intravenous application (lungs), this model was abandoned in favour of the more successful subcutaneous. Injection in the flank (refinement, reduction).

4.5.2 Intravenous Injection of mice with B16F10

Subsequently, this experiment was repeated twice with different numbers (dose) of melanoma cells. There were technical difficulties to apply full dose (volume) via the lateral tail veins. Intravenous models of tumour implantation may suffer from several limitations, such as the difficulty in estimating if injection of cells was done properly, as variation may occur due to mis-injection of some of the cells. In addition, the black tail of C57BL6 mice makes it difficult to locate the lateral tail

vein. Hence, it was difficult to assess if the same number of cells was delivered to all mice. The injection dose in the two intravenous experiments ranged from 3-4x10^5 cell/100µl. In these two experiments lung weight were measured as shown in Figure 43. The results showed that wildtype tumour bearing mice had greater lung weight as compared to properdin deficient mice. Lung weights of healthy control mice were the same between the two genotypes.

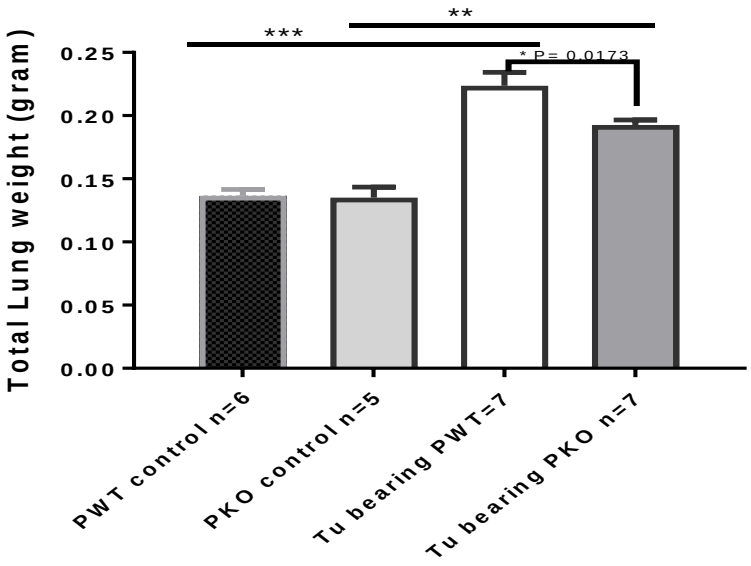

Figure 43: Total Lungs weight in PWT and PKO mice after intravenous injection of melanoma cells.

4×10^5 B16F10 cells were injected into the tail vein of 7 WT and 7 properdin deficient mice. Lungs of mice were removed after 10 days and weight was recorded in grams. The data are presented as means ±SEM. Statistical analysis was performed by one-tailed Mann-Whitney *U* test. * ($p < 0.05$).

Pigmented colonies were seen on the lungs as an indication of metastasis (as seen in Figure 5). Notably, the extent of pigmentation on the lungs of wildtype mice was more than that seen in properdin deficient mice.

4.5.3 Level of C5a in Intravenous syngeneic tumour PKO and PWT mice

Components of the complement system have been shown to play important roles in the response to tumours. One of those complement components is complement anaphylatoxin C5a. This complement component is a potent chemoattractant that activates and contributes in recruitment of immunosuppressive cells to primary tumour sites. Furthermore, C5a was found

to be a major player in immunosuppression, thereby facilitating metastasis (Vadrevu et al., 2014). Thus, the level of C5a was estimated in tumour bearing mice from wildtype and properdin mice as shown in Figure 44. The readings of the assayed samples were higher than that of the standards. Thus, the results of this experiment were expressed as optical density readings rather than concentration. The results showed that wildtype tumour bearing mice gave the highest OD reading indicating that C5a concentration was higher in this genotype. The reasons for this elevation, which presumably arises from complement activation, is not clear.

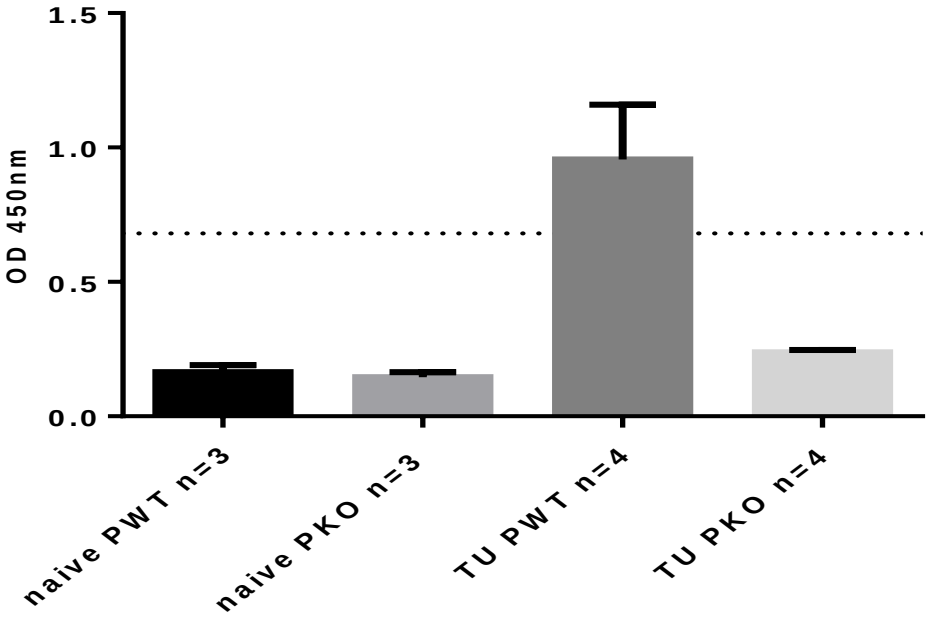

Figure 44: ELISA reading for C5a in tumour bearing mice.

Wildtype and Properdin deficient C57BL/6 mice were intravenously injected with $3X10^5$ cell/100µl of B16F10 cell suspension in tail vein. After 14 days, the mice were sacrificed and sera was collected for C5a quantification by ELISA. Lungs were macroscopically examined for pigmented colonies. PWT showed more intense pigmentation and also larger lung weight than PKO. The dotted line represents the cutoff of the standard curve.

4.5.4 Analysis of gene expression in mouse melanoma of wildtype and properdin deficient mice

Results presented in this chapter showed the abundance of $CD45^+CD11b^+Gr\text{-}1^+$ MDSCs was lower in properdin deficient compared to wildtype mice in tumour (4.5.9). Furthermore, $CD25^+CD4^+FOXP3^+$ Treg cell was lower in spleen of

properdin deficient compared to Wildtype mice. The cytokines transforming growth factor beta (TGF-β1) and IL-10 are associated with Treg production and are critical to immune homeostasis *in vivo* (Chen et al., 2009, Tsuji-Takayama et al., 2008).

FOXP3 transcription factor is the key driver of regulatory T cell differentiation and immunosuppressive function. In addition, FOXP3 has been reported to be expressed in many tumours, including melanoma. FOXP3 has also been suggested to facilitate tumourigenesis by enabling tumour cells to evade anti-tumour immunity (Niu et al., 2011). This has been demonstrated in pancreatic carcinoma and melanoma cell lines, where FOXP3 expression inhibits T cell proliferation in co-culture systems. TGF-β functions as an autocrine and paracrine factor that drives many cellular processes including tumour growth, invasion, escape from immune surveillance, angiogenesis and metastasis (Perrot et al., 2013).

It has been well documented that various cytokines, chemokines, and growth factors, including IL-1β, IL-6, IL-10, GM-CSF, VEGF, and TGF-β, are needed to drive MDSC migration into tumour lesions, and to keep their suppressive phenotype in tumour-bearing hosts (Gabrilovich and Nagaraj, 2009, Gabrilovich et al., 2012, Baniyash, 2006). Therefore, gene expression for IL-10, IL-17, FOXP3 , Crry (complement-receptor 1–related gene/protein y), TGF-β and VEGF in tumour of wildtype and properdin deficient mice was investigated. Crry is one of many surface regulators of complement activation which protect self-cells from the deleterious effects of cell-bound complement fragments. Murine Crry has the ability to inhibit the activation of C3 and protects self-tissues from complement-mediated damage (Molina, 2002).

The result represented by Figure 45 showed that wildtype mice had more FOXP3 and TGF-β mRNA (normalized to the housekeeping gene expression) compared to properdin deficient mice. Surprisingly, mRNA IL-10 expression showed no significant difference between the genotypes. While gene expression for IL-17, Crry and VEGF was similar between wildtype and properdin deficient mice. These results possibly indicate that the absence of properdin leads to less immune suppression in melanoma mouse model or different cell populations are recruited.

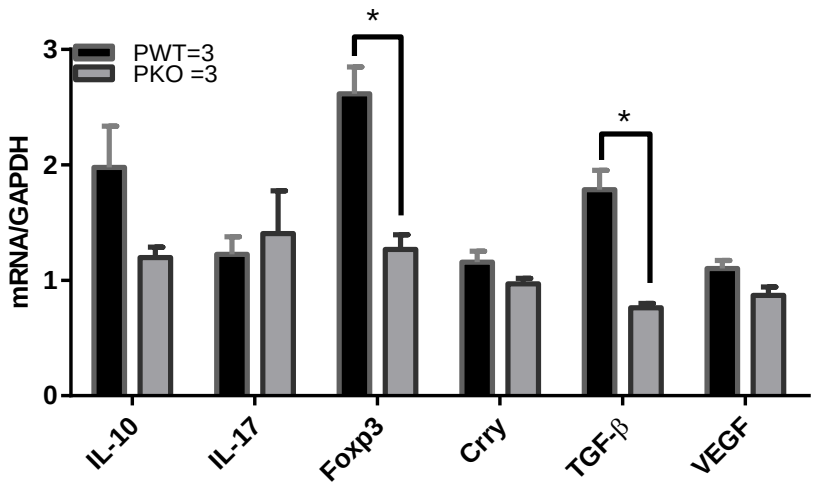

Figure 45: Analysis of mRNA expression in tumours of wildtype and properdin-deficient mice.

Wildtype (n=3) and properdin-deficient (n=3) mice were injected subcutaneously with 1.6×10^5 cell/100µl of B16F10 cell suspension. After 14 days the mice were sacrificed and dissected for collection of tumours. Total RNA was isolated from tumours and qPCR was conducted for gene expression of IL-10, IL-17, FOXP3 , Crry, TGF-β and VEGF to GAPDH, mRNA for GAPDH was stable, each set up in duplicate. The data are presented as means ±SEM. Statistical analyses were performed using one-tailed Mann-Whitney U test (significances with brackets). * Significantly different from the control group, $p<0.05$.

4.5.5 Protein macroarray for Tumour lysates.

Histological stains revealed a heterogeneous picture which did not relate to a certain genotype. Immunohistochemical analysis was attempted (CD86, CD88, VEGF, VWF and CD31),but did not prove successful as mentioned in 4.4.1. Therefore, to allow an efficient screen for relevant markers, tumours from three WT and three KO were pooled, lysate were prepared and antibody presenting membranes were hybridised. In this way, the presence and abundance of 18 chemokines could be interrogated at once.

Mouse Cytokine Array allows detection and measurement of a number of cytokines simultaneously. It involves the use of carefully selected capture antibodies which have been spotted on nitrocellulose membranes.

The Proteome ProfilerTM Array was used for determination of the relative levels of selected mouse cytokines and chemokines (18 in total) in tumour lysates from both wildtype and properdin deficient mice in an attempt to explore any difference between genotypes. The results represented by Figure 46 showed that this approach managed to identify 6 out of the 18 selected cytokines and chemokines.

The result showed that wildtype tumour bearing mice had higher levels of TIMP-1 (metallopeptidase inhibitor 1), IL-13, IL-1ra (Interleukin 1 Receptor Antagonist), JE CCL2 (Monocyte chemotactic protein-1) and MIP-1a/CCL3 (Macrophage Inflammatory Proteins 1a). CCL3 may be effective to enhance tumour immunity by attracting immature DCs to dying tumour cells (Mukaida et al., 2014). TIMP-1 has been shown to inhibit tumour-induced angiogenesis in experimental systems (Wojtowicz-Praga et al., 1997). Statistical analysis revealed that PWT tumour bearing mice had a significantly higher level of TIMP-1, CCL2 and CCL3 when compared to PKo mice which possibily could be linked to more cell recruitment.

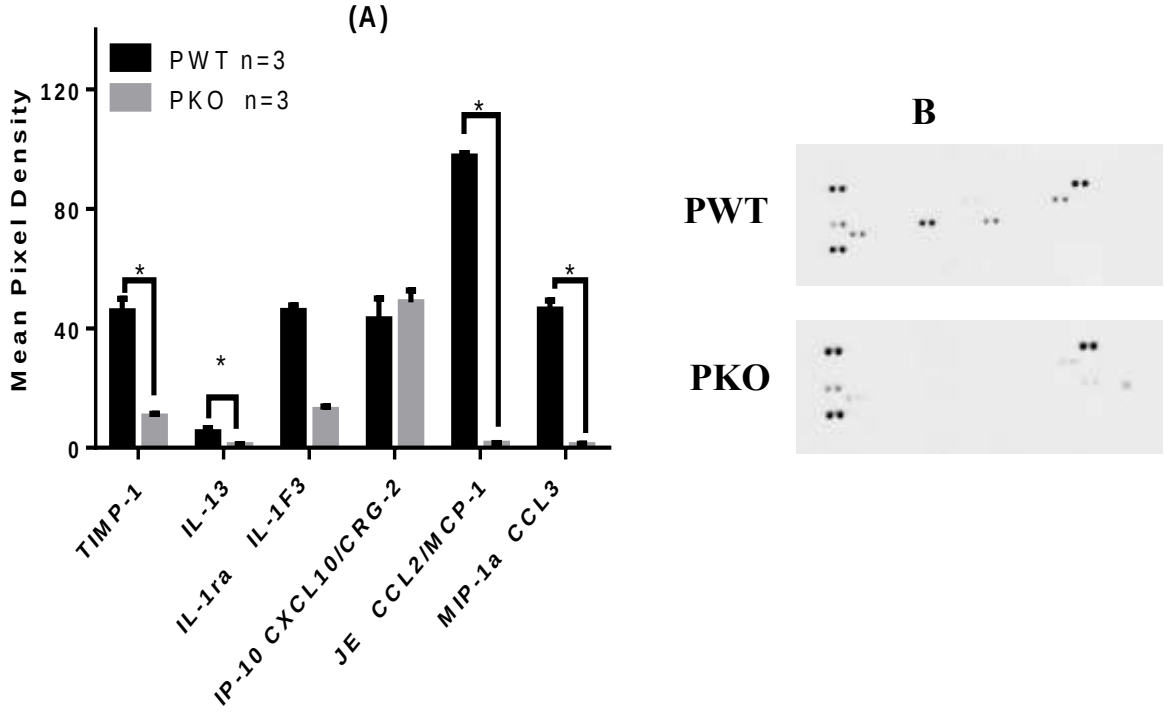

Figure 46: The Mouse Cytokine Array detects multiple analytes in tumour lysates of wildtype and deficient mice.

A- Wildtype and properdin deficient Mice were injected subcutaneously with 1.6 $X10^5$ B16F10 cell/100µl for 14 days. Tissues were excised and prepared as described in the Sample Collection and Storage section. 300µg of lysate was run on each array. CXCL13 ,C5/C5a,G-CSF, GM-CSF, CCL1, Exotoxin ,CCL11,sICAM-1, IFN-γ,IL-1α, IL-1β, IL-1F2, IL-2,IL-3,IL-4, IL-6, IL-7, IL-10, IL-13,IL-12 p70, IL-16,IL-17,IL-23, IL-27,CXCL11, CXCL1, M-CSF, CCL12,CXCL9, CCL3, CCL4, CXCL2, CCL5, CXCL12, CCL17, TNF-α, TREM-1 were undetected in these samples .Figure shows the 6 identified cytokines by the array. Data shown. B-array members are from a five minute exposure to X-ray film.The data are presented as means ±SEM. Statistical analysis was performed by one-tailed Mann-Whitney *U* test. * ($p < 0.05$).

4.5.6 Level of CCL2 in sera of Wildtype and properdin deficient tumour bearing mice

Other than its chemotactic function, CCL2 has recently been shown to be involved in tumour progression and metastasis (Li et al., 2013a). The previous results of protein microarray for tumour lysates demonstrated a significant difference in the level of CCL2 between PWT and PKO mice. To further confirm this difference, the level of CCL2 was measured in sera of PWT and PKO tumour bearing mice. Serum levels of CCL2 as measured by ELISA also showed that PWT tumour bearing mice had a significantly higher level when compared to its PKO counterparts (Figure 47). This difference was only seen after 14 days of tumour implantation. Although there was no significant difference after 7 days of tumour implantation, but there was also a trend of PWT having more CCL2. In contrast, measurement of CCL2 in sera of naïve mice revealed that PKO had a significantly higher levels of this chemokine which probably indicate more M2 macrophages in PKO mice. This result indicates CCL2 is a M2 marker for 14 day's tumour growth.

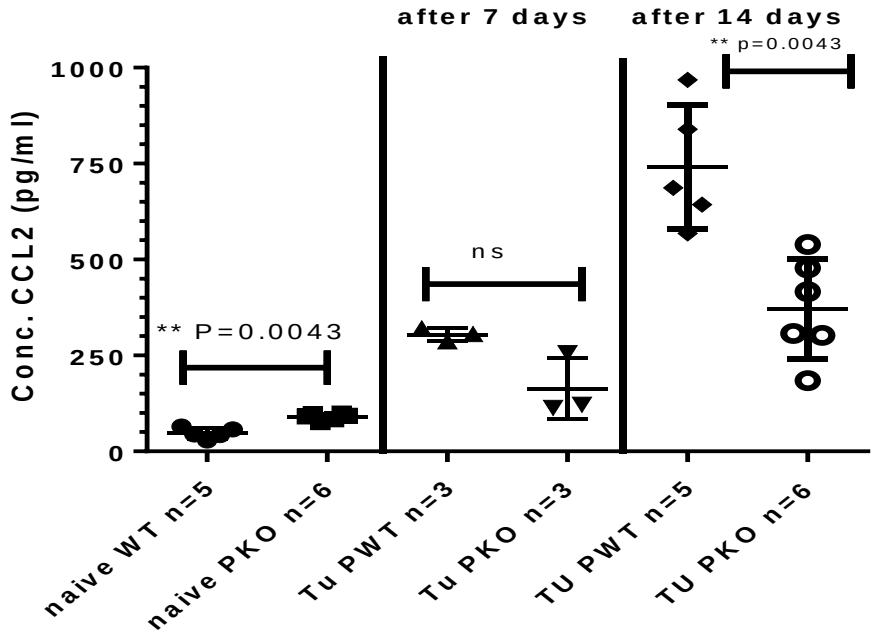

Figure 47: Levels of CCL2 in sera of naïve and tumour bearing mice from both genotypes. Mice were injected subcutaneously with 1.6×10^5 cell/100µl of B16F10 cell suspension. After 14 days, the mice were sacrificed and sera were collected for CCL2 measurement by ELISA. The data are presented as means ±SEM. Statistical analysis was performed by one-tailed Mann-Whitney *U* test. * ($p < 0.05$).

4.5.7 Analysis of tumour microenvironment by flow cytometry

The previously seen vascularisation in tumour, tendency towards greater tumour mass and high level of C5a reported in the PWT led to further investigations into various components of the tumour microenvironment (TME). There is an increasing body of evidence which has recognised the importance of studying the various components of TME as a means to further understand factors which promote tumour progression. Hence, part of this thesis was dedicated to studying some components of TME in both PWT and PKO mice.

4.5.8 T-regulatory ($CD25^+CD4^+FOXP3^+$) cells in Tumour of PWT and PKO mice.

One of the major players in the TME is T-regulatory lymphocytes (T-regs). Furthermore, T-regs have been reported to be one of the major obstacles which ultimately result in failure of anti-tumour immunotherapy (Zou, 2006). Earlier studies defined T-regs as $CD4^+CD25^+$ lymphocytes. Nevertheless, subsequent reports found that they also express the forkhead/winged helix family transcription factor FOXP3 . Thus, these markers were used to investigate the percentage of T-regs in tumours of PWT and PKO mice and the results are shown in Figure 48. Flow cytometry analysis of T-regulatory (CD25+CD4+FOXP3 +) cells in tumour showed no difference between genotypes. However, FOXP3 mRNA was high in PWT compared to PKO in tumour as mentioned previously (4.5.4). FACS analysis was done using three markers; CD25, CD4 and FOXP3 . The gating was done on $CD25^+$ cells, and the percent of populations of T-regs were calculated using Flow Jo software (see appendix).

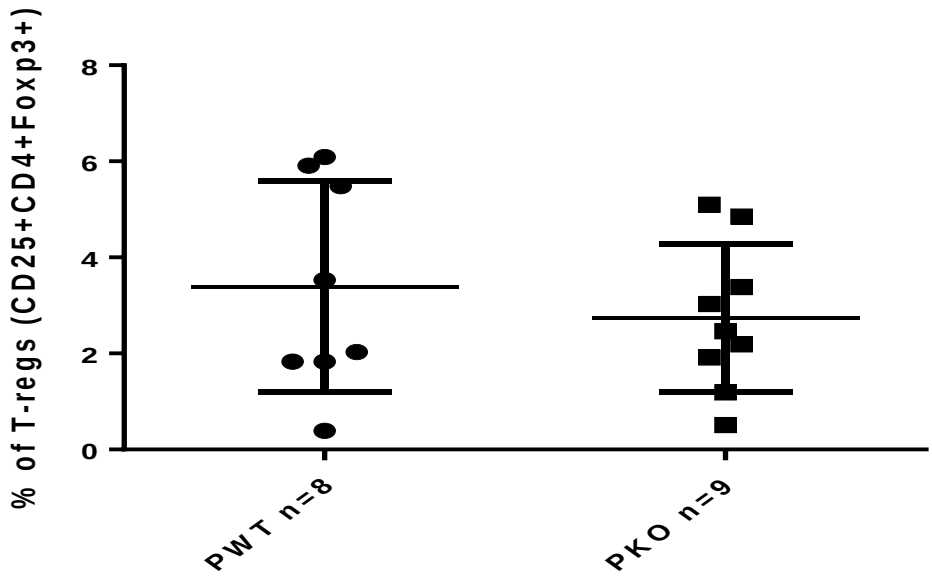

Figure 48: Percentage of T-regs in tumour of PWT and PKO mice.

Mice were injected subcutaneously with 1.6×10^5 cell/100µl of B16F10 cell suspension. After 14 days the mice were sacrificed and dissected for collection of tumour tissue. Tumour suspension from both genotypes were stained with three markers (CD25+, CD4+ and FOXP3 +) to distinguish T-reg. Then FACS was done and percentage of T-regs was obtained. The gating was on CD25, and the other two markers were used to calculate of total T-regs in tumour. The data are presented as means ±SEM. Statistical analysis was performed by one-tailed Mann-Whitney U test. * ($p < 0.05$).

4.5.9 Percentage of MDSCs cells in Tumour of PKO and PWT mice.

Tumour cells recruit myeloid derived suppressor cells (MDSC) and generate an immunosuppressive environment. Accumulation of MDSC have been linked to tumour growth. Thus, the frequency of MDSC was estimated in tumour tissue from both genotypes by flow cytometry analysis.

FACS analysis was done using three markers; CD45, Gr-1 and CD11b. The gating was done on $CD45^+$ cells, and the percent of populations of MDSC were calculated using flow jo software. Calculation of total number of MDSC in tumour showed that the highest percent of MDSC among $CD45^+$ was found in properdin wildtype mice. Interestingly, in both genotypes percentage of MSDCs in tumour correlated with tumour weight (see appendix).

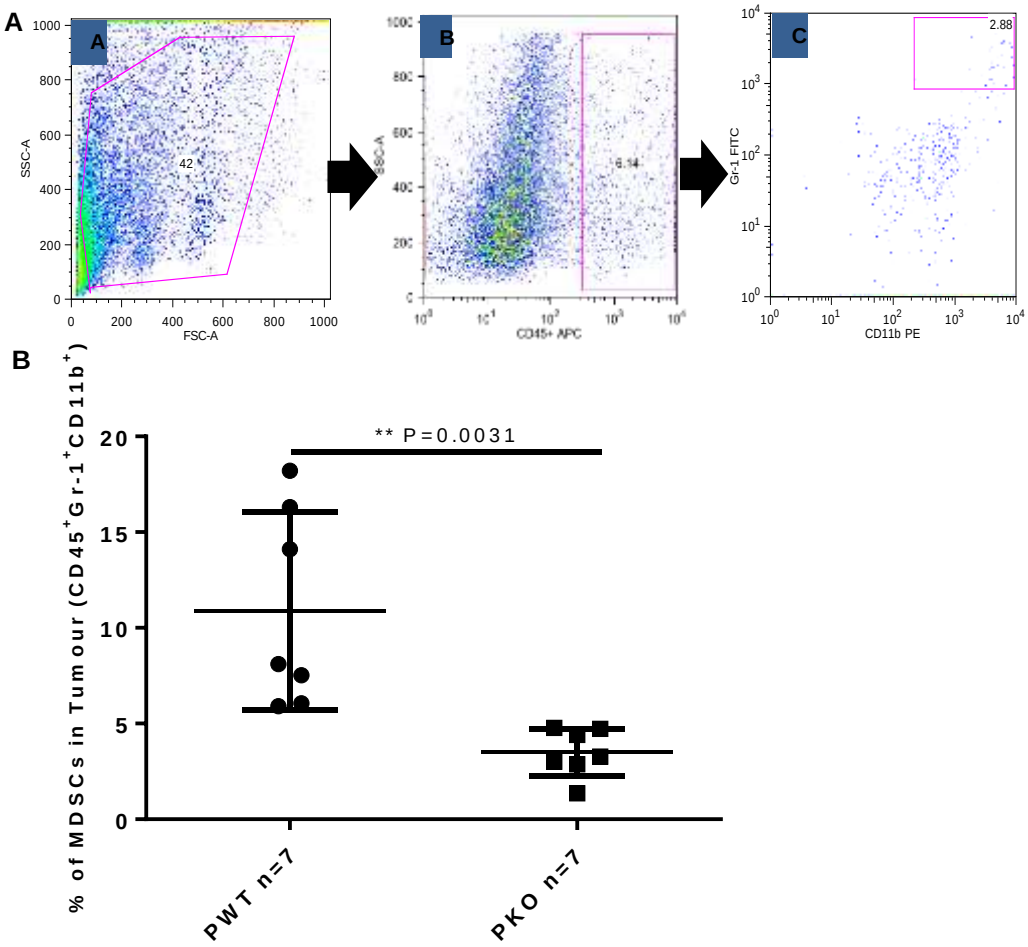

Figure 49: MDSC populations in tumour of wildtype and properdin deficient mice.

A) Flow cytometry analysis of Gr-1 and CD11b cells after gating on $CD45^+$cells in MDSCs from tumour, wildtype and properdin deficient mice. Numbers in the plots indicate the percent of gated cells. $CD45^+Gr\text{-}1^+CD11b^+$ represent percentage of MDSC. B) Populations of MDSCs in tumour of wildtype and properdin deficient mice. Mice were injected subcutaneously with 1.6×10^5 cell/100µl of B16F10 cell suspension. After 14 days the mice were sacrificed and dissected for collection of tumour tissue. Tumour suspension from both genotypes were stained with three markers (CD11b, Gr1 and CD45) to distinguish MDSC. Then FACS was done and percentage of MDSCs was obtained. The gating was on CD45, and the other two markers were used to calculate of total MDSC in tumour. The data are presented as means ±SEM. Statistical analysis was performed by one-tailed Mann-Whitney U test. * ($p < 0.05$).

4.5.10 Percentage of CD45+IL-10 and CD45+TGF-β cells in tumour of wildtype and Properdin deficient mice by flow cytometry

MDSCs can suppress anti-tumour immunity indirectly. Like M2 TAMs, MDSCs generate the cytokines IL-10 and TGF-β that can suppress antitumour TILs, generate T-regs in the tumour, and convert DCs into a regulatory phenotype.(Yang et al., 2006). MDSCs can also recruit T-regs to tumours in a TGF-β–independent pathway (Serafini et al., 2008).

Therefore, FACS for TGF-β and lL-10 positive cells in tumours of wildtype and properdin deficient mice was done. The strategy used for analysis of IL-10, TGF-β and lL-10 in tumour was the same as in that in Figure 50A.

FACS analysis showed that tumour of PWT had a significantly higher percentage of TGF-β^+ cells when compared to Properdin deficient mice, which is consistent with the result obtained by gene expression. However, IL-10 result showed no difference between the genotypes (as shown in Figure 50C) indicating that tumour cell analysis is more revealing for impaired immune reactant mobilisation in properdin deficient mice.

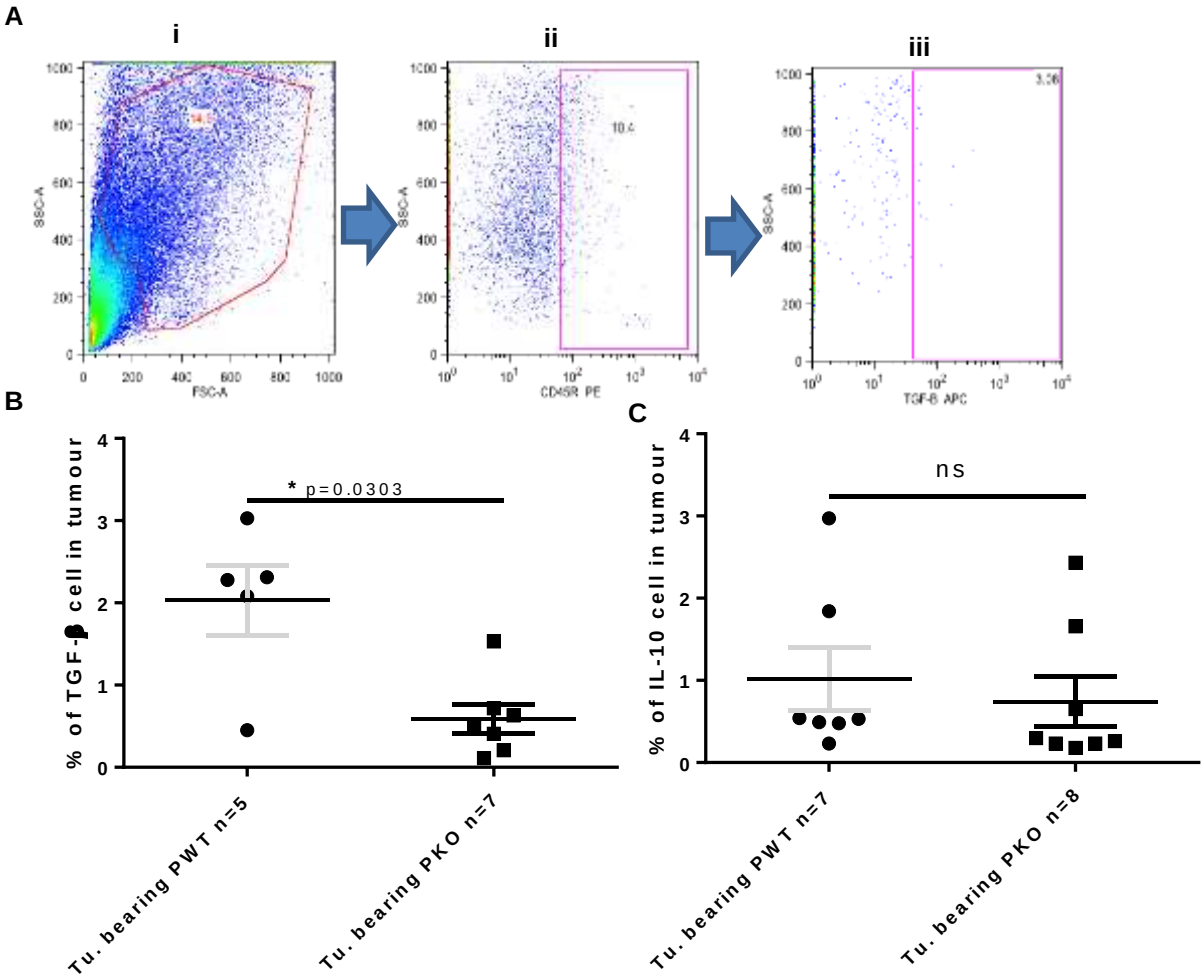

Figure 50: Strategy of FACS analysis of TGF-β⁺ cell in tumour.

A) Representative flow cytometry analysis of percentage TGF-β cells. After gating on CD45+cells in spleen. i- the gating on main population of tumour, ii- gating on CD45+ cells only, iii-gating on TGF-β cells. B) Mice were injected subcutaneously with 1.6×10^5 cell/100µl of B16F10 cell suspension. After 14 days the mice were sacrificed and dissected for collection of tumour. Tumour suspension from both genotypes were stained with two markers ($CD45^+$IL-10, $CD45^+$TGF-β. Then FACS was done and percentage of TGF-β were obtained. The data are presented as means ±SEM. Statistical analysis was performed by one-tailed Mann-Whitney U test. * ($p < 0.05$).

4.6 Complement activation in tumour bearing deficient mice.

Elements of the complement cascade contain some of the most powerful proinflammatory molecules, such as the anaphylatoxins C3a and C5a. The continuous activation and consumption of complement proteins in chronic inflammatory states such as cancer have long been recognised. Furthermore, complement proteins are direct and indirect players in angiogenesis which has been linked with tumour aggressiveness. Work by Markiewski and co-workers

has challenged the conventional anticancer role of complement in tumour growth and presented data demonstrating that components of the complement system may actually assist tumour growth. Their work has provided evidence that tumour cells may exploit complement components to generate an immunosuppressive environment, thereby providing a growth advantage (Markiewski et al., 2008). Given the important role of complement in tumour progression, this part of the thesis was dedicated to quantification of some complement components in tumour bearing mice.

4.6.1 Quantification of C5a in tumour lysates of tumour bearing wildtype and Properdin deficient mice.

C5a is one of complement effectors which has a capability to promote tumour growth (Markiewski et al., 2008). The level of this potent pro-inflammatory mediator was quantified using a commercially available mouse C5a ELISA kit. The results presented in Figure 51 showed that, as before for the i.v. model,(4.5.2), PWT tumour bearing mice had a significantly higher level of C5a when compared to PKO mice.

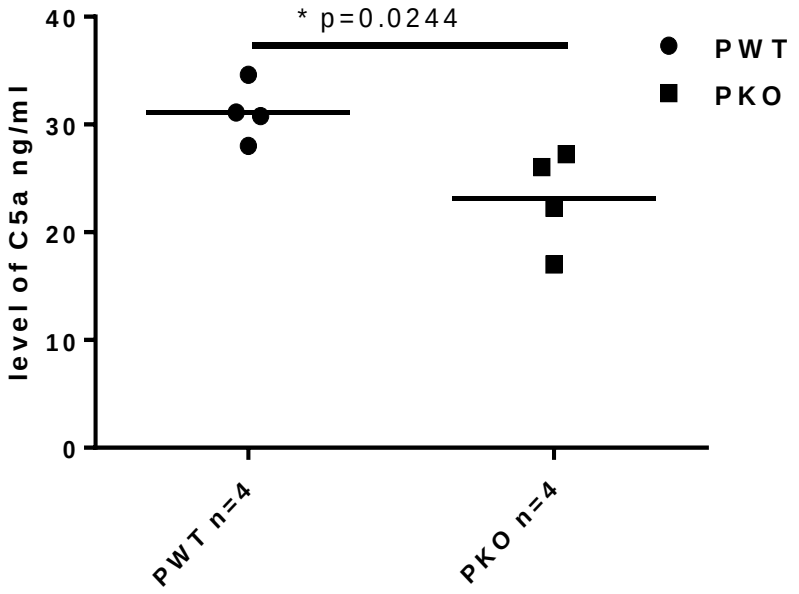

Figure 51: Level of C5a in tumour lysate of PWT and PKO mice.

Wildtype and Properdin deficient C57BL/6 mice were injected subcutaneously with 4×10^5 cell/100µl of B16F10 cell suspension. After 14 days, the mice were sacrificed and tumours were collected and prepared for C5a quantification by ELISA. The data are presented as means ±SEM. Statistical analysis was performed by one-tailed Mann-Whitney U test. * ($p < 0.05$).

4.6.2 Measurement of complement components C3 in sera of PWT and PKO tumour bearing mice.

The activation of complement system is one of the most important features characterising the host's immune response to tumours. C3 is a central molecule in the complement cascade and quantification of this molecule would provide further insights into the level of complement activation in cancer. Measurement of C3 in sera of tumour bearing mice revealed that PWT has a significantly higher level when compared to PKO (Figure 52). Levels of C3 in sera of tumour bearing mice were higher than that of naïve mice (Figure 52), however it did not reach statistical difference. It is not known whether this increase in C3 was a result of total C3 or due to an increase in the anaphylatoxin C3a, as the antibody used was one that reacts with all fragments of C3.

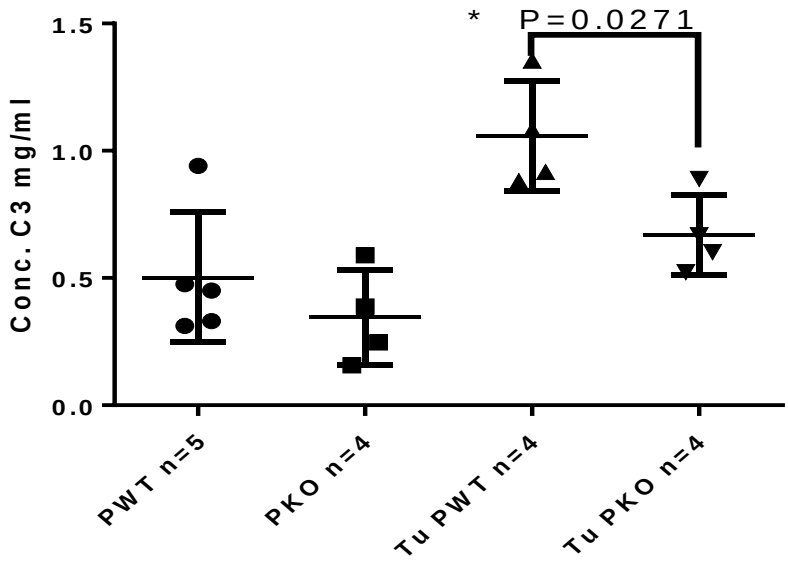

Figure 52: Level of C3 in sera of PWT and PKO tumour bearing mice.

Mice were injected subcutaneously with 1.6×10^5 cell/100µl of B16F10 cell suspension. After 14 days, the mice were sacrificed and sera was collected for C3 measurement by ELISA. The data are presented as means ±SEM. Statistical analysis was performed by one-tailed Mann-Whitney U test. * ($p < 0.05$).

4.6.3 C5a and C5b-9 in sera of PWT compared to PKO tumour bearing mice after 14 days of subcutaneous injection of B16F10.

The previous results revealed that C5a was higher in tumour lysates of PWT mice. The next step was to investigate if this anaphylatoxin was also increased in sera of tumour bearing mice. Quantification of C5a in sera of naïve and tumour bearing mice revealed that tumour bearing mice from both genotypes had a significant increase in C5a as shown in Figure 53. In addition, PWT tumour bearing mice had an increased serum level of C5a when compared to PKO. Interestingly, naïve mice showed no difference between genotypes in serum level of C5a. Notably, repeated measurements of C5a in sera of naïve mice consistently showed that PWT mice tended to have increased levels of C5a, however, this never reached statistical significance. The increased level of C5a in tumour bearing mice as compared with naïve mice raised the question whether this increase was a consequence of complement activation. It is well known that all three complement pathways involve cleavage of the central component C3 and the subsequent formation of C3a and C5a, in addition to the formation of the membrane attack complex C5b-9. Thus, levels of C5b-9 (MAC complex) as an indication of complement activation was investigated by ELISA as shown in Figure 53. The results demonstrated that PWT tumour bearing had a significantly higher level of serum C5b-9 when compared to its PKO counterparts. Surprisingly, no significant difference was found in serum level of C5b-9 between naïve and tumour bearing mice despite the difference seen in the level of C5a. Generation of C5a in the absence of C3 has previously been described. In the absence of C3, thrombin acts as a C5 convertase and generating C5 (Huber-Lang et al., 2006). These observations raised the question whether B16F10 can produce thrombin. Kirszberg and co-workers reported that B16F10 melanoma cells generate thrombin by promoting assembly of the prothrombinase complex (Kirszberg et al., 2005). Production of prothrombin by B16F10 was later confirmed in our lab by Western blotting (band is about 190 KDa). This was carried by subjecting B16F10 cell lysate to rat anti- Mouse prothrombin monoclonal antibody (Haematologies Technologies) as primary antibody and Goat anti-Rat IgG- HRP (anti- prothrombin) as secondary antibody. Human plasma containing 5Mm (EDTA) was used as a positive control.

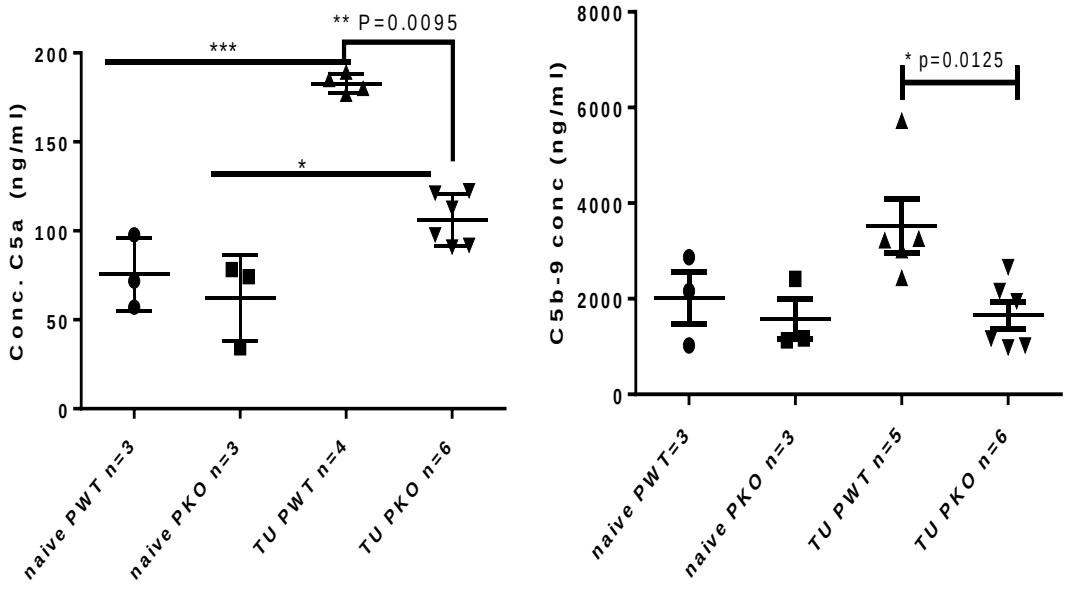

Figure 53: Level of C5a and C5b-9 in sera of tumour bearing mice.

Wildtype and properdin deficient C57BL/6 mice were injected subcutaneously with 1.6×10^5 cell/100µl of B16F10 cell suspension. After 14 days the mice were sacrificed and sera was collected for C5a and C5b-9 measurement by ELISA. The results showed a pattern of C5a and C5b-9 elevation for wildtype compared to properdin deficient tumour bearing mice. Tumour weight measurement showed an increase in PWT compared to properdin deficient mice. This indicates that high C5a coincides with limited tumour growth in Properdin WT.

4.6.4 Lectin pathway C9 activity in PWT and PKO tumour bearing mice

The previous results for C5a and C5b-9 showed high levels in sera of PWT tumour bearing mice as compared to PKO which could either be due to complement activation or other pathways. To confirm whether it was due to complement activation or not, ELISA for lectin pathway C9 activation was done on sera from tumour bearing mice. LP was chosen due to low immunogenicity of B16F10 which excludes classical pathway activation. The results represented by Figure 54 showed low C9 activity in PWT tumour bearing mice indicating more complement consumption, which is in line with the previous results for C5a and C5b-9. In naïve mice, no significant difference in C9 activity was detected between genotypes.

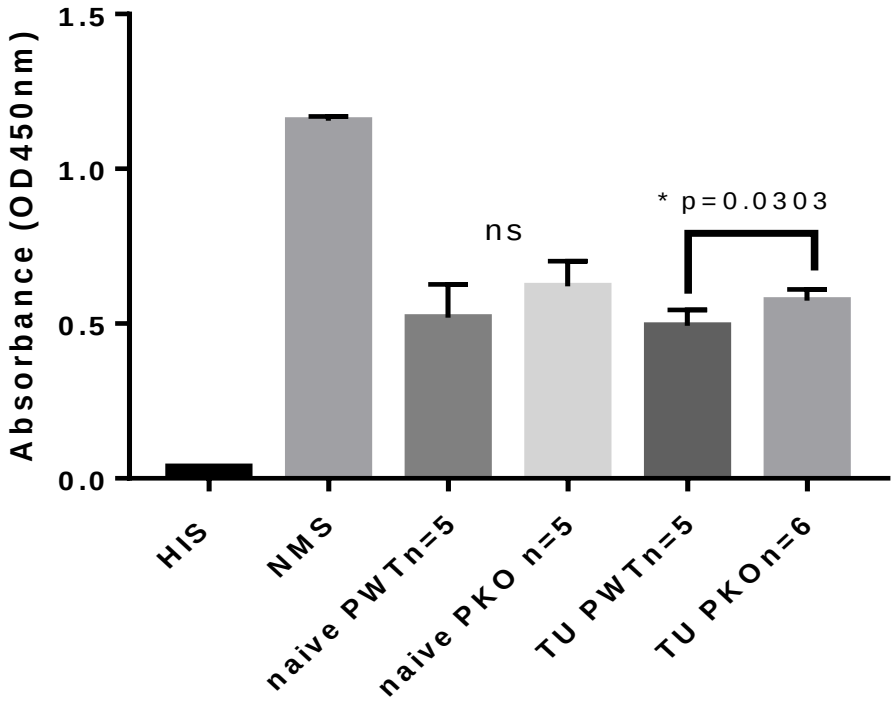

Figure 54: Determination of Lectin pathway functional complement activities at the level of C9 formation in sera of PWT n=5 and PKO n=6 tumour bearing mice.

Mice were injected subcutaneously with 1.6×10^5 cell/100µl of B16F10 cell suspension. After 14 days, the mice were sacrificed and sera was collected for LP measurement by ELISA. 20% heat inactivated serum (HIS), (serum heated at 56°C for 30 minutes). Normal mouse serum (NMS) was obtained commercialy for assessment. The absorbance was measured at 450 nm .The data are presented as means ±SEM. Statistical analysis was performed by one-tailed Mann-Whitney *U* test. * ($p < 0.05$).

4.7 Analysis of C5aR+Gr-1 cells

4.7.1 $C5aR^{+}Gr\text{-}1^{+}$ Cells: Gating strategy

Gr-1 is a myeloid differentiation antigen expressed on granulocytes and macrophages. Recently, it has been suggested that C5a and C5aR play an important role to tumour metastasis. C5a/C5aR signaling contribute to the recruitment and generation of immunosuppressive cells and thereby create an environment favoring tumour metastasis (Vadrevu et al., 2014). C5a is an anaphylatoxin which works after binding to the high affinity C5a receptor (CD88). Expression of C5aR was found in eripheral blood leukocytes (neutrophils, eosinophils, monocytes and macrophages). Furthermore, recent studies have demonstrated that C5aR expression can also be found in liver and lung cells (Haviland et al., 1995).

Studies on the role of C5a in tumour growth have concluded that C5a concentration plays an important role in determining tumour progression (Gunn et al., 2012). The percentage of $C5aR^{+}Gr\text{-}1^{+}$ Cells was investigated by flow cytometry analysis of BM and splenocytes. FACS analysis was done using two markers; Gr-1 and C5aR. The percent of populations of $C5aR^{+}Gr\text{-}1^{+}$ Cells were calculated in spleen and BM of PWT and PKO naïve and tumour bearing mice using Flow Jo software as shown in 4.7-A.

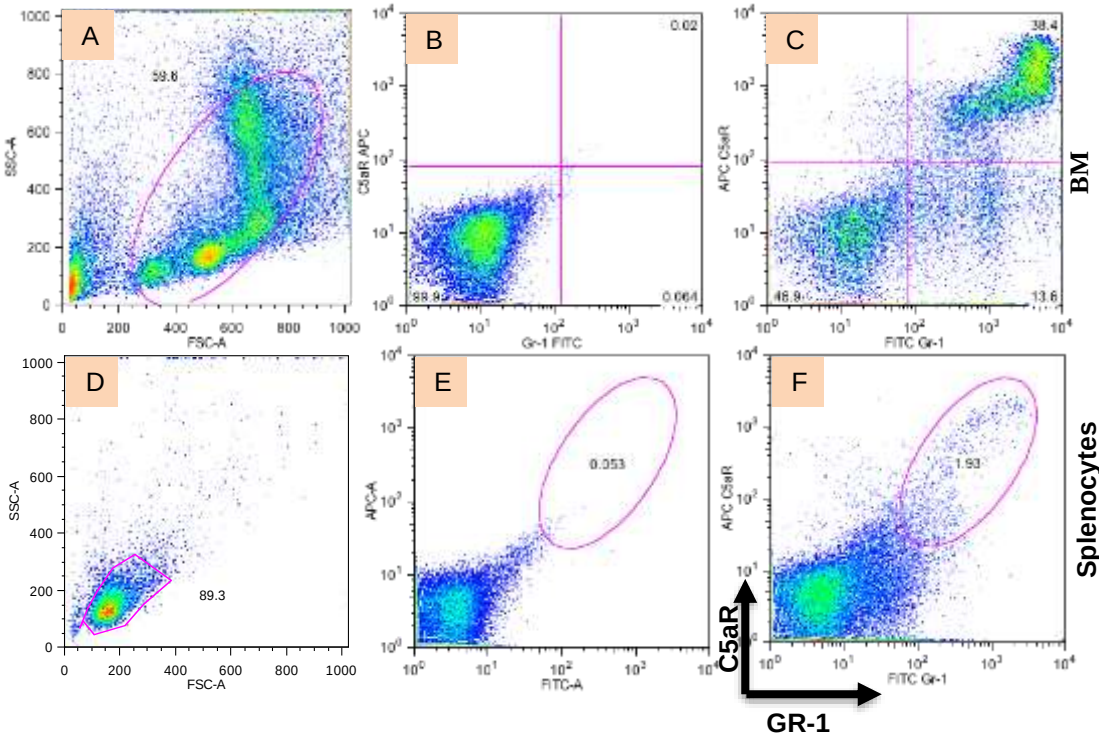

Figure 55 : C5aR+GR-1 populations in tumour bearing and naïve of wildtype and properdin deficient mice.

Flow cytometry analysis of Gr-1 FITC and C5aR APC cells in Spleen and BM from tumour bearing and naïve mice. A, B and C represent BM, where A: BM main population, B: unstain cell C:double positive cells $C5aR^{+}Gr\text{-}1^{+}$. D, E and F represent spleen where D: spleen main population E: control cells (unstain) for spleen and F:double positive cells $C5aR^{+}Gr\text{-}1^{+}$.

4.7.2 Percentage of $C5aR^{+}Gr\text{-}1^{+}$ cells in PWT compared to PKO tumour bearing mice in spleen

The aim of the current experiment was to study the expression of C5aR in spleen and the results are presented Figure 56. The results demonstrated that PKO tumour bearing mice have a significantly higher level of $C5aR^{+}Gr\text{-}1^{+}$ in splenocytes when compared to PWT counterparts. Similarly, PKO naïve mice showed higher levels of $C5aR^{+}Gr\text{-}1^{+}$ Cells than PWT naïve mice. Compared to naïve mice, expression of $C5aR^{+}Gr\text{-}1^{+}$ Cells was decreased in tumour bearing mice.

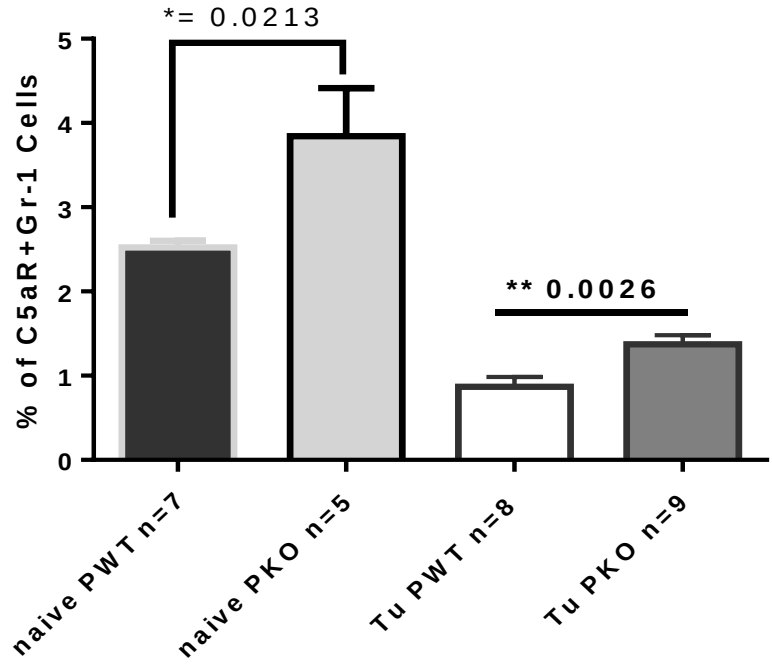

Figure 56: Percentage of C5aR$^+$GR-1$^+$ Cells in tumour bearing and naïve mice of PWT and PKO mice.

Populations of C5aR+Gr-1 cells in spleen of wildtype and properdin deficient mice. Mice were injected subcutaneously with 1.6×10^5 cell/100µl of B16F10 cell suspension. After 14 days the mice were sacrificed and dissected for collection of spleen. Spleen suspension from both genotypes were stained with two markers (Gr-1 FITC and C5aR APC). Then FACS was done and percentage of Gr-1$^+$C5aR was obtained.The data are presented as means ±SEM. Statistical analysis was performed by one-tailed Mann-Whitney U test. * ($p < 0.05$).

4.7.3 Percentage of C5aR$^+$Gr-1$^+$ cells in BM of PWT and PKO tumour bearing and naïve mice

In addition to BM, the percentage of C5aR$^+$Gr-1$^+$ cells were also investigated in spleen of PWT compared to PKO tumour bearing mice. Percentage of C5aR$^+$Gr-1$^+$ cells was significantly decreased in BM of PWT tumour bearing mice when compared to PKO as shown in Figure 57. Nevertheless, in naïve mice no significant difference in the percentage of C5aR$^+$Gr-1$^+$ cells was found between genotypes.

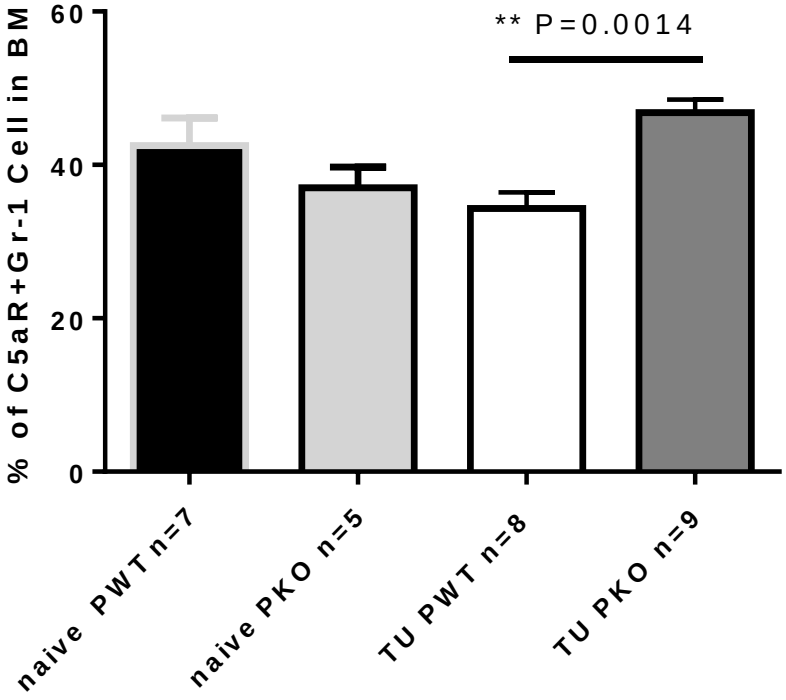

Figure 57: Percentage of C5aR$^+$Gr-1$^+$ cells PWT compared to PKO tumour bearing mice in BM.

Percentage of C5aR$^+$Gr-1$^+$ Cells in tumour bearing and naïve mice of PWT and PKO mice. Populations of C5aR$^+$Gr-1 cells in BM of wildtype and properdin deficient mice. Mice were injected subcutaneously with 1.6×10^5 cell/100µl of B16F10 cell suspension. After 14 days the mice were sacrificed and dissected for collection of BM. BM suspension from both genotypes were stained with two markers (Gr-1 and C5aR). Then FACS was done and percentage of Gr-1+C5aR was obtained. The data are presented as means ±SEM. Statistical analysis was performed by one-tailed Mann-Whitney U test. * ($p < 0.05$).

4.8 C5aR was downregulated on J774 1hr post C5a addition

The previous results showed that increased serum concentration of C5a coincided with decreased expression of C5aR in PWT tumour bearing mice in spleen and BM. To investigate the underlying reason for the aforementioned results, an *in vitro* experiment was set up which measures the expression of C5aR post exogenous addition of C5a. Previous reports have managed to demonstrate binding of exogenously added C5a with C5aR expressing cells. The macrophage-like cell line J774 has previously been reported to express classical types of the C5a and C3a chemokine receptors (Fan and McCloskey, 1994). Thus, J774 cells were *in vitro* stimulated by adding recombinant mouse C5a. Subsequently, FACs analysis was used to measure the expression of C5aR (CD88) after 1, 2, 3 and 5 hours of C5a addition. The results demonstrated (Figure 58) that expression of C5aR decreased after 1 hour of C5a addition when compared to control. Nevertheless, this decrease was not noticed after 2, 3 or 5 hours. Recently, van den Berg and co-workers reported that stimulation of macrophages with C5a resulted in downregulation of C5aR on these cells (van den Berg et al., 2014). Previously, it has been shown that macrophages tend to take up peptides within 1 hour and this probably explains downregulation of the receptor after 1 hour (Ehrenreich and Cohn, 1968).

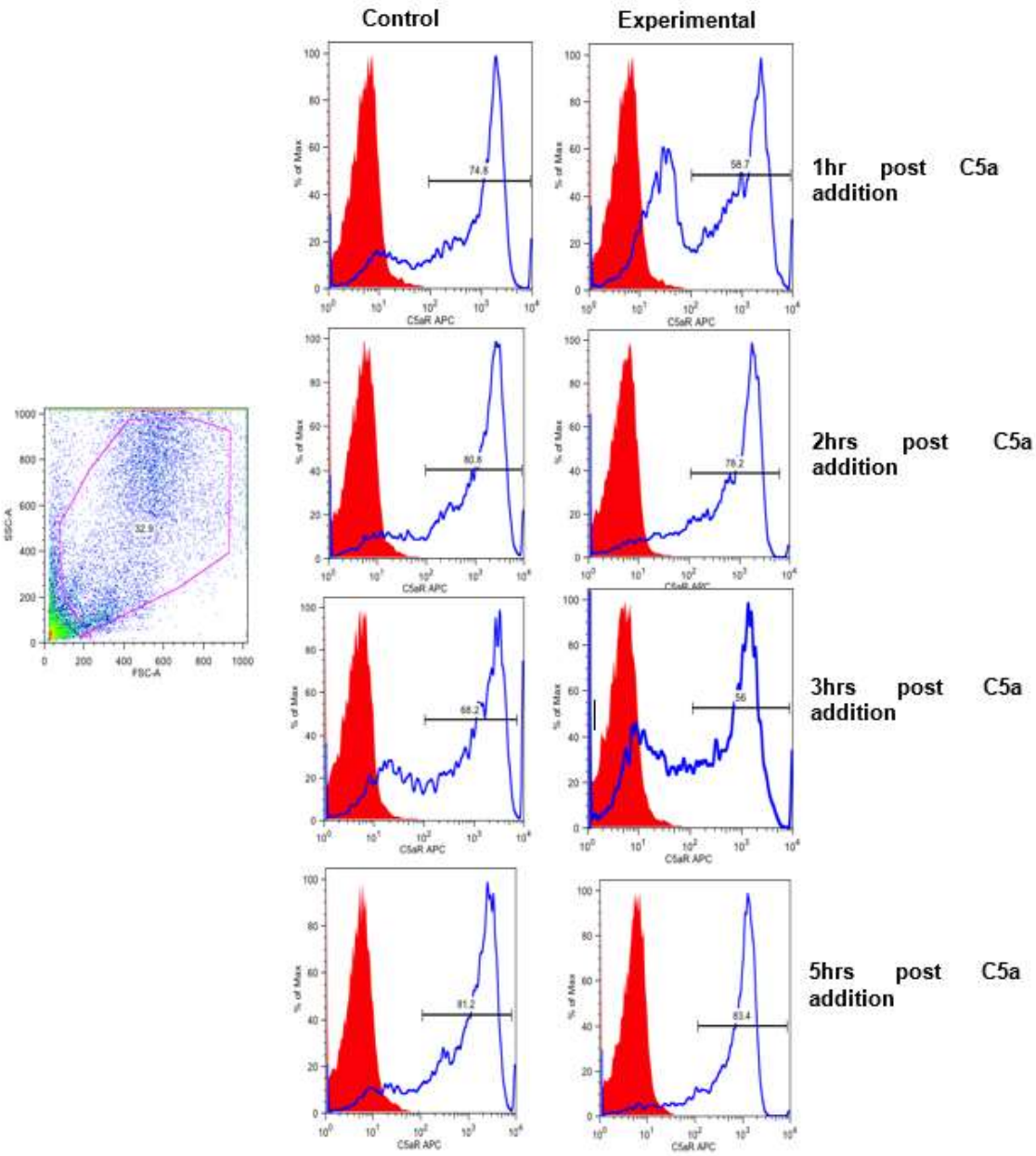

Figure 58: Expression of C5aR on J774 cells post C5a addition.

J774 cells were incubated with100nM of recombinant mouse C5a (R&D) for 1, 2, 3 and 5 hours. In addition, J774 was also incubated with medium only as a control. After each time point cells were collected and expression of C5aR (CD88) was analysed by flow cytometry after staining with mouse anti C5aR APC.

4.9 Strategy for identifying MDSCs in Spleen of wildtype, properdin deficient tumour bearing mice and naïve mice.

MDSCs were identified in spleen of PWT and PKO tumour bearing and naïve mice using the same strategy mentioned in 4.5.9. Unlike in tumour suspension, the percentage of CD45+ cells was about 90% in spleen as shown in Figure 59a. Animal models of disease have demonstrated that splenic haematopoiesis happens in a number of diseases including cancer. Interestingly, two scenarios have been put forward regarding the nature of these cells. The first postulates that cells accumulated in spleen are distinct from their BM counterparts. On the other hand, the second scenario postulates that the splenic niche is similar to that of BM and thus produce cells that are similar to their BM counterparts (Bronte and Pittet, 2013). Recent studies have reported the accumulation of immature MDSCs in spleens of tumour bearing mice (Gabrilovich et al., 2012). Investigating the expansion of MDSCs in the spleen has been the goal of several cancer research studies. In order to study the expansion of MDSCs in spleen of PWT and PKO tumour bearing and naïve mice, FACS analysis using $CD45^+Gr\text{-}1^+CD11b^+$ as markers for MDSCs was performed. The results showed higher percentage of MDSCs ($CD45^+Gr\text{-}1^+CD11b^+$) in spleen of PWT when compared to PKO tumour bearing mice as shown in Figure 59b. In spleen of naïve mice, no significant difference was found between PWT and PKO in naïve mice.

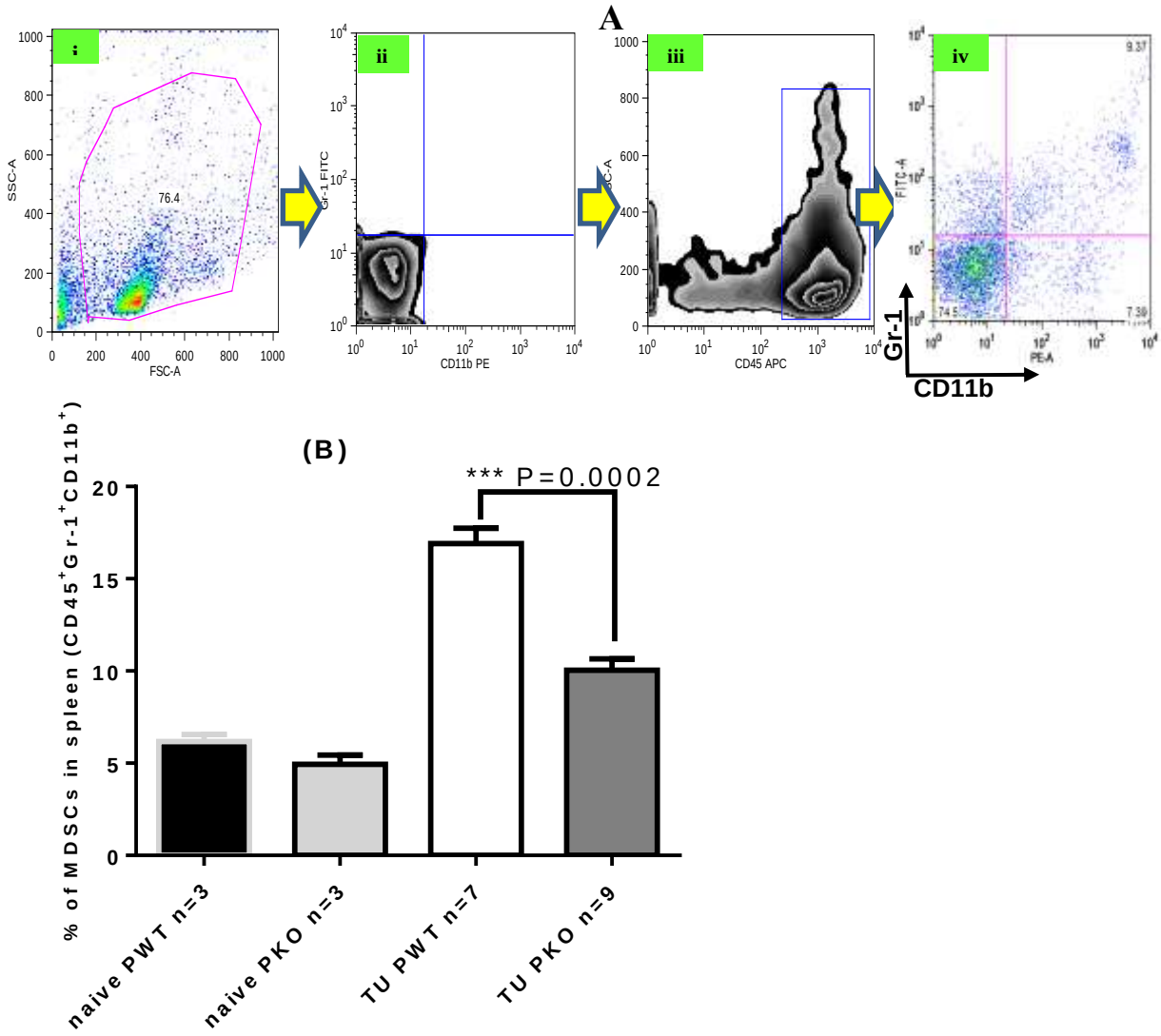

Figure 59: MDSC populations in spleen of wildtype and properdin deficient tumour bearing and naïve mice.

A-Flow cytometry analysis of Gr-1and CD11b cells after gating on CD45+cells in MDSCs from spleen. Numbers in the plots indicate the percent of gated cells. CD45+Gr-1+CD11b+ represent percentage of MDSC. i- the gating on main population of spenocytes, ii- unstained cells (control), iii- gating on CD45+ cells only, iv- gating on CD45+Gr-1+CD11b+ cells representing population of MDSCs.

B- Mice were injected subcutaneously with 1.6×10^5 cell/100µl of B16F10 cell suspension. After 14 days the mice were sacrificed and dissected for collection of spleen. Spleen suspension from both genotypes were stained with three markers (CD11b, Gr1 and CD45) to distinguish MDSC. Then FACS was done and percentage of MDSCs was obtained. The gating was on CD45, and the other two markers were used to calculate of total MDSC in spleen. The data are presented as means ±SEM. Statistical analysis was performed by one-tailed Mann-Whitney U test. * ($p < 0.05$).

4.10 Analysis of Splenocytic T-regulatory cells in wildtype, properdin deficient tumour bearing and naïve mice.

Other than MDSCs, T-regs represent one of the major immunosuppressive cells in tumour bearing hosts. These cells down regulate the function of immune cells via cell to cell contact and secretion of soluble factors. Increased accumulation of T-regs in tumour microenvironment has been linked with unfavourable prognosis (Fujimura et al., 2012a). Recently, it has been found that depletion of T-regs leads to downregulation of the immunosuppressive molecule B7-H1 on MDSCs, which coincided with reduced tumour growth. This finding suggest that there is a cross talk between T-regs and MDSCs. Therefore in addition to MDSCs, the percentage of T-regs in spleen of in PWT and PKO tumour bearing and naïve mice was investigated. The strategy used for analysis of T-regs in spleen was the same as in that in T-regulatory (CD25+CD4+FOXP3+) cells in Tumour of PWT and PKO mice. 4.5.8).

FACS analysis showed that spleens of PWT tumour bearing had a significantly higher percentage of T-regs when compared to PKO mice. In contrast, spleen of PKO naïve mice had a significantly higher percentage when compared to its percentage in PWT counterparts as shown in Figure 60a

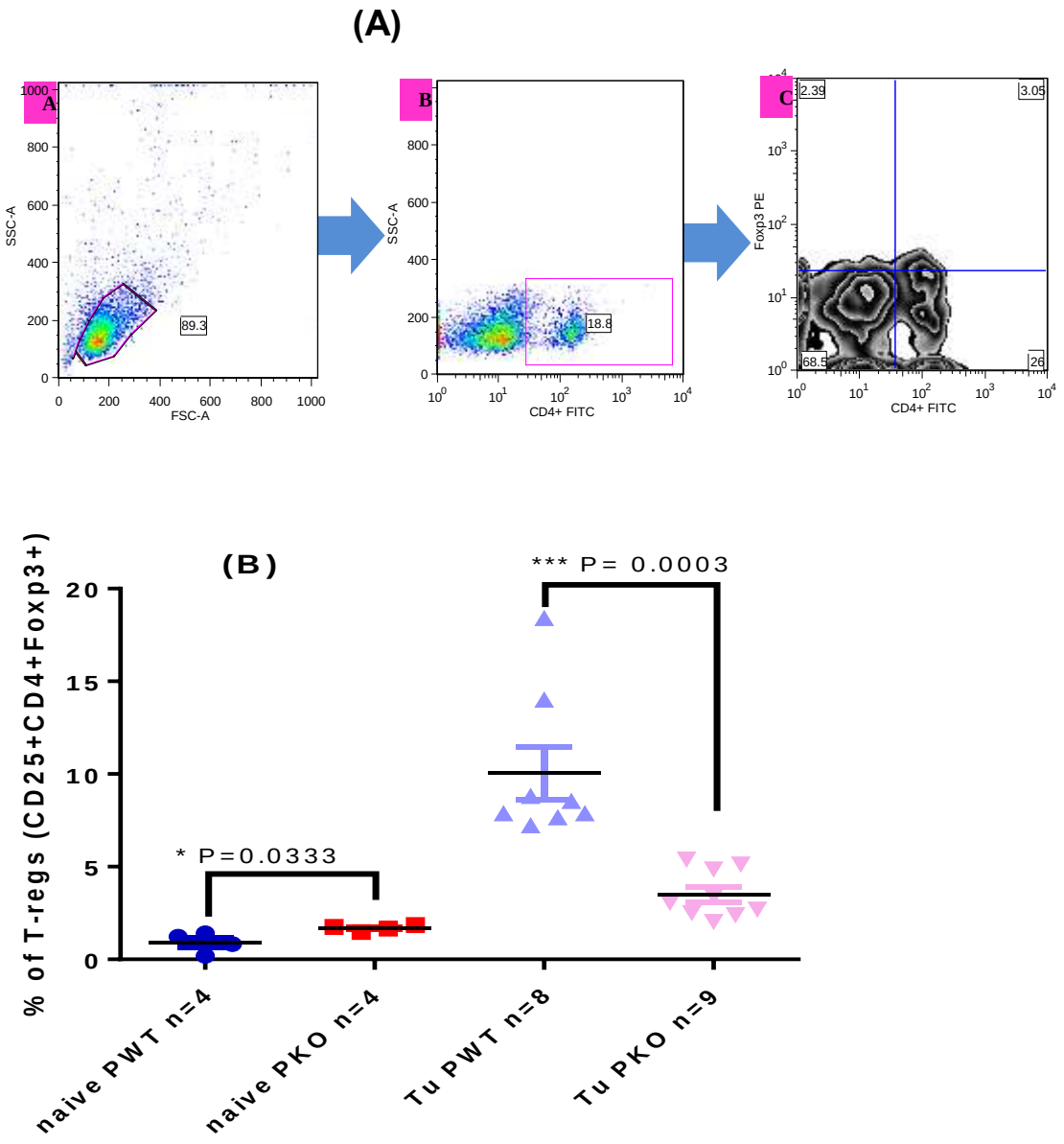

Figure 60: T-regs populations in spleen of PWT and PKO tumour-bearing and naïve mice.

A-Three markers were used to distinguish T-regulatory CD25, CD4 and FOXP3 . Then FACS was done and percentage of T-regs and phenotypes were calculated. (A) Splenocytes were gated. (B)The gating was on $CD4^+$ cells FITC. Then were used to calculate double positive (C) as percentage of total T-regulatory cells in Spleen.

B**-** Mice were injected subcutaneously with 1.6×10^5 cell/100µl of B16F10 cell suspension. After 14 days, the mice were sacrificed and dissected for collection of spleen. Spleen suspension from both genotypes were stained with three markers (CD4, CD25 and FOXP3) to distinguish T-regs. Then FACS was done and percentage of T-regs was obtained. The data are presented as means ±SEM. Statistical analysis was performed by one-tailed Mann-Whitney U test. * ($p < 0.05$).

4.11 Strategy for identifying the percentage of CD45+IL-10, CD45+TGF-β and CD45+IL-17 positive Splenic cells of tumour bearing wildtype and Properdin deficient mice by flow cytometry.

A previous study indicated that IL-10 could induce tumour growth in B16-melanoma model by stimulation of tumour-cell proliferation, angiogenesis and immunosuppression (Garcia-Hernandez et al., 2002).

It has been found at tumour sites of mouse melanoma model that IL-10 expression induces subsequent generation of $CD4^+$ T-regulatory cells and systemic collapse of anti-B16 melanoma immunity (Seo et al., 2001).

Transforming growth factor beta (TGF-beta) has sweeping inhibitory effects on the immune system, negatively affecting many immune cell types and functions (Gorelik and Flavell, 2002, Letterio, 2000). TGF-β is another key immunoregulatory cytokine frequently overexpressed in tumour microenvironment. Tumours reorient the differentiation of myeloid cells into alternatively activated macrophages that express increased levels of TGF-β, IL-10, VEGF and promote MDSC accumulation. VEGF production was recently identified as a key factor in the iNOS-dependent induction of $CD11b^+Gr^+$ MDSC in murine melanoma (Jayaraman et al., 2012, Murdoch et al., 2008).

IL-17 acts as a bridge between adaptive and innate immunity through the potent induction of a gene expression program typical of the inflammatory response, presenting a unique position in the immune response process (Kolls and Linden, 2004). IL-17 is produced by diverse T cell subsets, including $CD4^+$ T cells, $CD8^+$ Tcells, γδ T cells, and neutrophils (Dong, 2006).

IL-17R blockade inhibits B16 tumour growth and increases T cell migration while it reduces infiltration of myeloid-derived suppressor cells (MDSCs) and γδ cells at a late time point (Li et al., 2014).

The strategy used for analysis of IL-10, TGF-β and IL-17 postive cells in spleen is illustrated in Figure 61A. FACS analysis showed that spleen of properdin deficient tumour bearing had a significantly higher percentage of IL-10 and TGF-β positive cells when compared to wildtype mice. However, FACS IL-17 cells results showed no difference between the genotypes as shown in Figure 61.

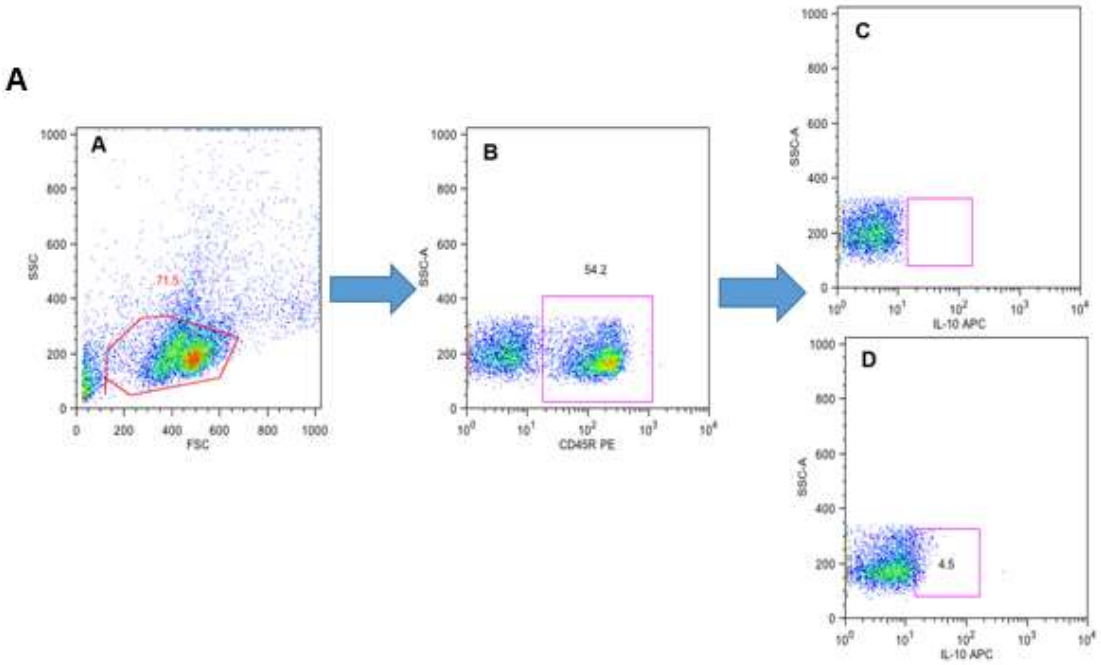
A
A
SSC
FSC
71.5
B
SSC-A
CD45R PE
54.2
C
SSC-A
IL-10 APC
D
SSC-A
IL-10 APC
4.5

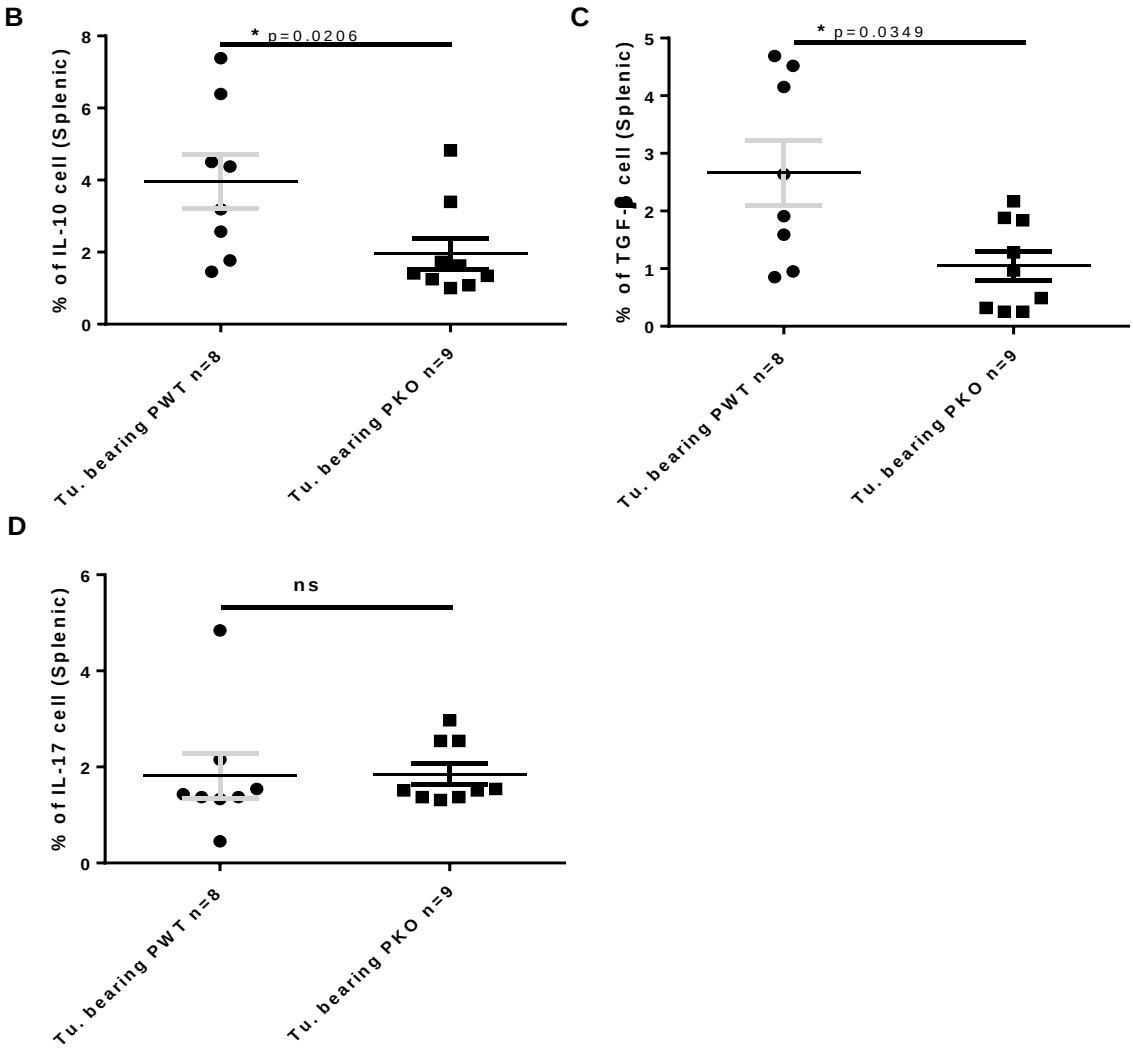

Figure 61: Strategy for FACS analysis of IL-10+, TGF-β and IL-17 cell in spleen.

A-Representative flow cytometry analysis of percentage IL-10 cells. After gating on CD45+cells in spleen. a- the gating on main population of splenocytes, b- gating on $CD45^+$ cells only, C-unstained cells (control), D-gating on IL-10+ cells. B-Mice were injected subcutaneously with 1.6×10^5 cell/100µl of B16F10 cell suspension. After 14 days the mice were sacrificed and dissected for collection of spleen. Spleen suspension from both genotypes were stained with two markers ($CD45^+$IL-10, $CD45^+$TGF-β and $CD45^+$IL-17). Then FACS was done and percentage of IL-10 (**B**), TGF-β (**C**) and IL-17 (**D**) were obtained. The data are presented as means ±SEM. Statistical analysis was performed by one-tailed Mann-Whitney U test. * ($p < 0.05$).

4.12 Percentage of cytotoxic T cells ($CD45^+CD3^+CD8^+$) in spleen of PWT compared to PKO tumour bearing mice.

Previous results for TGF-Beta in 4.1.24 showed high levels of TGF-Beta in wildtype compared to properdin deficient mice in tumour and spleen. Thomas and Massague have demonstrated that TGF-β acts on cytotoxic T lymphocytes (CTLs) to specifically inhibit the expression of five cytolytic gene products (Thomas and Massague, 2005). In this chapter the percentage of Regulatory T in spleen was investigated and the result showed wildtype have more Regulatory T cells compared to properdin deficient mice*.* According to Mempel and colleagues,Treg cells can reversibly blunt T cell responses by selectively modulating a terminal effector function of primed $CD8^+$ T cells.(Mempel et al., 2006).Therefore, the percentage of T-cytotoxic in spleen of PWT and PKO tumour bearing and naïve mice was investigated. The strategy used for analysis of T-cytotoxic in spleen is shown in Figure 62.

FACS analysis showed that spleen of properdin deficient tumour bearing mice had a significantly higher percentage of T-cytotoxic cells when compared to wildtype tumour bearing mice. In addition, fewer $CD8^+$ T cells spleens of tumour bearing mice of both genotypes than naïve counterparts as shown in Figure 62.However, a significant small numerical difference may conflict a biological significance in the tumour immune response. The aforementioned data show depression of T-cytotoxic cells in tumour bearing mice, possibility indicating the effect of another influential element such as C5a and T-regs which were high in tumour bearing mice. Alternative explanation for the depression of T-cytotoxic in tumour bearing mice is the possibility of migration of cells as from spleen, into tumour site. In addition, technical reasons influencing the viability of cells may account for the low numbers of T-cells in tumour bearing mice.

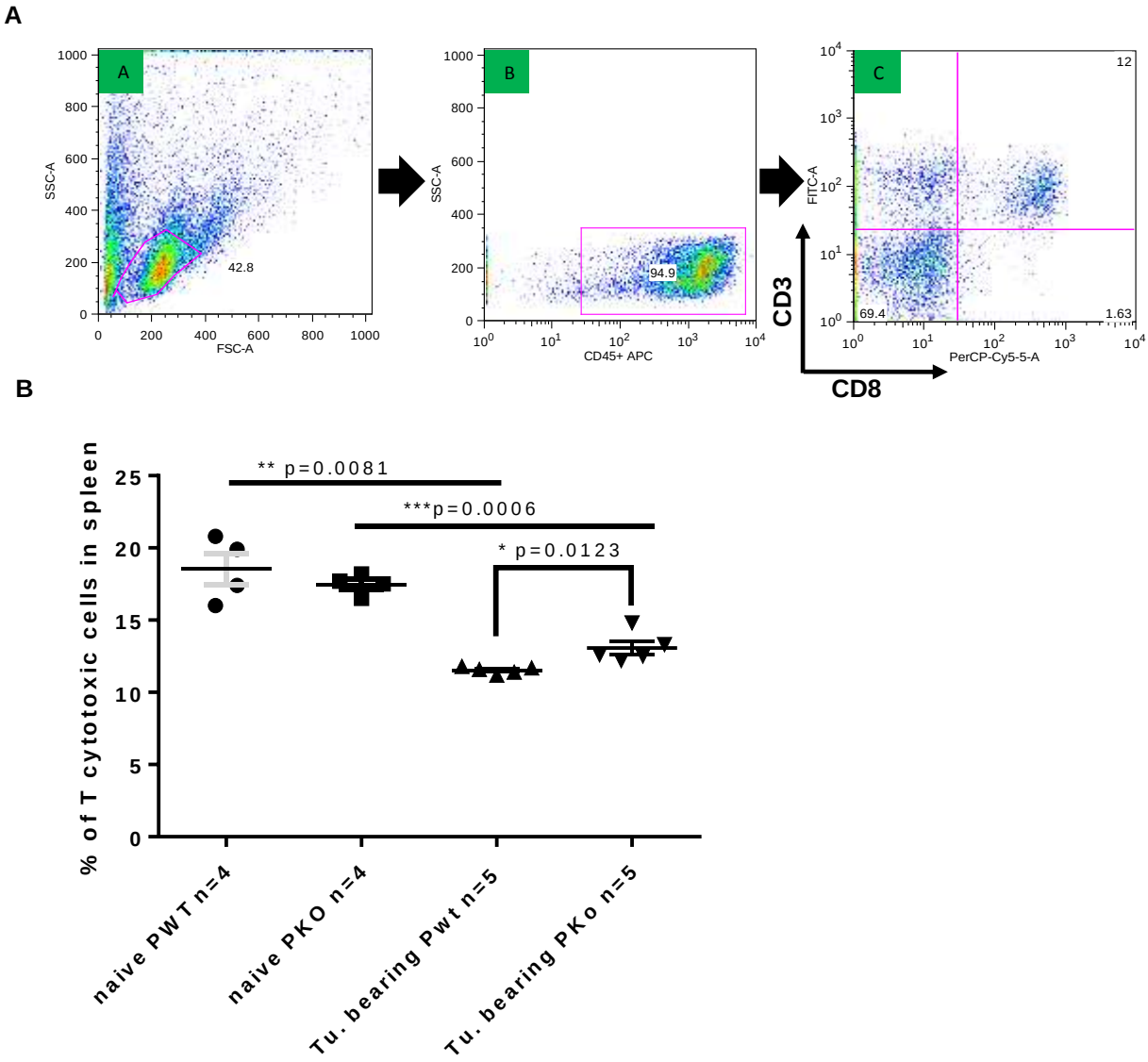

Figure 62:T-cytotoxic populations in spleen of wildtype and properdin deficient mice.

A- Flow cytometry analysis of $CD45^{+}CD3^{+}CD8^{+}$ cells after gating on $CD45^{+}$cells from in spleen from wildtype and properdin deficient mice. Numbers in the plots indicate the percent of gated cells. $CD45^{+}CD3^{+}CD8^{+}$ represent percentage of T-cytotoxic after subcutaneous injection of 1.6 $X10^{5}$ cells of B16F10. B- Populations of T-cytotoxic in tumour of wildtype and properdin deficient mice. Mice were injected subcutaneously with 1.6×10^{5} cell/100µl of B16F10 cell suspension. After 14 days the mice were sacrificed and dissected for collection of spleen. Spleen suspension from both genotypes were stained with three markers (CD45, CD3 and CD8) to distinguish T-cytotoxic. Then FACS was done and percentage of T-cytotoxic cells was obtained. The gating was on CD45, and the other two markers were used to calculate of total T-cytotoxic cells in spleen. The data are presented as means ±SEM. Statistical analysis was performed by one-tailed Mann-Whitney U test. * ($p < 0.05$).

4.13 Strategy of identifying Gamma delta T cells (γδ T cells) in Spleen of wildtype, properdin deficient tumour bearing mice and naïve mice.

γδ T cells are T cells that express a unique T-cell receptor (TCR) composed of one γ-chain and one δ-chain. γδ T cells are of low abundance in the body, are found in the mucosa and in skin. They are involved in the initiation and propagation of immune responses (Silva-Santos et al., 2015).

These cells may be involved in both establishing and regulating the inflammatory response. Moreover, γδ T cells and αβ T cells are clearly distinct in their antigen recognition and activation requirements as well as in the development of their antigen-specific repertoire and effector functions. These aspects allow γδ T cells to occupy unique temporal and functional niches in host immune defense (Chien et al., 2014). Moreover, γδ T cells were also protective against in the widely used B16-F0 melanoma transplantable model (Gao et al., 2003, Lanca et al., 2013).However, a recent study showed that IL-7 could trigger the expansion of γδ T cells, and IL-7/IL-7R promotes lymphangiogenesis in cancer at later time point (He et al., 2010).

Therefore, the percentage of γδ T cells in spleen of in PWT and PKO tumour bearing and naïve mice was investigated. The strategy used for analysis of γδ T cells in spleen is illustrated in Figure 63A.

In order to study of γδ T cells in spleen of PWT and PKO tumour bearing and naïve mice, FACs analysis using $CD45^{+}CD3^{+}$TCR γδ as markers for γδ T cells was performed. Although the results show higher percentage of γδ T cells ($CD45^{+}CD3^{+}$TCR γδ) in spleen of PWT and PKO naïve mice compared to tumour bearing mice (as shown in Figure 63B), no significant difference was found between PWT and PKO mice indicating that these cells are of less importance in our melanoma mouse model.

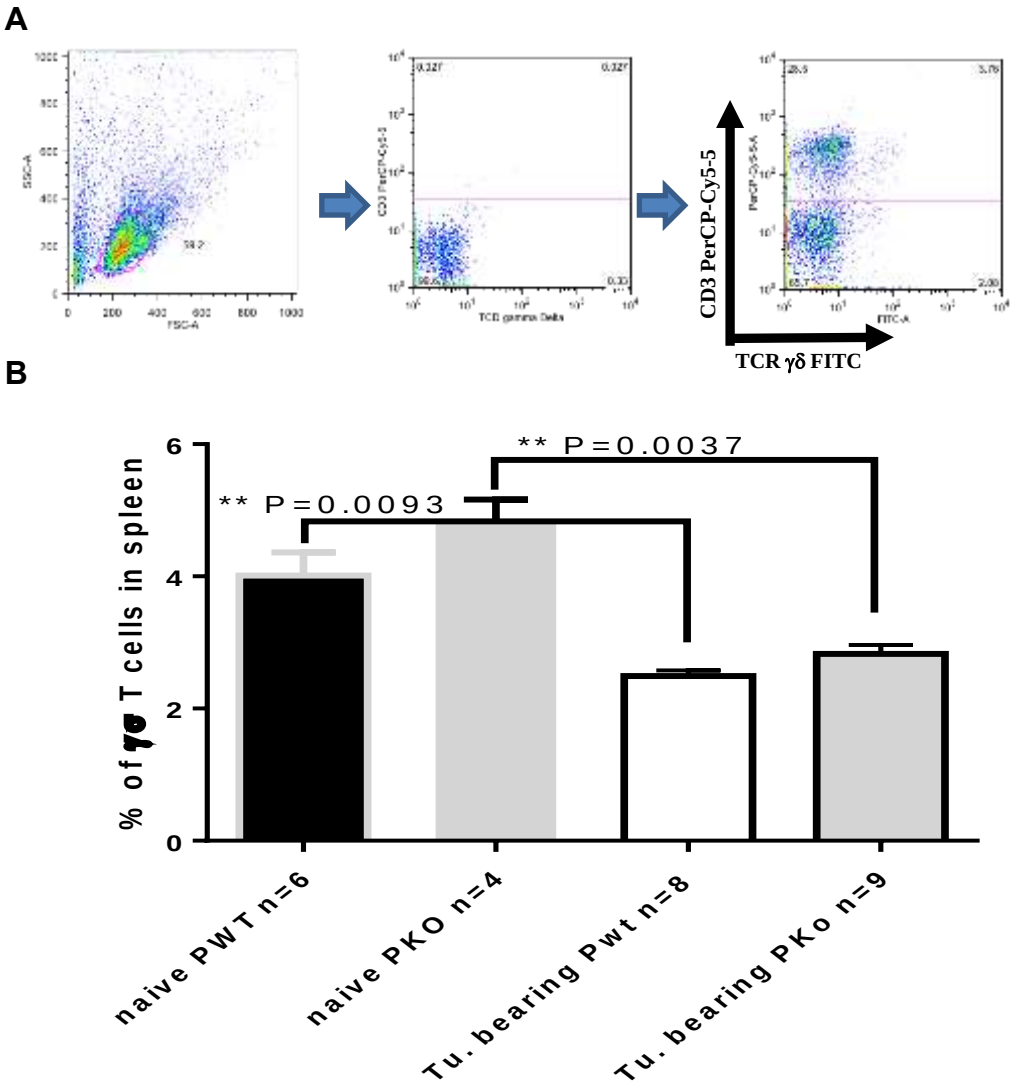

Figure 63: γδ T cells populations in spleen of wildtype and properdin deficient mice.

A)Flow cytometry analysis of $CD45^+CD3^+$ γδ TCR^+ cells after gating on $CD45^+$cells in spleen of wildtype and properdin deficient mice. Numbers in the plots indicate the percent of gated cells. $CD45^+CD3^+$ γδ TCR^+ represent percentage of γδ T cells after subcutaneous injection of 1.6 X105 cells of B16F10. B) Populations of γδ T in tumour of wildtype and properdin deficient mice. Mice were injected subcutaneously with 1.6×105 cell/100µl of B16F10 cell suspension. After 14 days the mice were sacrificed and dissected for collection of spleen. The data are presented as means ±SEM. Statistical analysis was performed by one-tailed Mann-Whitney *U* test. * ($p < 0.05$).

4.14 Strategy for identifying MDSCs in BM of wildtype, properdin deficient tumour bearing mice and naïve mice.

In order to identify clear population of MDSCs in BM, cells were stained with CD45, Gr-1 and CD11b. $CD45^+$ cells were gated first followed by $CD45^+Gr\text{-}1^+$ cells. Percentage of MDSCs in PWT and PKO tumour bearing mice were then calculated.

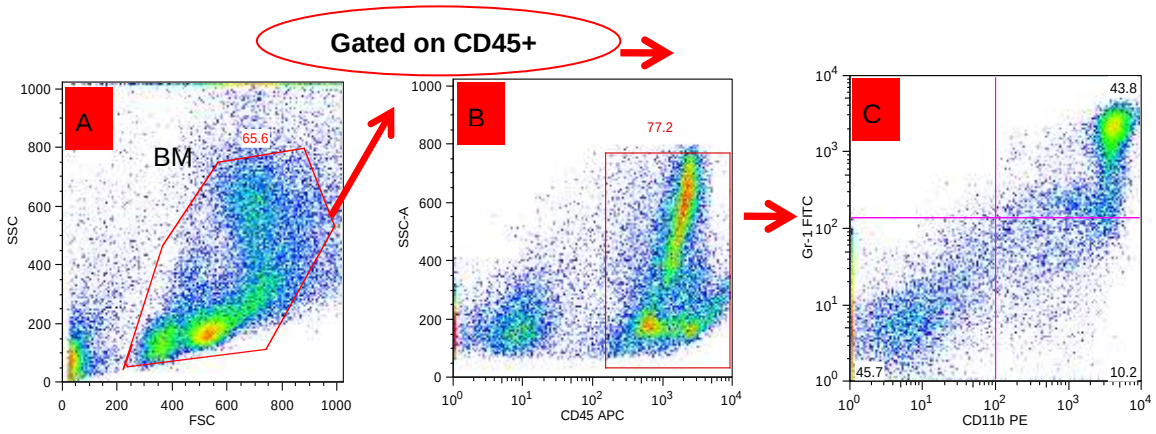

Figure 64: Repesentive dots plot to identify MDSCs in BM.

Populations of MDSCs in bone marrow of PWT and PKO tumour bearing mice and naïve mice. Three markers were used to distinguish MDSC CD11b, Gr1 and CD45. Then FACS was done and % of MDSC and phenotypes were calculated. (A) Bone marrow population was gated. (B)The gating was on CD45+ APC (C) Gr-1 FITC and CD11b PE were used to calculate double positive as percentage of total MDSC in bone marrow.

4.15 FACS analysis of M-MDSCs and PMN-MDSCs Cells in BM of wildtype, properdin deficient and tumour bearing mice and naïve mice.

The process of myelopoiesis is disrupted in cancer resulting in increase of immature and activated myeloid cells such as MDSCs. MDSCs are negative regulators of the immune response and are thought to have a role in tumour metastasis and angiogenesis. In addition, they have a role in regulating the immune response in a variety of conditions such as autoimmune disease and chronic infectious diseases (Youn et al., 2013). Two groups of MDSCs have been identified, the first with monocytic morphology known as M-MDSCs and the second with polymorphonuclear morphology known as PMN-MDSCs. Both groups are identified by the expression of both Gr-1 and CD11b markers. M-MDSCs are thought to have low Gr-1 expression and are highly immune suppressive (Figure 65). On the other hand, PMN-MDSCs are thought to have high expression of Gr-1 with moderate immunosuppressive ability (Youn et al., 2013).

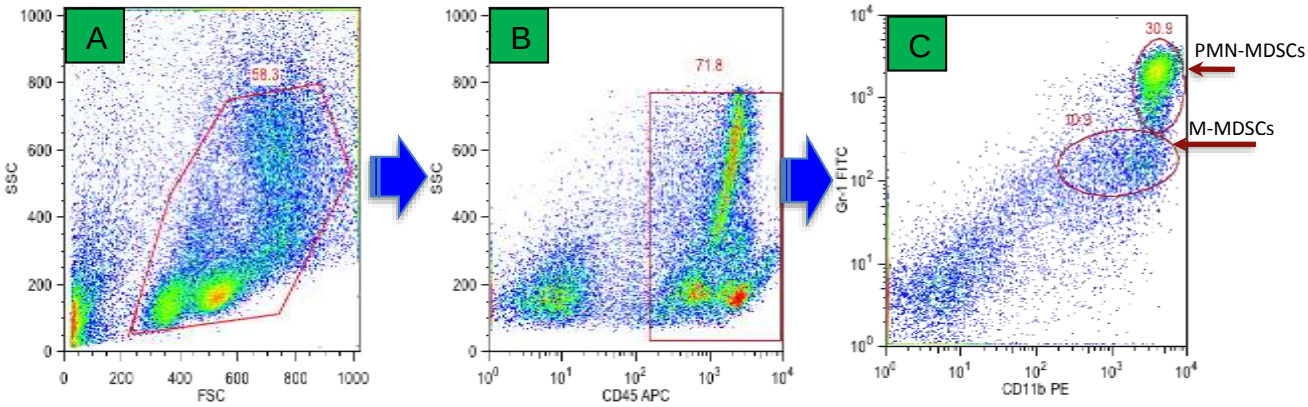

Figure 65: FACS analysis of identified PMN-MDSCs and M-MDSCs in BM.

Populations of PMN-MDSCs and M-MDSCs in bone marrow of PWT and PKO tumour bearing mice and naïve mice. Three markers were used to distinguish MDSC CD11b, Gr1 and CD45. Then FACS was done and % of MDSC and phenotypes were calculated. A) Bone marrow population was gated. (B)The gating was on CD45+ APC (C) Gr-1 FITC and CD11b PE were used to calculate double positive as percentage of total MDSC in bone marrow. Then, two subgroups were identified.

4.16 Percentage of MDSCs ($CD45^+Gr\text{-}1^+CD11b^+$) cells in BM of PWT compared to PKO tumour bearing mice.

Calculation of percentage of MDSCs in bone marrow of tumour bearing mice showed no difference in the total percent of MDSC for all the tested genotypes. However, both genotypes had higher percentage of MDSCs in tumour bearing mice when compared to naïve mice as shown in Figure 66a. Assessment of the accumulation of M-MDCS and PMN-MDSCs was done according the phenotypic criteria of M-MDSCs as Gr-1 ^{low}, $CD11b^+CD45^+$ and of PMN-MDSC as Gr-1^{Hi}, $CD11b^+CD45^+$ (Youn et al., 2013). Depending on the previous criteria, the percentage of PMN-MDSCs was calculated and the results showed no difference between tumour bearing and naïve mice. In addition, no difference was found between genotypes within each group of tumour bearing and naïve mice as shown in Figure 66b. As for the percentage of M-MDSC in BM, a significant increase was seen in PWT tumour bearing mice when compared to their PKO counterparts Figure 66C). Nevertheless, the percentage of M-MDSCs in BM of naïve mice, showed no significant difference between genotypes. It was expected that properdin deficient mice would have more immunosuppressive population as it has been previously published that this genotype has macrophage population

skewed relatively more to M2 phenotype compared to its congenic control (Dupont et al., 2014).

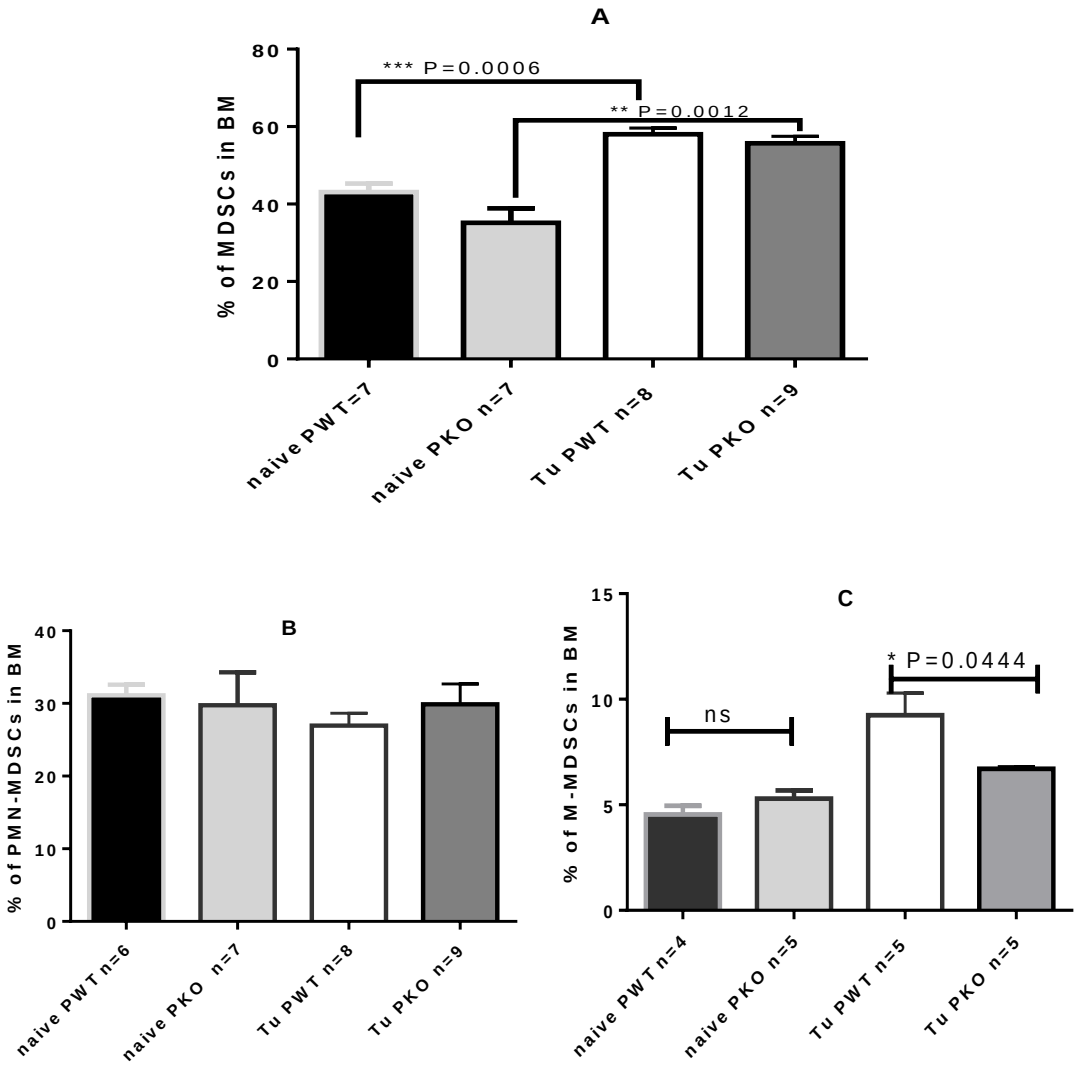

Figure 66: Percentage of MDSCs in BM from PWT and PKO tumour bearing, and naïve mice.

Mice were injected subcutaneously with 1.6×10^5 cell/100µl of B16F10 cell suspension. After 14 days the mice were sacrificed and dissected for collection of BM. BM cells from tumour bearing and naïve mice were stained with a mixture of CD11b, CD45 and Gr-1 Abs. then FACS analysis was done and percentage of total and sub populations of MDSCs were calculated. A-total percentage of MDSCs in BM B-percentage of PMN-MDSCs in BM. C- Percentage of M-MDSCs in BM. The data are presented as means ±SEM. Statistical analysis was performed by one-tailed Mann-Whitney *U* test. * ($p < 0.05$).

4.17 Percentage of CD206 +F4/80+ in spleen of PWT and PKO tumour bearing mice.

It is well documented that M2 macrophages has the ability to promote tumour growth and metastasis, in part by secreting a wide range of proangiogenic factors and growth factors. Moreover, M2 tumour associated macrophages are thought to enhance tumour growth and metastasis by suppressing the activity of CD8+ T cells (Melancon et al., 2012). Surface markers CD206 and F4/80 were used to investigate the percentage of M2 macrophages in spleen. Comparison between PWT and PKO tumour bearing mice showed that PWT had a significantly higher percentage of splenic M2 macrophages characterised by the markers CD206 and F4/80 (Figure 67). Nevertheless in naïve mice, the percentage of splenic M2 macrophages were similar in both genotypes.

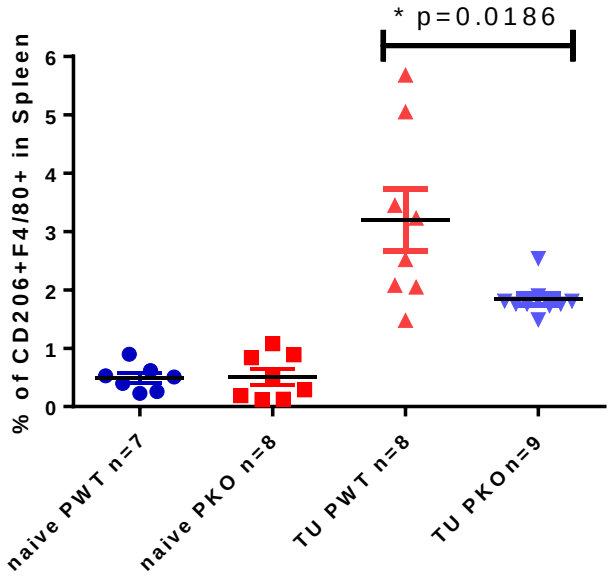

Figure 67: Percentage of CD206 $^{+}$F4/80^{+} cells in spleen of PWT and PKO tumour bearing and naïve mice.

Mice were injected subcutaneously with 1.6×10^{5} cell/100µl of B16F10 cell suspension. After 14 days the mice were sacrificed and dissected for collection of spleen. Spleen suspension from both genotypes were stained with F4/80 FITC and CD206 APC. The data are presented as means ±SEM. Statistical analysis was performed by one-tailed Mann-Whitney U test. * ($p < 0.05$).

4.18 Surface expression of CD80, MHC-II and CD86 of splenic dendritic cells

CD80, CD86 and MHCII are some of the surface markers that characterise antigen presenting cells. These up-regulate the molecules necessary for their role within the adaptive immune response. Antibodies specific for these molecules can be used to characterise the extent of maturation of dendritic cells. In addition, these molecules may participate in the antitumour immune response because several studies have shown that induction of CD80 and/or CD86 expressions on tumour cells promotes antitumour immunity (Rudy et al., 1997, McCarthy et al., 2000, Douin-Echinard et al., 2000, Johnson et al., 2003).

Generally, tumour cells do not express CD80 or CD86 costimulatory molecules except for some lymphomas, leukemias, or carcinoma cell lines. However, some melanoma cell lines, spontaneously or treated with IFN-γ moderately express CD80 and/or CD86 costimulatory molecules (Bernsen et al., 2003).

It has also been shown that induction of costimulatory molecule expression on tumour cells promotes antitumour immunity and the antigenicity of the melanoma cells varies with the level of their expression (Driessens et al., 2009, Douin-Echinard et al., 2000).

To study the surface expression of dendritic cells (in spleen) from wildtype mice compared to properdin-deficient mice after tumour melanoma implantation, an approach of double staining with the dendritic cell marker $CD11c^+$ was taken. The expression was measured by flow cytometry. The analysis was done on cells that were double positive for $CD11c^+CD80^+$, $CD11c^+CD86^+$ and $CD11c^+$MHC class II^+ with the double positive quadrant determined by the isotype control profile. The level of expression of $CD80^+$, $CD86^+$ and MHC class II was calculated using the median fluorescence intensity and comparing them to their relevant individual isotype controls (Figure 68).

The percentages of dendritic cells positive for MHC-II^+ and $CD80^+$ in spleen of wildtype naïve were higher than in properdin-deficient naïve mice (Figure 68 panels A and B). However, Figure 68A shows the levels of surface markers CD80 was higher in properdin-deficient compared with wildtype in tumour bearing mice. The percentages of positive CD86 in both genotypes were comparable in tumour bearing and naïve mice cells, but after tumour melanoma implantation the

percentages were higher in dendritic cells from properdin-deficient compared to dendritic cells from wildtype, although the percentages of MHC-II in tumour bearing mice showed no difference in either genotype. (Figure 68.C)

These data emphasize that immune dysfunction in properdin deficient tumour bearing compared to wildtype mice, particularly the recruitment of more immune suppressor cells (MDSCs) and T-reg may be lead to downregulation of costimulatory molecules, and occurs early in tumour progression (Tirapu et al., 2006).

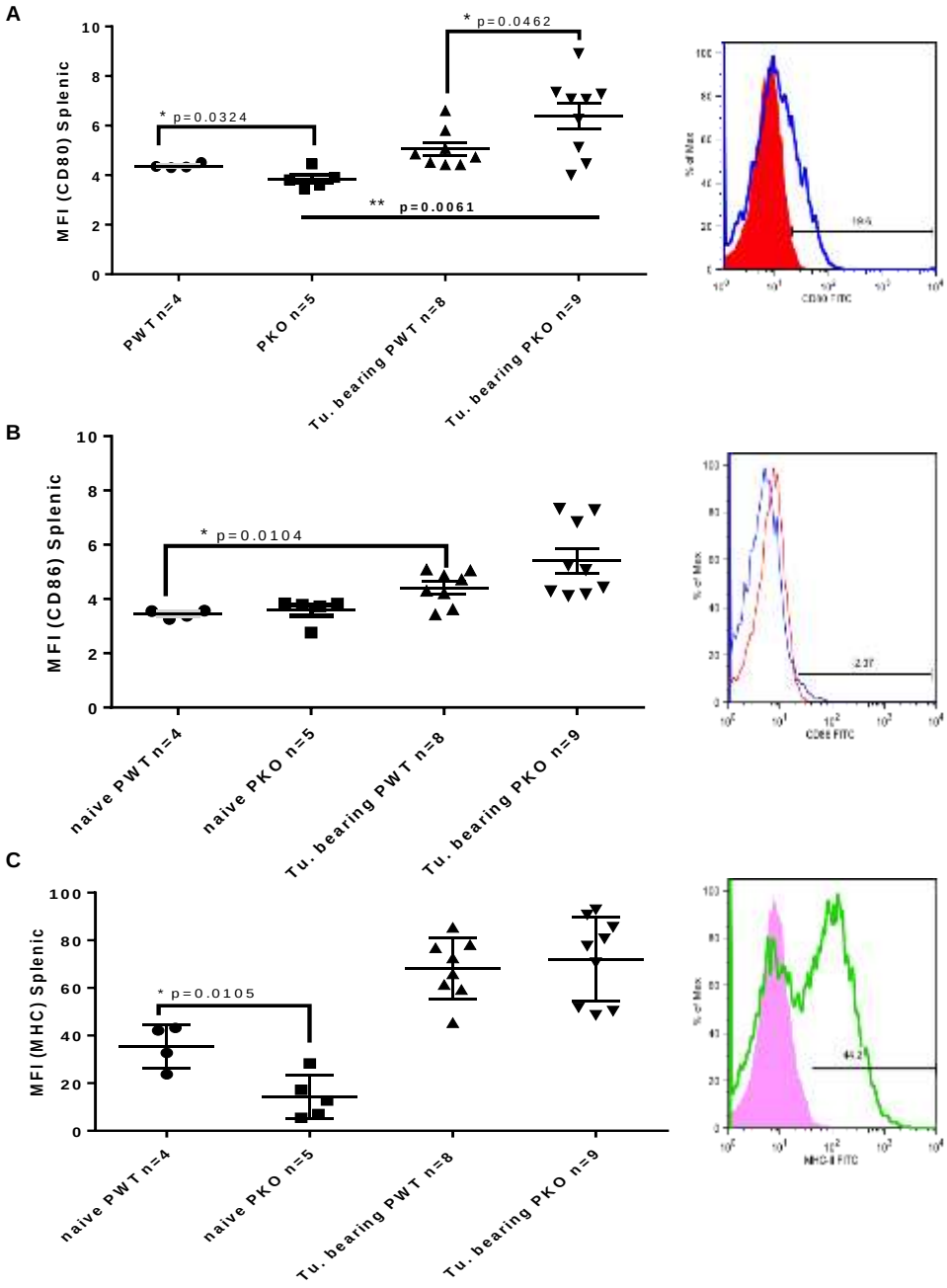

Figure 68: Flow cytometric analysis of CD80, CD86 and MHC-II surface expression on CD11c⁺ cells in splenic of naïve and tumour bearing mice.

Mice were injected subcutaneously with 1.6×10^5 cell/100µl of B16F10 cell suspension. After 14 days, the mice were sacrificed and dissected for collection of spleen. Spleen suspension from both CD11c⁺ genotypes were stained with markers (CD80, CD86 and MHC-II). Flow cytometry histogram of the MFI value of CD80 (A) and CD86 (B) and MHC-II (C). The population were gated by the size for and FITC for CD80 in density plot (The histograms show the data for 10,000 gated events from each sample) after the FITC/PE plot is gated then present in the histograms. Results are expressed mean using MFI (mean fluorescence intensity) value. The data are presented as means ±SEM. Statistical analysis was performed by one-tailed Mann-Whitney *U* test. * ($p < 0.05$).

4.19 Strategy for identifying of percentage $B220^{+}CD19^{+}CD80$ Splenic cell of tumour bearing wildtype and Properdin deficient mice by flow cytometry.

Animal models of melanoma have demonstrated the involvement of $CD4^{+}$T cells, $CD8^{+}$T cells and B cells mounting a response against cancer (Ramirez-Montagut et al., 2003). CD80 (B7.1), expressed on macrophages, activated B cells, and some B lymphomas, has been shown to deliver a costimulatory signal to T cells through binding to its natural ligand CD28 constitutively expressed by most naïve $CD4^{+}$ T cells (Sahoo et al., 2002, Lim et al., 2012).

In order investigate the expression of CD80 on activated B-cells in spleen in wildtype and properdin deficient tumour bearing mice, FACS was used to analysed cell surface expression of CD80 in B-cells.

Splenocytes from wildtype and properdin-deficient mice were prepared as described in Material and Methods. Cells were stained for B-cells with PE-B220 and PE-Cy-7–CD19 (B-cell markers). The strategy used for analysis of B220+CD19+CD80 spleen was the same as in that in Figure 69 A.

The results showed slightly higher percentage of activated B-cells ($B220^{+}CD19^{+}CD80^{+}$) in spleen of PWT when compared to PKO tumour bearing mice as shown in Table 14,however statistical analysis did not show any significant difference between the genotypes.

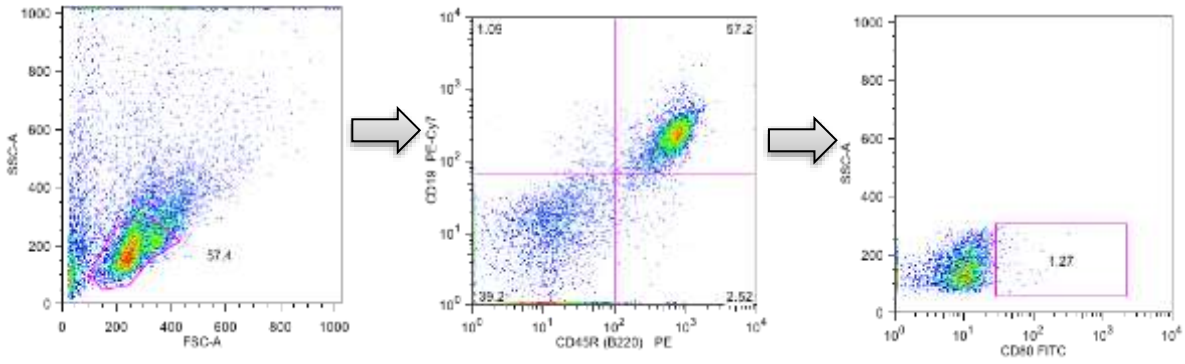

Figure 69: Flow cytometry analysis of CD80+ expression on B-cells in spleen of tumour bearing mice.

Flow cytometry analysis after gating on double positive cells of $B220^{+}CD19^{+}$cells from spleen in wildtype and properdin deficient mice. Numbers in the plots indicate the percent of gated cells. $B220^{+}CD19^{+}CD80^{+}$, after subcutaneous injection of 1.6 $X10^{5}$ cells of B16F10. Spleen suspension from both genotypes were stained with three markers (B220, CD19 and CD80) to distinguish activated B-cells. Then FACS was done and percentage of B-cells was obtained. The gating was on CD45, and the other two markers were used to calculate of total t-cytotoxic in spleen. The data are presented as means ±SEM. Statistical analysis was performed by one-tailed Mann-Whitney *U* test. * ($p < 0.05$).

Table 14: $B220^{+}CD19^{+}CD80^{+}$ positive cells in spleen of tumour bearing mice.

WT	6.574	± 2.15	n=7
KO	2.554	±0.5844	n=8

4.20 Flow cytometric analysis of CD16/CD32 surface expression in splenic cells

FcγRs are a family of membrane glycoproteins expressed on hematopoietic cells (Ravetch and Bolland, 2001).In dendritic cells, but not in other cell types, FcγR-mediated internalization very efficiently targets antigen for a unique dendritic cell–specific antigen transport pathway resulting in delivery to the cytosol. Once in the cytosol, internalized antigens are degraded by the proteasome. The resulting peptides are translocated into the lumen and loaded on MHC class I molecules (Ravetch and Bolland, 2001). These results suggested that antigen-specific humoral immune responses may promote the generation of specific cytotoxic T lymphocytes (CTLs).(Baker et al., 2014)

Dendritic cells were used as a model system for the control of immune activation to further study the role of properdin in activation of immune cells through FcγRs This experiment focused on expression of FcγR in dendritic cells to investigate any differences between wildtype and properdin-deficient mice cells. FACS was used to analysed cell surface expression of FcγR in dendritic cells.

Splenocytes from wildtype and properdin-deficient mice were prepared as described in Materials and Methods. Cells were stained markers with PE- rat anti-mouse CD11c (dendritic cell marker) and FITC rat anti-mouse CD16/CD32 (FcγIII/II receptor) and were analysed by FACS. CD16/CD32 is an antibody that recognises both FcγRIII and FcγRII.

This was done for wildtype and properdin-deficient naïve mice for isotypes as background control and for positive expression dendritic-cells for CD16/CD32.The result showed high percentage of dendritic (CD11c+CD16/32) in wildtype compared to properdin deficient mice as shown in Figure 70. However, there was no chance to investigate the expression of these markers in tumour bearing mice.

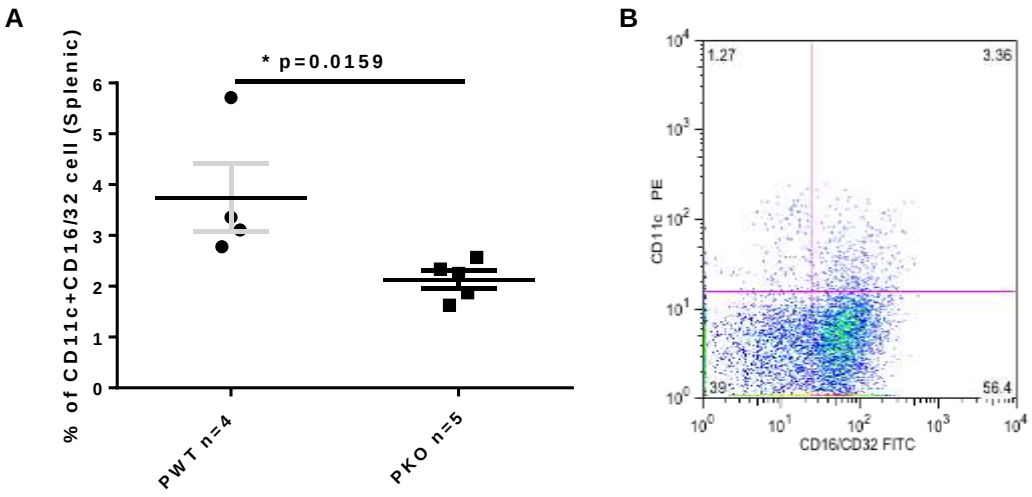

Figure 70: Flow cytometric analysis of dendritic (CD11c^{+}CD16/32) expression in spleens of wildtype and properdin deficient naïve mice.

Mice were sacrificed and dissected for collection of spleen. Spleen suspension from both genotypes were stained with markers (CD11c PE+CD16/32 FITC). The data are presented as means ±SEM. Statistical analysis was performed by one-tailed Mann-Whitney U test. * ($p < 0.05$).

4.21 Discussion & Conclusion

4.21.1 Discussion

The aim of the animal model used in this chapter was to set up a model of syngeneic tumour growth, then define the role of properdin in tumour growth and composition of the tumour microenvironment (TME). In vivo experiments were set up to induce tumour implantation using properdin deficient mice and their wildtype control. This was done through two models: the first model was syngeneic subcutaneous tumour model to study tumour growth, while the second was syngeneic intravenous tumour model to study tumour metastasis. In these models 100µl of B16F10 (containing $1X10^5$- $4X10^5$ cell) were injected through two routes. The first is subcutaneous into the flank as described by Baird and colleagues, and the second is intravenous via the tail vein as previously described (Eberting et al., 2004, Baird et al., 2013, Takeda et al., 2011, Lv et al., 2009).

It is well documented that subcutaneous injection of B16F10 into C57/BL6 mice leads to the development of progressive solid tumours. This cell line has also been utilised to study lung metastasis (Almendros *et al.*, 2013). Additionally, B16F10 are pigmented (due to the production of melanin) and this criterion is documented to be used in assessing the extent of lung metastasis by counting the number of black pigmented colonies which appear on the lung. For the subcutaneous model, a suspension of B16F10 was injected in the right flank as injections in the flank are considered to cause the least distress to mice and are orthotopic. Tumour implantation in research animals is considered one of the critically important experimental procedures which necessities careful assessment of the effect of tumour on the animals. Therefore, mice were carefully monitored daily until the mice reached the endpoint specified in the animal licence. Mice usually reached the endpoint within 7-14 days, after which the mice were sacrificed, macroscopically examined for tumour formation, and tumour tissue and spleens were collected for analysis. Tumour size (volume) was measured by calipers. Calipers had been traditionally used to measure tumour size; however measurement of tumour size by this method may often be affected by errors resulting from variable tumour shape, subcutaneous fat layer and skin, difference in compressibility of the tumour and subjectivity of the investigator

(Jensen et al., 2008). Furthermore, this method is generally based on volumetric measurement of tumour mass, which does not take into account oedema formation and necrosis. Measurement of tumour size by calipers from a number of independent subcutaneous tumour implantations showed no significant difference between PWT and PKO mice. Similarly, measurement of tumour weight did not show a difference between genotypes. The results obtained from this study showed that the subcutaneous tumour model was successful; however there is a need to develop a more accurate method to measure tumour volume. A number of imaging techniques for monitoring tumour progression and metastasis have recently become available. Of those techniques, bioluminescence imaging has demonstrated an ability to detect microscopic tumours with high accuracy (Puaux et al., 2011).

Bioluminescent approaches for measuring tumour growth depend on the use of tumour cell lines which have been transfected with a luciferase gene of the firefly Photinus pyralis. In the presence of ATP, luciferase converts luciferin into the light-emitting product oxyluciferin. Subsequent bioluminescence measurements give an indication of tumour growth in the animal. Thus, BLI is a sensitive non-invasive imaging technique which enables monitoring of the tumour burden and progression in the animal body in a timely manner without the need to sacrifice the animal. Tumour growth can be quantified by counting the number of photons emitted from the animals (O'Neill et al., 2010). This method reduces the number of animals used in each experiment as each animal serves as its own control over the period of the experiment. Luciferase- expressing B16F10 was injected subcutaneously into PWT and PKO mice, followed by administration of the substrate, luciferin. At the indicated time points, tumour growth was measured by counting the number of photons emitted from the animals. The results of the pilot BLI experiment demonstrated that light emission could be detected from the regions of interest which confirms that BLI was able to detect melanomic tumours. Following the pilot experiment, another subcutaneous injection was carried out using B16F10-luc, and the photon emission was carried out at day 8 and 12 of tumour implantation. The bioluminescence result showed no significant difference between the genotypes.

The B16F10 mouse model of melanoma was chosen for this project because it is widely used in many cancer studies to investigate some aspects of tumour lung

metastasis via the lateral tail veins (Intravenous injection) (Nguyen et al., 2007, Gautam et al., 2002) In addition, The fact that B16F10 is pigmented (due to the production of melanin) makes it a widely used cell line to study the metastasis in the lungs, by counting the number of black pigmented colonies after injecting the mice with these cells (Burghoff et al., 2014). However, it has been reported that these malignant cells migrate from the tumour through its blood vessels and attach to the vessel wall of the affected organ. Then they migrate to the parenchyma leading to the formation of new tumours (Geiger and Peeper, 2009). Furthermore, there were technical difficulties to apply full dose (volume) via the lateral tail veins. Intravenous models of tumour implantation may suffer from several limitations, such as the difficulty in estimating if injection of cells was done properly, as variation may occur due to mis-injection of some of the cells. In addition, the black tail of C57BL6 mice makes it difficult to locate the lateral tail vein. Hence, it was difficult to assess if the same number of cells was delivered to all mice for these reasons this model was abandoned.

4.21.1.1 Cellular immune response in syngeneic tumour melanoma

To gain insights into the role of properdin in cell-mediated responses during syngeneic mouse melanoma, this project investigated phenotypic changes in differentiated cells from properdin-deficient and wildtype mice in tumour, spleen and bone marrow.

One of the most fundamental mechanisms employed by malignant tumours to suppress the immune response to tumour antigens is dysfunctional myelopoiesis and the recruitment of myelomonocytic cells to the tumour site and peripheral lymphoid organs such as spleen (Sica and Bronte, 2007, Chanmee et al., 2014). MDSCs have been recognised as critical mediators of tumour progression in numerous solid tumours through their inhibition of tumour-specific immune responses (Serafini et al., 2006). These cells, identified by the co-expression of Gr-1 and CD11b as well as CD45 in mice (Movahedi et al., 2008, Youn et al., 2008), are the immature counterparts of myeloid-derived antigen-presenting cells. MDSCs are able to suppress antitumour T cell-mediated responses and tumour cytotoxicity in tumour bearing mice (Monu and Frey, 2012).

One of the major host factors contributing to the generation of an immunosuppressive microenvironment is an increase in the number of myeloid-

derived suppressor cells (MDSCs). Characterised by $CD11b^{+}Gr\text{-}1^{+}$, MDSCs are an important population of innate regulatory cells mainly comprising monocytic MDSCs (M-MDSCs) and granulocytic MDSCs (G-MDSCs). The percentage of MDSCs was investigated in tumour tissue, bone marrow and spleen of wildtype and properdin deficient tumour bearing mice. MDSC within tumour showed that the highest percent of MDSC was found in properdin wildtype mice. Similarly, in spleen, the highest percentage of MDSCs was in PWT when compared to PKO tumour bearing mice. However, In BM of naïve mice, no significant difference was found between PWT and PKO. These findings indicated that properdin may contribute to the accumulation of MDSCs in spleen, as well as to the migration of these cells into tumours. Similar findings were obtained by Markiewski et al., 2008 who found that the percentage of total MDSCs isolated from tumours of wildtype mice was higher than the percentage of these cells in tumour tissue from C5aR-deficient mice. The peripheral localisation of myeloid cells in the tumours of properdin deficient mice might also suggest that the chemotactic activity of C5a contributes to the migration of these cells throughout the tumour tissue. Markiewski and co-workers reached a conclusion that the existence of C5a receptors on the cell surface of MDSCs enables direct binding of C5a which subsequently results in stimulation of MDSCs.

In measuring the ratio of M-MDSC in BM, M-MDSC was significantly higher in BM from PWT tumour bearing mice than in BM of PKO mice. Nevertheless, properdin deficient mice were expected to have a more immunosuppressive population, as it has been previously published that this genotype has more M2 macrophage population (Dupont et al., 2014). Similarly, comparison between PWT C57BL/6 with C5a expressing tumours and those without C5a expressing tumours showed higher frequency of CD11b+ MDSC in mice with C5a expressing tumour (Gunn et al., 2012).

Using a syngeneic model of melanoma developed in C57BL/6 WT and C1q-deficient (C1qa-/-) mice, Bulla et al. detected slower tumour growth in C1q-deficient (C1q-/-) mice as compared to their wildtype counterparts. However, they failed to detect higher frequency of MDSC in wildtype mice (Bulla et al., 2016). Their finding that wildtype and C1q-/- mice had similar frequency of MDSC may be attributed to the high number of B16/F10 ($2X10^{6}$) used for tumour implantation (Bulla et al., 2016) which was almost 10 times higher than the number used in

this project. Similarly, Nunez-Cruz and co-workers found no difference in the frequency of tumour-infiltrating macrophages, B cells, and MDSCs between with mice partial deficiency in C3 and their wildtype controls using a model of spontaneous ovarian cancer (Nunez-Cruz et al., 2012). This apparent contradiction in frequency of MDSC could be attributed to different models and experimental settings used by different research groups. The increase in number of MDSCs in tumour bearing mice was also reported by others. The level of MDSCs expansion in various tumour models are thought to be influenced by the nature of tumour derived factors, which explains the often contradictory results reported in various studies (Youn et al., 2008).

In addition to MDSCs, T-regs are another population of cells which contribute to the generation of an immunosuppressive microenvironment. Accumulation of both T-regs and MDSCs in tumour microenvironment represents a major hurdle for antitumour immune responses (Weiss et al., 2014). In addition to their immunosuppressive role, recent studies have demonstrated that T regs may also play a role in promoting angiogenic reprogramming of the tumour microenvironment (Facciabene et al., 2011). Investigation into the percentage of T-regs in spleen of tumour bearing mice revealed that PWT tumour bearing had a significantly higher percentage of T-regs when compared to PKO mice. Nevertheless, spleens of PKO naïve mice had a significantly higher percentage when compared to its percentage in PWT counterparts. This result is consistent with others, who have concluded that progressing mouse tumours can be linked with enhanced T-regs activity (Weiss et al., 2014, Mempel et al., 2006, Holmgaard et al., 2015). Unexpectedly, investigations into the percentage of T-regs within tumour tissue showed comparable levels in both genotypes. One reason for the inability of our experimental settings to show a difference between genotypes is that we were restricted with tumour size and thus the latest time point did not exceed 12-14 days. Thus, it could not be ruled out that leaving the tumour to grow more than 2 weeks might show in a difference in percentage of T-regs within tumour tissue. Recent studies have highlighted the existence of a cross talk between T-regs and MDSCs during melanoma growth (Fujimura et al., 2012a). In addition to their immunosuppressive ability, T-regs modified the phenotype of tumour infiltrating MDSCs to express inhibitory B7-H molecules and to produce IL-10 (Fujimura et al., 2012b).

4.21.1.2 Role of properdin in cellular immune response in syngeneic tumour melanoma

TGF- β is one of the cytokines that are critical to immune homeostasis *in vivo* and has been linked with T-regs and MDSC production. TGF-β has the ability to negatively affect a number of immune cell types and thereby exert an immense inhibitory effects on the immune system, (Gorelik and Flavell, 2002, Letterio, 2000). PWT mice had a significantly higher level of TGF- β, both in spleen and within tumour when compared to PKO mice.

Recently, Liu and co-workers demonstrated that TGF-β was the main tumour-derived factor responsible for the upregulation of microRNA-494 in MDSC. Expression of microRNA-494 enhances CXCR4-mediated MDSC chemotaxis and alters the intrinsic apoptotic/survival signal and thus contributes to the accumulation of MDSCs in tumour tissues and facilitates tumour cell invasion and metastasis (Liu et al., 2012). Increased expression and activation of TGF-β by tumour cells stimulates extracellular matrix deposition and chemoattraction of fibroblasts, promoting tumour growth and angiogenesis (Roberts et al., 1986, Zheng et al., 1997, Derynck et al., 2001). TGF-β expression by melanoma cells can modify the surrounding stroma with increased production and deposition of extracellular matrix proteins, which favour increased metastatic spread and survival (Berking et al., 2001). TGF-β is an ubiquitous cytokine with paradoxical functions in melanoma tumour progression (Medrano, 2003).

Tumour associated macrophage infiltration and angiogenesis have been associated with expression of CCL2 and VEGF (Valkovic et al., 2002). CCL2 has been implicated in promoting tumour proliferation, migration, invasion and survival. Furthermore, CCL2 enhances the recruitment of macrophages and cytotoxic T lymphocytes, thereby this chemokine is one of the main mediators of interactions between tumour and host cells. In addition to other stromal cells, tumour cells are suggested to be the main source of CCL2 in tumour microenvironment (Zhao et al., 2013). The extent of CCL2 expression determines whether this cytokine reduces or promotes melanoma tumour growth (Knight et al., 2013). Protein macroarray results revealed that PKO tumour bearing mice had significantly lower levels of TIMP-1, IL-13, CCL2 and CCL3 when compared to their wildtype counterparts, a possible indicator of less cell recruitment. Moreover, serum levels of CCL2 (measured by ELISA) showed that PKO tumour

bearing mice had a significantly lower level when compared to its PWT counterparts at 14 of tumour implantation but not at 7 days. Notably, after 7 days of tumour implantation there was a trend of PKO having less CCL2 but this did not reach statistical significance. In contrast to its level in tumour bearing mice, measurement of CCL2 in sera of naïve mice revealed that PKO had a significantly higher level of this chemokine. It has been demonstrated that CCL2 is involved in recruitment of a number of immunosuppressive cells including MDSCs. Moreover, CCL2 has been directly linked with the generation of immunosuppressive Treg cells. Thus the low level of both MDSCs and T-regs seen in PKO tumour bearing mice may be a consequence of the decrease in CCL2. It would be reasonable to suggest that MDSCs and T-regs migrate in response to CCL2 in the tumour microenvironment. Similar assumptions were made be Zhao and colleagues who linked recruitment of MDSCs via CCL2/CCR2 with the development of colorectal cancer liver metastasis (Zhao et al., 2013).

In tumour microenvironment, both host stromal cells and tumour cells secrete a number of factors. Among those is the complement activation product C5a.

Cellular immune response in tumour melanoma can also be affected by the level of this potent chemoattractant. C5a influences haemostasis and has the ability to recruit immune cells such as monocytes, neutrophils and MDSCs, and thus is a factor which can contribute to disease pathogenesis (Ricklin et al., 2010). C5a in tumour microenvironment leads to recruitment of MDSCs into tumour tissue, thereby suppressing cytotoxic $CD8^+$ T cells (Markiewski et al., 2008). Given the ability this complement activation product in the cellular response in tumour microenvironment, C5a level was investigated in tumour tissue and in sera of PWT and PKO mice. Compared to PWT tumour bearing mice, PKO tumour bearing mice had a significantly lower level of C5a within tumour tissue. Similarly, measurement of C5a level in serum showed that PKO tumour bearing mice had a significantly lower level as compared to their PWT counterparts. On the other hand, naïve mice showed no difference between genotypes in serum level of C5a. Although repeated measurements consistently showed that naïve PWT mice seem to have increased serum levels of C5a, however this never reached statistical significance.

The high level of C5a seen in tumour bearing mice may possibly be due to increased complement activation. As all three complement pathways lead to

cleavage of C3 and the generation of C3a, C5a and ultimately the membrane attack complex C5b-9, level of the aforementioned complex was investigated as an indicator of complement activation. As with C5a, C5b-9 was significantly lower in PKO tumour bearing mice when compared to PWT. Despite the difference in the level of C5a between naïve and tumour bearing mice, the results showed no difference in serum level of C5b-9. Published data have revealed the existence of a complex crosstalk between the complement and the coagulation systems, whereby thrombin can directly cleave C3 and C5 respectively and lead to the generation of more chemoattractant C5a (Markiewski et al., 2007, Rittirsch et al., 2008). Moreover in the absence of C3, thrombin can function as a C5 convertase leading to the generation of C5a (Amara et al., 2008).

B16F10 were reported as a potential source of thrombin, raising the possibility that high levels of C5a in tumour bearing mice was due to its production from melanomic cells. Subsequently, our lab managed to generate results which confirmed the production of prothrombin by B16F10.

Complement activation and complement products have been found to have an important role in determining the extent of tumour growth. In particular, it was found that C5a can promote tumour growth by inhibition of $CD8^+$ T–cells response. The suppression of $CD8^+$ was accompanied by an increase in the number of myeloid derived suppressor cells in the tumour microenvironment which subsequently produces reactive oxygen species (ROS) and reactive nitrogen species (Markiewski *et al.*, 2008). In addition, C5a may create a favourable environment for lung cancer cells growth and progression which may be linked to the induction of angiogenesis and immunosuppression (Corrales *et al.*, 2012). Investigations into the level of T-cytotoxic cells revealed that spleen of PKO tumour bearing mice had a significantly lower percentage of T-cytotoxic cells as compared to PWT tumour bearing mice. Furthermore, spleen of PWT/PKO tumour bearing mice had a significantly lower percentage when compared to its percentage in PWT/PKO naïve counterpart's possibly indicating depression of T-cytotoxic cells in tumour bearing mice. Migration of the cells away from tumour site might be the reason for depression of T-cytotoxic cells in tumour bearing mice. Furthermore, binding of C5a with C5aR on MDSCs promotes their migration and augments their production of immunosuppressive molecules such as reactive oxygen species and reactive nitrogen species, leading to a decrease

in cytotoxic $CD8^+$ T cells. Thus $CD8^+$ T-cell suppression can be a consequence of high C5a levels.

It is important to note that many parameters were investigated in spleens only but not in tumour tissue due to the small size of tumours which ultimately results in insufficient number of cells. Therefore, the priority was to use single cell suspensions from tumour tissue to investigate for MDSCs and T-regs. Spleen is an important extramedullary site and tumour associated macrophage precursors are localised in this organ, subsequently relocating to the tumour stroma. Furthermore, removal of spleen leads to decrease in the accumulation of tumour associated macrophages and less tumour growth (tumour-associated macrophages (Cortez-Retamozo et al., 2012). Between optimisation of experiment with different dose of injection and carrying out the actual experiment, 150-200 mice have been used in this study.

4.21.2 Conclusions

Despite the low immunogenicity of B16F10 tumour cells, apoptotic B16F10 tumour cells have been found to induce a strong immune response in the tumour-bearing mice (Dou et al., 2007, Banchereau and Steinman, 1998).

Tumour growth in properdin and wildtype mice was evaluated by three different methods: Tumour size by calipers, tumour weight and bioluminescence from a number of independent subcutaneous tumour implantations showed no significant difference between PWT and PKO mice. However, there was a tendency toward smaller tumours in properdin deficient mice.

MDSCs, C5a, CCL2, TGF-β^+ cells and $FOXP3^+$ cells were significantly less in tumour of properdin deficient mice compared to wildtype.

In spleen, MDSCs, regulatory T cells, M2 macrophage($CD206^+F4/80^+$) and TGF-β were decreased significantly in properdin deficient compared with wildtype mice (control) after subcutaneous injection with B16F10 cells, indicating that properdin may contribute to the accumulation of MDSCs in spleen, as well as to the migration of these cells into tumours. MDSCs play a fundamental role in regulating the antitumour immune response (Vatner and Formenti, 2015).

Notably, expression of CD86 on dendritic cells was very faint which could either be due to relatively low expression of this marker on Dendritic cells under our

experimental conditions or due to the use of FITC fluorochrome in staining. This limitation stresses the need for further experiments to confirm these results.

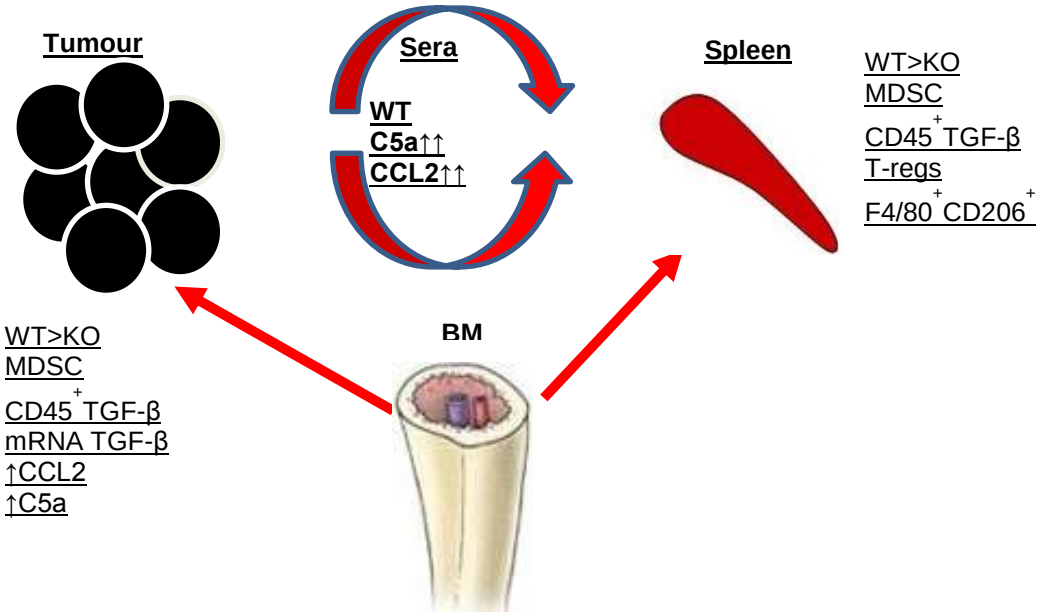

Figure 71: Tumour induces more MDSC and T –regs (up to naïve) also C5a, TGF and CCL2 in PWT.

Chapter 5 Analysis of tumour burden in LDLR$^{-/-}$PWT and LDLR$^{-/-}$ PKO mice.

5.1 Results

5.1.1 Tumour size and weight in LDLDR$^{+/+}$(PWT/PKO) and LDLR$^{-/-}$

Comparison in melanoma tumour growth was done between LDLR$^{+/+}$ and LDLR$^{-/-}$ mice to investigate the effect of hypercholesteremia and the role of properdin on tumour growth (tumour weight and size). In addition, melanoma tumour growth between LDLDR$^{+/+}$(PWT/PKO) and LDLR$^{-/-}$ mice was investigated. Data from more than four independent experiments performed using the same procedures were combined and statistical analysis was done. Tumour growth was expected to be more in LDLR$^{-/-}$ as they have more M2 macrophages compared to wildtype however no difference was seen at this time point.

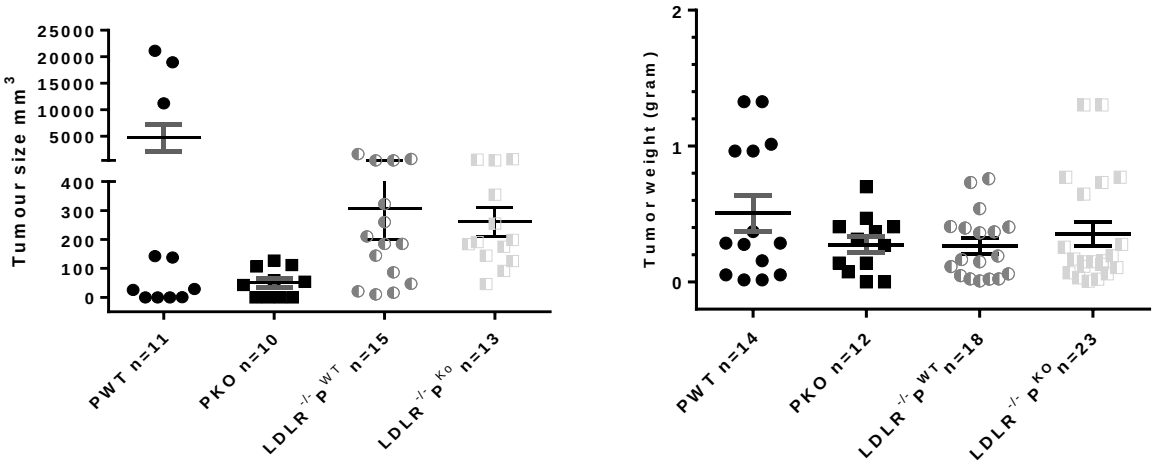

Figure 72: Tumour weight and Size in LDLR-/- (PWT/PKO) and LDLR-/- mice on C57BL/6 background.

Sex and age matched mice (male& female) were injected subcutaneously in the flank with 100µl (1.6x10^{5}cells) of freshly prepared B16F10 cell suspension. After 14 days, mice were culled and dissected. Their flanks were macroscopically examined for tumour formation, tumour size was measured using carbon dial calipers (upto150mm) and tumours were weighed. Tumour was not invasive and there was no evidence of melanotic lymph nodes and necrosis**.** The data are presented as means ±SEM. Statistical analysis was performed by one-tailed Mann-Whitney U test. * ($p < 0.05$). Statistical analyses were performed using two-way ANOVA with Tukey's multiple comparisons test.

5.1.2 Percentage of CD206^{+}F4/80^{+} in spleen of LDLR$^{-/-}$P^{WT} and LDLR$^{-/-}$P^{KO} tumour bearing mice.

As mentioned previously, M2 macrophages have been associated with promoting tumour growth and metastasis via suppressing the activity of CD8^{+} T cells (Melancon et al., 2012). Surface markers CD206 and F4/80 were used to investigate the percentage of M2 macrophages in spleen (Jablonski et al., 2015, Roszer, 2015). Comparison between LDLR$^{-/-}$P^{WT} and LDLR$^{-/-}$P^{KO} tumour bearing mice showed that LDLR$^{-/-}$P^{KO} had a significantly higher percentage of splenic M2 macrophages characterised by the markers CD206 and F4/80 (Figure 73). In addition, tumour bearing mice have more M2 macrophages than naïve mice. Nevertheless, in naïve mice, the percentage of splenic M2 macrophages was similar in both genotypes. Based on the markers CD206 and F4/80, the results previously reported in chapter 3 reveal that PWT/PKO group of naïve mice have lower percentage of splenic M2 macrophages than their counterparts in LDLR$^{-/-}$ background. Because of the significant differences in M2 phenotype abundance, LDLR$^{-/-}$ mice were pursued further in this model.

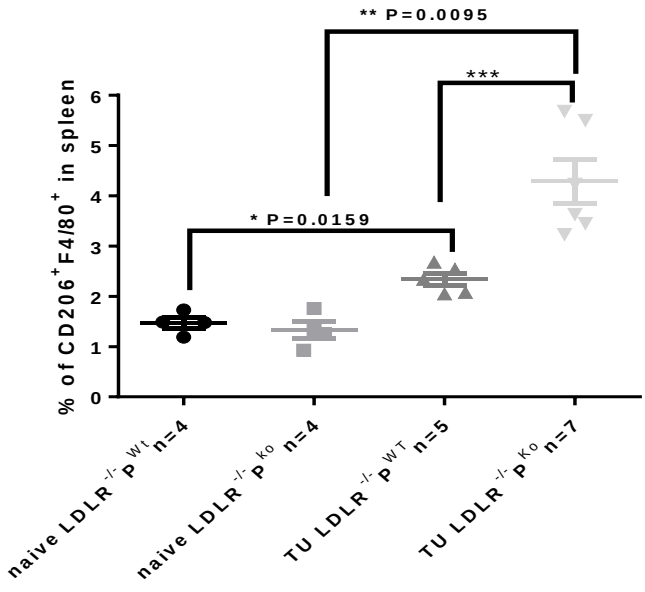

Figure 73: Percentage of CD206 +F4/80+ cells in spleen of LDLR$^{-/-}$P^{WT} and LDLR$^{-/-}$P^{KO} tumour bearing and naïve mice.

Mice were injected subcutaneously with 1.6×10^{5} cell/100µl of B16F10 cell suspension. After 14 days the mice were sacrificed and dissected for collection of spleen. Spleen suspension from both genotypes was stained. The data are presented as means ±SEM. Statistical analysis was performed by one-tailed Mann-Whitney U test. * ($p < 0.05$).

5.1.3 Percentage of CD11b^{+}CD205^{+} in of LDLR$^{-/-}$P^{WT} and LDLR$^{-/-}$P^{KO} tumour bearing mice.

Due to its abundant expression in dendritic cells, CD205^{+} is used as a marker for a subset of dendritic cells (DCs)(Yamazaki et al., 2008). This receptor is reported to direct captured antigens from the extracellular space to specialised antigen processing compartments. Mouse splenic dendritic cell subsets marked by the presence of CD205 can induce T-helper 1 response. Thus, the percentage of CD11b^{+}CD205^{+} cells was quantified in spleen of LDLR$^{-/-}$P^{WT} and LDLR$^{-/-}$P^{KO} tumour bearing mice and naïve mice as an indicator of Th1 inducing subset of DC. The result showed that spleen of LDLR$^{-/-}$P^{WT}/ LDLR$^{-/-}$P^{KO} tumour bearing mice had a significantly higher percentage when compared to its percentage in LDLR$^{-/-}$P^{WT}/ LDLR$^{-/-}$P^{KO} naïve counterparts, a sign of immune activation in tumour bearing mice. (Figure 74). However, no difference was seen in either naïve or tumour bearing mice between PWT and PKO genotypes.

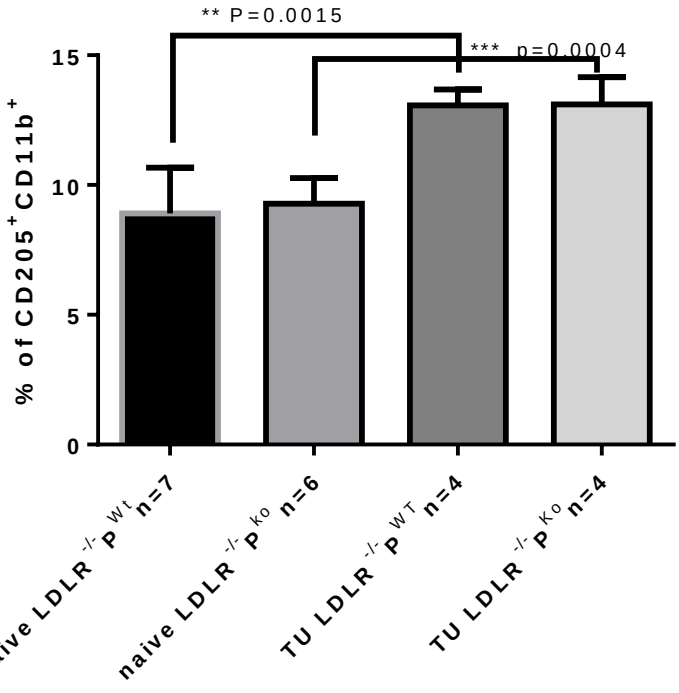

Figure 74: Percentage of CD205^{+}CD11b^{+} cells in spleen of LDLR$^{-/-}$P^{WT} and LDLR$^{-/-}$P^{KO} tumour bearing and naïve mice.

Mice were injected subcutaneously with 1.6×10^{5} cell/100µl of B16F10 cell suspension. After 14 days the mice were sacrificed and dissected for collection of spleen. Spleen suspension from both genotypes were stained. The data are presented as means ±SEM. Statistical analysis was performed by one-tailed Mann-Whitney U test. * ($p < 0.05$).

5.1.4 Analysis of tumour burden in LDLR$^{-/-}$P^{WT} and LDLR$^{-/-}$ P^{KO}

5.1.4.1 Tumour weight

In order to investigate any difference in tumour weight LDLR$^{-/-}$PWT and LDLR$^{-/-}$ PKO mice, data from three independent experiments performed using the same procedures were combined and statistical analysis was done. The results showed no statistical difference in tumour weight between wildtype and properdin deficient mice.

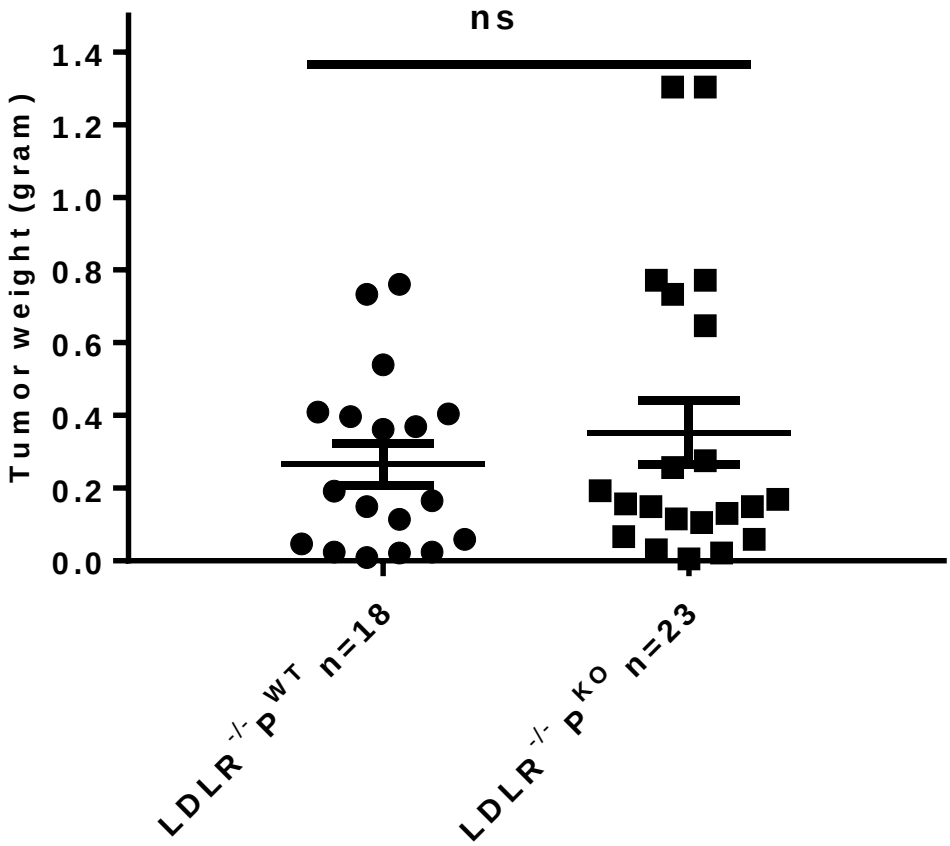

Figure 75: Tumour weight in PWT and PKO LDLR$^{-/-}$ mice on C57BL/6 background.
Sex and age matched mice (male & female) were injected subcutaneously in the flank with 100µl (1.6x10^{5}cells) of freshly prepared B16F10 cell suspension. After 14 days, mice were culled and dissected. Their flanks were macroscopically examined for tumour formation, tumour size was measured using carbon dial calipers (upto150mm) and tumours were weighed. Tumour was not invasive and there was no evidence of melanotic lymph nodes and necrosis**.** The data are presented as means ±SEM. Statistical analysis was performed by one-tailed Mann-Whitney *U* test. * ($p < 0.05$).

Notably, this project used male and female mice in tumour implantation experiments; however the results of tumour weight from these experiments showed contradictory results between genotypes. Hence, an experiment was carried out on males only in an attempt to exclude any variation. However, the results showed that male mice from both genotypes had no difference in tumour weight (data not shown).

5.1.4.2 Tumour size

Tumour size was measured by calipers after each subcutaneous tumour implantation experiment. Data collected from two independent experiments showed that male, wildtype mice tend to have a slightly larger tumour size. However, both wildtype and properdin deficient female mice had similar tumour size as shown by Figure 76.

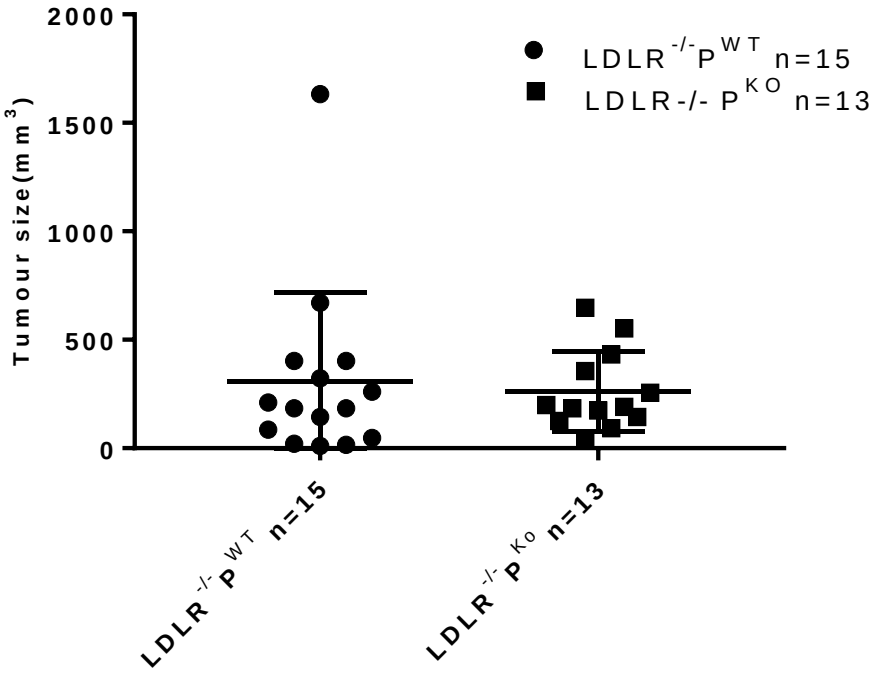

Figure 76: size of subcutaneous tumours of LDLR$^{-/-}$PKO and LDLR$^{-/-}$PWT.
C57BL/6 mice (female) were injected subcutaneously with 1.6x10^5 cell of B16F10. After 14 days the mice were sacrificed and tumour size was measured by calipers. Values are expressed as mean ± SEM from two independent experiments. The data are presented as means ±SEM. Statistical analysis was performed by one-tailed Mann-Whitney *U* test. * ($p < 0.05$).

5.1.5 FACS analysis of tumour microenvironment in LDLR$^{-/-}$P^{WT} and LDLR$^{-/-}$P^{KO}.

Studying the level of some immunological parameters will help to gain better understanding of the interaction between tumour cells and the immune system. The data generated from these studies will eventually aid in developing better knowledge of the tumour microenvironment. Implanting tumour in both $LDLR^{-/-}P^{WT}$ and $LDLR^{-/-}P^{KO}$ mice will aid in understanding the role that properdin might play in the tumour microenvironment. Hence the aim of this experiment was to compare between tumour bearing wildtype and properdin deficient mice with regards to % $CD45^{+}$, % $CD4^{+}$, $CD8^{+}$, % Treg, %IL-10^{+} and % TGF-B^{+}cells in tumour as key descriptors of tumour development and immune cell infiltration. It has been shown that regulatory T cells (T-regs) have the ability to inhibit self - reactive cells resulting in protecting the host from autoimmune disorders. Moreover, T-regs also have the ability to suppress antitumour immune responses. Some studies have reported that T-regs increase in the tumour microenvironment. It is thought that the suppressive ability of T-regs is attributed to inhibition of IL-2. Both human and murine T-regs have the capability of producing transforming growth factor (TGF-B) and interleukin-10 (IL-10) (Plitas and Rudensky, 2016).

Complement and complement activation products have been found to have an important role in determining the extent of tumour growth. In particular, it was found that C5a can promote tumour growth by inhibition of $CD8^{+}$ T–cells response. The suppression of $CD8^{+}$ was accompanied by an increase in the number of MDSCs in the tumour microenvironment which subsequently produces reactive oxygen species and reactive nitrogen species (Markiewski et al., 2008). In addition, C5a create a favourable environment for lung cancer cells growth and progression which may be linked to the induction of angiogenesis and immunosuppression (Corrales et al., 2012). It is well documented that M2 macrophages have the ability to promote tumour growth and metastasis, in part by secreting a wide range of proangiogenic factors and growth factors. Moreover, M2 tumour associated macrophages are thought to enhance tumour growth and metastasis by suppressing the activity of $CD8^{+}$ T cells (Melancon et al., 2012).

Previous data has shown that tumour bearing wildtype $LDLR^{-/-}$ mice tend to have larger tumour size and higher percentage of MDSCs when compared with properdin deficient tumour bearing mice.

Analysis of the tumour microenvironment revealed that the average percentage of CD8+ cells was lower in the wildtype group when compared to the properdin deficient group (12.49 ± 1.66 and 23.11 ± 9.19 respectively) as shown in Table 15. On the other hand, the percentage of $CD45^+$cells was higher (2.34± 0.43) in wildtype mice when compared with properdin deficient mice (1.48±0.14). The average percentage of TGF-β positive cells was higher (0.963±0.23) in properdin deficient mice compared to 0.52± 0.23 in wildtype mice as illustrated by Table 15. In order to gain better understanding of the tumour microenvironment in both genotypes, individual mice from each genotype with similar tumour weight were compared with each other. For example mice with tumour weight of 0.11g (represented by number 5341 in wildtype mice and number 5334 in the properdin deficient mice). For this tumour weight, the wildtype had lower percentage of CD45+ cells (0.33) when compared to the properdin deficient mouse which had 1.02%. Moreover, the percentage of $CD8^+$ cells, T-regs ($CD45^+$, FOXP3 $^+$ and $CD4^+$) and TGF-β^+cell was lower (17.2, 0.61 and 0.67 respectively) in wildtype mouse when compared to 26.1, 1.03 and 1.37 respectively in the properdin deficient mouse. Another pair that was compared together was mice with tumour weight ranging from 0.006 and 0.009g represented by mouse number 5340 in the wildtype group and mouse number 5336 in the properdin deficient group. The percentage of $CD45^+$ and $CD4^+$ cells showed that there was no difference between the wildtype and the properdin deficient mice. The wildtype mice had higher (13.3) percentage of CD8+ and lower (4.98) percentage of T-regs when compared with properdin deficient mice which had 7.46 and 12.7% respectively. Comparison between mouse number 5347 (in the wildtype group) and mouse number 5332 (in the properdin deficient group) which had tumour weight of 0.02g showed that both had similar $CD45^+$ percentage. On the other hand, the wildtype mouse had lower percentage of $CD4^+$, $CD8^+$ and T-regs (0.58, 14.3 and 1.3 respectively) when compared to the properdin deficient mouse which had 1.24% of $CD4^+$ cells, 23.8% of $CD8^+$ cells and 2.31% of T-regs as shown in Table 15.

The aforementioned data shows that the small weight of tumour observed in properdin deficient mice was accompanied by higher percentage of T-regs which could mean that T-regs tend to be higher at early stages of tumour formation. Cell migration does not appear to be impaired in the absence of properdin.

It has been reported that IL-17 secreting Th cells (Th17) play a role in promoting inflammation and are responsible for immunopathology in both cancer and several autoimmune disorders. The results of various murine tumour model studies have suggested that Th17 cells may be associated with tumour initiation (Kawakami et al., 2009;Wang et al., 2009;Wu et al., 2009b).

Table 15: Percentage of $CD45^+$, $CD4^+$, $CD8^+$, T-reg ($CD45^+$, $CD4^+$, $FOXP3^+$), $CD45^+IL\text{-}10^+$ and $CD45^+TGF\text{-}B^+$ cells in melanoma tumour suspension after 14 days of B6F10 implantation in $LDLR^{-/-}P^{WT}$ and $LDLR^{-/-}P^{KO}$ (by FACS).

Genotype	Tumour weight/g	Mean ± SEM	$CD45^+$	Mean ± SEM	% $CD4^+$	Mean ± SEM	%$CD8^+$	Mean ± SEM	$CD45^{+*}$	Mean ± SEM	%T-regs in tumour	Mean ± SEM	$CD45^+$ %IL-10	Mean ± SEM	$CD45^+$ %TGF-β	Mean ± SEM
$LDLR^{-/-}$ PWT	0.114	0.101 ± 0.036	5.91	7.680 ± 1.333	0.33	0.536 ± 0.201, n=5	17.2	12.49 ± 1.657, n=5	2.89	2.343 ± 0.436	0.61	1.692 ± 0.830	0.33	0.420 ± 0.051	0.67	0.520 ± 0.229
	0.166		5.22		0.2		7.85		2.66		0.84		0.42		0.82	
	0.192		5.62		0.27		9.8		1.48		0.73		0.51		0.07	
	0.009		11.9		1.3		13.3				4.98					
	0.024		9.75		0.58		14.3				1.3					
$LDLR^{-/-}$ PKO	0.031	0.0562 ± 0.022	8.57	8.852 ± 1.044	0.3	0.808 ± 0.196, n=5	2.98	23.11 ± 9.191, n=5	1.64	1.487 ± 0.148	0.75	3.554 ± 2.303	0.72	0.423 ± 0.151	0.94	0.963 ± 0.228
	0.116		5.16		1.02		26.1		1.19		1.03		0.33		1.37	
	0.106		9.03		0.37		55.2		1.63		0.98		0.22		0.58	
	0.022		10.1		1.11		23.8				2.31					
	0.006		11.4		1.24		7.46				12.7					

5.1.6 Percentage of MDSCs in bone marrow, spleen and tumour of LDLR$^{-/-}$P^{WT} and LDLR$^{-/-}$P^{KO}

The process of myelopoiesis is altered in cancer resulting in increase of immature and activated myeloid cells such as Myeloid Derived Suppressor Cells (MDSCs). MDSCs are negative regulators of the immune response and have a role in tumour metastasis and angiogenesis. In addition, they have a role in regulating the immune response in a variety of conditions such as autoimmune disease and chronic infectious diseases (Youn et al., 2013).

MDSCs are a heterogeneous group of cells consisting of both myeloid progenitors and immature myeloid cells. Immature myeloid cells are produced in the bone marrow, where they differentiate into macrophages, dendritic cells or mature granulocytes. However, certain pathological conditions such as cancer and autoimmune disease, lead to an increase of these cells. These immature myeloid cells tend to possess an immunosuppressive activity and are generally known as MDSCs (Kusmartsev et al., 2004). It has been shown that in healthy mice, 20-30% of cells in bone marrow and 2-4% of cells in spleen are MDSCs (Almand et al., 2001).

In cancer, MDSCs accumulate in peripheral lymphoid organs and eventually migrate to tumour site, where they possess immunosuppressive properties. There have been some indications that MDSCs might even play a role in the expansion of T regs (Gabrilovich and Nagaraj, 2009). Two groups of MDSC have been identified, the first with monocytic characteristics known as M-MDSCs and the second with polymorphonuclear characteristics Known as PMN-MDSCs. While both groups are identified by the expression of both Gr-1 and CD11b markers, M-MDSCs are thought to have low Gr-1 expression and are highly immune suppressive. PMN-MDSCs have high expression of Gr-1 with a moderate immunosuppressive ability, hence the aims of this experiment to investigate the percentage of MDSCs in bone marrow, spleen and tumour in both genotypes as well as in naïve mice as a control. In order to investigate the role of properdin in tumour growth, C57BL/6 mice (LDLR$^{-/-}$P^{WT} and LDLR$^{-/-}$P^{KO} sex and age matched) were injected subcutaneously in the flank with 1.6x10^{5} B16F10 cells suspension. After 14 days the mice were culled and dissected and were macroscopically examined for tumour formation. Bone marrow derived cells and splenocytes were prepared from tumour bearing mice. FACS analysis was done

using three markers; CD45, Gr-1 and CD11b. Assessment of the accumulation of M-MDCS and PMN-MDSCs was done according to the phenotypic criteria of M-MDSCs as Gr-1 low, CD11b+CD45+ and of PMN-MDSC as Gr-1 Hi, CD11b+CD45+ (Youn et al., 2013). The results showed that there was no difference in the total percentage of MDSCs in bone marrow of tumour bearing and naïve mice (data not shown) for both tested genotypes as shown in Figure 77. Additionally, there was no apparent difference in numbers of the PMN-MDSC and M-MDSC populations of MDSCs (Data not shown). However, assessment of expansion of MDSC subset in bone marrow showed that wildtype tumour bearing mice had more M-MDSC than KO tumour bearing mice. In addition, of $LDLR^{-/-}P^{WT}$ mice had the highest percentage of M-MDSCs population (up to 18.4±4.5%) which are reported to be highly suppressive. It was expected that this genotype would have more immunosuppressive population as it has been previously published that this genotype has more M2 macrophage population. Table 16 shows that $LDLR^{-/-}P^{WT}$ seem to have more MDSCs (14.70 ±3.120) than $LDLR^{-/-}P^{KO}$ (9.270±1.747) in tumour microenvironment though this does not reach statistical significance (for 5 mice in each group). But there was no obvious relation to tumour size.

FACS analysis showed that spleen of properdin deficient tumour bearing mice had a significantly lower percentage of MDSCs when compared to wildtype tumour bearing mice. However, spleen of of $LDLR^{-/-}P^{WT}$/$LDLR^{-/-}P^{KO}$ tumour bearing mice had a significantly lower percentage when compared to its percentage in $LDLR^{-/-}P^{WT}$/$LDLR^{-/-}P^{KO}$ naïve counterparts as shown in Figure 77. Analysis of percentage of MDSCs in tumour showed no significant difference between the genotypes. Although not significant, $LDLR^{-/-}P^{WT}$ tumour bearing mice had a tendency to higher percentage of MDSCs compared to $LDLR^{-/-}P^{Ko.}$

Table 16: Percentage of MDSC (CD45+Gr-1+CD11b+) cells in mouse melanoma tumour.
After 14 days of B16F10 implantation in $LDLR^{-/-}P^{WT}$ and $LDLR^{-/-}P^{Ko}$ (by FACS).
Mice were injected subcutaneously with 1.6×10^5 cell/100µl of B16F10 cell suspension. After 14 days the mice were sacrificed and dissected for collection of spleen. Spleen suspension from both genotypes were stained with three markers (CD11b+Gr1 and CD45) to distinguish MDSC. Then FACS was done and percentage of MDSCs was obtained. The gating was on CD45, and the other two markers were used to calculate of total MDSC in spleen.

Genotype	ID	Genotype	%MDSCs Tumour	Mean ± SEM
$LDLR^{-/-}P^{WT}$	5341	$LDLR^{-/-}P^{WT}$	24.00	14.70 ± 3.120
	5342	$LDLR^{-/-}P^{WT}$	6.08	
	5346	$LDLR^{-/-}P^{WT}$	10.80	
	5340	$LDLR^{-/-}P^{WT}$	18.90	
	5347	$LDLR^{-/-}P^{WT}$	13.70	
$LDLR^{-/-}P^{KO}$	5333	$LDLR^{-/-}P^{KO}$	5.26	9.270 ± 1.747
	5334	$LDLR^{-/-}P^{KO}$	7.66	
	5335	$LDLR^{-/-}P^{KO}$	12.60	
	5332	$LDLR^{-/-}P^{KO}$	6.63	
	5336	$LDLR^{-/-}P^{KO}$	14.20	

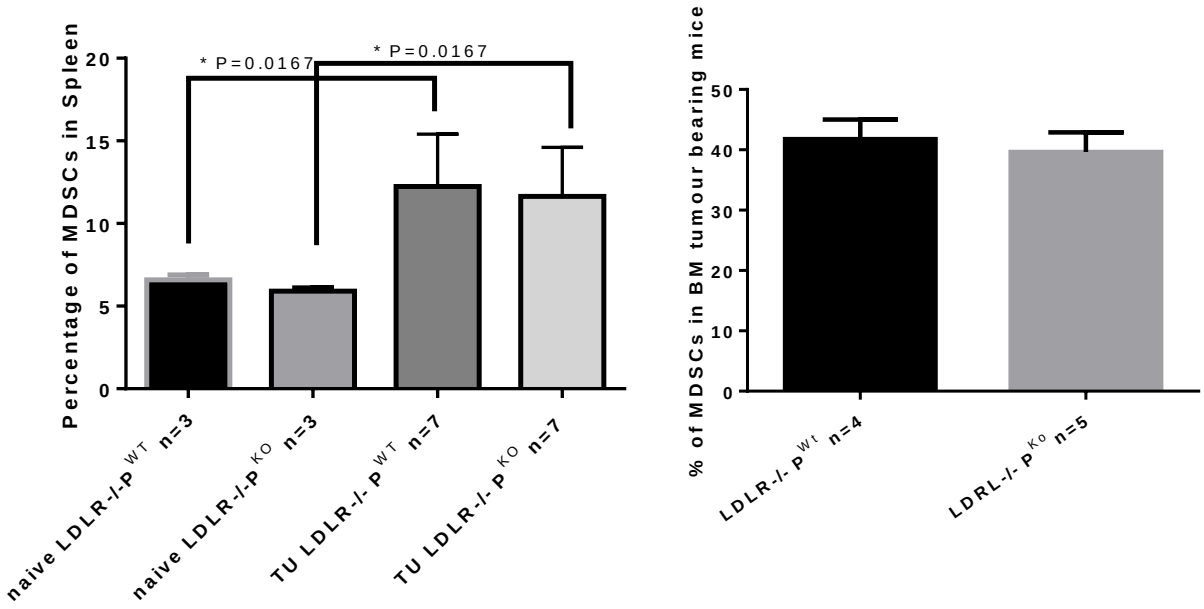

Figure 77: **MDSC populations in spleen and BM of LDLR$^{-/-}$P^{WT}/LDLR$^{-/-}$P^{KO} tumour bearing and naïve mice.**

Mice were injected subcutaneously with 1.6×10^5 cell/100µl of B16F10 cell suspension. After 14 days the mice were sacrificed and dissected for collection of spleen. Spleen suspension from both genotypes were stained with three markers (CD11b, Gr1 and CD45) to distinguish MDSC. Then FACS was done and percentage of MDSCs was obtained. The gating was on CD45, and the other two markers were used to calculate of total MDSC in spleen. The data are presented as means ±SEM. Statistical analysis was performed by one-tailed Mann-Whitney *U* test. * ($p < 0.05$).

5.1.7 Percentage of T-regulatory cells (CD25+CD4+FOXP3 +) in spleen of LDLR$^{-/-}$P^{WT} and LDLR$^{-/-}$P^{KO} tumour bearing and naïve mice.

FACS analysis showed that spleen of LDLR$^{-/-}$P^{WT}/ LDLR$^{-/-}$P^{KO} tumour bearing mice had a significantly higher percentage of T-regs when compared to its percentage in LDLR$^{-/-}$P^{WT}/ LDLR$^{-/-}$P^{KO} naïve counterparts as shown in Figure 78. However, there was no difference between of LDLR$^{-/-}$P^{WT} compared to LDLR$^{-/-}$P^{KO} tumour bearing mice.

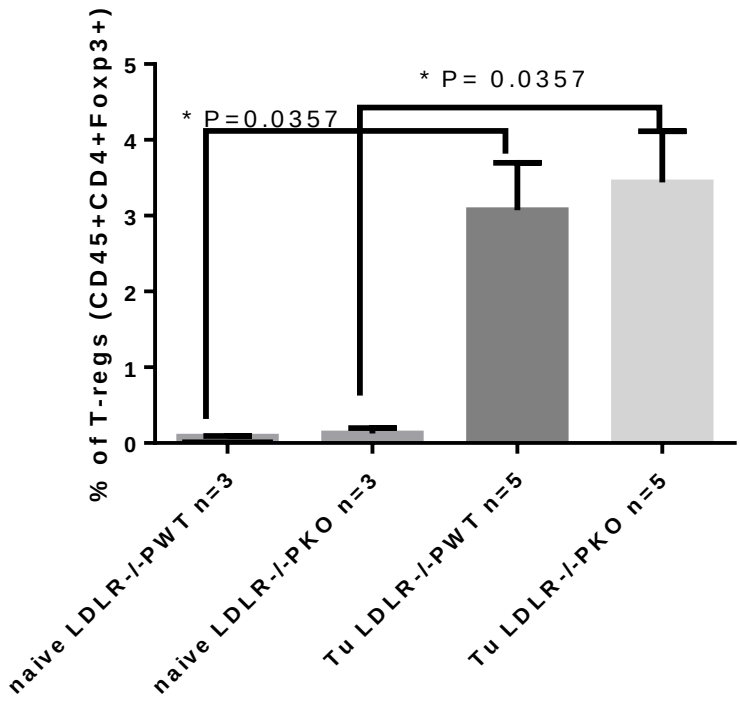

Figure 78: T-regs populations in spleen of LDLR$^{-/-}$P^{WT}/LDLR$^{-/-}$P^{KO} tumour-bearing and naïve mice.

Mice were injected subcutaneously with 1.6×10^5 cell/100µl of B16F10 cell suspension. After 14 days the mice were sacrificed and dissected for collection of spleen. Spleen suspension from both genotypes was stained with three markers (CD4, CD25 and FOXP3) to distinguish T-regs. Then FACS was done and percentage of T-regs was obtained.The data are presented as means ±SEM. Statistical analysis was performed by one-tailed Mann-Whitney U test. * ($p < 0.05$).

5.1.8 Percentage of NK cells (NKP46+CD3+CD45+) in spleen.

Natural killer (NK) cells play critical roles in host immunity against cancer. In animal studies, they have been shown to play an important role in the control of tumour growth and metastasis and to provide innate immunity against infection with certain viruses. Following activation, NK cells release cytokines and chemokines that induce inflammatory responses; modulate monocyte, dendritic cells, and granulocyte growth and differentiation; and influence subsequent adaptive immune responses. In order to investigate the percentage of NK cells in spleen of LDLR$^{-/-}$P^{WT} and LDLR$^{-/-}$P^{KO} mice. FACS analysis was done using NKP46+CD45 and the result showed that spleens of LDLR$^{-/-}$P^{WT}/ LDLR$^{-/-}$P^{KO} tumour bearing mice had a significantly lower percentage of NK cells when compared to its percentage in LDLR$^{-/-}$P^{WT}/ LDLR$^{-/-}$P^{KO} naïve counterparts, as shown in Figure 79 B. However, there was no difference between the percentage of NK cells in LDLR$^{-/-}$P^{WT} compared to LDLR$^{-/-}$P^{KO} tumour bearing mice. Similar

results were obtained for NKT cells ($CD45^+CD3^+NKP46^+$) in both genotypes, however $LDLR^{-/-}P^{WT}$ tumour bearing mice showed no difference compared to naïve mice.

In conclusion, both NK and NKT cells seem to decrease in tumour bearing mice. This decrease may possibly be due to the action of the immune suppressive cells, MDSCs and T-regs.

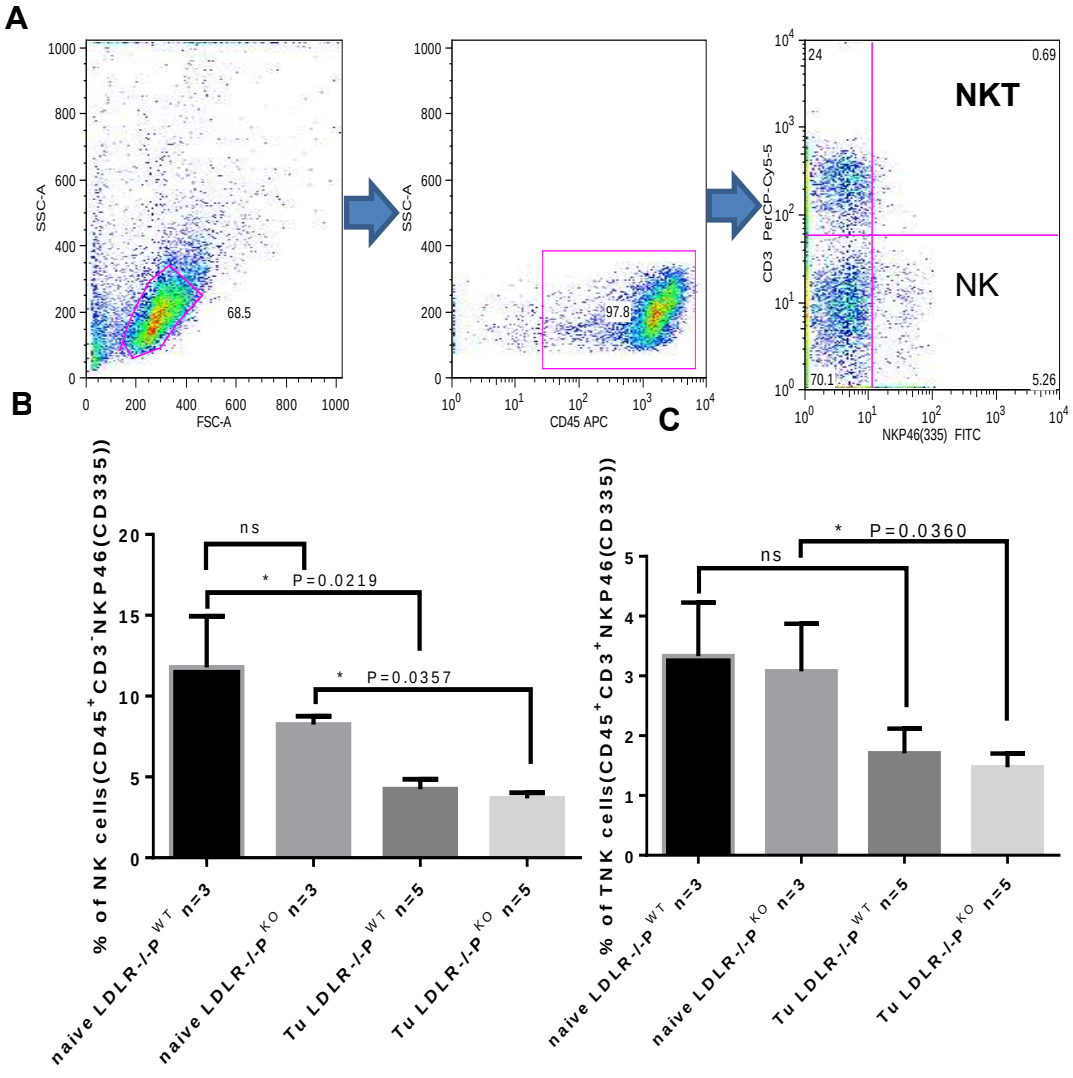

Figure 79: NK and TNK cells populations in spleen of $LDLR^{-/-}P^{WT}$/$LDLR^{-/-}P^{KO}$ mice.
A) Flow cytometry analysis of $CD45^+CD3^+$ $NKP46^+$ cells after gating on $CD45^+$cells in spleen of $LDLR^{-/-}P^{WT}$/LDLR-/-P^{KO} mice. Numbers in the plots indicate the percent of gated cells. $CD45^+CD3^+NKP46^+$ represent percentage of NKT cells and $CD45^+CD3^-NKP46^+$ represent percentage of NK cells, after subcutaneous injection of 1.6 $X10^5$ cells of B16F10. B) Populations of NK cells. C) Populations of NKT in tumour of wildtype and properdin deficient mice. Mice were injected subcutaneously with 1.6×10 cell/100µl of B16F10 cell suspension. After 14 days the mice were sacrificed and dissected for collection of spleen. The data are presented as means ±SEM. Statistical analysis was performed by one-tailed Mann-Whitney U test. * ($p < 0.05$).

5.1.9 Percentage of cytotoxic T cells ($CD45^+CD3^+CD8^+$) in spleen of LDLR-/- P^{WT} compared to LDLR-/-P^{KO} tumour bearing mice.

In this chapter, the percentage of M2 macrophages ($F4/80^+CD206^+$) in spleen was investigated, and the result showed more M2 cells in $LDLR^{-/-}P^{KO}$ compared to $LDLR^{-/-}P^{WT}$ mice, T-reg cells can reversibly blunt T cell responses by selectively modulating a terminal effector function of primed $CD8^+$ T cells(Mempel et al., 2006).Therefore, the percentage of cytotoxic T cells in spleen of $LDLR^{-/-}P^{WT}$ and $LDLR^{-/-}P^{KO}$ tumour bearing and naïve mice was investigated. The result showed that tumour bearing mice from both genotypes had similar percentage of cytotoxic T cells in spleens.

Furthermore, FACS analysis showed that spleens of $LDLR^{-/-}P^{WT}$/$LDLR^{-/-}P^{KO}$ tumour bearing mice had a significantly lower percentage of cytotoxic T cells when compared to its percentage in $LDLR^{-/-}P^{WT}$/$LDLR^{-/-}P^{KO}$ naïve counterparts as shown in Figure 80. However, a significant numerical difference may not be of biological significance in tumour immune response. The aforementioned data show depression of cytotoxic T cells in tumour bearing mice, possibility indicating the effect of another influential element such as C5a and T-regs which were high in tumour bearing mice. An alternative explanation for the depression of cytotoxic Tcells in tumour bearing mice is the possibility of migration of cells away from spleen site.

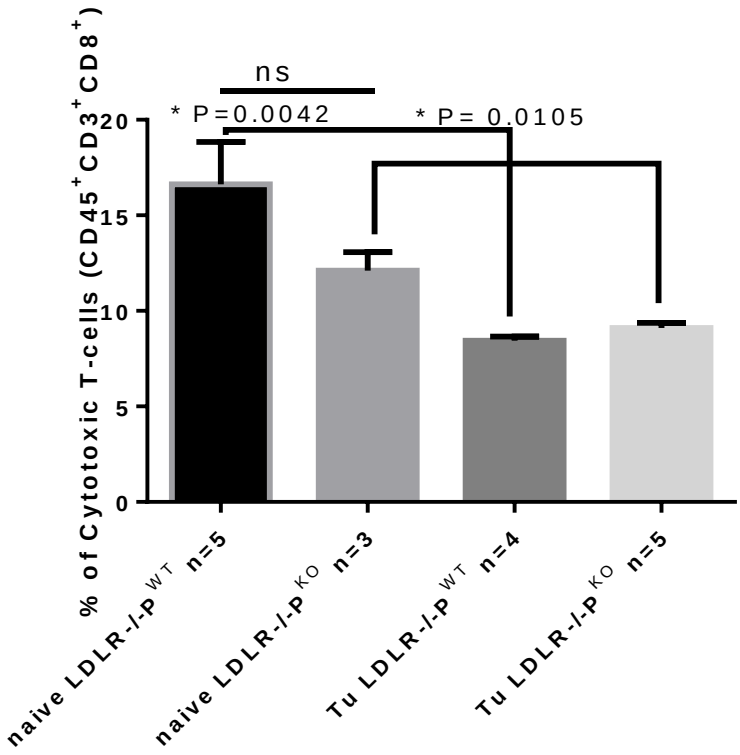

Figure 80: Cytotoxic T cell populations in spleens of LDLR$^{-/-}$P^{WT} and LDLR$^{-/-}$P^{KO} mice.

Mice were injected subcutaneously with 1.6×10^5 cell/100µl of B16F10 cell suspension. After 14 days, the mice were sacrificed and dissected for collection of spleen. Spleen suspension from both genotypes were stained with three markers (CD45, CD3 and CD8) to distinguish cytotoxic T cells. Then FACS was done, and percentage of cytotoxic T cells was obtained. The gating was on CD45. The data are presented as means ±SEM. Statistical analysis was performed by one-tailed Mann-Whitney U test. * ($p < 0.05$).

5.1.10 T-regulatory cells (CD25+CD4+FOXP3+) in spleen of LDLR$^{-/-}$P^{WT} and LDLR$^{-/-}$P^{KO} mice.

FACS analysis showed that spleens of LDLR$^{-/-}$P^{WT}/ LDLR$^{-/-}$P^{KO} tumour bearing mice had a significantly higher percentage of regulatory T cells when compared to its percentage in LDLR$^{-/-}$P^{WT}/ LDLR$^{-/-}$P^{KO} naïve counterparts as shown in Figure 81. However, there was no difference between the genotypes.

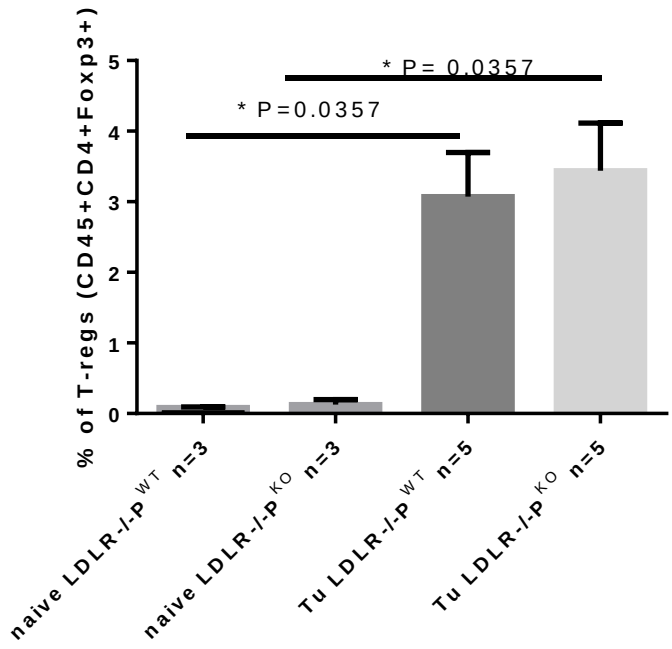

Figure 81: T-regs populations in spleen of LDLR$^{-/-}$P^{WT} and LDLR$^{-/-}$P^{KO} tumour-bearing and naïve mice.

Mice were injected subcutaneously with 1.6×10^5 cell/100µl of B16F10 cell suspension. After 14 days the mice were sacrificed and dissected for collection of spleens. Spleen suspension from both genotypes were stained with three markers (CD4, CD25 and FOXP3) to distinguish T-regs cells. The data are presented as means ±SEM. Statistical analysis was performed by one-tailed Mann-Whitney *U* test. * ($p < 0.05$).

5.1.11 Measurement of complement component C3 in sera of LDLR$^{-/-}$PWT and LDLR$^{-/-}$PKO tumour bearing mice.

C3, the central molecule in the complement cascade, was quantified in sera of LDLR$^{-/-}$P^{WT} and LDLR$^{-/-}$P^{KO} tumour bearing mice. Recent findings by Markiewski

and colleagues have presented results indicating that complement C3 activation can give a tumour growth advantage (Markiewski et al., 2008). Measurement of C3 in sera of tumour bearing mice revealed that LDLR$^{-/-}$P^{WT} has a significantly higher level when compared to LDLR$^{-/-}$P^{KO} (Figure 82). Notably, the ELISA kit used was one capable of detecting both fragments of C3. Thus, there is a possibility that increased C3 level may arise from increase in total C3 and anaphylatoxin C3a.

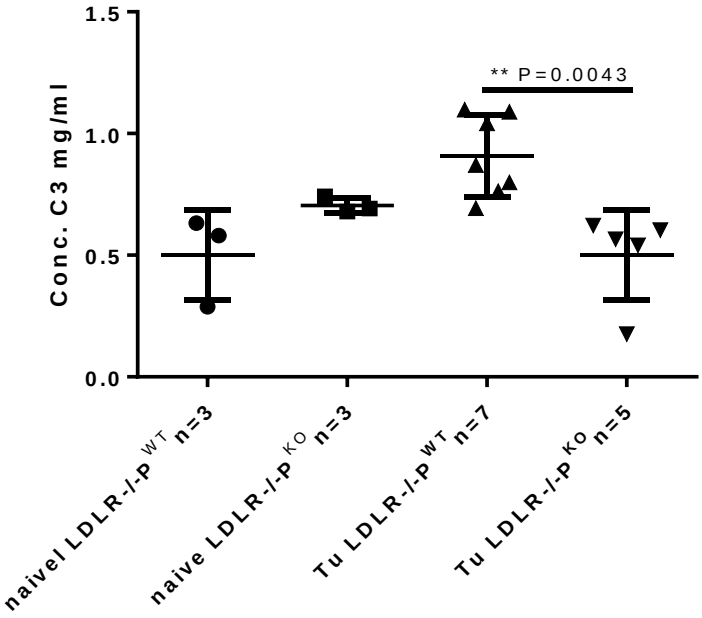

Figure 82: Level of C3 in sera of LDLR$^{-/-}$P^{WT} and LDLR$^{-/-}$P^{KO} tumour bearing mice.
Mice were injected subcutaneously with 1.6×10^5 cell/100µl of B16F10 cell suspension. After 14 days, the mice were sacrificed and sera was collected for C3 measurement by ELISA. The data are presented as means ±SEM. Statistical analysis was performed by one-tailed Mann-Whitney *U* test. * ($p < 0.05$).

5.1.12 Investigation into the extent of complement mediated activation in melanoma of LDLR$^{-/-}$P^{WT} and LDLR$^{-/-}$P^{KO} mice using Western blot.

The increased serum level of C3 in LDLR$^{-/-}$P^{WT} tumour bearing mice reported in 5.1.11, prompted further investigation into C3 reactive products in tumour lysate from both genotypes. The effect of properdin on complement C3 activation in melanoma after subcutaneous injection of mice from LDLR$^{-/-}$P^{WT} and LDLR$^{-/-}$P^{KO} with 1.6×10^5 cell/100µl of B16F10 cell suspension for 14 days was addressed in this experiment. The aim of this experiment was to study the activation of complement in mouse tumour lysate from LDLR$^{-/-}$P^{WT} and LDLR$^{-/-}$P^{KO} mice. C3

cleavage products in tumour lysate was detected by western blot. C3 fragments, iC3b (68 KDa) and C3dg (41 KDa) in tumour lysate were separated by size and are reactive with Goat anti-C3 antibody. The results represented by Figure 83 revealed that tumour lysates from $LDLR^{-/-}P^{WT}$ mice had more abundant iC3b and C3dg as compared to $LDLR^{-/-}P^{KO}$ mice. Nevertheless, this difference was not obvious in all $LDLR^{-/-}P^{WT}$ samples. This finding may possibly indicate more cleavage of C3 in tumour of in $LDLR^{-/-}P^{WT}$.

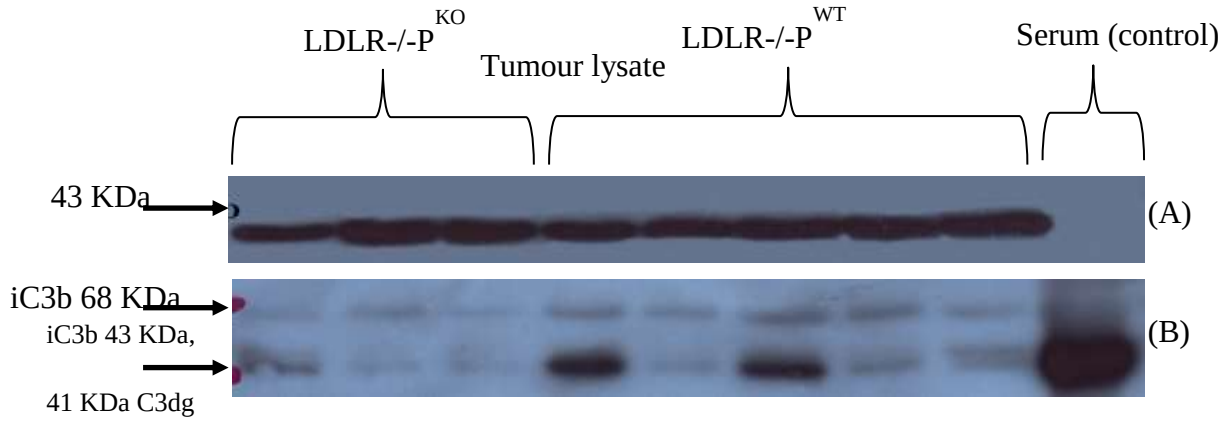

Figure 83: Western blot analysis of C3 reactive products in tumour lysate of LDLR$^{-/-}$P^{WT} ,LDLR$^{-/-}$P^{KO} and serum as a control.

A- Western Blot with anti-Beta Actin Loading Monoclonal Antibody [BA3R] (MA5-15739), Western blot analysis of Beta-Actin was performed by loading 20ug of tumour cell lysate per well onto a SDS-PAGE gel. Proteins were transferred to a PVDF membrane and blocked with 5% non-fat milk in TBST for 1 hour at room temperature. The membrane was probed with a Beta-Actin monoclonal antibody (Product # MA5-15739) at a dilution of 1:1000 overnight at 4°C, washed in TBST, and probed with an HRP-conjugated goat anti-mouse IgG secondary at a dilution of 1:4,000 for 1 hour at room temperature. Chemiluminescent detection was performed using ECL substrate. B- Western blot analysis of C3 reactive products on LDLR$^{-/-}$P^{WT} and LDLR$^{-/-}$P^{KO} tumour lysate. Membrane was probed with Goat anti-C3 (biorbyt) at a dilution of 1:5000 overnight at 4°C, and developed with Donkey anti-goat -HRP (Santa Cruz Biotechnology). Films were exposed for 50 seconds.

5.1.13 C5a and C5b-9 in sera of LDLR$^{-/-}$P^{WT} and LDLR-/-P^{KO} naïve and tumour bearing mice.

As mentioned in Chapter 4, C5a is an inflammatory peptide with a broad spectrum of functions and chemotactic activity for neutrophils, monocytes, macrophages and MDSCs. The level of C5a was measured in sera of naïve and tumour bearing mice due to the importance of this anaphylatoxin in the activation of a number of cellular responses involved in tumour growth and progression (Vadrevu et al., 2014). The results showed that LDLR$^{-/-}$P^{WT}/LDLR$^{-/-}$P^{KO} tumour bearing mice from both genotypes had a significant increase in C5a, as shown in Figure 84 compared with naïve mice. Nevertheless, neither naïve or tumour bearing mice showed a difference between genotypes in serum level of C5a. An increase in complement activation may possibly be behind the difference in the level of C5a in tumour bearing mice when compared with naïve mice, thus the level of C5b-9 (MAC complex) as an indication of complement activation was investigated by ELISA. As with C5a level in serum, tumour bearing mice from both genotypes had higher serum levels of C5b-9 when compared with naïve mice (Figure 84).

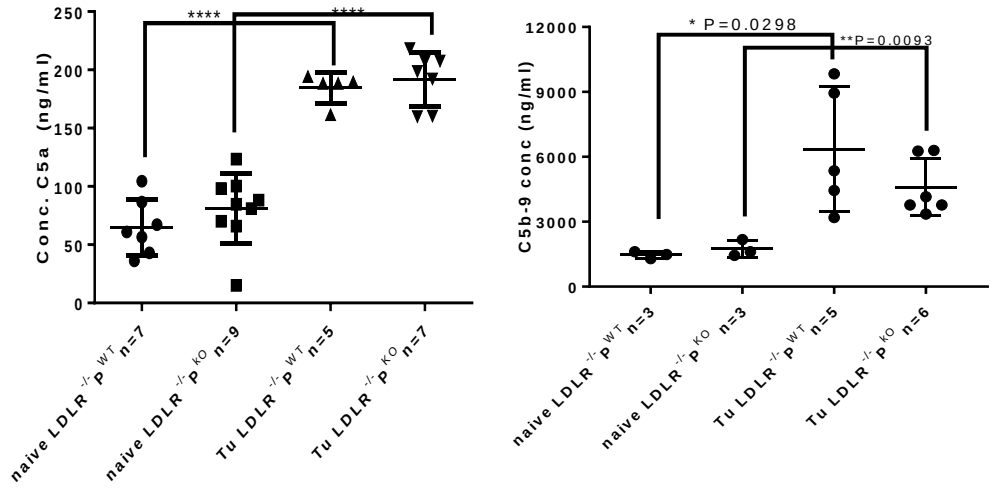

Figure 84: Level of C5a and C5b-9 in tumour bearing and naïve LDLR$^{-/-}$P^{WT} and LDLR$^{-/-}$P^{KO} C57BL/6 mice

Mice were injected subcutaneously with 1.6×10^5 cell/100µl of B16F10 cell suspension. After 14 days the mice were sacrificed and sera was collected for C5a and C5b-9 measurement by ELISA. The results showed a pattern of C5a elevation for properdin wildtype compared to wildtype mice. The data are presented as means ±SEM. Statistical analysis was performed by t student test. * ($p < 0.05$).

5.1.14 Analysis of C5aR in Bone marrow and spleen of tumour bearing and naïve mice (LDLR$^{-/-}$ P^{WT} and LDLR$^{-/-}$P^{KO})

The previous results had shown that the level of C5a was higher in sera of tumour bearing LDLR$^{-/-}$P^{WT}/LDLR$^{-/-}$P^{Ko} mice when compared with naïve mice. Nevertheless, no significant difference was found between the two genotypes. To investigate a hypothesised feedback response between cleaved C5a and relatively decreased C5aR expression in LDLR$^{-/-}$P^{WT} compared to LDLR$^{-/-}$P^{KO}, the percentage of C5a receptor and Gr1+ cells in BM and spleen of tumour bearing mice from both genotypes was investigated. Measurement of the concentration of C5aR in BM revealed that LDLR$^{-/-}$P^{WT} tumour bearing mice had a significantly lower percentage of C5aR positive cells when compared to their LDLR$^{-/-}$P^{KO} counterparts (Figure 85). Similarly, LDLR$^{-/-}$P^{WT} tumour bearing mice had lower concentration of C5aR in spleen when compared to their LDLR$^{-/-}$P^{KO} counterparts. However, in both genotypes no significant difference was detected between tumour bearing and naïve mice possibly indicating that elevation of C5a in sera of LDLR$^{-/-}$P^{WT} tumour bearing mice lead to downregulation of C5aR.

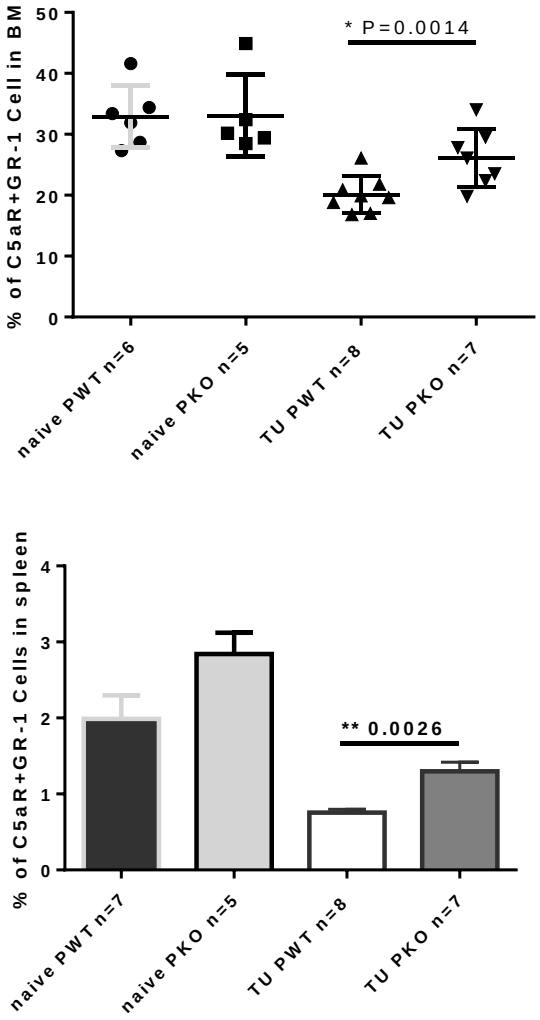

Figure 85: Percentage of C5aR+GR-1 Cells in tumour bearing and naïve LDLR$^{-/-}$P^{WT} and LDLR$^{-/-}$P^{KO} mice.

Populations of C5aR+Gr-1 cells in BM and spleen of LDLR$^{-/-}$P^{WT} and LDLR$^{-/-}$P^{KO} mice. Mice were injected subcutaneously with 1.6×10^5 cell/100µl of B16F10 cell suspension. After 14 days the mice were sacrificed and dissected for collection of BM and spleen. BM and spleen suspension from both genotypes were stained with two markers (Gr-1 FITC and C5aR APC). Then FACS was done and percentage of Gr-1+C5aR was obtained. The data are presented as means ±SEM. Statistical analysis was performed by one-tailed Mann-Whitney *U* test. * ($p < 0.05$).

5.1.15 Histological analysis of tumours from LDLR$^{-/-}$PWT and LDLR$^{-/-}$PKO mice.

H&E staining was performed on tumour tissue sections from LDLR$^{-/-}$P^{WT} and LDLR$^{-/-}$P^{KO} mice and the results are presented in Figure 38. No apparent difference was found between the genotypes.

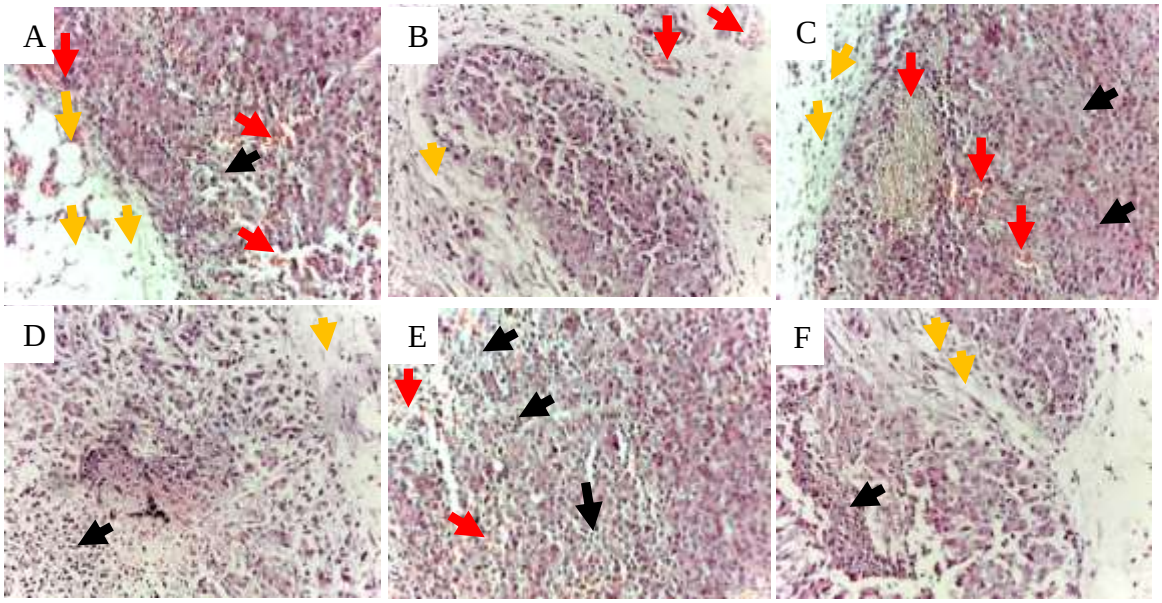

Figure 86: Tumour sections from LDLR$^{-/-}$P^{WT} and LDLR$^{-/-}$P^{KO} were examined by H&E staining.

LDLR$^{-/-}$ Wildtype and LDLR$^{-/-}$ Properdin deficient C57BL/6 mice were injected subcutaneously with 4×10^5 cell/100µl of B16F10 cell suspension. Fourteen days after injection, tumour mass was isolated from mice and fixed. Tumour tissue was sectioned and examined by H&E staining. Representative images of PWT (A, B and C) and PKO (D, E, F) mice. Area of necrosis (Black arrows), blood vessels (red arrows) and fat vacuoles (yellow arrows) are indicated. Compact tumours mass can also be seen. All images were taken at 20x magnification

5.2 Discussion & Conclusion

Published studies reported that tumour from high-cholesterol (hypercholesterolemic) mice had higher microvessel density, linking hypercholesterolemia with induction of angiogenesis and more tumour growth *in vivo* (Pelton et al., 2014). Accumulation of cholesterol and other lipids have been previously described in solid tumours. Furthermore, tumourgenesis was found to be enhanced by cholesterol, cholesterol oxidation products (Oxysterols) and cholesterol precursor (mevalonate) (Llaverias et al., 2011). Based on the aforementioned findings, it was postulated that $LDLR^{-/-}$ mice would be prone to larger tumours and more metastasis than PWT/PKO group. To our knowledge, no previous study has investigated the effect of knocking out the LDL receptor combined with complement deficiency on tumour growth and tumour microenvironment. Analysis of tumour weight and tumour size in tumour bearing $LDLR^{-/-}P^{WT}$ and $LDLR^{-/-}P^{KO}$ mice showed no significant difference between genotypes. Investigations into macrophage content and phenotype has been carried out in several cancer studies due to their crucial role in the immune response. In melanomas, the macrophage contents ranges from 0 to 30%. Melanoma cells interact with macrophages via the release of soluble factors which either prevent or promote tumour growth. In early stages of neoplastic transformation, tumour cells are subjected to non-specific killing by macrophages. Furthermore, macrophages act as antigen presenting cells for T-lymphocytes which subsequently produce macrophage activating cytokines (Hussein, 2006). Tumour associated macrophages and related subset of M2 (alternatively-activated) macrophages enhance tumour cell proliferation. With regards to Tumour associated macrophages, several studies have have presented findings showing that tumour-associated macrophages (TAMs) exhibit predominantly the anti-inflammatory M2 phenotype. During cancer, M2 macrophages assist tumour growth via production of a number of growth factors and proangiogenic cytokines (Okwan-Duodu et al., 2013). In aggressive melanomas, the presence of increased number of M2 macrophages is an indication of host response against the tumours (Hussein, 2006). Due to their proangiogenic and tumour-promoting potential, M2 macrophages ($F4/80^{+}CD206^{+}$) have been investigated in this chapter in spleen of tumour

bearing and naïve mice from both genotypes. In naïve mice, results for $CD206^{+}F4/80^{+}$ cells showed that $LDLR^{-/-}$ group of mice had higher percentage of cells when compared to PWT/PKO group, a possible indicator that $LDLR^{-/-}$ group of mice have more M2 macrophages. Similar observations were also reported in tumour bearing mice. In addition, the level of C5a in serum was slightly higher in $LDLR^{-/-}P^{KO}$ mice than $LDLR^{+/+}P^{KO}$. These findings also raise the possibility whether $LDLR^{-/-}P^{WT}$/$LDLR^{-/-}P^{KO}$ group of tumour bearing mice had more tumour size and weight that their PWT/PKO counterparts. Analysis of tumour weight and tumour size in tumour bearing LDLR-/-P^{WT} and $LDLR^{-/-}P^{KO}$ mice found no significant difference between genotypes. This finding was the results of three independent experiments after 14 days of B16F10 injection. The reason for choosing 14 days time point has been previously outlined (see Chapter 4). Although no difference was found at 14 days timepoint we cannot rule out the possibility of finding a difference in tumour size/weight if the mice would have been left for longer.

FACS analysis of tumour microenvironment in $LDLR^{-/-}P^{WT}$ and $LDLR^{-/-}P^{KO}$ was carried out via implanting tumours in both wildtype and properdin deficient mice, in order to understand the role that properdin plays in shaping tumour microenvironment. The following markers were investigated $\%CD45^{+}$, $\%\ CD4^{+}$, $CD8^{+}$, %Tregs, %IL-10 and %TGF-B cells as key descriptors of tumour development and immune cell infiltration. The results showed no clear difference between genotypes at this time point. Investigations into the percentage of MDSCs in BM, spleen and tumour tissue revealed higher percentage in spleen of tumour bearing mice when compared to naïve mice. Nevertheless, no significant difference was found between genotypes. In BM, no difference was found in percentage of MDSCs between genotypes. Estimation of subpopulations of MDSCs showed no difference in either Mo-MDSCs or PM-MDSCs (data not shown). Although the percentage of MDSCs in tumour tissue was higher in $LDLR^{-/-}P^{WT}$ than $LDLR^{-/-}P^{KO}$, however this did not reach statistical significance. Myeloid-derived suppressor cells (MDSCs) are a heterogeneous population of cells which suppress the immune response during cancer and several other diseases. MDSCs supress T-cells by increasing the expression of immune suppressive factors. Furthermore, MDSCs can enhance de novo development of FOXP3 , resulting in increased levels of regulatory T cells (Tregs) which efficiently

suppress effector T cells. Several studies have reported the expression of FOXP3 in a number of solid human tumours including melanoma. Miranda-Hernández and co-workers have studied the expression of FOXP3 in B16F10 melanoma cells *in vitro* and detected expression of this marker on B16F10 cells in culture and in the intratumoral B16F10 cells (Miranda-Hernandez et al., 2013). However, analysis of FOXP3 expression in our B16F10 cells *in vitro* by qPCR and FACs did not detect expression of this marker in our clone of B16F10 (see data in appendix). In addition, no significant difference was seen in expression of FOXP3 in tumour tissue between genotypes. Similarly, no difference was found in level of T-regs in spleen between genotypes. Nevertheless, in both genotypes, spleen of tumour bearing mice had significantly higher levels of T-regs when compared to naïve mice. This difference between naïve and tumour bearing mice probably reflects the difference also reported in the level of MDSC in spleen, as MDSCs can modulate the *de novo* development and induction of Treg cells (Lindau et al., 2013). The percentage of NK cells as recognised by $NKP46^{+}CD3^{+}CD45^{+}$ markers was significantly lower in spleens of tumour bearing mice when compared to naïve mice from both genotypes. This result was expected as previous reports have indicated that NK cells from spleen were significantly impaired in tumour-bearing mice. Additionally, it was shown that down-regulation of NK cell function is inversely correlated with the marked increase of MDSC in liver and spleen (Li et al., 2009).

Complement activation is a cornerstone of innate immunity and may ultimately contribute in shaping the cellular immune response. $LDLR^{-/-}P^{WT}$ tumour bearing mice had a significantly higher level of C3 in serum when compared to $LDLR^{-/-}P^{KO}$. Surprisingly, similar serum levels of C3 were found in naïve and tumour bearing mice from both genotypes. Western blot results for iC3b and C3dg in tumour lysates showed more abundance of both fragments in $LDLR^{-/-}P^{WT}$. Although levels of C5a and C5b-9 were higher in serum of tumour bearing mice as compared to naïve mice no significant difference was found between genotypes. Interestingly, ELISA for lectin pathway performed by another PhD student in our lab showed that $LDLR^{-/-}P^{KO}$ had significant reduction of this pathway. However, a significant numerical difference may not be of biological significance in immune response. The aforementioned data suggest that there more complement activation in $LDLR^{-/-}P^{WT}$, which contrasts the finding of more

M2 macrophages in LDLR-/-P^{KO} reported in the beginning of this chapter. $LDLR^{-/-}$ mouse model combined with complement-deficient mouse lines has been previously used to give a broader understanding of the role that complement plays in disease such as atheromatous lesions. A model of murine atherosclerosis using $LDLR^{-/-}$ Properdin knockout ($LDLR^{-/-}P^{KO}$) and $LDLR^{-/-}P^{WT}$ mice found that properdin plays a beneficial role in the development and progression of early atherosclerotic lesions. Interestingly, Complement C3 levels were increased in $LDLR^{-/-}P^{KO}$ mice regardless of diet type or gender (Steiner et al., 2014).

In conclusion, the data did not show a significant impact of properdin on tumour growth in $LDLR^{-/-}$mice.

Chapter 6 Supportive analysis of Patients with Pancreatic Cancer Undergoing Treatment with Gemcitabine and omega-3 Fatty Acids

6.1 Introduction

Pancreatic cancer is the fourth most common cancer with an incidence of 8 per 100,000 (Raimondi et al., 2009). Pancreatic cancer has the worst prognosis of all solid organ tumours, with a median survival of 12 weeks and a 5-year survival of 2-3% (Macmillan Cancer, December2014). The poor prognosis for pancreatic cancer is mainly due to late diagnosis of the disease, with the majority of patients presenting with locally advanced or distant metastases. Only 10% of patients with pancreatic cancers are suitable for curative surgical resection (Arshad et al., 2011).

Omega-3 (n-3) fatty acids are a group of fatty acids with the first double bond three carbons from the methyl end. The human body is unable to desaturate the n-3, hence are essential fatty acids (EFA); they must be consumed with the diet (Arshad et al., 2011). These polyunsaturated fatty acids are found in cold water fish mainly as eicosapentaenoic acid (EPA) or docosahexaenoic acid (DHA). Extensive research has unveiled its role in augmenting cancer therapy and anti-inflammatory properties. Specific to pancreatic cancer, numerous *in-vivo* and *in-vitro* studies show a reduction in pro-inflammatory eicosanoids such as prostaglandin E2 (PGE2) via inhibition of the COX pathway and Interleukin-6 (Hardman, 2002, Larsson et al., 2004, Runau et al., 2015).

Fish Oils in Pancreatic Cancers: Preclinical Studies

EPA and DHA acids found in cold water fish were shown to have the ability to inhibit the growth of human pancreatic adenocarcinoma cell lines in a dose dependant manner (Falconer et al., 1994, Ravichandran et al., 2000). Apoptosis was induced in these cells in a dose-dependent manner (Lai et al., 1996, Merendino et al., 2003, Zhang et al., 2007), as well as inhibition of proliferation in gemcitabine-resistant cell lines irrespective of the level of gemcitabine resistance (Hering et al., 2007). It has been predicted that the therapeutic effect include induction of apoptosis in cancer cell lines via alteration at the cell-cycle level, intracellular glutathione depletion (Dekoj et al., 2007), and inhibition of NF-κB (Hardman, 2002). Angiogenesis is the growth of new blood vessels, which must occur for cancers to grow. ω-3 fatty acids induce their effect via suppression of vascular (Yang et al., 1998, Tsuji et al., 2003) endothelial growth factor–stimulated cell proliferation, migration, and tube formation during angiogenesis.

They have also been shown to induce the reduction of the levels of platelet-derived growth factors from vascular endothelial cells. Inhibition of vascular smooth muscle proliferation (Fox and DiCorleto, 1988, Terano et al., 1996) have also been reported as a result of ω-3 fatty acids. Furthermore, ω-3 fatty acids been shown to reduce the production of proinflammatory eicosanoids, such as prostaglandin E2, which promotes cell proliferation and tumour angiogenesis via inhibition of the COX pathway. The COX pathway is also partly regulated by NF-κB, which is inhibited by ω-3 fatty acids. Another factor of interest is the effect of ω-3 fatty acids on peroxisome proliferator-activated receptors (PPARs). These are ligand-activated transcription factors that are implicated in the regulation of lipid metabolism and homeostasis, but they have also been found to be involved in cell proliferation, differentiation, and inflammatory responses. PPARγ has been shown to be upregulated by EPA and PPARδ by DHA: this has both antiproliferative and proapoptotic effects, as shown in *in vitro* and *in vivo* studies (Larsson et al., 2004).

Complement is a hierarchically arranged system of zymogens which is activated as part of the innate inflammatory response on the surface of pathogens (via pattern recognition molecules MBL, mannan binding lectin, or Ficolins), histones, DNA, annexins and immune complexes (via the multimeric classical pathway recognition molecule C1q). Apart from its pro-inflammatory and clearance function, complement activation also has a role in triglyceride synthesis. Ongoing complement activation is strengthened in the presence of properdin, the only positive regulator of the system and controlled by soluble and membrane bound down-regulators. An inflammatory increase in complement activation exerts a modulatory role for adaptive immunity (via opsonisation using C3b and B cell activation using C3dg) and, via split products such as C5a, is involved in shaping cell phenotypes (Barber et al., 2001).

Previous work has shown that properdin significantly contributes to the expression of a pro-inflammatory, M1-type, macrophage phenotype(Dupont et al., 2014). The production site for complement components is primarily the liver but also leukocytes and endothelial cells. Complement has recently been identified as a potentially targetable modulator of tumour growth, though approaches vary in treating parenchymatous tumours vs leukaemias (Rutkowski et al., 2010, Dupont et al., 2014, Stover, 2010, Kolev et al., 2014, Pio et al., 2013).

Properdin stabilised complement activity has been measured in patients with cancers but since the avenue of commercially available properdin ELISA kits, levels have not been studied and related to prognosis (Lokhatiuk et al., 1974).

It has previously been shown that restoration of the Mannose Binding Lectin complement activity is associated with improved outcome in patients with advanced unresectable pancreatic adenocarcinoma treated with gemcitabine and intravenous n-3 fatty acids (Arshad et al., 2014). The aim of this chapter was to investigate properdin levels as a viable marker of prognosis and efficacy of treatment correlating this to clinical outcomes in a similar cohort of patients.

6.2 Results

There were 29 patients in the gemcitabine and n-3 fatty acid group (labelled G## in appendix) and 5 patients in the gemcitabine only group (Labelled C## in appendix). Serial properdin levels as well as the demographics of the two groups are listed in the appendix. Mean age is 66.0 years old and the male:female ratio is 23:11. In the healthy control group, there were 30 volunteers representing a normal Dutch ethnic group (16 male:14 female) and mean age 55.3 years old.

To be able to objectively measure disease response, only patients who survived to 8 weeks of treatment to have a CT scan according to the RECIST criteria were selected for subsequent analysis (Patients C01, 02, 03, 06 were removed). As death is the end point for overall survival, two patients (G44 and C04) were subsequently removed from survival analysis on Kaplan-Meier tests. Details describing the patient cohort is shown in the appendix.

Test for normality was performed on the data set for properdin levels: on the D'Agostino and Pearson omnibus normality test, p value >0.05, suggesting a normal distribution, hence parametric tests were used for analysis.

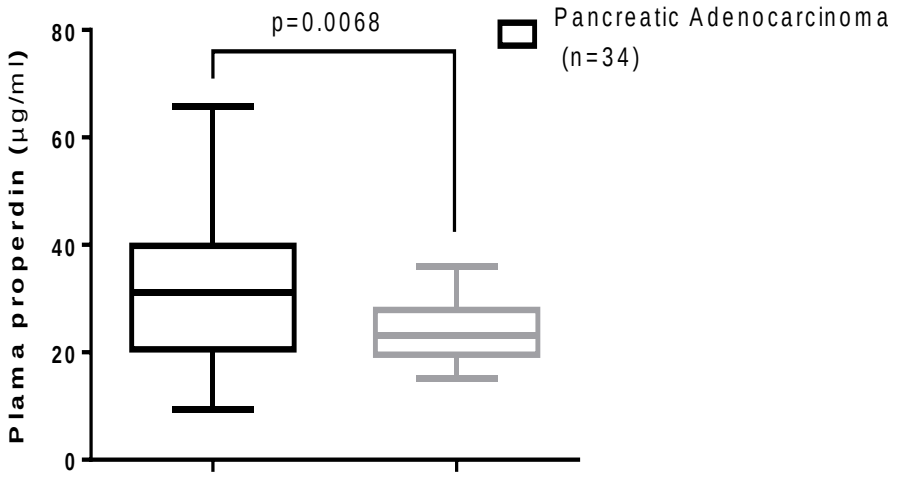

Figure 87: Properdin levels of pancreatic adenocarcinoma patients and healthy Dutch Controls at week 0 (Baseline)

At baseline (Week 0, prior to any intervention), patients with unresectable pancreatic adenocarcinoma had a significantly higher value of properdin compared to healthy volunteers as shown in Figure 87.

Comparing the group receiving intravenous n-3 fatty acid and without, there was no significant difference in properdin levels in serial measurements on Pearson correlation tests (as shown in Figure 88). Subsequent analysis of serial properdin levels comparing sex, tumour load, neutrophil count, CA19-9 and albumin levels also yielded no statistical significant differences or correlations (see appendix).

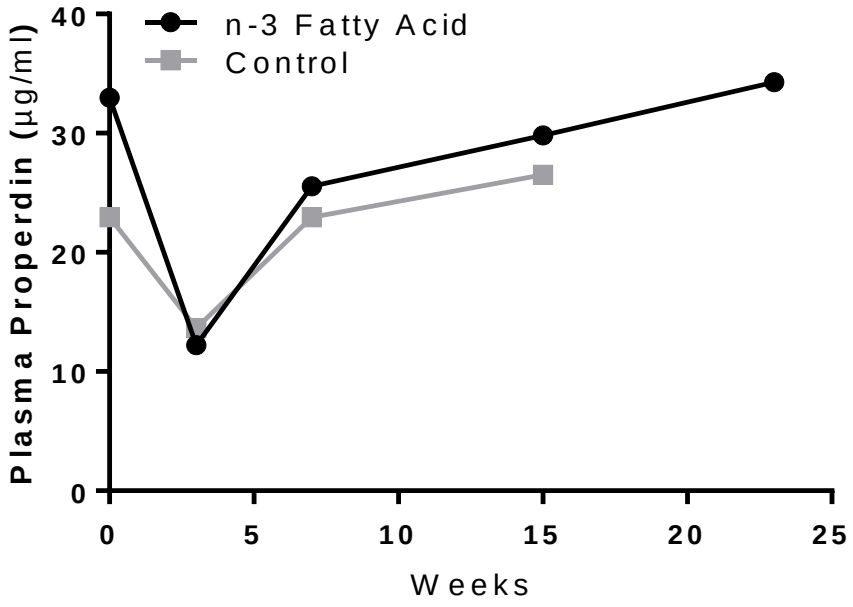

Figure 88: Serial measurement of properdin levels between n-3 Fatty Acid vs Control Arm (Pancreatic Adenocarcinoma & Gemcitabine only). No significant difference statistically, though only 5 patient in the control arm of which only 1 (C04) treated to 16 weeks.

Serial properdin levels were investigated in comparing the groups according to response to treatment (Partial Response (PR), Stable disease (SD) and Progressive Disease (PD) with complete follow up (i.e. once an outcome of death has been achieved). There was a visible and significant difference (p=0.038) in baseline properdin levels between the worst Progressive Disease group and the Partial Response and Stable Disease group (as shown in Figure 89). However, on Pearson's correlation, there was no significant difference between the groups on serial measurement over time.

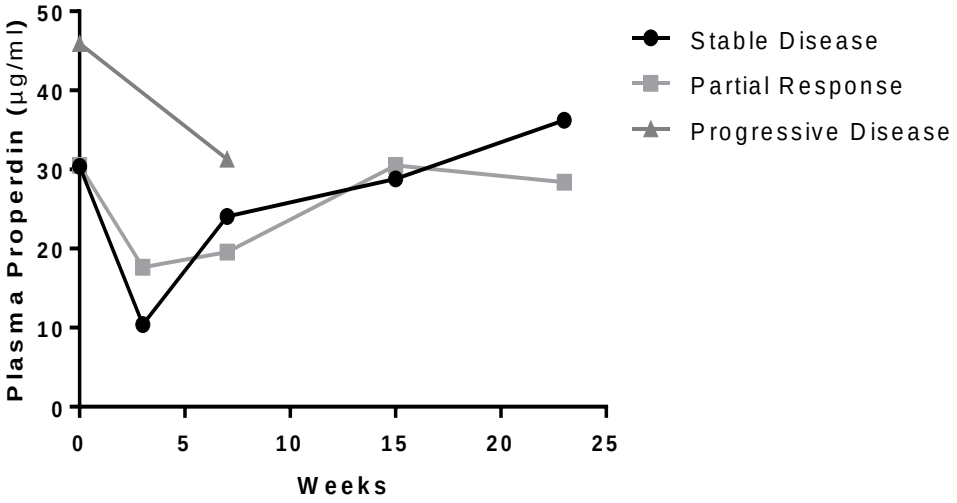

Figure 89: Serial Properdin Measurement in Partial Response (PD), Stable Disease (SD) and Progressive Disease (PR).

Based on the difference in the baseline measurement, the arithmetic midpoint properdin value between Progressive Disease versus Partial Response + Stable Disease was calculated to be 38.17 µg/ml. This also correlated to a standard error of the mean (SEM) value of 2.8 times less than the mean of the Progressive Disease group. (Mean = 45.93, SEM 2.68). This was used as the mean cut off to illustrate two groups with baseline Low (<38.17 µg/ml) and High (>38.17 µg/ml) properdin levels.

On subsequent Kaplan-Meier analysis using the Gehan-Breslow-Wilcoxon Test, there was a significant difference in both Overall Survival (OS) and Progression Free Survival (PFS) between the mean cut off Low and High properdin groups. On overall survival, the median survival in the Low properdin group is 7.60

months versus 4.90 months for the High properdin group (p=0.0003). For Progression, Free Survival, the median time to progression was 5.50 months in the Low properdin group compared to 2.60 months in the High properdin group (p=0.0007). These are illustrated in Figure 90 and Figure 91.

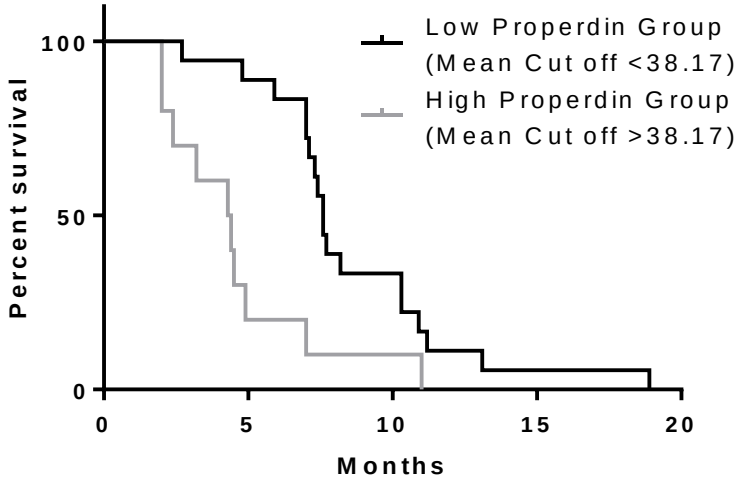

Figure 90: Kaplan-Meier Curve - Overall Survival: High and Low Properdin Group.

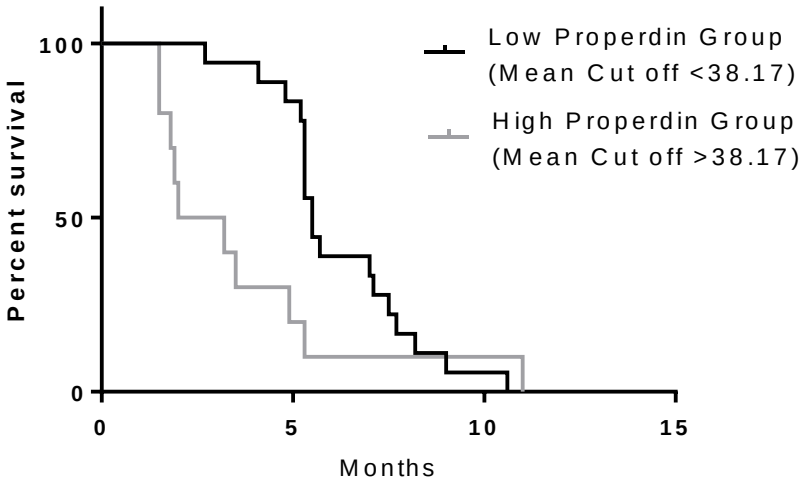

Figure 91: Kaplan-Meier Curve - Progression Free Survival: High and Low Properdin Group.

6.2.1 Level of properdin in healthy individuals

The level of properdin in healthy groups was measured in Iraqi individuals resident in Leicester (n=7) and compared to levels obtained for Dutch individuals (n=30), and the results showed a high level of properdin in the Iraqi group. This may possibly be linked to genetic factors. The context of variation in complement component levels due ethnic differences have been reported by others. Previous studies have shown that some genetic components may influence the levels of serum complement C3 and C4 in healthy subjects (Yang et al., 2012). Similar observations were also noted by others who reported that serum C3 and C5b-9 components were elevated in healthy South Asian subjects compared with their healthy Caucasian counterparts. These studies contribute to the understanding of genetic components that affect individual level of complement variation (Somani et al., 2012, Somani et al., 2006, Siezenga et al., 2009).

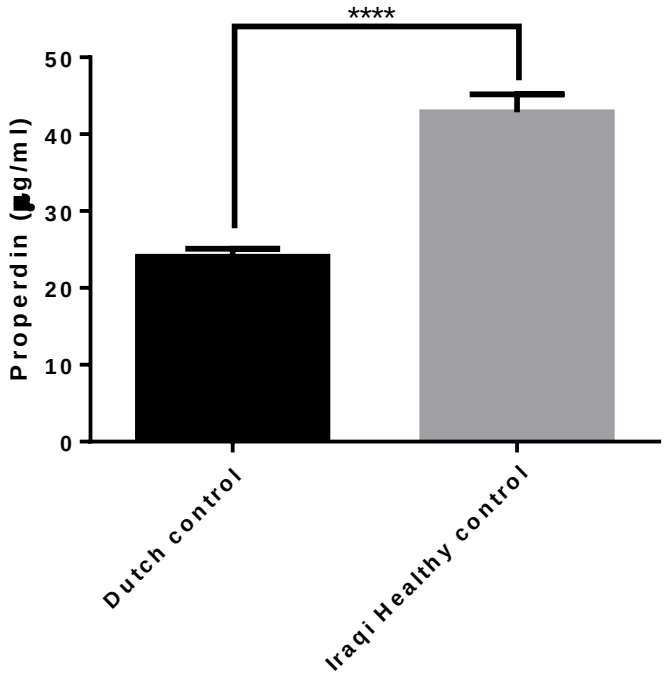

Figure 92: Level of properdin in Iraqi healthy group and Dutch group.
Serum properdin levels were measured by ELISA. The data are presented as means ±SEM. Statistical analysis was performed by one-tailed Mann-Whitney U test. * ($p < 0.05$).

6.2.2 Level of ITG/CD11b in Pancreatic Adenocarcinoma patients

A previous MSc student working on analysing the link between survival of cancer patients and complement component genes found a link between ITG/CD11b and malignant melanoma (I. Alhabib, 2015 University of Leicester, MSc Bioinformatics). This gene encodes the integrin alpha M chain. Integrins are heterodimeric integral membrane proteins composed of an alpha chain and a beta chain. The I-domain containing alpha integrin combines with the beta 2 chain (ITGB2) to form a leukocyte-specific integrin referred to as macrophage receptor 1 (Mac-1), or inactivated-C3b (iC3b) receptor 3 (CR3). The alpha M beta 2 integrin is important in the adherence of neutrophils and monocytes to stimulated endothelium and in the phagocytosis of complement coated particles. Multiple transcript variants encoding different isoforms have been found for this gene. The aim of the present experiment was to investigate the level of this protein in advanced Pancreatic Adenocarcinoma patients and healthy subjects. The results represented by figure 92 showed significantly higher levels of this protein in serum of advanced Pancreatic Adenocarcinoma patients receiving gemcitabine chemotherapy than healthy controls. Furthermore, pancreatic carcinoma patients receiving fish oil in addition to gemcitabine chemotherapy had significantly lower levels of ITG/CD11b when compared with pancreatic carcinoma patients receiving gemcitabine chemotherapy only. To determine whether this is an effect specific for cancer, samples from a sepsis trial (Stover et al., 2015) were tested as well and found to follow the same pattern: elevation in sepsis (“NIS” on admission, day 1), lower levels on recovery and lowest levels in matched controls (“VNIS”). The result showed ITG/CD11b is not a specific marker for only cancer but also for acute inflammation. Increased levels of ITG/CD11b in both advanced Pancreatic Adenocarcinoma patients and sepsis patients implies that this protein is not specific for cancer.

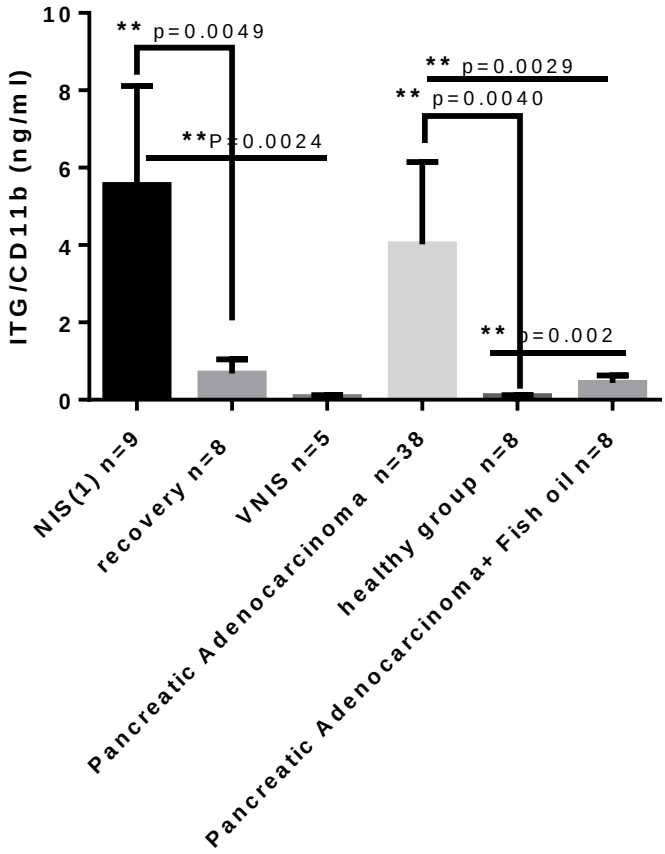

Figure 93: ITG/CD11b levels in patients with advanced Pancreatic Adenocarcinoma patient, septicaemia patients and healthy control group

levels of ITG/CD11b were measured in serum of patients with advanced Pancreatic Adenocarcinoma treated with Gemcitabine only, advanced pancreatic adenocarcinoma treated with weekly fatty acids intravenous infusion plus gemcitabine chemotherapy, septicaemia patients and healthy control group. The data are presented as means ±SEM. Statistical analysis was performed by Student t-test. * ($p < 0.05$).

6.2.3 Discussion

To the best of my knowledge, this is the first study aimed at describing the relationship of a raised properdin level with clinical outcome in pancreatic adenocarcinoma. The results presented in this chapter have linked higher properdin levels with poorer outcome in terms of progression free survival and overall survival in patients with pancreatic adenocarcinoma.

It is well established that there is a link between cancers and inflammation, as first proposed by Rudolf Virchow (Grivennikov et al., 2010). Various studies have found activation of the complement system in solid tumours and raised complement activity in the sera of patients with neoplastic disease. Properdin up-regulates the alternative pathway of the innate immune response by stabilising

the C3bBb complex which ultimately activates the central C3 component which leads to activation of the complement system (Kouser et al., 2013). A link between properdin and malignant tumours was first expressed in 1958, though the method of measuring properdin has developed since then (Rottino et al., 1958). More recently, an association of raised expression of properdin levels in mice lung tumour models have been identified using proteomic methods (Chatterji and Borlak, 2009). This is in keeping with these findings that patients with pancreatic adenocarcinoma have a raised baseline properdin level compared to a healthy control population. It would be reasonable to postulate that the presence of pancreatic adenocarcinoma leads to an anti-inflammatory response which leads to an increase in the alternative pathway and raised plasma properdin levels. An alternate hypothesis is the direct stimulation by pancreatic adenocarcinoma cell lines on the alternative pathway may lead to increased properdin levels.

Properdin is a soluble glycoprotein found in plasma. It is mainly synthesised in the liver though another primary extrahepatic source of properdin are from neutrophils (Kouser et al., 2013). The results of this chapter shows no significant correlation between properdin levels and serum levels of albumin (a marker of liver biosynthesis) and neutrophils taken at the same time point in pancreatic adenocarcinoma patients who receive both gemcitabine and intravenous n-3 fatty acids (see the appendix). This suggests that properdin may be an independent marker for pancreatic adenocarcinoma.

Tumour load is derived by the totalling up of measurable disease on CT scan based on the RECIST 1.1 criteria. (Adding up the size of the primary pancreatic adenocarcinoma tumour and any additional metastatic disease, i.e. liver, lung or lymph node metastases.) No significant correlation between serial measurements of properdin and overall tumour load were found. Previous studies have already proven that larger pancreatic tumour size is associated with lower survival and poorer prognosis (Agarwal et al., 2008). However, in the present cohort, all the patients have stage IV unresectable pancreatic adenocarcinoma receiving palliative gemcitabine chemotherapy with or without intravenous n-3 fatty acid. This negates the hypothesis that the size of the tumour affects prognosis, as all the patients in this cohort have terminal disease. However, it may be worth correlating properdin levels with pancreatic adenocarcinoma

tumour size in different disease stage as a future study to identify any potential correlation between the two.

Based on the best outcome following at least one RECIST measurement (completed 8 weeks of treatment), a difference was seen at baseline properdin measurements between the worse performing group (Progressive Disease) and better performing groups (Partial Response and Stable Disease). It was decided to combine the Partial Response and Stable Disease group together, as eventually all the patients will succumb and show signs of progressive disease. The severity and poor overall prognosis of the disease also meant the best statistical test for survival was the Gehan-Breslow-Wilcoxon Test , as this placed more emphasis on looking at survival/progression at early time points. Using the midpoint baseline properdin level between Progressive Disease and Partial Response/Stable Disease, patients were subdivided to High and Low properdin groups. On Kaplan—Meier analysis, it was shown that a high properdin level at baseline is associated with shorter overall survival and quicker progression of pancreatic adenocarcinoma. This may reflect the fact that the higher properdin load is a consequence of a heavier disease burden, which leads to the poorer outcome and survival. The fact that no correlation of properdin with tumour size (albeit all the patients have stage IV unresectable pancreatic adenocarcinoma which may negate the effect of the tumour load) were shown or that properdin shows any association with albumin and neutrophil count suggest that properdin may be useful as a new independent marker of diagnosis and surrogate marker of disease severity.

One limitation of the study is that the cohort of healthy controls was from a previous study of healthy Dutch volunteers. The patient cohort was not matched in terms of age or ethnicity to the pancreatic adenocarcinoma group of patients, but were not known to have any serious underlying malignancy. The measurement of properdin was consequently done in a different lab, but the same ELISA kit was used and similarly plasma properdin was measured, which would have been comparable to this study.

In conclusion, the results of this chapter suggests that Properdin may be used as a novel independent marker in this cohort of advanced unresectable pancreatic adenocarcinoma compared to a normal healthy population. Furthermore, higher properdin levels may possibly be associated with poorer outcome and survival in

this debilitating condition, hence properdin may potentially be applicable as a surrogate marker of severity as well as efficacy to treatment, in this cohort receiving palliative gemcitabine and intravenous n-3 fatty acid. This warrants further clinical trials looking specifically at properdin as a potential marker of diagnosis as well as a marker for prognosis. Measurement of properdin in two healthy control groups has shown higher levels of this complement protein in the Iraqi healthy group was higher which suggest that genetic factors arising from ethnic difference is the propable cause. Increased levels of ITG/CD11b in advanced Pancreatic Adenocarcinoma patients as well as sepsis patients implies that this protein is not specific for cancer.

Chapter 7 Final Conclusions and Future work

7.1 Conclusion

Cancer remains a leading cause of death worldwide, claiming the lives of more than 8 million people each year. In 2012, malignant melanoma of skin increased to 1.5% of cancer cases in adults (Ferlay et al., 2012). Skin melanomas are tumours arising from skin melanocytes present in hair follicles, interfollicular epidermal and dermal layers. Malignant melanoma can be highly aggressive when they metastasise to distant organs (Kuzu et al., 2015). *In vivo* murine melanoma models have been widely used to broaden scientists understanding of tumour biology, as these models offer the ability to simulate natural tumour progression, from proliferation to invasion and metastasis. Cancer cells exist as diverse entities and the crosstalk between cancer cells and the surrounding microenvironment is a major determinant in the outcome of malignancy. Mice possess a functional immune system enabling murine models such as syngeneic transplantation models to evaluate immunotherapies. In addition, data generated from these models help to gain better understanding of the interaction between the immune system and tumour microenvironment (TME). As such, information gained via these models may possibly lead to the development of novel immune modulators (Kuzu et al., 2015).

Traditionally, researchers have considered the complement system as an integral part of the body's immune surveillance against tumour cells. Nevertheless, a growing body of evidence has accumulated during the past decade to challenge this conventional view and support the association of some complement components with tumour progression. A syngeneic mouse model in which C57BL/6 mice were subcutaneously injected with the cervical cancer cell line TC-1, showed that C3 cleavage products were deposited in the tumour vasculature of the mice, in contrast with little C3 deposition in the benign tissue surrounding the tumour (Nabizadeh et al., 2016). Furthermore, C3 deficient mice had significantly smaller tumours when compared to the wildtype (Nabizadeh et al., 2016). Blockade of C5aR in tumour bearing wildtype mice resulted in retardation of tumour growth in those mice, which supports that C5a promotes tumour growth (Markiewski et al., 2008). Subsequently, Corrales and colleagues used a mouse syngeneic lung cancer model to show that C5a promotes tumour growth. Treatment of mice with C5aR antagonist resulted in less microvessel formation

and decrease in the level of angiogenic factor bFGf (basic fibroblast growth factor), as well as decrease in granulocytic MDSCs. These results provide further evidence that C5a creates a favorable environment for cancer cells growth and progression, which may be linked to the induction of angiogenesis and immunosuppression (Corrales et al., 2012). Another study reported that over activation of the infiltrating cells due to high concentration of C5a may result in suppression of antitumour T cells, while low concentration of C5a can lead to a powerful antitumour immune response (Gunn et al., 2012). Nunez-Cruz and colleagues showed that complement activation plays a critical role in the formation of ovarian tumours. In their study, transgenic mice C57BL/6 TgMISIIR-Tag that can develop spontaneous epithelial ovarian cancer were crossed with two lines of mice with genetic complement deficiencies C3 (B6.129S4-C3tm1Crr/J) (B6.129S4-C3tm1Crr/J) or C5aR (C5ar1tm1Cge/J). The resulting transgenes with deficiency in either C3 or C5aR either developed no ovarian tumours or a small and poorly vascularized tumour which implies that complement activation plays a critical role in the formation of ovarian tumours. The composition of tumour infiltration leucocytes was studied and the results showed no difference in tumour infiltrating leukocytes between the mice that had partial deficiency in C3 and the wildtype except in $CD8^+$ (which was increased in mice with partial C3 deficiency) and $CD4^+$ T cells (which was decreased in mice with partial C3 deficiency). This study concluded that activation of complement plays a major role in oncogene driven carcinogenesis (Nunez-Cruz et al., 2012). All of the aforementioned findings strongly suggest that complement proteins may promote angiogenesis and participate in tumour cell invasion and migration, thereby promoting malignancy. In line with this hypothesis, this thesis used a murine syngeneic melanoma model to study the role of the complement protein properdin in tumour growth and cell recruitment. Both *in vitro* and *in vivo* investigations were carried out using the B16F10 cell line.

7.1.1 Phenotypic Skewing of Macrophages after culturing with B16F10 conditioned medium

Research on inflammation in cancer led to the identification of components of the immune system that can be both beneficial and deleterious for patient prognosis. Among those components are the macrophages, which are a heterogeneous group of cells that can display both tumour suppressing (M1 macrophages) and

tumour promoting functions (M2 macrophages). One of the aims of this thesis was to investigate whether *in vitro* tumour secreted factors could preferentially active macrophage phenotypes. B16F10, a well characterised subline of C57BL/6J melanoma was used as a tumour cell line to generate conditioned medium. Bone marrow derived macrophages from properdin-deficient and wildtype mice were cultured with B16F10 conditioned medium and the phenotype of BMDM compared to unstimulated BM cells was subsequently evaluated. The results showed an increased mRNA expression of IL-1β, IL-10, Arginase and TNF-α in both genotypes after culturing with B16F10 conditioned medium. Unlike wildtype BMDM, PKO cells showed more MCP-1 upon stimulation with B16F10 conditioned medium. Similarly, the percent of $CD206^{+}CD11b$ cells was only increased in PKO cells after culturing with B16F10 conditioned medium. The results presented in this thesis indicate that B16F10 supernatant can activate BM cells and polarise macrophages. Most importantly, culturing with tumour cell conditioned medium in the absence of properdin leads to greater M2 skewing of macrophages. In contrast, more levels of IFN-ɣ and IL-12 were found in WT cells, indicating that WT cells show a more M1 skewed immune response. In conclusion, the results of the *in vitro* studies presented in this thesis reveal a significantly altered phenotype of BMDM from properdin deficient mice in response to tumour cell conditioned medium compared to wildtype mice. Based on these findings it would be reasonable to suggest that complement protein properdin plays a role in modulating the phenotypic skewing of macrophages towards tumour cell conditioned medium. It remains, however, to be elucidated as to the relevance of a macrophage phenotype with strong features of tumour associated macrophage population in the absence of properdin for tumour growth and development, as well as for the shaping of the tumour microenvironment. Further *in vitro* as well as *in vivo* studies are required to define the differences in intracellular signalling of macrophages differentiated from properdin-deficient and wildtype mice that yield a distinct inflammatory response to melanoma cell conditioned medium. Such investigation will provide new insights into the role of properdin in melanoma progression and possibly metastasis.

7.1.2 Complement component properdin and melanoma tumourgenesis in Properdin wildtype and Properdin deficient mice

Decades of research has highlighted the complex interplay between the various components of the immune system and tumour cells. The complement system is a central component of innate immunity, as well as being one of the immune players present in the tumour microenvironment. Data accumulated during the last decade have proposed complement mediated tumour progression. Complement components such as C5a, C1q and C3a have been linked with promoting tumour growth (Markiewski et al., 2008, Bulla et al., 2016, Nabizadeh et al., 2016). Nevertheless, this thesis was the first to investigate the role of properdin, the only known positive regulator of complement activation, in tumour growth and cell recruitment. Measurement of tumour growth by calipers in a syngeneic murine B16F10 melanoma model established in wildtype and PKO deficient mice showed that wildtype mice have a tendency for larger tumour size and weight at 14 days of tumour implantation, however no significant difference was found between the genotypes. Similarly, measurement of tumour burden by BLI showed no significant difference between the two genotypes at either 8 or 12 days of tumour implantation. It is important to note that, due to animal licence restrictions, the experiment had to be ended once tumours reached the predetermined size (up to 1 cm) which was usually 14 days. Thus, it is not known whether leaving the tumours to grow beyond 14 days would have resulted in a significant difference between the genotypes, as the wildtype had a tendency for larger tumours. Recent studies using the B16F10 melanoma mouse model which have presented results stating that some complement components have tumour promoting capabilities have used higher injection dose and let the tumours grow to a size up to 1.5 and 6 cm respectively (Nabizadeh et al., 2016, Bulla et al., 2016). Furthermore, it must be emphasized that B16F10 cultures from different laboratories differ in various aspects such degree of pigmentation, minimal tumourigenic dose and growth rate in mice (Overwijk and Restifo, 2001). Therefore, it was not feasible to compare the results of the aforementioned studies with our results. The results presented in this thesis showed some phenotypic differences in differentiated cells from PKO and wildtype mice in tumour, spleen and bone marrow. Of those changes, wildtype tumour bearing mice had higher MDSCs within tumour and in spleens than their PKO

counterparts. This increase suggests that properdin may contribute to the accumulation of MDSCs in spleen, as well as to the migration of these cells into tumours. Another important difference between wildtype and PKO tumour bearing mice was that the percentage of T-regs in spleen were higher in wildtype mice, another indication of more immunosuppressive phenotypes in wildtype mice. TGF- β is one of the key cytokines linked with T-regs and MDSC production and therefore higher levels of this cytokine in wildtype mice both in spleen and within tumour tissue, was an expected result. Similarly, the level of IL-10 was increased in wildtype tumour bearing mice as compared to their PKO counterparts. Production of the immunosuppressive cytokines TGF-β and IL-10 is one of the pathways by which MDSCs induce immune suppression (Kumar et al., 2016), thus the measurements confirm functionally that wildtype tumour bearing mice undergo relatively more immune suppression than PKO tumour bearing mice. C5a, an influential player in haemostasis and immune cell recruitment, was increased in sera and tumour tissue of PWT tumour bearing mice as compared to PKO. Interestingly, this difference between the two genotypes was not found in naïve mice indicating that it was the result of melanomic tumour. This increase in C5a was also accompanied by increased levels of C5b-9 suggesting that PWT tumour bearing mice have more complement activation. A marked difference between the two genotypes was the finding that CCL2, a chemokine associated with tumour progression, was higher in wildtype tumour bearing mice.

7.1.3 Complement component properdin and melanoma tumourgenesis in LDLR$^{-/-}$ mice

The overall objective of using LDLR$^{-/-}$ mice in our B16F10 melanoma model was to address whether hypercholesterolemia induced an exaggerated inflammatory response to tumour, and whether combined deficiency of properdin and LDR receptor would result in significantly smaller tumours when compared to wildtype. LDLR$^{-/-}$ naïve mice had higher levels of F4/80^{+}CD206^{+} on splenic macrophages. Similar results were also found in LDLR$^{-/-}$ tumour bearing mice, possibly indicating that this group have more M2 macrophages. Increased levels of serum C5a was found in LDLR$^{-/-}$P^{KO} than LDLR$^{+/+}$P^{KO} of tumour bearing mice. Analysis of tumour weight and size did not reveal any significant difference between the two genotypes, although it must be stressed again that this was at 14 days and

we cannot rule out the possibility of finding a difference if tumours were left to grow larger in size.

Analysis of tumour microenvironment by FACS showed no significant difference between the genotypes at 14 days of injection with B16F10. MDSCs in spleen was higher tumour bearing mice when compared to naïve mice. Similarly, higher percentage of T-regs was found in spleens of tumour bearing mice as compared to naïve mice. Both MDSCs and T-regs cells are major players in the immunosuppressive networks and thus both cells are expected to increase during cancer. A marked difference between the genotypes was that $LDLR^{-/-}P^{WT}$ tumour bearing mice had a significantly higher level of C3 in serum when compared to $LDLR^{-/-}P^{KO}$. Furthermore, tumour lysates of $LDLR^{-/-}P^{WT}$ had more abundance of iC3b and C3dg, indicating greater in situ complement activation in $LDLR^{-/-}P^{WT}$.

7.1.4 Major differences among PWT/PKO and $LDLR^{-/-}$ groups of tumour bearing mice

This thesis has employed PWT/PKO group and $LDLR^{-/-}$ groups ($LDLR^{-/-}P^{WT}$ and $LDLR^{-/-}P^{KO}$) of mice in a syngeneic murine B16F10 melanoma model. Tumour burden and tumour microenvironment were studied in both cases, and the results highlighted some similarities and differences between the PWT/PKO group and $LDLR^{-/-}$ of mice. In both these groups, no significant difference in either tumour weight or size was detected between the PWT/PKO group and $LDLR^{-/-}$($LDLR^{-/-}P^{WT}$ and $LDLR^{-/-}P^{KO}$) genotypes. Although not significant, it was noted that PKO mice showed a tendency to have smaller tumour weight and size. However, no such observation was noted in $LDLR^{-/-}P^{KO}$ mice. Analysis of MDSCs, C5a, TGF-β and FOXP3 in tumour tissue of PWT/PKO group of mice revealed that PKO mice had significantly lower levels when compared to PWT. Nevertheless, analysis of the aforementioned parameters showed no difference between $LDLR^{-/-}P^{WT}$ and $LDLR^{-/-}P^{KO}$ tumour bearing mice. Similarly, spleens of PKO tumour bearing mice had lower levels of MDSCs, T-regs, IL-10 and TGF-β when compared to PWT. However, similar levels of splenic MDSCs, T-regs, IL-10 and TGF-β were found in $LDLR^{-/-}P^{WT}$ and $LDLR^{-/-}P^{KO}$ tumour bearing mice. Furthermore, serum levels of C5a and C5b-9 were lower in PKO tumour bearing but not $LDLR^{-/-}P^{KO}$ tumour bearing mice as compared with their wildtype tumour bearing counterparts. From the above findings, it would be reasonable to speculate that the absence of LDL receptor in $LDLR^{-/-}P^{KO}$ resulted in similar levels

of the parameters that have been previously shown to be significantly lower in $LDLR^{+/+}P^{KO}$ tumour bearing mice. One possible reason for this difference that knocking out the LDL receptor may have eliminated any difference previously seen between PWT and PKO mice.

Between optimisation of experiments with different doses of injection as well as carrying out the actual experiment, 150-200 mice were used in this study. It is important to note the challenges encountered during isolation of cells from tumour tissue due to the inherent difficulties associated with obtaining sufficient cell numbers and purity from the primary tumour. Therefore, some flow cytometry markers were investigated in spleen but not in tumour due to the small size of tumour, which ultimately results in insufficient number of cells. The use of the available single cell suspensions from tumour tissue to investigate for MDSCs and T-regs was prioritised in this project due to the importance of these cells. Furthermore, there were technical difficulties with obtaining clear population of MDSCs and T-regs using FACS Caliber machine. After several trials, it was decided to move to using a FACS canto machine, which is more sensitive and accurate. Difficulties also arose from the large scale of work that had to carried out when tissues from these mice were harvested once tumours reached the endpoint (1 cm in one dimension of tumour growth). Time was restricted, as mice had to be dissected, cell prepared from tumour, bone marrow and spleen for staining with different Abs and finally samples run on FACS machine. Experiments were planned to ensure analysis of tumours, spleen as well as bone marrow cells in individual mice rather than conducting experiment targeting one organ, in order to get a more accurate overview of the tumour microenvironment. Besides these limitations, additional technical aspects that had to be carefully considered included that tumour samples had to be processed within a few hours of removal to avoid tissue degradation and antigen alteration. The various manipulation steps from trypsin treatment after differentiation, treatment with brefeldin, PMA and ionomycin for six hours, staining, with washing steps in between, resulted in low number of cells, which was insufficient to perform flow cytometry analysis. Providing individual analyses for the intracellular detection of IL-12 and IL-10 from BMDM was hampered by this limitation and thus pooled samples from three mice of each age, genotype and sex matched to achieve the minimal number of cells required for analysis.

7.1.5 High levels of properdin in pancreatic adenocarcinoma patients

The results presented in this thesis showed increased level of properdin in pancreatic adenocarcinoma patients as compared to healthy controls. Decrease in the level of properdin was observed after treatment with Gemcitabine, a possible result of bone marrow suppression (as neutrophil count was low). Interestingly, the Iraqi healthy control group had higher levels of properdin when compared to the healthy Dutch group. Genetic factors due to ethnic differences is the most probable cause for this difference in healthy groups. It is important to note that serum samples from the Dutch and the Iraqi control groups were not collected at the same time. Furthermore, the healthy Dutch control samples were stored for longer periods than the Iraqi control samples. A number of studies have investigated the effect of storage and freeze–thawing-induced concentration changes on some proteins in human serum/plasma samples with some being susceptible to freeze–thawing-induced protein concentration changes, while others were slightly susceptible.

7.2 Future work

After successful establishment of the syngeneic melanoma model, this work will be carried forward with new Home Office license approval to study the role of obesity in tumour growth, by examining the effects of high-fat diet (HFD) on melanoma progression. HFD-fed C57BL/6 PWT and PKO mice will be subcutaneously injected with syngeneic B16F10 melanoma cells. Because of additional *in vitro* observation of an inhibitory effect of β-estradiol on mitochondrial activity of B16F10 cells (data not shown), a diet free of phytoestrogen will be chosen for the future project. Because PropKO and PropWT mice were on the same soybean meal containing diet for this work, the comparisons made are valid for these genotypes under these conditions.

During the last few years a number of studies have emphasized the importance of studying the relationship between immune signalling and metabolic pathways affecting T-reg function (Galgani et al., 2016). Published data has revealed that local environmental conditions and the availability of certain metabolites are influential elements in the function and metabolism of T-regs. Due to their association with poor prognosis in cancer, studying the link between the

availability of specific metabolites in the microenvironment and the suppressive function of T-regs would be an interesting field to explore.

APPENDIX

Appendix **1**

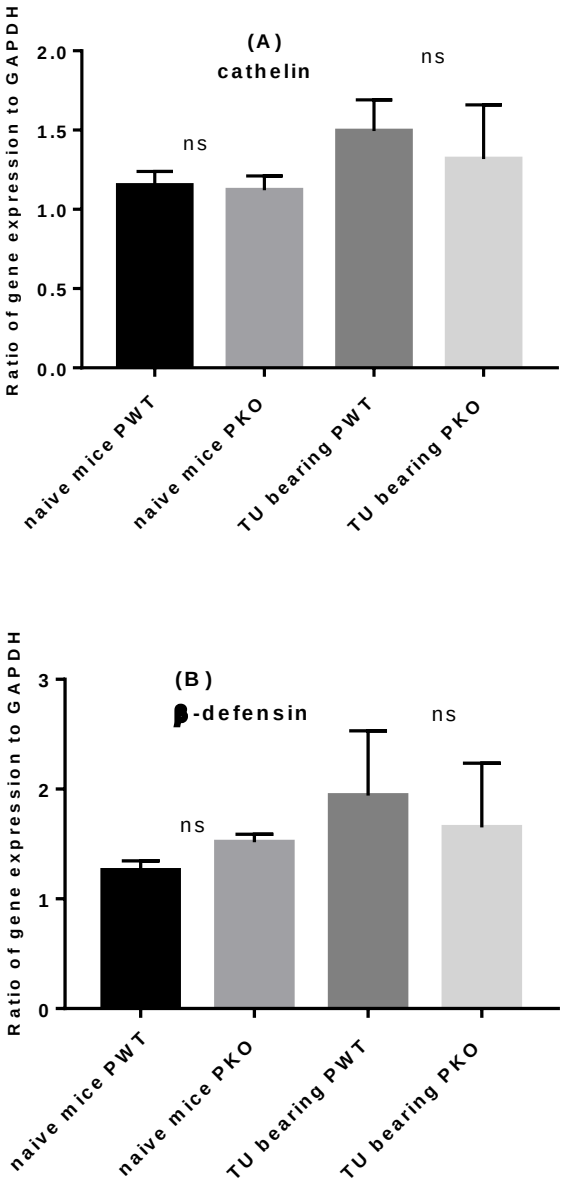

Figure 1-1: Analysis of mRNA expression in spleen of wildtype and properdin-deficient and naive mice. Wildtype (n=3) and properdin-deficient (n=3) mice were injected subcutaneously with 1.6×10^5 cell/100µl of B16F10 cell suspension. After 14 days the mice were sacrificed and dissected for collection of spleens. Total RNA was isolated from spleens and qPCR was conducted for gene expression of A- Cathelin B-β-defensin to GAPDH, mRNA for GAPDH was stable, each set up in duplicate. The data are presented as means ±SEM. Statistical analyses were performed using one-tailed Mann-Whitney U test (significances with brackets). * Significantly different from the control group, $p<0.05$.

Appendix 2

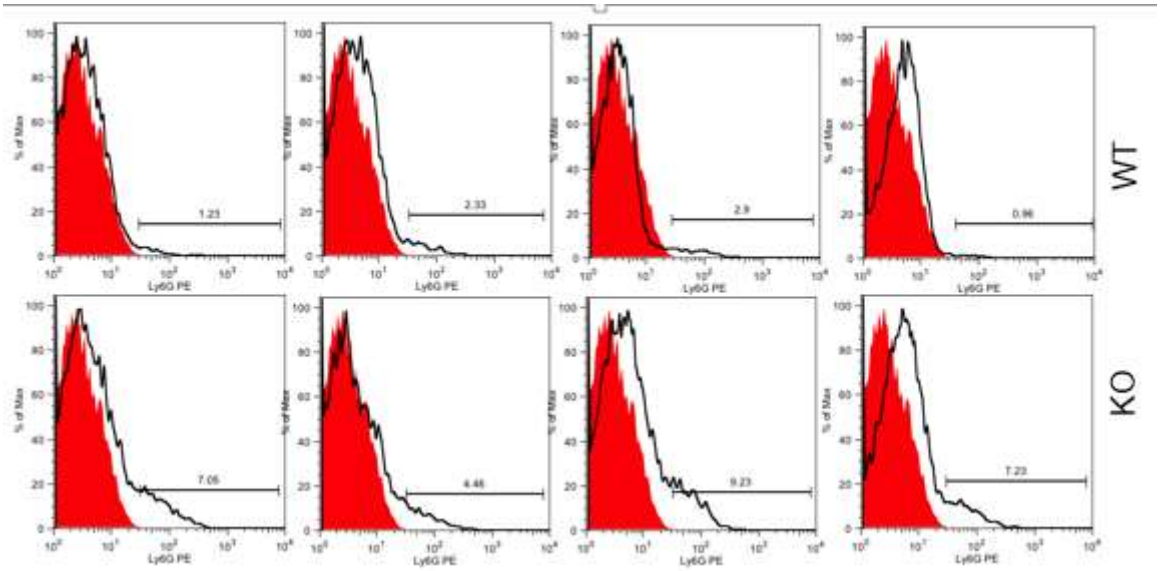

Figure 4-1: Expression of Ly6G in BMDM of and properdin deficient mice after stimulation. Macrophages from wildtype and properdin deficient tumour bearing mice were differentiated *in vitro* with GM-CSF for eight days and then stimulated either with LPS (100ng/ml), IL-4 (20ng/ml) or B16F10 supernatant for 24 hours. Unstimulated cells were used as controls. Samples were stained for the expression of Gr-1 FITC and CD11b PE. The above results represent pooled BMDM sample where n= 4 in wildtype and n=5 in properdin deficient mice.

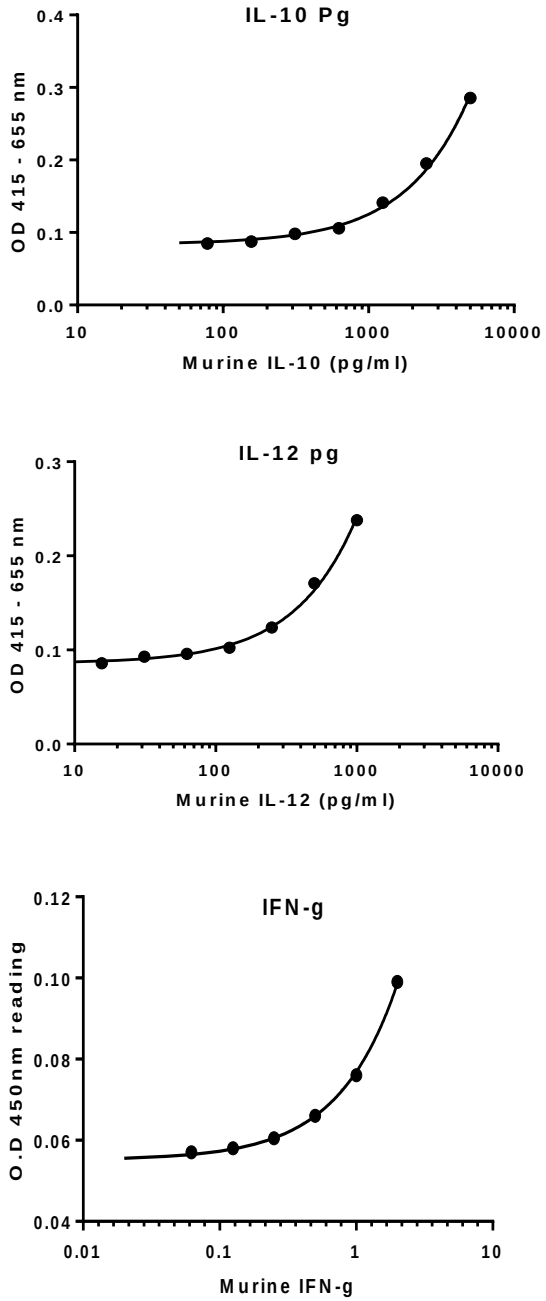

Figure 4-2: Standard curve of mouse ELISA for IL-10, IL-12 and IFN-g.

Appendix 3

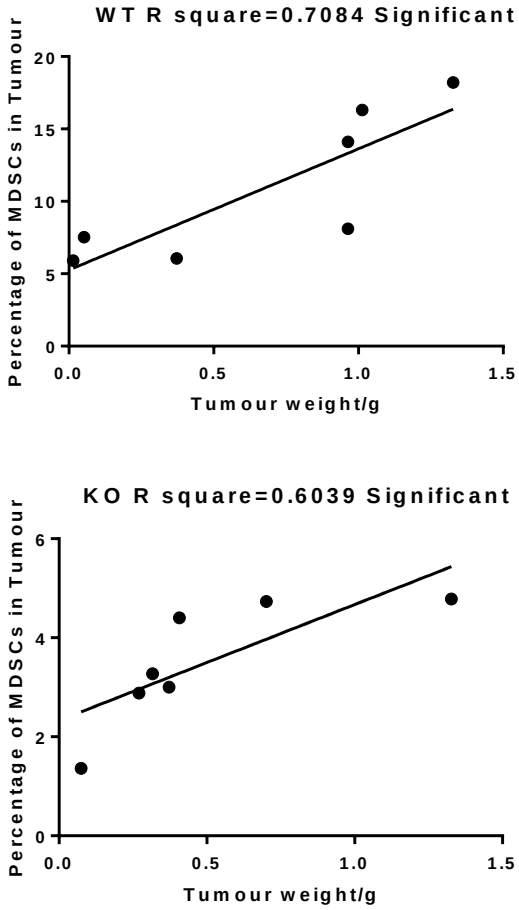

Figure 5-1: Correlation between Tumour weight and percentage of MDSCs. In tumour wildtype and properdin deficient mice, mice were injected subcutaneously with 1.6×10^5 cell/100µl of B16F10 cell suspension. After 14 days the mice were sacrificed and dissected for collection of tumour tissue. Tumour suspension from both genotypes were stained with three markers (CD11b, Gr1 and CD45) to distinguish MDSC.

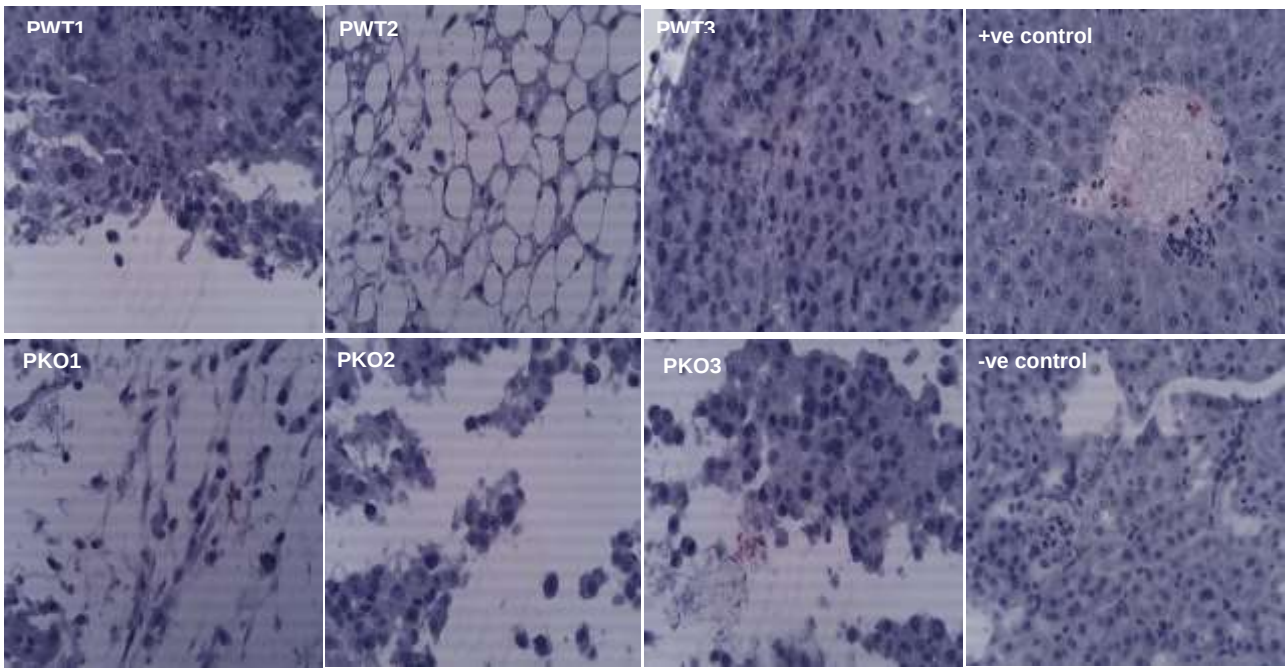

Figure 5-2: Tumour sections from both genotypes were examined by VWF immunohistochemistry staining. Wildtype and Properdin deficient C57BL/6 mice were injected subcutaneously with 4×10^5 cell/100µl of B16F10 cell suspension. Fourteen days after injection, tumour mass was isolated from mice and fixed. Tumour tissue was sectioned and examined by VWF staining, Anti-Von Willebrand Factor (ab6994 Abcam) sheep polyclonal antibody was used and anti-rabbit/mouse IgG, DAKO kit. The control (mouse kidney section) gave positive results, however tumour sections stained with this antibody gave inconsistent results staining. Representative images of PWT and PKO and. All images were taken at 40x magnification.

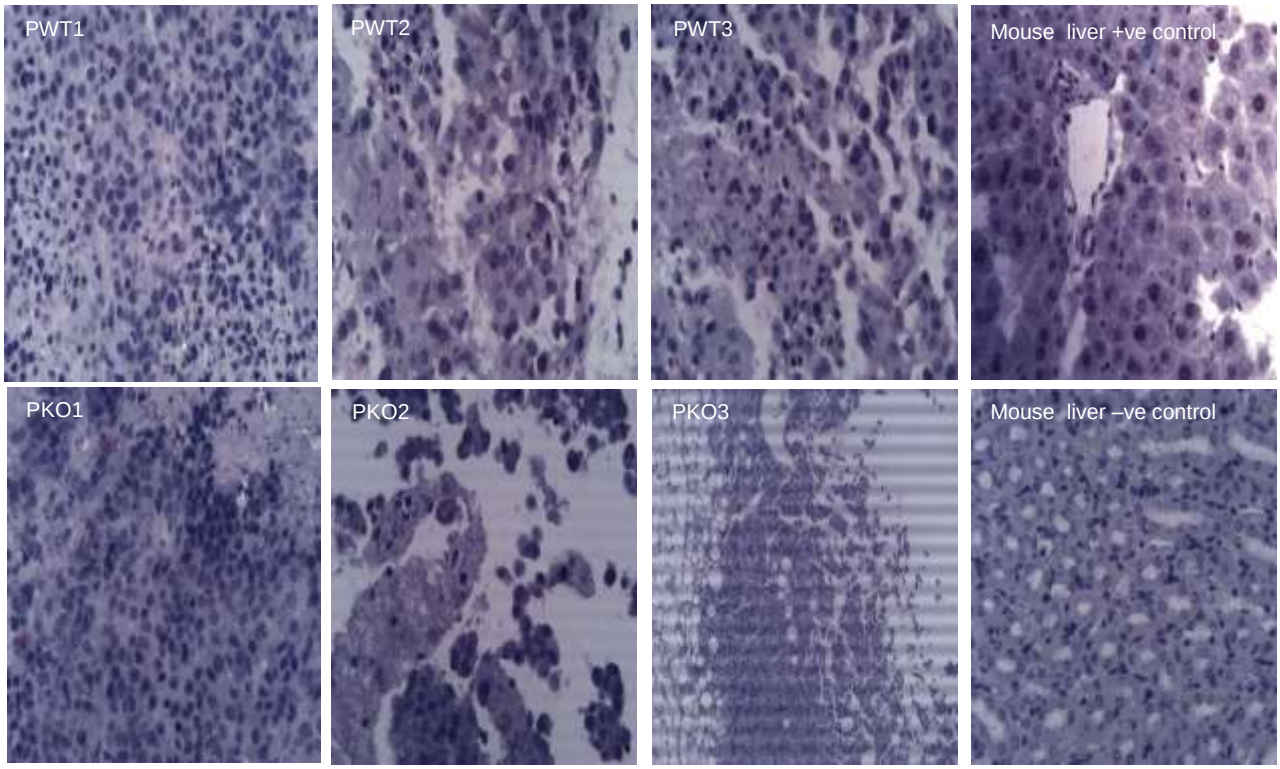

Figure 5-3: Tumour sections from both genotypes were examined by VEGF immunohistochemistry staining. Wildtype and Properdin deficient C57BL/6 mice were injected subcutaneously with 4×10^5 cell/100µl of B16F10 cell suspension. Fourteen days after injection, tumour mass was isolated from mice and fixed. Tumour tissue was sectioned and examined by Rabbit polyclonal antibody to VEGF (orb11554 , biorbyt) and anti-rabbit/mouse IgG, DAKO kit. Representative images of PWT and PKO and. All images were taken at 40x magnification**.**

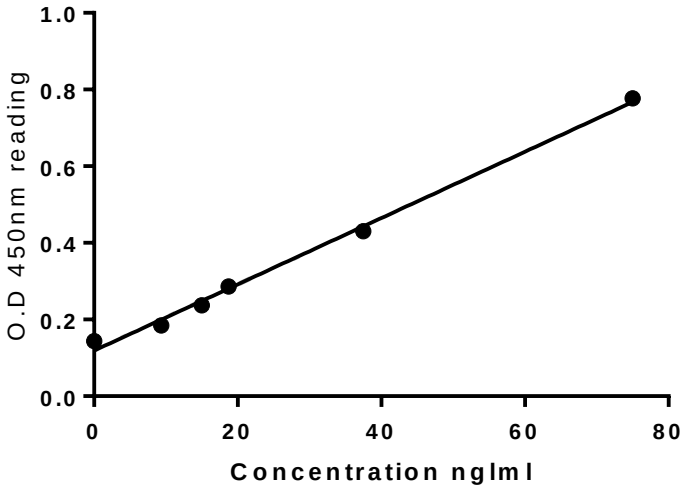

Figure 5-4: Standard curve of mouse ELISA for C5a.

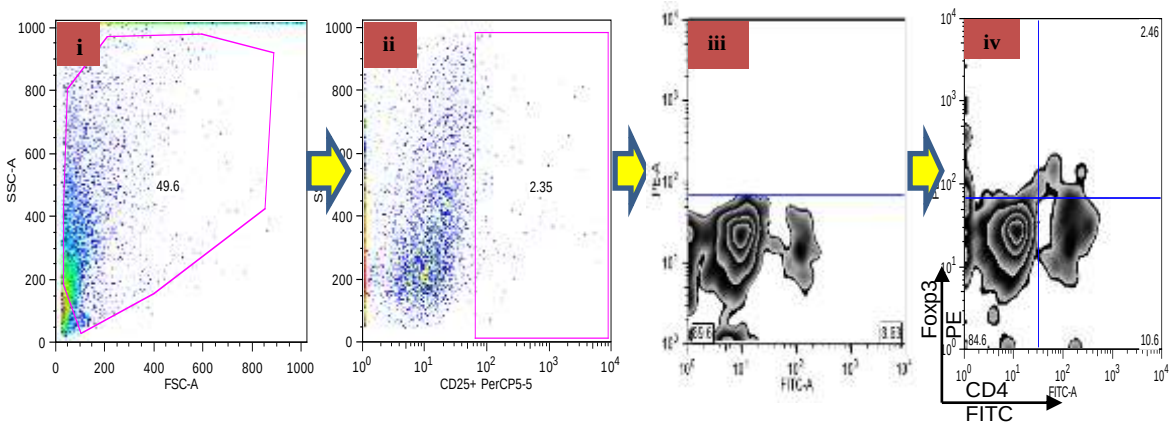

Figure 5-5: Strategy for identifying MDSC populations in tumour of wildtype and properdin deficient tumour bearing and naïve mice. Flow cytometry analysis of Gr-1and CD11b cells after gating on CD25^{+}cells in MDSCs from tumour Numbers in the plots indicate the percent of gated cells. CD25+Gr-1+CD11b+ represent percentage of MDSC. i- the gating on main population of tumour cells, ii- gating on CD25^{+} only iii- gating on CD25^{+}(PerCP5.5) cells, CD4^{+} and Foxp3^{-}(PE) negative control (isotype), iv- gating on CD25^{+}Gr-1^{+}CD11b^{+} cells representing population of MDSCs.

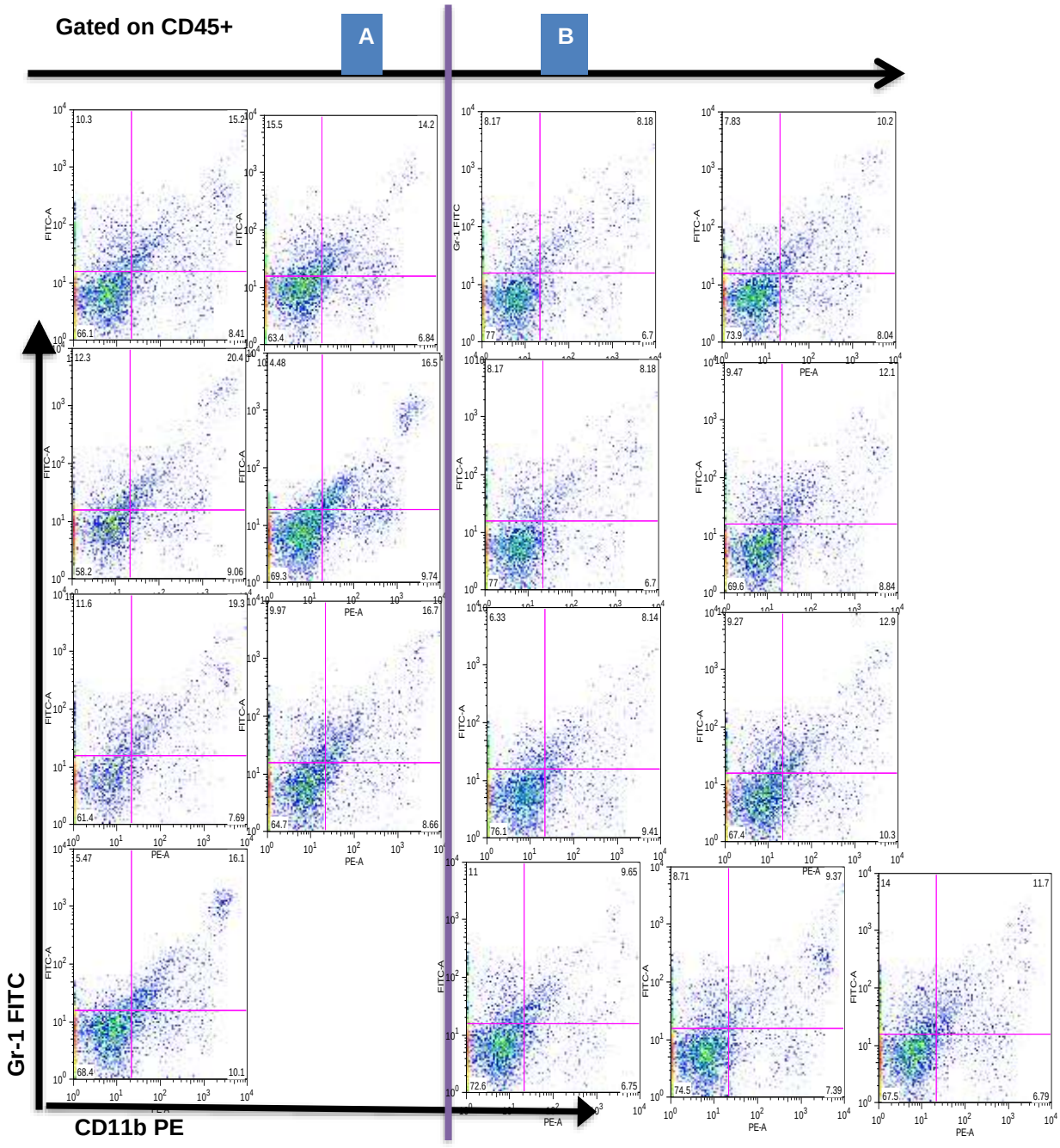

Figure 5-6: MDSC populations in spleen of wildtype and properdin deficient tumour bearing and naïve mice. Flow cytometry analysis of Gr-1and CD11b cells after gating on CD45+cells in MDSCs from spleen. Numbers in the plots indicate the percent of gated cells. $CD45^{+}Gr\text{-}1^{+}CD11b^{+}$ represent percentage of MDSC. Mice were injected subcutaneously with 1.6×105 cell/100µl of B16F10 cell suspension. After 14 days the mice were sacrificed and dissected for collection of spleen. Spleen suspension from both genotypes were stained with three markers (CD11b, Gr1 and CD45) to distinguish MDSC. Then FACS was done and percentage of MDSCs was obtained. The gating was on CD45, and the other two markers were used to calculate of total MDSC in spleen.

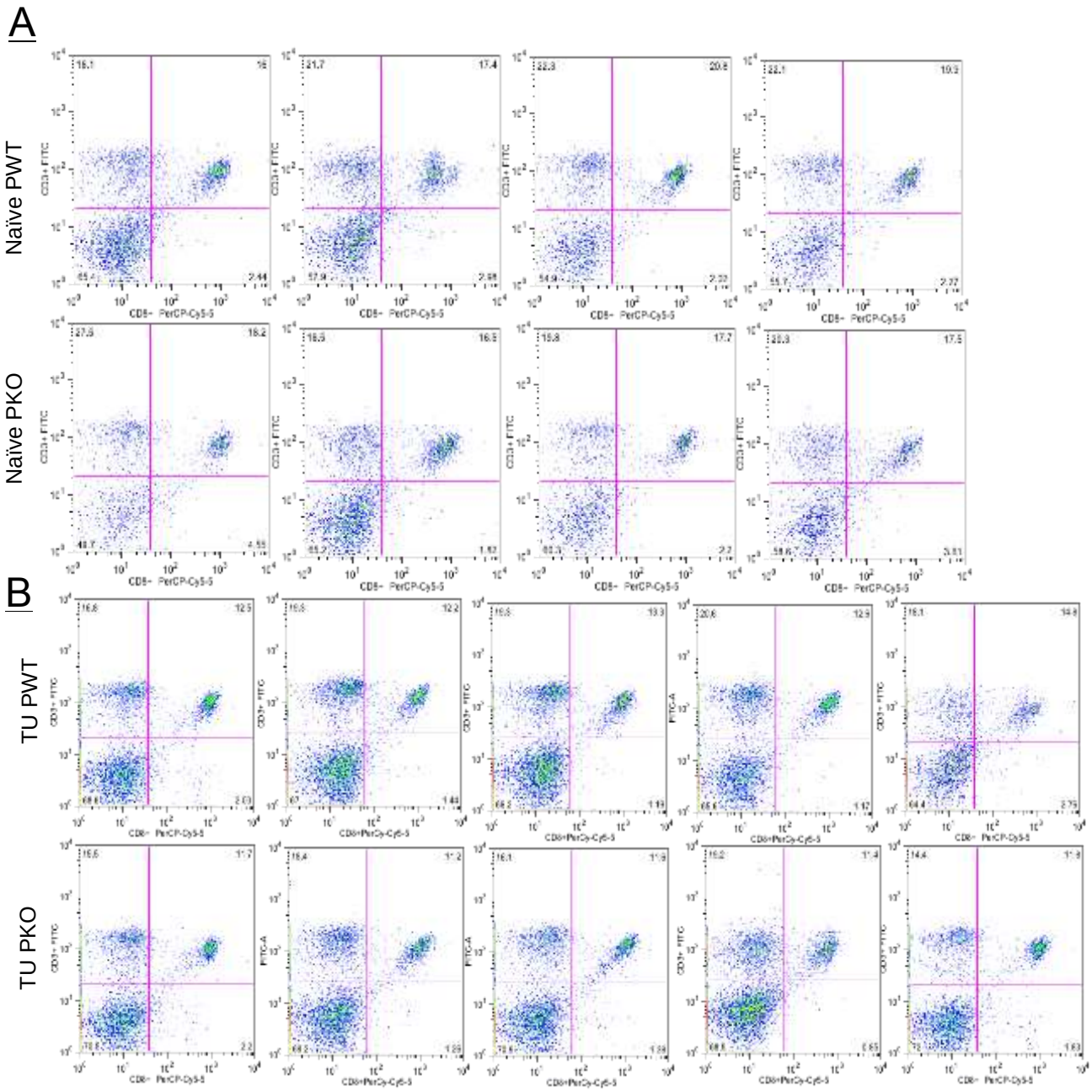

Figure 5-7: T-cytotoxic populations in spleen of wildtype and properdin deficient mice. Flow cytometry analysis of $CD45^+CD3^+CD8^+$ cells after gating on $CD45^+$cells from in spleen from wildtype and properdin deficient mice. Numbers in the plots indicate the percent of gated cells. $CD45^+CD3^+CD8^+$ represent percentage of T-cytotoxic after subcutaneous injection of 1.6 $X10^5$ cells of B16F10. Populations of T-cytotoxic in tumour of wildtype and properdin deficient mice. Mice were injected subcutaneously with 1.6×10^5 cell/100µl of B16F10 cell suspension. After 14 days the mice were sacrificed and dissected for collection of spleen. Spleen suspension from both genotypes were stained with three markers (CD45, CD3 and CD8) to distinguish T-cytotoxic. Then FACS was done and percentage of T-cytotoxic cells was obtained. The gating was on CD45, and the other two markers were used to calculate of total T-cytotoxic cells in spleen**.**

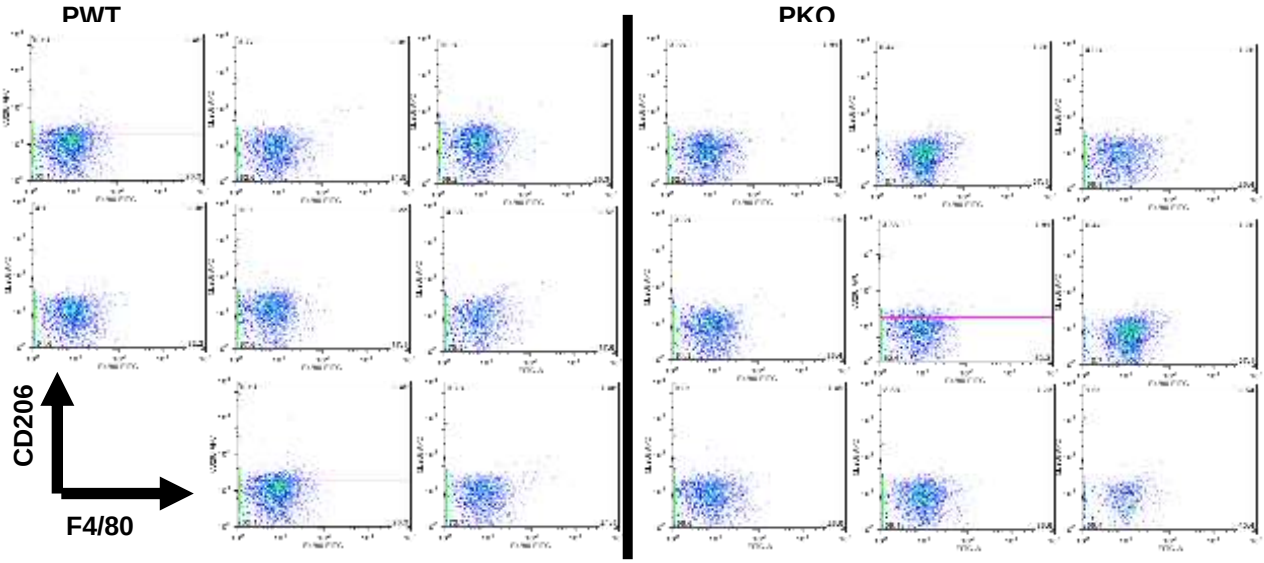

Figure 5-8: Percentage of CD206 +F4/80+ cells in spleen of PWT and PKO tumour bearing and naïve mice. Mice were injected subcutaneously with 1.6×10^5 cell/100µl of B16F10 cell suspension. After 14 days the mice were sacrificed and dissected for collection of spleen. Spleen suspension from both genotypes were stained with F4/80 FITC and CD206 APC

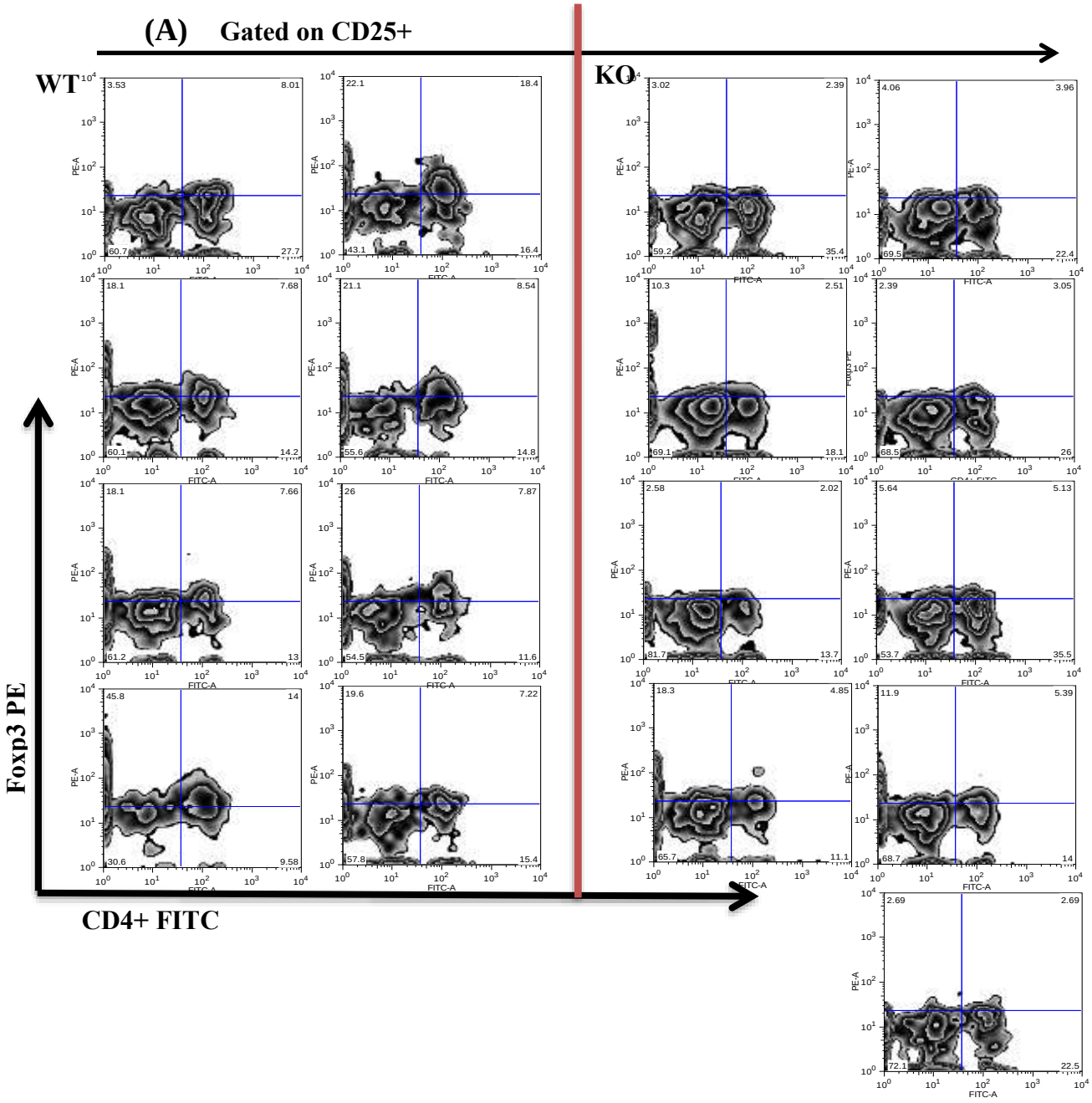
(A) Gated on CD25+
WT
KO
Foxp3 PE
CD4+ FITC
PE-A
FITC-A
3.53
8.01
60.7
27.7
22.1
18.4
43.1
16.4
3.02
2.39
59.2
35.4
4.06
3.96
69.5
22.4
18.1
7.68
60.1
14.2
21.1
8.54
55.6
14.8
10.3
2.51
69.1
18.1
2.39
3.05
68.5
26
18.1
7.66
61.2
13
26
7.87
54.5
11.6
2.58
2.02
81.7
13.7
5.64
5.13
53.7
35.5
45.8
14
30.6
9.58
19.6
7.22
57.8
15.4
18.3
4.85
65.7
11.1
11.9
5.39
68.7
14
2.69
2.69
72.1
22.5

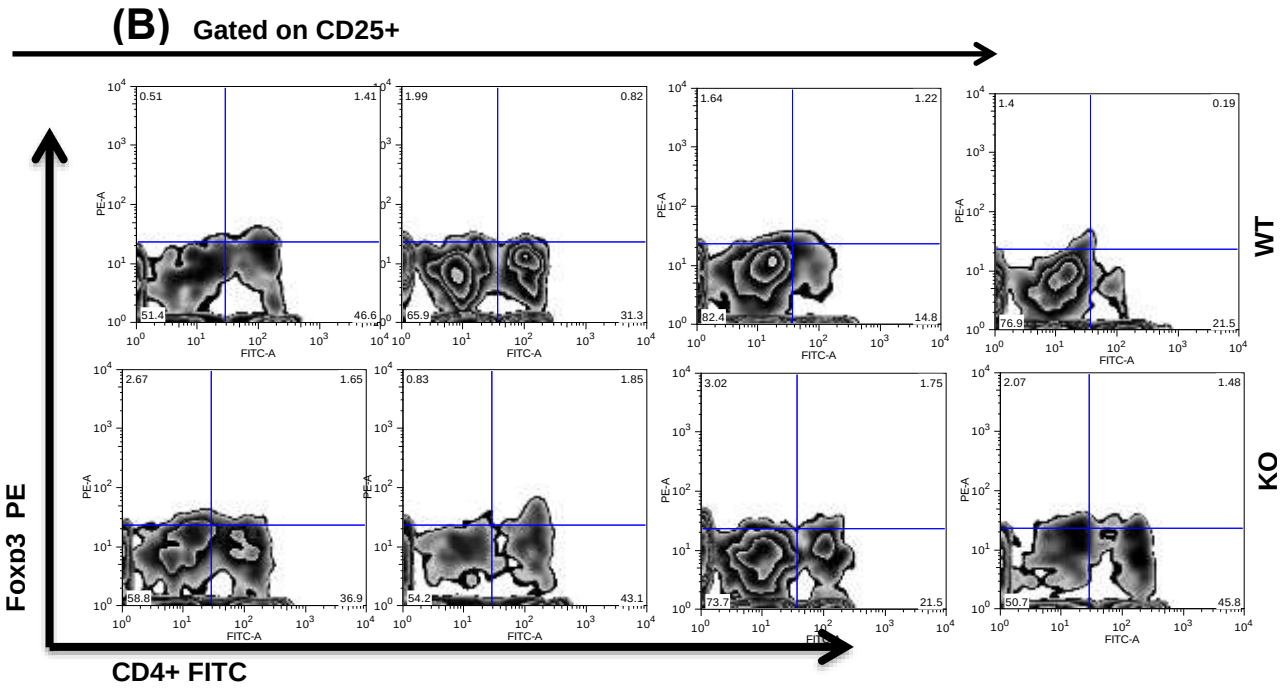

Figure 5-9: T-regs populations in spleen of PWT and PKO tumor-bearing and naïve mice. Three markers were used to distinguish T-regulatory CD25, CD4 and Foxp3. Then FACS was done and percentage of T-regs and phenotypes were calculated. Mice were injected subcutaneously with 1.6×105 cell/100µl of B16F10 cell suspension. After 14 days, the mice were sacrificed and dissected for collection of spleen. Spleen suspension from both genotypes were stained with three markers (CD4, CD25 and Foxp3) to distinguish T-regs. Then FACS was done and percentage of T-regs was obtained. A-t-regs in spleen of tumour bearing mice B-t-regs in spleen of naïve mice.

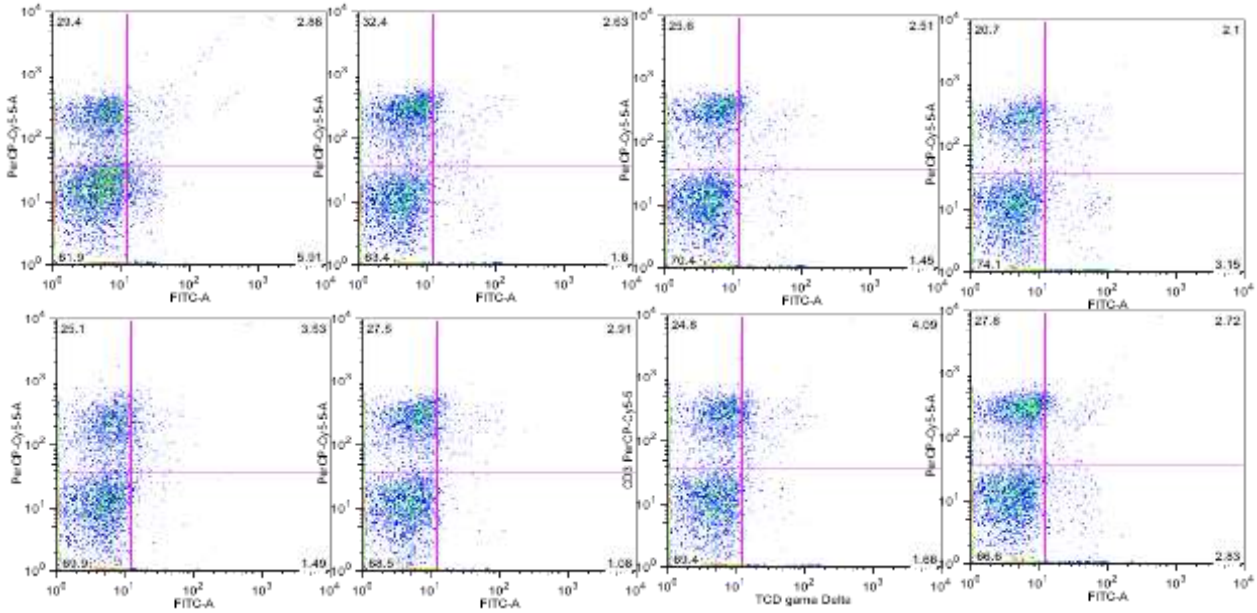

Figure 5-10: γδ T cells populations in spleen of wildtype and properdin deficient mice. Flow cytometry analysis of $CD45^+CD3^+$ γδ TCR^+ cells after gating on $CD45^+$cells in spleen of wildtype and properdin deficient mice. Numbers in the plots indicate the percent of gated cells. $CD45^+CD3^+$ γδ TCR^+ represent percentage of γδ T cells after subcutaneous injection of 1.6 $X10^5$ cells of B16F10.

Appendix 4

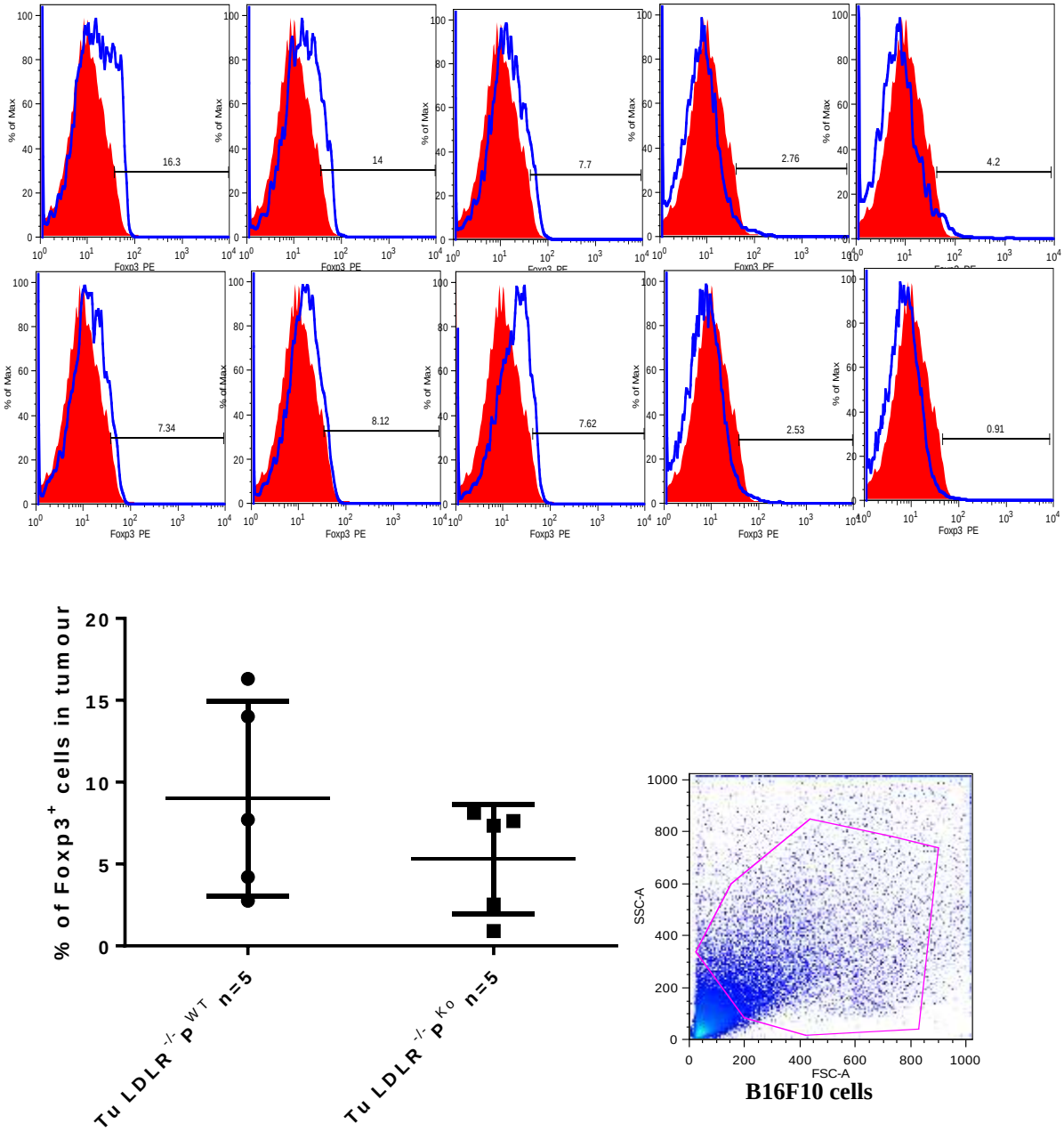

Figure 6-1: Percentage of Foxp3 cell in tumour of LDLR$^{-/-}$PWT and LDLR$^{-/-}$PKO tumour-bearing and naïve mice. Mice were injected subcutaneously with 1.6×10^5 cell/100µl of B16F10 cell suspension. After 14 days the mice were sacrificed and dissected for collection of tumour. Tumour suspension from both genotypes were stained with Foxp3. The data are presented as means ±SEM. Statistical analysis was performed by one-tailed Mann-Whitney U test.

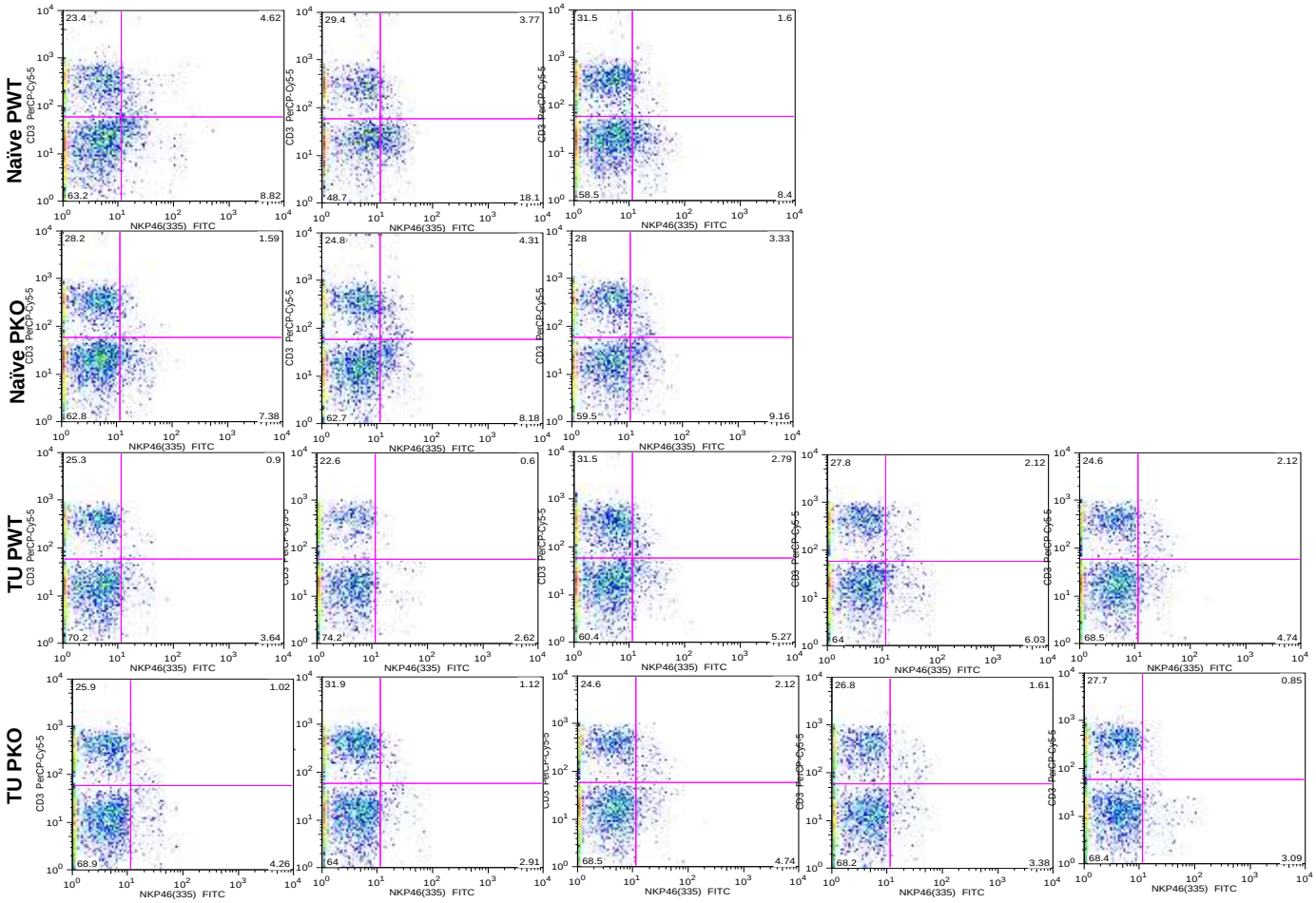

Figure 6-2: NK and TNK cells populations in spleen of wildtype and properdin deficient mice.

Flow cytometry analysis of $CD45^+CD3^+$ $NKP46^+$ cells after gating on $CD45^+$cells in spleen of wildtype and properdin deficient mice. Numbers in the plots indicate the percent of gated cells. $CD45^+CD3^+NKP46^+$ represent percentage of NKT cells and $CD45^+CD3^-NKP46^+$ represent percentage of NK cells, after subcutaneous injection of 1.6 $X10^5$ cells of B16F10.

Appendix 5

Table 17: pancreatic cancer patients data.

Group	Patient	Interval week	Properdin value	Best Response	Overall Survival	Progression Free Survival	Sex	Age	Ethnicity
Treatment arm (Gemcitabine + n-3 fatty acid group)	G01	0	15.3	SD	7	5.3	Male	70	Caucasian
		3	11.3						
		7	18.65						
		15	37.32						
		23	33.31						
	G02	0	65.81	PR	2	2	male	78	Caucasian
		7	27.11						
	G03	0	10.6	SD	10.9	5.7	male	54	Caucasian
		3	5.3						
		7	11.3						
		15	28.69						
		23	25.61						
	G05	0	21.95	SD	7	5.2	female	64	Caucasian
		3	11.95						
		7	13.3						
		15	23.25						
		23	22.2						
	G06	0	35.3	SD	11.2	5.3	female	52	Oriental
		7	25.14						
		15	23.82						
	G07	0	25.95	SD	7.4	5.3	female	40	Caucasian
		3	13.95						
		7	12.6						
		15	38.44						
		23	62.1						
	G08	0	49.42	PD	4.5	1.9	female	66	Caucasian
		3							
		7	55.83						
	G10	0	54.42	SD	4.3	3.5	male	64	Caucasian
		3							
		7	23.79						
		15	10.27						
	G11	0	11.3	PR	10.3	9	male	66	Caucasian
		3	20.65						
		7	15.3						

	G12	0	36.81	SD	7.7	5.5	male	83	Caucasian
		3							
		7	30.51						
		15	28.27						
	G13	0	20.65	PR	13.1	7.5	male	70	Caucasian
		3	14.65						
		7	11.3						
		15	40.91						
		23	34.56						
	G15	0	11.95	SD	8.2	8.2	male	71	Caucasian
		3	8.6						
		7	8.6						
		15	30.36						
		23	29.09						
	G18	0	38.74	PD	2.4	1.5	male	80	Caucasian
		3							
		7	18.48						
	G19	0	15.95	SD	2.7	2.7	male	65	Caucasian
		3	11.3						
		7	9.3						
	G20	0	37.28	SD	18.9	10.6	female	77	Caucasian
		3							
		7	36.04						
		15	22.02						
		23	20.13						
	G21	0	20.34	SD	7.6	7	male	70	Caucasian
		3							
		7	17.82						
	G24	0	45.01	PD	4.4	1.5	female	56	Caucasian
		3							
		7	25.43						
	G25	0	50.53	PD	2	1.8	female	61	Caucasian
		3							
		7	25.52						
	G26	0	32.15	SD	4.8	4.8	male	51	Caucasian
		3							
		7	21.13						
		15	26.6						
	G31	0	29.9	SD	7.6	5.5	male	68	Caucasian
		3							
		7	24.74						
		15	51.17						
	G33	0	35.41	SD	5.9	4.1	female	76	Caucasian
		3							
		7	30.59						

		15	24.75						
	G36	0	46.38	SD	7	5.3	male	66	Caucasian
		3							
		7	40.14						
		15	14.41						
		23	45.09						
	G37	0	38.78	SD	4.9	4.9	male	60	Caucasian
		3							
		7	40.8						
	G38	0	42.87	SD	3.2	3.2	male	73	Asian
		3							
		7	16.06						
	G43	0	24.74	SD	7.1	7.1	male	72	Caucasian
		3							
		7	43.14						
		15	19.36						
	G44	0	43.14	PR	-	-	female	65	Caucasian
		3							
		7	55.47						
		15	44.27						
		23	28.16						
	G47	0	33.52	SD	7.3	5.3	male	69	Caucasian
		3							
		7	32.86						
		15	49.05						
		23	46.26						
	G51	0	24.38	PR	10.3	7.7	female	68	Caucasian
		3							
		7	24.57						
		15	20.11						
		23	22.27						
	G52	0	38.18	SD	11	11	female	66	Caucasian
		3							
		7	24.97						
		15	33.26						
		23	42.42						
Control arm (Gemcitabine only group)	C01	0	9.3	-	1	1	male	66	Caucasian
		2	5.95						
	C02	0	15.95	-	1	1	male	58	Asian
		3	10.6						
	C03	0	30.33	-	7	2	male	50	Caucasian
		3	25.4						
	C04	0	30.13	SD	-	-	male	75	Caucasian
		3							
		7	22.96						

		15	26.5						
	C06	0	29	-	2.9	2.9	male	75	Caucasian
		3	12.69						
Dutch Healthy Volunteer [min-max]	N=30	0	Mean = 24.07 [15.07 - 36.03]	-	-	-	Male 16: Female 14	Mean Age = 55.3 [29 - 71]	-

Figure 07-1: Flow Chart of patient analysis.

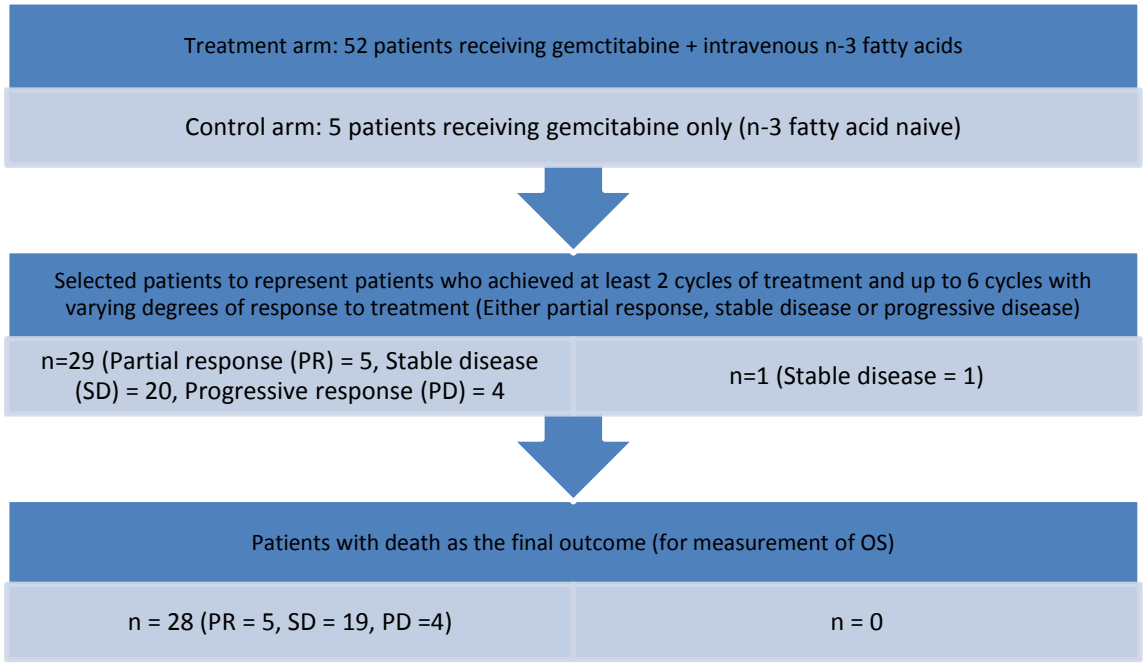

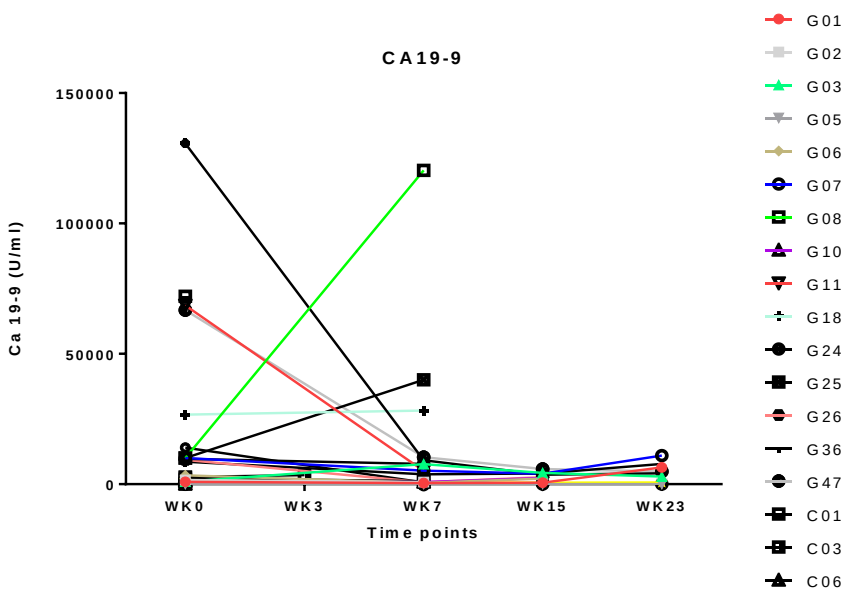

Figure 7-2: Ca19-9 levels in patients with advanced Pancreatic Adenocarcinoma.

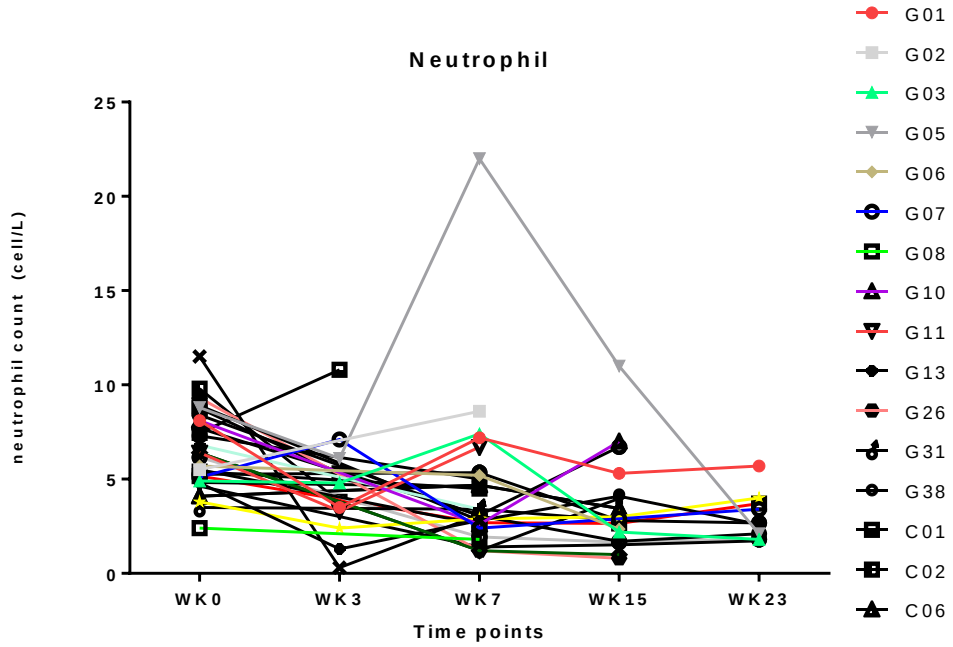

Figure 7-3: neutrophil count in patients with advanced Pancreatic Adenocarcinoma.

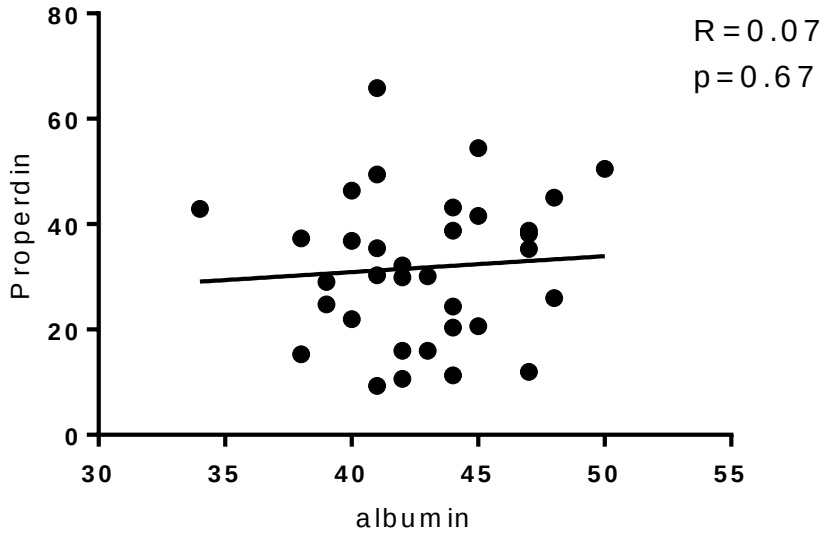

Figure 7-4: correlation of albumin and properdin in patients with advanced Pancreatic Adenocarcinoma.

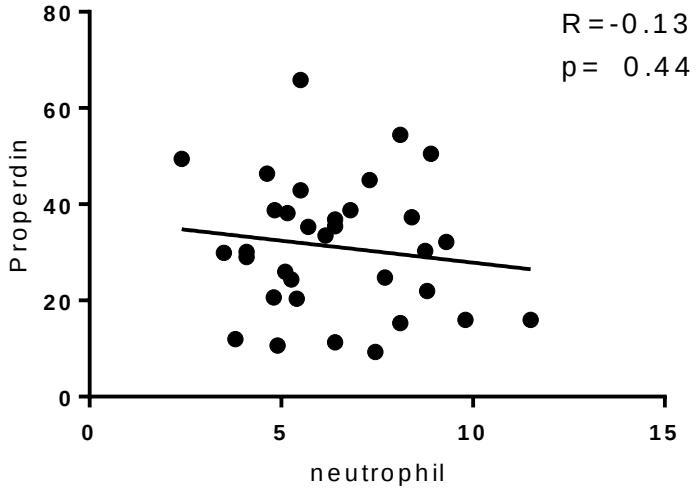

Figure 7-5: Correlation of neutrophil count and properdin in patients with advanced Pancreatic Adenocarcinoma.

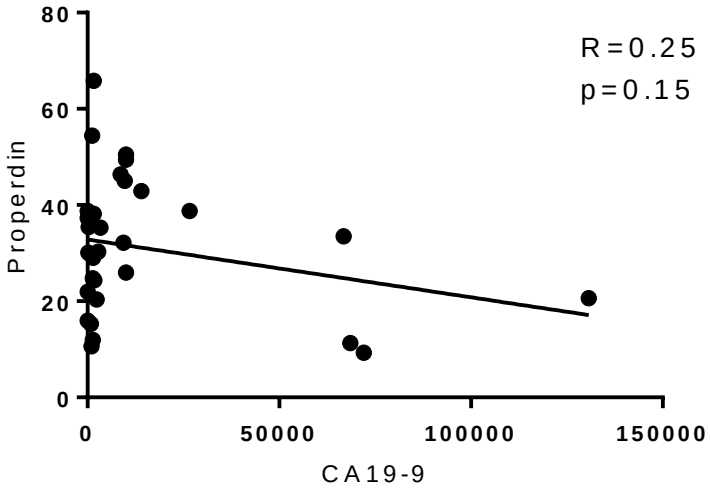

Figure 7-6: Correlation of Ca19-9 and properdin in patients with advanced Pancreatic Adenocarcinoma

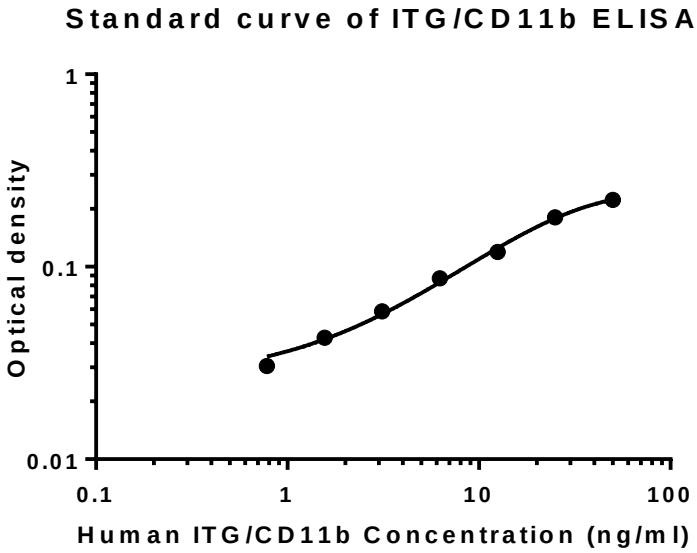

Figure 0-7: Standard curve of ITG/CD11b ELISA.

.

REFERENCES

ADEEGBE, D. O. & NISHIKAWA, H. 2013. Natural and induced T regulatory cells in cancer. *Front* Immunol*,* 4**,** 190.

AGARWAL, B., CORREA, A. M. & HO, L. 2008. Survival in pancreatic carcinoma based on tumor size. *Pancreas,* 36**,** e15-20.

AGBANOMA, G., LI, C., ENNIS, D., PALFREEMAN, A. C., WILLIAMS, L. M. & BRENNAN, F. M. 2012. Production of TNF-alpha in macrophages activated by T cells, compared with lipopolysaccharide, uses distinct IL-10-dependent regulatory mechanism. *J Immunol,* 188**,** 1307-17.

AL-RAYAHI, I. A. M., BROWNING, M. J. & STOVER, C. 2016. Tumour cell conditioned medium reveals greater M2 skewing of macrophages in the absence of properdin. . *Immunity, Inflammation and Disease,*.

ALCORLO, M., TORTAJADA, A., RODRIGUEZ DE CORDOBA, S. & LLORCA, O. 2013. Structural basis for the stabilization of the complement alternative pathway C3 convertase by properdin. *Proc Natl Acad Sci U S A,* 110**,** 13504-9.

ALMAND, B., CLARK, J. I., NIKITINA, E., VAN BEYNEN, J., ENGLISH, N. R., KNIGHT, S. C., CARBONE, D. P. & GABRILOVICH, D. I. 2001. Increased production of immature myeloid cells in cancer patients: a mechanism of immunosuppression in cancer. *J Immunol,* 166**,** 678-89.

ALRAYAHI, I. & SANYI, R. 2015. The overlapping roles of antimicrobial peptides and complement in recruitment and activation of tumour-associated inflammatory cells. *Name: Frontiers in Immunology,* 6.

AMARA, U., FLIERL, M. A., RITTIRSCH, D., KLOS, A., CHEN, H., ACKER, B., BRUCKNER, U. B., NILSSON, B., GEBHARD, F., LAMBRIS, J. D. & HUBER-LANG, M. 2010. Molecular intercommunication between the complement and coagulation systems. *J Immunol,* 185**,** 5628-36.

AMARA, U., RITTIRSCH, D., FLIERL, M., BRUCKNER, U., KLOS, A., GEBHARD, F., LAMBRIS, J. D. & HUBER-LANG, M. 2008. Interaction between the coagulation and complement system. *Adv Exp Med Biol,* 632**,** 71-9.

AMJADI, F., JAVANMARD, S. H., ZARKESH-ESFAHANI, H., KHAZAEI, M. & NARIMANI, M. 2011. Leptin promotes melanoma tumor growth in mice related to increasing circulating endothelial progenitor cells numbers and plasma NO production. *J Exp Clin Cancer Res,* 30**,** 21.

ARANGO DUQUE, G. & DESCOTEAUX, A. 2014. Macrophage cytokines: involvement in immunity and infectious diseases. *Front Immunol,* 5**,** 491.

ARSHAD, A., AL-LESWAS, D., STEPHENSON, J., METCALFE, M. & DENNISON, A. 2011. Potential applications of fish oils rich in n-3 fatty acids in the palliative treatment of advanced pancreatic cancer. *Br J Nutr,* 106**,** 795-800.

ARSHAD, A., CHUNG, W., ISHERWOOD, J., STEWARD, W., METCALFE, M. & DENNISON, A. 2014. Restoration of mannose-binding lectin complement activity is associated with improved outcome in patients with advanced pancreatic cancer treated with gemcitabine and intravenous omega-3 fish oil. *JPEN J Parenter Enteral Nutr,* 38**,** 214-9.

ASCIERTO, P. A., MARINCOLA, F. M. & ATKINS, M. B. 2015. What's new in melanoma? Combination! *J Transl Med,* 13**,** 213.

ATKINS, M. B., LOTZE, M. T., DUTCHER, J. P., FISHER, R. I., WEISS, G., MARGOLIN, K., ABRAMS, J., SZNOL, M., PARKINSON, D., HAWKINS, M., PARADISE, C., KUNKEL, L. & ROSENBERG, S. A. 1999. High-dose recombinant interleukin 2 therapy for patients with metastatic melanoma: analysis of 270 patients treated between 1985 and 1993. *J Clin Oncol,* 17**,** 2105-16.

BAIRD, J. R., BYRNE, K. T., LIZOTTE, P. H., TORAYA-BROWN, S., SCARLETT, U. K., ALEXANDER, M. P., SHEEN, M. R., FOX, B. A., BZIK, D. J., BOSENBERG, M., MULLINS, D. W., TURK, M. J. & FIERING, S. 2013. Immune-mediated regression of established B16F10 melanoma by intratumoral injection of attenuated Toxoplasma gondii protects against rechallenge. *J Immunol,* 190**,** 469-78.

BAJIC, G., YATIME, L., SIM, R. B., VORUP-JENSEN, T. & ANDERSEN, G. R. 2013. Structural insight on the recognition of surface-bound opsonins by the integrin I domain of complement receptor 3. *Proc Natl Acad Sci U S A,* 110**,** 16426-31.

BAKER, K., RATH, T., PYZIK, M. & BLUMBERG, R. S. 2014. The Role of FcRn in Antigen Presentation. *Front Immunol,* 5**,** 408.

BALABAN, S., LEE, L. S., SCHREUDER, M. & HOY, A. J. 2015. Obesity and cancer progression: is there a role of fatty acid metabolism? *Biomed Res Int,* 2015**,** 274585.

BALLANTI, E., PERRICONE, C., GRECO, E., BALLANTI, M., DI MUZIO, G., CHIMENTI, M. S. & PERRICONE, R. 2013. Complement and autoimmunity. *Immunol Res,* 56**,** 477-91.

BANCHEREAU, J. & STEINMAN, R. M. 1998. Dendritic cells and the control of immunity. *Nature,* 392**,** 245-52.

BANIYASH, M. 2006. Chronic inflammation, immunosuppression and cancer: new insights and outlook. *Semin Cancer Biol,* 16**,** 80-8.

BARBER, M. D., FEARON, K. C., TISDALE, M. J., MCMILLAN, D. C. & ROSS, J. A. 2001. Effect of a fish oil-enriched nutritional supplement on metabolic mediators in patients with pancreatic cancer cachexia. *Nutr Cancer,* 40**,** 118-24.

BASTIAN, B. C. 2014. The molecular pathology of melanoma: an integrated taxonomy of melanocytic neoplasia. *Annu Rev Pathol,* 9**,** 239-71.

BERKING, C., TAKEMOTO, R., SCHAIDER, H., SHOWE, L., SATYAMOORTHY, K., ROBBINS, P. & HERLYN, M. 2001. Transforming growth factor-beta1 increases survival of human melanoma through stroma remodeling. *Cancer Res,* 61**,** 8306-16.

BERNSEN, M. R., HAKANSSON, L., GUSTAFSSON, B., KRYSANDER, L., RETTRUP, B., RUITER, D. & HAKANSSON, A. 2003. On the biological relevance of MHC class II and B7 expression by tumour cells in melanoma metastases. *Br J Cancer,* 88**,** 424-31.

BETTS, G., TWOHIG, J., VAN DEN BROEK, M., SIERRO, S., GODKIN, A. & GALLIMORE, A. 2007. The impact of regulatory T cells on carcinogen-induced sarcogenesis. *Br J Cancer,* 96**,** 1849-54.

BHARDWAJ, N. 2007. Harnessing the immune system to treat cancer. *J Clin Invest,* 117**,** 1130-6.

BIEGHS, V., VAN GORP, P. J., WOUTERS, K., HENDRIKX, T., GIJBELS, M. J., VAN BILSEN, M., BAKKER, J., BINDER, C. J., LUTJOHANN, D., STAELS, B., HOFKER, M. H. & SHIRI-SVERDLOV, R. 2012. LDL receptor knock-out mice are a physiological model particularly vulnerable to study the onset of inflammation in non-alcoholic fatty liver disease. *PLoS One,* 7**,** e30668.

BLATT, A. Z., SAGGU, G., KULKARNI, K. V., CORTES, C., THURMAN, J. M., RICKLIN, D., LAMBRIS, J. D., VALENZUELA, J. G. & FERREIRA, V. P. 2016. Properdin-Mediated C5a Production Enhances Stable Binding of Platelets to Granulocytes in Human Whole Blood. *J Immunol,* 196**,** 4671-80.

BRANDON, E. L., GU, J. W., CANTWELL, L., HE, Z., WALLACE, G. & HALL, J. E. 2009. Obesity promotes melanoma tumor growth: role of leptin. *Cancer Biol Ther,* 8**,** 1871-9.

BRODY, J. R., COSTANTINO, C. L., BERGER, A. C., SATO, T., LISANTI, M. P., YEO, C. J., EMMONS, R. V. & WITKIEWICZ, A. K. 2009. Expression of

indoleamine 2,3-dioxygenase in metastatic malignant melanoma recruits regulatory T cells to avoid immune detection and affects survival. *Cell Cycle,* 8**,** 1930-4.

BRONTE, V., KASIC, T., GRI, G., GALLANA, K., BORSELLINO, G., MARIGO, I., BATTISTINI, L., IAFRATE, M., PRAYER-GALETTI, T., PAGANO, F. & VIOLA, A. 2005. Boosting antitumor responses of T lymphocytes infiltrating human prostate cancers. *J Exp Med,* 201**,** 1257-68.

BRONTE, V. & PITTET, M. J. 2013. The spleen in local and systemic regulation of immunity. *Immunity,* 39**,** 806-18.

BUI, J. D., UPPALURI, R., HSIEH, C. S. & SCHREIBER, R. D. 2006. Comparative analysis of regulatory and effector T cells in progressively growing versus rejecting tumors of similar origins. *Cancer Res,* 66**,** 7301-9.

BULLA, R., TRIPODO, C., RAMI, D., LING, G. S., AGOSTINIS, C., GUARNOTTA, C., ZORZET, S., DURIGUTTO, P., BOTTO, M. & TEDESCO, F. 2016. C1q acts in the tumour microenvironment as a cancer-promoting factor independently of complement activation. *Nat Commun,* 7**,** 10346.

BURGHOFF, S., GONG, X., VIETHEN, C., JACOBY, C., FLOGEL, U., BONGARDT, S., SCHORR, A., HIPPE, A., HOMEY, B. & SCHRADER, J. 2014. Growth and metastasis of B16-F10 melanoma cells is not critically dependent on host CD73 expression in mice. *BMC Cancer,* 14**,** 898.

CANCER & RESEARCH UK. 2017.

Ranking of 20 most common cancers in the UK [Online]. Available: http://www.cancerresearchuk.org/health-professional/cancer-statistics/statistics-by-cancer-type/skin-cancer [Online]. [Accessed 20/04/2017].

CHANMEE, T., ONTONG, P., KONNO, K. & ITANO, N. 2014. Tumor-associated macrophages as major players in the tumor microenvironment. *Cancers (Basel),* 6**,** 1670-90.

CHATTERJI, B. & BORLAK, J. 2009. A 2-DE MALDI-TOF study to identify disease regulated serum proteins in lung cancer of c-myc transgenic mice. *Proteomics,* 9**,** 1044-56.

CHEN, H., QIN, J., WEI, P., ZHANG, J., LI, Q., FU, L., LI, S., MA, C. & CONG, B. 2009. Effects of leukotriene B4 and prostaglandin E2 on the differentiation of murine Foxp3+ T regulatory cells and Th17 cells. *Prostaglandins Leukot Essent Fatty Acids,* 80**,** 195-200.

CHEN, J., ROWLEY, D. A., CLARK, T., LEE, S., ZHOU, G., BECK, C., ROWLEY, J. D. & WANG, S. M. 2001. The pattern of gene expression in mouse Gr-1(+) myeloid progenitor cells. *Genomics,* 77**,** 149-62.

CHIEN, Y. H., MEYER, C. & BONNEVILLE, M. 2014. gammadelta T cells: first line of defense and beyond. *Annu Rev Immunol,* 32**,** 121-55.

CHO, E., ROSNER, B. A. & COLDITZ, G. A. 2005. Risk factors for melanoma by body site. *Cancer Epidemiol Biomarkers Prev,* 14**,** 1241-4.

CLEMENT, E., LAZAR, I., MULLER, C. & NIETO, L. 2017. Obesity and melanoma: could fat be fueling malignancy? *Pigment Cell Melanoma Res*.

CONDAMINE, T. & GABRILOVICH, D. I. 2011. Molecular mechanisms regulating myeloid-derived suppressor cell differentiation and function. *Trends Immunol,* 32**,** 19-25.

CORRALES, L., AJONA, D., RAFAIL, S., LASARTE, J. J., RIEZU-BOJ, J. I., LAMBRIS, J. D., ROUZAUT, A., PAJARES, M. J., MONTUENGA, L. M. & PIO, R. 2012. Anaphylatoxin C5a creates a favorable microenvironment for lung cancer progression. *J Immunol,* 189**,** 4674-83.

CORTES, C., OHTOLA, J. A., SAGGU, G. & FERREIRA, V. P. 2012. Local release of properdin in the cellular microenvironment: role in pattern recognition and amplification of the alternative pathway of complement. *Front Immunol,* 3**,** 412.

CORTEZ-RETAMOZO, V., ETZRODT, M., NEWTON, A., RAUCH, P. J., CHUDNOVSKIY, A., BERGER, C., RYAN, R. J., IWAMOTO, Y., MARINELLI, B., GORBATOV, R., FORGHANI, R., NOVOBRANTSEVA, T. I., KOTELIANSKY, V., FIGUEIREDO, J. L., CHEN, J. W., ANDERSON, D. G., NAHRENDORF, M., SWIRSKI, F. K., WEISSLEDER, R. & PITTET, M. J. 2012. Origins of tumor-associated macrophages and neutrophils. *Proc Natl Acad Sci U S A,* 109**,** 2491-6.

CURTIN, J. A., FRIDLYAND, J., KAGESHITA, T., PATEL, H. N., BUSAM, K. J., KUTZNER, H., CHO, K. H., AIBA, S., BROCKER, E. B., LEBOIT, P. E., PINKEL, D. & BASTIAN, B. C. 2005. Distinct sets of genetic alterations in melanoma. *N Engl J Med,* 353**,** 2135-47.

DANCIU, C., FALAMAS, A., DEHELEAN, C., SOICA, C., RADEKE, H., BARBU-TUDORAN, L., BOJIN, F., PINZARU, S. C. & MUNTEANU, M. F. 2013. A characterization of four B16 murine melanoma cell sublines molecular fingerprint and proliferation behavior. *Cancer Cell Int,* 13**,** 75.

DE HAAS, N., DE KONING, C., SPILGIES, L., DE VRIES, I. J. & HATO, S. V. 2016. Improving cancer immunotherapy by targeting the STATe of MDSCs. *Oncoimmunology,* 5**,** e1196312.

DE LA HOZ, C. & BAROJA, A. 1993. Proliferative behaviour of high-ploidy cells in two murine tumour lines. *J Cell Sci,* 104 (Pt 1)**,** 31-6.

DEKOJ, T., LEE, S., DESAI, S., TREVINO, J., BABCOCK, T. A., HELTON, W. S. & ESPAT, N. J. 2007. G2/M cell-cycle arrest and apoptosis by n-3 fatty acids in a pancreatic cancer model. *J Surg Res,* 139**,** 106-12.

DERYNCK, R., AKHURST, R. J. & BALMAIN, A. 2001. TGF-beta signaling in tumor suppression and cancer progression. *Nat Genet,* 29**,** 117-29.

DISCIPIO, R. G., SMITH, C. A., MULLER-EBERHARD, H. J. & HUGLI, T. E. 1983. The activation of human complement component C5 by a fluid phase C5 convertase. *J Biol Chem,* 258**,** 10629-36.

DONALD, C. D., SUN, C. Q., LIM, S. D., MACOSKA, J., COHEN, C., AMIN, M. B., YOUNG, A. N., GANZ, T. A., MARSHALL, F. F. & PETROS, J. A. 2003. Cancer-specific loss of beta-defensin 1 in renal and prostatic carcinomas. *Lab Invest,* 83**,** 501-5.

DONG, C. 2006. Diversification of T-helper-cell lineages: finding the family root of IL-17-producing cells. *Nat Rev Immunol,* 6**,** 329-33.

DOU, J., CHU, L., ZHAO, F., TANG, Q., ZHANG, A., ZHANG, L., WANG, Y., LI, Y., CAO, M. & GU, N. 2007. Study of immunotherapy of murine myeloma by an IL-21-based tumor vaccine in BALB/C mice. *Cancer Biol Ther,* 6**,** 1871-9.

DOUIN-ECHINARD, V., BORNES, S., ROCHAIX, P., TILKIN, A. F., PERON, J. M., BONNET, J., FAVRE, G. & COUDERC, B. 2000. The expression of CD70 and CD80 by gene-modified tumor cells induces an antitumor response depending on the MHC status. *Cancer Gene Ther,* 7**,** 1543-56.

DRIESSENS, G., KLINE, J. & GAJEWSKI, T. F. 2009. Costimulatory and coinhibitory receptors in anti-tumor immunity. *Immunol Rev,* 229**,** 126-44.

DUPONT, A., MOHAMED, F., SALEHEN, N., GLENN, S., FRANCESCUT, L., ADIB, R., BYRNE, S., BREWIN, H., ELLIOTT, I., RICHARDS, L., DIMITROVA, P., SCHWAEBLE, W., IVANOVSKA, N., KADIOGLU, A., MACHADO, L. R., ANDREW, P. W. & STOVER, C. 2014. Septicaemia models using Streptococcus pneumoniae and Listeria monocytogenes: understanding the role of complement properdin. *Med Microbiol Immunol,* 203**,** 257-71.

EBERTING, C. L., SHRAYER, D. P., BUTMARC, J. & FALANGA, V. 2004. Histologic progression of B16 F10 metastatic melanoma in C57BL/6 mice over a six week time period: distant metastases before local growth. *J Dermatol,* 31**,** 299-304.

EHRENREICH, B. A. & COHN, Z. A. 1968. Pinocytosis by macrophages. *J Reticuloendothel Soc,* 5**,** 230-42.

ELLERHORST, J. A., DIWAN, A. H., DANG, S. M., UFFORT, D. G., JOHNSON, M. K., COOKE, C. P. & GRIMM, E. A. 2010. Promotion of melanoma growth by the metabolic hormone leptin. *Oncol Rep,* 23**,** 901-7.

ENGLEN, M. D., VALDEZ, Y. E., LEHNERT, N. M. & LEHNERT, B. E. 1995. Granulocyte/macrophage colony-stimulating factor is expressed and secreted in cultures of murine L929 cells. *J Immunol Methods,* 184**,** 281-3.

FACCIABENE, A., PENG, X., HAGEMANN, I. S., BALINT, K., BARCHETTI, A., WANG, L. P., GIMOTTY, P. A., GILKS, C. B., LAL, P., ZHANG, L. & COUKOS, G. 2011. Tumour hypoxia promotes tolerance and angiogenesis via CCL28 and T(reg) cells. *Nature,* 475**,** 226-30.

FALCONER, J. S., ROSS, J. A., FEARON, K. C., HAWKINS, R. A., O'RIORDAIN, M. G. & CARTER, D. C. 1994. Effect of eicosapentaenoic acid and other fatty acids on the growth in vitro of human pancreatic cancer cell lines. *Br J Cancer,* 69**,** 826-32.

FAN, Y. & MCCLOSKEY, M. A. 1994. Dual pathways for GTP-dependent regulation of chemoattractant-activated K+ conductance in murine J774 monocytes. *J Biol Chem,* 269**,** 31533-43.

FARRIES, T. C., FINCH, J. T., LACHMANN, P. J. & HARRISON, R. A. 1987. Resolution and analysis of 'native' and 'activated' properdin. *Biochem J,* 243**,** 507-17.

FEARON, D. T. & AUSTEN, K. F. 1975. Initiation of C3 cleavage in the alternative complement pathway. *J Immunol,* 115**,** 1357-61.

FILIPAZZI, P., HUBER, V. & RIVOLTINI, L. 2012. Phenotype, function and clinical implications of myeloid-derived suppressor cells in cancer patients. *Cancer Immunol Immunother,* 61**,** 255-63.

FISCHER, A. H., JACOBSON, K. A., ROSE, J. & ZELLER, R. 2008. Hematoxylin and eosin staining of tissue and cell sections. *CSH Protoc,* 2008**,** pdb.prot4986.

FLEETWOOD, A. J., LAWRENCE, T., HAMILTON, J. A. & COOK, A. D. 2007. Granulocyte-macrophage colony-stimulating factor (CSF) and macrophage CSF-dependent macrophage phenotypes display differences in cytokine profiles and transcription factor activities: implications for CSF blockade in inflammation. *J Immunol,* 178**,** 5245-52.

FOX, P. L. & DICORLETO, P. E. 1988. Fish oils inhibit endothelial cell production of platelet-derived growth factor-like protein. *Science,* 241**,** 453-6.

FUJIMURA, T., KAMBAYASHI, Y. & AIBA, S. 2012a. Crosstalk between regulatory T cells (Tregs) and myeloid derived suppressor cells (MDSCs) during melanoma growth. *Oncoimmunology,* 1**,** 1433-1434.

FUJIMURA, T., RING, S., UMANSKY, V., MAHNKE, K. & ENK, A. H. 2012b. Regulatory T cells stimulate B7-H1 expression in myeloid-derived suppressor cells in ret melanomas. *J Invest Dermatol,* 132**,** 1239-46.

GABRILOVICH, D. I. & NAGARAJ, S. 2009. Myeloid-derived suppressor cells as regulators of the immune system. *Nat Rev Immunol,* 9**,** 162-74.

GABRILOVICH, D. I., OSTRAND-ROSENBERG, S. & BRONTE, V. 2012. Coordinated regulation of myeloid cells by tumours. *Nat Rev Immunol,* 12**,** 253-68.

GAETANO, C., MASSIMO, L. & ALBERTO, M. 2010. Control of iron homeostasis as a key component of macrophage polarization. *Haematologica,* 95**,** 1801-3.

GALGANI, M., DE ROSA, V., LA CAVA, A. & MATARESE, G. 2016. Role of Metabolism in the Immunobiology of Regulatory T Cells. *J Immunol,* 197**,** 2567-75.

GALLIMORE, A. M. & SIMON, A. K. 2008. Positive and negative influences of regulatory T cells on tumour immunity. *Oncogene,* 27**,** 5886-93.

GAO, Y., YANG, W., PAN, M., SCULLY, E., GIRARDI, M., AUGENLICHT, L. H., CRAFT, J. & YIN, Z. 2003. Gamma delta T cells provide an early source of interferon gamma in tumor immunity. *J Exp Med,* 198**,** 433-42.

GARBE, C., TERHEYDEN, P., KEILHOLZ, U., KOLBL, O. & HAUSCHILD, A. 2008. Treatment of melanoma. *Dtsch Arztebl Int,* 105**,** 845-51.

GARCIA-HERNANDEZ, M. L., HERNANDEZ-PANDO, R., GARIGLIO, P. & BERUMEN, J. 2002. Interleukin-10 promotes B16-melanoma growth by inhibition of macrophage functions and induction of tumour and vascular cell proliferation. *Immunology,* 105**,** 231-43.

GATENBY, R. A. & BROWN, J. 2017. Mutations, evolution and the central role of a self-defined fitness function in the initiation and progression of cancer. *Biochim Biophys Acta*.

GAUTAM, A., WALDREP, J. C., DENSMORE, C. L., KOSHKINA, N., MELTON, S., ROBERTS, L., GILBERT, B. & KNIGHT, V. 2002. Growth inhibition of established B16-F10 lung metastases by sequential aerosol delivery of p53 gene and 9-nitrocamptothecin. *Gene Ther,* 9**,** 353-7.

GEIGER, T. R. & PEEPER, D. S. 2009. Metastasis mechanisms. *Biochim Biophys Acta,* 1796**,** 293-308.

GORELIK, L. & FLAVELL, R. A. 2002. Transforming growth factor-beta in T-cell biology. *Nat Rev Immunol,* 2**,** 46-53.

GRAILER, J. J., BOSMANN, M. & WARD, P. A. 2012. Regulatory effects of C5a on IL-17A, IL-17F, and IL-23. *Front Immunol,* 3**,** 387.

GRANOVETTER, M. 2016. IRF4 SNP is predictive of melanoma subtypes. *Lancet Oncol,* 17**,** e96.

GRIVENNIKOV, S. I., GRETEN, F. R. & KARIN, M. 2010. Immunity, inflammation, and cancer. *Cell,* 140**,** 883-99.

GUNN, L., DING, C., LIU, M., MA, Y., QI, C., CAI, Y., HU, X., AGGARWAL, D., ZHANG, H. G. & YAN, J. 2012. Opposing roles for complement component C5a in tumor progression and the tumor microenvironment. *J Immunol,* 189**,** 2985-94.

HANAHAN, D. & WEINBERG, R. A. 2000. The hallmarks of cancer. *Cell,* 100**,** 57-70.

HANAHAN, D. & WEINBERG, R. A. 2011. Hallmarks of cancer: the next generation. *Cell,* 144**,** 646-74.

HARBOE, M., JOHNSON, C., NYMO, S., EKHOLT, K., SCHJALM, C., LINDSTAD, J. K., PHARO, A., HELLERUD, B. C., NILSSON EKDAHL, K., MOLLNES, T. E. & NILSSON, P. H. 2017. Properdin binding to complement activating surfaces depends on initial C3b deposition. *Proc Natl Acad Sci U S A,* 114**,** E534-e539.

HARBOE, M., ULVUND, G., VIEN, L., FUNG, M. & MOLLNES, T. E. 2004. The quantitative role of alternative pathway amplification in classical pathway induced terminal complement activation. *Clin Exp Immunol,* 138**,** 439-46.

HARDMAN, W. E. 2002. Omega-3 fatty acids to augment cancer therapy. *J Nutr,* 132**,** 3508s-3512s.

HART, I. R. 1979. The selection and characterization of an invasive variant of the B16 melanoma. *Am J Pathol,* 97**,** 587-600.

HAVILAND, D. L., MCCOY, R. L., WHITEHEAD, W. T., AKAMA, H., MOLMENTI, E. P., BROWN, A., HAVILAND, J. C., PARKS, W. C., PERLMUTTER, D. H. & WETSEL, R. A. 1995. Cellular expression of the C5a anaphylatoxin receptor (C5aR): demonstration of C5aR on nonmyeloid cells of the liver and lung. *J Immunol,* 154**,** 1861-9.

HE, D., LI, H., YUSUF, N., ELMETS, C. A., LI, J., MOUNTZ, J. D. & XU, H. 2010. IL-17 promotes tumor development through the induction of tumor promoting microenvironments at tumor sites and myeloid-derived suppressor cells. *J Immunol,* 184**,** 2281-8.

HE, Y., CHENG, G., XIE, L., NIE, Y., HE, B. & GU, Z. 2013. Polyethyleneimine/DNA polyplexes with reduction-sensitive hyaluronic acid derivatives shielding for targeted gene delivery. *Biomaterials,* 34**,** 1235-45.

HERBUT, P. A. & KRAEMER, W. H. 1958. The properdin system in transplantable cancer (Gardner lymphosarcoma 6C3HED). *Am J Pathol,* 34**,** 911-20.

HERBUT, P. A., KRAEMER, W. H. & PILLEMER, L. 1958. The effects of components of guinea pig serum on lymphosarcoma 6C3HED in C3H mice. *Blood,* 13**,** 732-9.

HERING, J., GARREAN, S., DEKOJ, T. R., RAZZAK, A., SAIED, A., TREVINO, J., BABCOCK, T. A. & ESPAT, N. J. 2007. Inhibition of proliferation by omega-3 fatty acids in chemoresistant pancreatic cancer cells. *Ann Surg Oncol,* 14**,** 3620-8.

HILLEN, F., BAETEN, C. I., VAN DE WINKEL, A., CREYTENS, D., VAN DER SCHAFT, D. W., WINNEPENNINCKX, V. & GRIFFIOEN, A. W. 2008. Leukocyte infiltration and tumor cell plasticity are parameters of aggressiveness in primary cutaneous melanoma. *Cancer Immunol Immunother,* 57**,** 97-106.

HIWATASHI, K., TAMIYA, T., HASEGAWA, E., FUKAYA, T., HASHIMOTO, M., KAKOI, K., KASHIWAGI, I., KIMURA, A., INOUE, N., MORITA, R., YASUKAWA, H. & YOSHIMURA, A. 2011. Suppression of SOCS3 in macrophages prevents cancer metastasis by modifying macrophage phase and MCP2/CCL8 induction. *Cancer Lett,* 308**,** 172-80.

HOLMGAARD, R. B., ZAMARIN, D., LI, Y., GASMI, B., MUNN, D. H., ALLISON, J. P., MERGHOUB, T. & WOLCHOK, J. D. 2015. Tumor-Expressed IDO Recruits and Activates MDSCs in a Treg-Dependent Manner. *Cell Rep,* 13**,** 412-24.

HOSKIN, D. W. & RAMAMOORTHY, A. 2008. Studies on anticancer activities of antimicrobial peptides. *Biochim Biophys Acta,* 1778**,** 357-75.

HOURCADE, D. E. 2006. The role of properdin in the assembly of the alternative pathway C3 convertases of complement. *J Biol Chem,* 281**,** 2128-32.

HUANG, B., PAN, P. Y., LI, Q., SATO, A. I., LEVY, D. E., BROMBERG, J., DIVINO, C. M. & CHEN, S. H. 2006. Gr-1+CD115+ immature myeloid suppressor cells mediate the development of tumor-induced T regulatory cells and T-cell anergy in tumor-bearing host. *Cancer Res,* 66**,** 1123-31.

HUBER-LANG, M., SARMA, J. V., ZETOUNE, F. S., RITTIRSCH, D., NEFF, T. A., MCGUIRE, S. R., LAMBRIS, J. D., WARNER, R. L., FLIERL, M. A., HOESEL, L. M., GEBHARD, F., YOUNGER, J. G., DROUIN, S. M., WETSEL, R. A. & WARD, P. A. 2006. Generation of C5a in the absence of C3: a new complement activation pathway. *Nat Med,* 12**,** 682-7.

HUBER-LANG, M., YOUNKIN, E. M., SARMA, J. V., RIEDEMANN, N., MCGUIRE, S. R., LU, K. T., KUNKEL, R., YOUNGER, J. G., ZETOUNE, F. S. & WARD, P. A. 2002. Generation of C5a by phagocytic cells. *Am J Pathol,* 161**,** 1849-59.

HUME, D. A. & GORDON, S. 1983. Mononuclear phagocyte system of the mouse defined by immunohistochemical localization of antigen F4/80. Identification of resident macrophages in renal medullary and cortical interstitium and the juxtaglomerular complex. *J Exp Med,* 157**,** 1704-9.

HUSSEIN, M. R. 2006. Tumour-associated macrophages and melanoma tumourigenesis: integrating the complexity. *Int J Exp Pathol,* 87**,** 163-76.

INABA, K., INABA, M., ROMANI, N., AYA, H., DEGUCHI, M., IKEHARA, S., MURAMATSU, S. & STEINMAN, R. M. 1992. Generation of large numbers of dendritic cells from mouse bone marrow cultures supplemented with granulocyte/macrophage colony-stimulating factor. *J Exp Med,* 176**,** 1693-702.

ISHIBASHI, S., BROWN, M. S., GOLDSTEIN, J. L., GERARD, R. D., HAMMER, R. E. & HERZ, J. 1993. Hypercholesterolemia in low density lipoprotein receptor knockout mice and its reversal by adenovirus-mediated gene delivery. *J Clin Invest,* 92**,** 883-93.

IYER, S. S., GHAFFARI, A. A. & CHENG, G. 2010. Lipopolysaccharide-mediated IL-10 transcriptional regulation requires sequential induction of type I IFNs and IL-27 in macrophages. *J Immunol,* 185**,** 6599-607.

JABLONSKI, K. A., AMICI, S. A., WEBB, L. M., RUIZ-ROSADO JDE, D., POPOVICH, P. G., PARTIDA-SANCHEZ, S. & GUERAU-DE-ARELLANO,

M. 2015. Novel Markers to Delineate Murine M1 and M2 Macrophages. *PLoS One,* 10**,** e0145342.

JACKAMAN, C., RADLEY-CRABB, H. G., SOFFE, Z., SHAVLAKADZE, T., GROUNDS, M. D. & NELSON, D. J. 2013. Targeting macrophages rescues age-related immune deficiencies in C57BL/6J geriatric mice. *Aging Cell,* 12**,** 345-57.

JACOBS, J. F., NIERKENS, S., FIGDOR, C. G., DE VRIES, I. J. & ADEMA, G. J. 2012. Regulatory T cells in melanoma: the final hurdle towards effective immunotherapy? *Lancet Oncol,* 13**,** e32-42.

JAGUIN, M., HOULBERT, N., FARDEL, O. & LECUREUR, V. 2013. Polarization profiles of human M-CSF-generated macrophages and comparison of M1-markers in classically activated macrophages from GM-CSF and M-CSF origin. *Cell Immunol,* 281**,** 51-61.

JAYARAMAN, P., PARIKH, F., LOPEZ-RIVERA, E., HAILEMICHAEL, Y., CLARK, A., MA, G., CANNAN, D., RAMACHER, M., KATO, M., OVERWIJK, W. W., CHEN, S. H., UMANSKY, V. Y. & SIKORA, A. G. 2012. Tumor-expressed inducible nitric oxide synthase controls induction of functional myeloid-derived suppressor cells through modulation of vascular endothelial growth factor release. *J Immunol,* 188**,** 5365-76.

JENSEN, M. M., JØRGENSEN, J. T., BINDERUP, T. & KJÆR, A. 2008. Tumor volume in subcutaneous mouse xenografts measured by microCT is more accurate and reproducible than determined by 18F-FDG-microPET or external caliper. *BMC Medical Imaging,* 8**,** 1-9.

JOHNSON, B. D., YAN, X., SCHAUER, D. W. & ORENTAS, R. J. 2003. Dual expression of CD80 and CD86 produces a tumor vaccine superior to single expression of either molecule. *Cell Immunol,* 222**,** 15-26.

KARIMI, K., LINDGREN, T. H., KOCH, C. A. & BRODELL, R. T. 2016. Obesity as a risk factor for malignant melanoma and non-melanoma skin cancer. *Rev Endocr Metab Disord*.

KARIMKHANI, C., GREEN, A. C., NIJSTEN, T., WEINSTOCK, M. A., DELLAVALLE, R. P., NAGHAVI, M. & FITZMAURICE, C. 2017. The Global Burden of Melanoma: Results from Global Burden of Disease Study 2015. *Br J Dermatol*.

KEMPER, C., ATKINSON, J. P. & HOURCADE, D. E. 2010. Properdin: emerging roles of a pattern-recognition molecule. *Annu Rev Immunol,* 28**,** 131-55.

KHANNA, C. & HUNTER, K. 2005. Modeling metastasis in vivo. *Carcinogenesis,* 26**,** 513-23.

KIRSZBERG, C., RUMJANEK, V. M. & MONTEIRO, R. Q. 2005. Assembly and regulation of prothrombinase complex on B16F10 melanoma cells. *Thromb Res,* 115**,** 123-9.

KOLEV, M., LE FRIEC, G. & KEMPER, C. 2014. Complement--tapping into new sites and effector systems. *Nat Rev Immunol,* 14**,** 811-20.

KOLLS, J. K. & LINDEN, A. 2004. Interleukin-17 family members and inflammation. *Immunity,* 21**,** 467-76.

KOSTNER, K., DENZER, N., MULLER, C. S., KLEIN, R., TILGEN, W. & REICHRATH, J. 2009. The relevance of vitamin D receptor (VDR) gene polymorphisms for cancer: a review of the literature. *Anticancer Res,* 29**,** 3511-36.

KOTIMAA, J., VAN DER POL, P., LEIJTENS, S., KLAR-MOHAMMAD, N., SCHILDERS, G., DAHA, M. R., RUTJES, H. & VAN KOOTEN, C. 2014. Functional assessment of rat complement pathway activities and quantification of soluble C5b-9 in an experimental model of renal ischemia/reperfusion injury. *J Immunol Methods,* 412**,** 14-23.

KOUSER, L., ABDUL-AZIZ, M., NAYAK, A., STOVER, C. M., SIM, R. B. & KISHORE, U. 2013. Properdin and factor h: opposing players on the alternative complement pathway "see-saw". *Front Immunol,* 4**,** 93.

KRETZER, I. F., MARIA, D. A. & MARANHAO, R. C. 2012. Drug-targeting in combined cancer chemotherapy: tumor growth inhibition in mice by association of paclitaxel and etoposide with a cholesterol-rich nanoemulsion. *Cell Oncol (Dordr),* 35**,** 451-60.

KRISINGER, M. J., GOEBELER, V., LU, Z., MEIXNER, S. C., MYLES, T., PRYZDIAL, E. L. & CONWAY, E. M. 2012. Thrombin generates previously unidentified C5 products that support the terminal complement activation pathway. *Blood,* 120**,** 1717-25.

KUMAR, V., PATEL, S., TCYGANOV, E. & GABRILOVICH, D. I. 2016. The Nature of Myeloid-Derived Suppressor Cells in the Tumor Microenvironment. *Trends Immunol*.

KURANO, M., TSUKAMOTO, K., HARA, M., OHKAWA, R., IKEDA, H. & YATOMI, Y. 2015. LDL receptor and ApoE are involved in the clearance of ApoM-associated sphingosine 1-phosphate. *J Biol Chem,* 290**,** 2477-88.

KUSMARTSEV, S., NEFEDOVA, Y., YODER, D. & GABRILOVICH, D. I. 2004. Antigen-specific inhibition of CD8+ T cell response by immature myeloid

cells in cancer is mediated by reactive oxygen species. *J Immunol,* 172**,** 989-99.

KUZU, O. F., NGUYEN, F. D., NOORY, M. A. & SHARMA, A. 2015. Current State of Animal (Mouse) Modeling in Melanoma Research. *Cancer Growth Metastasis,* 8**,** 81-94.

LACEY, D. C., ACHUTHAN, A., FLEETWOOD, A. J., DINH, H., ROINIOTIS, J., SCHOLZ, G. M., CHANG, M. W., BECKMAN, S. K., COOK, A. D. & HAMILTON, J. A. 2012. Defining GM-CSF- and macrophage-CSF-dependent macrophage responses by in vitro models. *J Immunol,* 188**,** 5752-65.

LADANYI, A., MOHOS, A., SOMLAI, B., LISZKAY, G., GILDE, K., FEJOS, Z., GAUDI, I. & TIMAR, J. 2010. FOXP3+ cell density in primary tumor has no prognostic impact in patients with cutaneous malignant melanoma. *Pathol Oncol Res,* 16**,** 303-9.

LAI, P. B., ROSS, J. A., FEARON, K. C., ANDERSON, J. D. & CARTER, D. C. 1996. Cell cycle arrest and induction of apoptosis in pancreatic cancer cells exposed to eicosapentaenoic acid in vitro. *Br J Cancer,* 74**,** 1375-83.

LANCA, T., COSTA, M. F., GONCALVES-SOUSA, N., REI, M., GROSSO, A. R., PENIDO, C. & SILVA-SANTOS, B. 2013. Protective role of the inflammatory CCR2/CCL2 chemokine pathway through recruitment of type 1 cytotoxic gammadelta T lymphocytes to tumor beds. *J Immunol,* 190**,** 6673-80.

LARSSON, S. C., KUMLIN, M., INGELMAN-SUNDBERG, M. & WOLK, A. 2004. Dietary long-chain n-3 fatty acids for the prevention of cancer: a review of potential mechanisms. *Am J Clin Nutr,* 79**,** 935-45.

LAWRENCE, T. & NATOLI, G. 2011. Transcriptional regulation of macrophage polarization: enabling diversity with identity. *Nat Rev Immunol,* 11**,** 750-61.

LEONG, P. P., MOHAMMAD, R., IBRAHIM, N., ITHNIN, H., ABDULLAH, M., DAVIS, W. C. & SEOW, H. F. 2006. Phenotyping of lymphocytes expressing regulatory and effector markers in infiltrating ductal carcinoma of the breast. *Immunol Lett,* 102**,** 229-36.

LETTERIO, J. J. 2000. Murine models define the role of TGF-beta as a master regulator of immune cell function. *Cytokine Growth Factor Rev,* 11**,** 81-7.

LEUSCHNER, C. & HANSEL, W. 2004. Membrane disrupting lytic peptides for cancer treatments. *Curr Pharm Des,* 10**,** 2299-310.

LI, H., HAN, Y., GUO, Q., ZHANG, M. & CAO, X. 2009. Cancer-expanded myeloid-derived suppressor cells induce anergy of NK cells through membrane-bound TGF-beta 1. *J Immunol,* 182**,** 240-9.

LI, J., LIU, J., MAO, X., TANG, Q. & LU, H. 2014. IL-7 receptor blockade inhibits IL-17-producing gammadelta cells and suppresses melanoma development. *Inflammation,* 37**,** 1444-52.

LI, M., KNIGHT, D. A., L, A. S., SMYTH, M. J. & STEWART, T. J. 2013a. A role for CCL2 in both tumor progression and immunosurveillance. *Oncoimmunology,* 2**,** e25474.

LI, M., XU, F., MULLER, J., HEARING, V. J. & GORELIK, E. 1998. Ecotropic C-type retrovirus of B16 melanoma and malignant transformation of normal melanocytes. *Int J Cancer,* 76**,** 430-6.

LI, X., LIANG, L., ZHANG, M., SONG, F., NAN, H., WANG, L. E., WEI, Q., LEE, J. E., AMOS, C. I., QURESHI, A. A. & HAN, J. 2013b. Obesity-related genetic variants, human pigmentation, and risk of melanoma. *Hum Genet,* 132**,** 793-801.

LIM, E., MODI, K. D. & KIM, J. 2009. In vivo bioluminescent imaging of mammary tumors using IVIS spectrum. *J Vis Exp*.

LIM, T. S., GOH, J. K., MORTELLARO, A., LIM, C. T., HAMMERLING, G. J. & RICCIARDI-CASTAGNOLI, P. 2012. CD80 and CD86 differentially regulate mechanical interactions of T-cells with antigen-presenting dendritic cells and B-cells. *PLoS One,* 7**,** e45185.

LIN, R. L. & ZHAO, L. J. 2015. Mechanistic basis and clinical relevance of the role of transforming growth factor-beta in cancer. *Cancer Biol Med,* 12**,** 385-93.

LINDAU, D., GIELEN, P., KROESEN, M., WESSELING, P. & ADEMA, G. J. 2013. The immunosuppressive tumour network: myeloid-derived suppressor cells, regulatory T cells and natural killer T cells. *Immunology,* 138**,** 105-15.

LIU-SMITH, F., FARHAT, A. M., ARCE, A., ZIOGAS, A., TAYLOR, T., WANG, Z., YOURK, V., LIU, J., WU, J., MCELIGOT, A. J., ANTON-CULVER, H. & MEYSKENS, F. L. 2017. Sex differences in the association of cutaneous melanoma incidence rates and geographic ultraviolet light exposure. *J Am Acad Dermatol,* 76**,** 499-505.e3.

LIU, V. C., WONG, L. Y., JANG, T., SHAH, A. H., PARK, I., YANG, X., ZHANG, Q., LONNING, S., TEICHER, B. A. & LEE, C. 2007. Tumor evasion of the immune system by converting CD4+CD25- T cells into CD4+CD25+ T

regulatory cells: role of tumor-derived TGF-beta. *J Immunol,* 178**,** 2883-92.

LIU, Y., LAI, L., CHEN, Q., SONG, Y., XU, S., MA, F., WANG, X., WANG, J., YU, H., CAO, X. & WANG, Q. 2012. MicroRNA-494 is required for the accumulation and functions of tumor-expanded myeloid-derived suppressor cells via targeting of PTEN. *J Immunol,* 188**,** 5500-10.

LIVAK, K. J. & SCHMITTGEN, T. D. 2001. Analysis of relative gene expression data using real-time quantitative PCR and the 2(-Delta Delta C(T)) Method. *Methods,* 25**,** 402-8.

LLAVERIAS, G., DANILO, C., MERCIER, I., DAUMER, K., CAPOZZA, F., WILLIAMS, T. M., SOTGIA, F., LISANTI, M. P. & FRANK, P. G. 2011. Role of cholesterol in the development and progression of breast cancer. *Am J Pathol,* 178**,** 402-12.

LOKHATIUK, A. S., SMOL'IANINOV, E. S., KAZANTSEV, N. P. & NEMIROVSKAIA, L. 1974. [Properdin and complement activity in patients with stomach cancer]. *Vopr Onkol,* 20**,** 22-5.

LOUIE, S. M., ROBERTS, L. S. & NOMURA, D. K. 2013. Mechanisms linking obesity and cancer. *Biochim Biophys Acta,* 1831**,** 1499-508.

LUTZ, H. U., FUMIA, S., SCHURTENBERGER, C. & ALAIA, V. 2007. Opinion paper: Stimulation of complement amplification or activation of the alternative pathway of complement? *Mol Immunol,* 44**,** 3862-5.

LV, H. F., CUI, F., YU, C. H., DENG, L. L., JI, J. J., LU, D., YANG, Y., WANG, W. X. & XU, Y. Q. 2009. Inhibition of lung metastasis in mice by intravascular injection of dendritic cells and natural killer cells. *Biotechnol Lett,* 31**,** 1709-15.

MACCIONI, L., RACHAKONDA, P. S., SCHERER, D., BERMEJO, J. L., PLANELLES, D., REQUENA, C., HEMMINKI, K., NAGORE, E. & KUMAR, R. 2013. Variants at chromosome 20 (ASIP locus) and melanoma risk. *Int J Cancer,* 132**,** 42-54.

MACMICKING, J., XIE, Q. W. & NATHAN, C. 1997. Nitric oxide and macrophage function. *Annu Rev Immunol,* 15**,** 323-50.

MAKITA, N., HIZUKURI, Y., YAMASHIRO, K., MURAKAWA, M. & HAYASHI, Y. 2015. IL-10 enhances the phenotype of M2 macrophages induced by IL-4 and confers the ability to increase eosinophil migration. *Int Immunol,* 27**,** 131-41.

MARGOLIN, K. 2016. The Promise of Molecularly Targeted and Immunotherapy for Advanced Melanoma. *Curr Treat Options Oncol,* 17**,** 48.

MARIGO, I., BOSIO, E., SOLITO, S., MESA, C., FERNANDEZ, A., DOLCETTI, L., UGEL, S., SONDA, N., BICCIATO, S., FALISI, E., CALABRESE, F., BASSO, G., ZANOVELLO, P., COZZI, E., MANDRUZZATO, S. & BRONTE, V. 2010. Tumor-induced tolerance and immune suppression depend on the C/EBPbeta transcription factor. *Immunity,* 32**,** 790-802.

MARKIEWSKI, M. M., DEANGELIS, R. A., BENENCIA, F., RICKLIN-LICHTSTEINER, S. K., KOUTOULAKI, A., GERARD, C., COUKOS, G. & LAMBRIS, J. D. 2008. Modulation of the antitumor immune response by complement. *Nat Immunol,* 9**,** 1225-35.

MARKIEWSKI, M. M., NILSSON, B., EKDAHL, K. N., MOLLNES, T. E. & LAMBRIS, J. D. 2007. Complement and coagulation: strangers or partners in crime? *Trends Immunol,* 28**,** 184-92.

MARTINEZ, F. O. & GORDON, S. 2014. The M1 and M2 paradigm of macrophage activation: time for reassessment. *F1000Prime Rep,* 6**,** 13.

MCCARTHY, D. O., GLOWACKI, N., SCHELL, K., EMLER, C. A. & ALBERTINI, M. R. 2000. Antigenicity of human melanoma cells transfected to express the B7-1 co-stimulatory molecule (CD80) varies with the level of B7-1 expression. *Cancer Immunol Immunother,* 49**,** 85-93.

MEDICUS, R. G., SCHREIBER, R. D., GOTZE, O. & MULLER-EBERHARD, H. J. 1976. A molecular concept of the properdin pathway. *Proc Natl Acad Sci U S A,* 73**,** 612-6.

MEDRANO, E. E. 2003. Repression of TGF-beta signaling by the oncogenic protein SKI in human melanomas: consequences for proliferation, survival, and metastasis. *Oncogene,* 22**,** 3123-9.

MELANCON, B. J., LAMERS, A. P., BRIDGES, T. M., SULIKOWSKI, G. A., UTLEY, T. J., SHEFFLER, D. J., NOETZEL, M. J., MORRISON, R. D., DANIELS, J. S., NISWENDER, C. M., JONES, C. K., CONN, P. J., LINDSLEY, C. W. & WOOD, M. R. 2012. Development of a more highly selective M(1) antagonist from the continued optimization of the MLPCN Probe ML012. *Bioorg Med Chem Lett,* 22**,** 1044-8.

MELIS, C., ROGIERS, A., BECHTER, O. & VAN DEN OORD, J. J. 2017. Molecular genetic and immunotherapeutic targets in metastatic melanoma. *Virchows Archiv***,** 1-13.

MEMPEL, T. R., PITTET, M. J., KHAZAIE, K., WENINGER, W., WEISSLEDER, R., VON BOEHMER, H. & VON ANDRIAN, U. H. 2006. Regulatory T cells

reversibly suppress cytotoxic T cell function independent of effector differentiation. *Immunity,* 25**,** 129-41.

MERENDINO, N., MOLINARI, R., LOPPI, B., PESSINA, G., M, D. A., TOMASSI, G. & VELOTTI, F. 2003. Induction of apoptosis in human pancreatic cancer cells by docosahexaenoic acid. *Ann N Y Acad Sci,* 1010**,** 361-4.

MERLE, N. S., CHURCH, S. E., FREMEAUX-BACCHI, V. & ROUMENINA, L. T. 2015a. Complement System Part I - Molecular Mechanisms of Activation and Regulation. *Front Immunol,* 6**,** 262.

MERLE, N. S., NOE, R., HALBWACHS-MECARELLI, L., FREMEAUX-BACCHI, V. & ROUMENINA, L. T. 2015b. Complement System Part II: Role in Immunity. *Front Immunol,* 6**,** 257.

MILLS, C. D. 2012. M1 and M2 Macrophages: Oracles of Health and Disease. *Crit Rev Immunol,* 32**,** 463-88.

MILLS, C. D. 2015. Anatomy of a discovery: m1 and m2 macrophages. *Front Immunol,* 6**,** 212.

MIRACCO, C., MOURMOURAS, V., BIAGIOLI, M., RUBEGNI, P., MANNUCCI, S., MONCIATTI, I., COSCI, E., TOSI, P. & LUZI, P. 2007. Utility of tumour-infiltrating CD25+FOXP3+ regulatory T cell evaluation in predicting local recurrence in vertical growth phase cutaneous melanoma. *Oncol Rep,* 18**,** 1115-22.

MIRANDA-HERNANDEZ, D. F., FRANCO-MOLINA, M. A., MENDOZA-GAMBOA, E., ZAPATA-BENAVIDES, P., SIERRA-RIVERA, C. A., CORONADO-CERDA, E. E., ROSAS-TARACO, A. G., TAMEZ-GUERRA, R. S. & RODRIGUEZ-PADILLA, C. 2013. Expression of Foxp3, CD25 and IL-2 in the B16F10 cancer cell line and melanoma is correlated with tumor growth in mice. *Oncol Lett,* 6**,** 1195-1200.

MOCELLIN, S., PASQUALI, S., ROSSI, C. R. & NITTI, D. 2010. Interferon alpha adjuvant therapy in patients with high-risk melanoma: a systematic review and meta-analysis. *J Natl Cancer Inst,* 102**,** 493-501.

MOLINA, H. 2002. The murine complement regulator Crry: new insights into the immunobiology of complement regulation. *Cell Mol Life Sci,* 59**,** 220-9.

MONU, N. R. & FREY, A. B. 2012. Myeloid-derived suppressor cells and anti-tumor T cells: a complex relationship. *Immunol Invest,* 41**,** 595-613.

MOSSER, D. M. & EDWARDS, J. P. 2008. Exploring the full spectrum of macrophage activation. *Nat Rev Immunol,* 8**,** 958-69.

MOVAHEDI, K., GUILLIAMS, M., VAN DEN BOSSCHE, J., VAN DEN BERGH, R., GYSEMANS, C., BESCHIN, A., DE BAETSELIER, P. & VAN GINDERACHTER, J. A. 2008. Identification of discrete tumor-induced myeloid-derived suppressor cell subpopulations with distinct T cell-suppressive activity. *Blood,* 111**,** 4233-44.

MUKAIDA, N., SASAKI, S. & BABA, T. 2014. Chemokines in cancer development and progression and their potential as targeting molecules for cancer treatment. *Mediators Inflamm,* 2014**,** 170381.

MURDOCH, C., MUTHANA, M., COFFELT, S. B. & LEWIS, C. E. 2008. The role of myeloid cells in the promotion of tumour angiogenesis. *Nat Rev Cancer,* 8**,** 618-31.

MURRAY, P. J., ALLEN, J. E., BISWAS, S. K., FISHER, E. A., GILROY, D. W., GOERDT, S., GORDON, S., HAMILTON, J. A., IVASHKIV, L. B., LAWRENCE, T., LOCATI, M., MANTOVANI, A., MARTINEZ, F. O., MEGE, J. L., MOSSER, D. M., NATOLI, G., SAEIJ, J. P., SCHULTZE, J. L., SHIREY, K. A., SICA, A., SUTTLES, J., UDALOVA, I., VAN GINDERACHTER, J. A., VOGEL, S. N. & WYNN, T. A. 2014. Macrophage activation and polarization: nomenclature and experimental guidelines. *Immunity,* 41**,** 14-20.

MURRAY, P. J. & WYNN, T. A. 2011. Protective and pathogenic functions of macrophage subsets. *Nat Rev Immunol,* 11**,** 723-37.

NABIZADEH, J. A., MANTHEY, H. D., STEYN, F. J., CHEN, W., WIDIAPRADJA, A., MD AKHIR, F. N., BOYLE, G. M., TAYLOR, S. M., WOODRUFF, T. M. & ROLFE, B. E. 2016. The Complement C3a Receptor Contributes to Melanoma Tumorigenesis by Inhibiting Neutrophil and CD4+ T Cell Responses. *J Immunol,* 196**,** 4783-92.

NAGARAJ, S., GUPTA, K., PISAREV, V., KINARSKY, L., SHERMAN, S., KANG, L., HERBER, D. L., SCHNECK, J. & GABRILOVICH, D. I. 2007. Altered recognition of antigen is a mechanism of CD8+ T cell tolerance in cancer. *Nat Med,* 13**,** 828-35.

NAJJAR, Y. G. & FINKE, J. H. 2013. Clinical perspectives on targeting of myeloid derived suppressor cells in the treatment of cancer. *Front Oncol,* 3**,** 49.

NEILL, D. R., FERNANDES, V. E., WISBY, L., HAYNES, A. R., FERREIRA, D. M., LAHER, A., STRICKLAND, N., GORDON, S. B., DENNY, P., KADIOGLU, A. & ANDREW, P. W. 2012. T regulatory cells control susceptibility to invasive pneumococcal pneumonia in mice. *PLoS Pathog,* 8**,** e1002660.

NGUYEN, N. Q., CORNET, A., BLACHER, S., TABRUYN, S. P., FOIDART, J. M., NOEL, A., MARTIAL, J. A. & STRUMAN, I. 2007. Inhibition of tumor

growth and metastasis establishment by adenovirus-mediated gene transfer delivery of the antiangiogenic factor 16K hPRL. *Mol Ther,* 15**,** 2094-100.

NIU, J., JIANG, C., LI, C., LIU, L., LI, K., JIAN, Z. & GAO, T. 2011. Foxp3 expression in melanoma cells as a possible mechanism of resistance to immune destruction. *Cancer Immunol Immunother,* 60**,** 1109-18.

NUNEZ-CRUZ, S., GIMOTTY, P. A., GUERRA, M. W., CONNOLLY, D. C., WU, Y. Q., DEANGELIS, R. A., LAMBRIS, J. D., COUKOS, G. & SCHOLLER, N. 2012. Genetic and pharmacologic inhibition of complement impairs endothelial cell function and ablates ovarian cancer neovascularization. *Neoplasia,* 14**,** 994-1004.

O'FLYNN, J., DIXON, K. O., FABER KROL, M. C., DAHA, M. R. & VAN KOOTEN, C. 2014. Myeloperoxidase directs properdin-mediated complement activation. *J Innate Immun,* 6**,** 417-25.

O'NEILL, K., LYONS, S. K., GALLAGHER, W. M., CURRAN, K. M. & BYRNE, A. T. 2010. Bioluminescent imaging: a critical tool in pre-clinical oncology research. *J Pathol,* 220**,** 317-27.

OKWAN-DUODU, D., UMPIERREZ, G. E., BRAWLEY, O. W. & DIAZ, R. 2013. Obesity-driven inflammation and cancer risk: role of myeloid derived suppressor cells and alternately activated macrophages. *Am J Cancer Res,* 3**,** 21-33.

OLIVEIRA, M. A., LIMA, G. M., SHIO, M. T., LEENEN, P. J. & ABRAHAMSOHN, I. A. 2003. Immature macrophages derived from mouse bone marrow produce large amounts of IL-12p40 after LPS stimulation. *J Leukoc Biol,* 74**,** 857-67.

OVERWIJK, W. W. & RESTIFO, N. P. 2001. B16 as a mouse model for human melanoma. *Curr Protoc Immunol,* Chapter 20**,** Unit 20.1.

PANGBURN, M. K. 1989. Analysis of the natural polymeric forms of human properdin and their functions in complement activation. *J Immunol,* 142**,** 202-7.

PANGBURN, M. K. & MULLER-EBERHARD, H. J. 1986. The C3 convertase of the alternative pathway of human complement. Enzymic properties of the bimolecular proteinase. *Biochem J,* 235**,** 723-30.

PAPO, N., SHAHAR, M., EISENBACH, L. & SHAI, Y. 2003. A novel lytic peptide composed of DL-amino acids selectively kills cancer cells in culture and in mice. *J Biol Chem,* 278**,** 21018-23.

PAPO, N. & SHAI, Y. 2005. Host defense peptides as new weapons in cancer treatment. *Cellular and Molecular Life Sciences CMLS,* 62**,** 784-790.

PATTABIRAMAN, D. R. & WEINBERG, R. A. 2014. Tackling the cancer stem cells - what challenges do they pose? *Nat Rev Drug Discov,* 13**,** 497-512.

PEDERSEN, D. V., ROUMENINA, L., JENSEN, R. K., GADEBERG, T. A., MARINOZZI, C., PICARD, C., RYBKINE, T., THIEL, S., SORENSEN, U. B., STOVER, C., FREMEAUX-BACCHI, V. & ANDERSEN, G. R. 2017. Functional and structural insight into properdin control of complement alternative pathway amplification. *Embo j,* 36**,** 1084-1099.

PELTON, K., COTICCHIA, C. M., CURATOLO, A. S., SCHAFFNER, C. P., ZURAKOWSKI, D., SOLOMON, K. R. & MOSES, M. A. 2014. Hypercholesterolemia induces angiogenesis and accelerates growth of breast tumors in vivo. *Am J Pathol,* 184**,** 2099-110.

PERROT, C. Y., JAVELAUD, D. & MAUVIEL, A. 2013. Overlapping activities of TGF-beta and Hedgehog signaling in cancer: therapeutic targets for cancer treatment. *Pharmacol Ther,* 137**,** 183-99.

PILLEMER, L., BLUM, L., LEPOW, I. H., ROSS, O. A., TODD, E. W. & WARDLAW, A. C. 1954. The properdin system and immunity. I. Demonstration and isolation of a new serum protein, properdin, and its role in immune phenomena. *Science,* 120**,** 279-85.

PIO, R., AJONA, D. & LAMBRIS, J. D. 2013. Complement inhibition in cancer therapy. *Semin Immunol,* 25**,** 54-64.

PLITAS, G. & RUDENSKY, A. Y. 2016. Regulatory T Cells: Differentiation and Function. *Cancer Immunol Res,* 4**,** 721-5.

POLLEY, M. J. & NACHMAN, R. 1978. The human complement system in thrombin-mediated platelet function. *J Exp Med,* 147**,** 1713-26.

POSCHKE, I. & KIESSLING, R. 2012. On the armament and appearances of human myeloid-derived suppressor cells. *Clin Immunol,* 144**,** 250-68.

PUAUX, A. L., ONG, L. C., JIN, Y., TEH, I., HONG, M., CHOW, P. K., GOLAY, X. & ABASTADO, J. P. 2011. A comparison of imaging techniques to monitor tumor growth and cancer progression in living animals. *Int J Mol Imaging,* 2011**,** 321538.

QIAN, B. Z. & POLLARD, J. W. 2010. Macrophage diversity enhances tumor progression and metastasis. *Cell,* 141**,** 39-51.

RAIMONDI, S., MAISONNEUVE, P. & LOWENFELS, A. B. 2009. Epidemiology of pancreatic cancer: an overview. *Nat Rev Gastroenterol Hepatol,* 6**,** 699-708.

RAMIREZ-MONTAGUT, T., TURK, M. J., WOLCHOK, J. D., GUEVARA-PATINO, J. A. & HOUGHTON, A. N. 2003. Immunity to melanoma: unraveling the relation of tumor immunity and autoimmunity. *Oncogene,* 22**,** 3180-7.

RAVETCH, J. V. & BOLLAND, S. 2001. IgG Fc receptors. *Annu Rev Immunol,* 19**,** 275-90.

RAVICHANDRAN, D., COOPER, A. & JOHNSON, C. D. 2000. Effect of 1-(gamma)linolenyl-3-eicosapentaenoyl propane diol on the growth of human pancreatic carcinoma in vitro and in vivo. *Eur J Cancer,* 36**,** 423-7.

RAYCHAUDHURI, B., RAYMAN, P., IRELAND, J., KO, J., RINI, B., BORDEN, E. C., GARCIA, J., VOGELBAUM, M. A. & FINKE, J. 2011. Myeloid-derived suppressor cell accumulation and function in patients with newly diagnosed glioblastoma. *Neuro Oncol,* 13**,** 591-9.

RENEHAN, A. G., FRYSTYK, J. & FLYVBJERG, A. 2006. Obesity and cancer risk: the role of the insulin-IGF axis. *Trends Endocrinol Metab,* 17**,** 328-36.

RICKLIN, D., HAJISHENGALLIS, G., YANG, K. & LAMBRIS, J. D. 2010. Complement: a key system for immune surveillance and homeostasis. *Nat Immunol,* 11**,** 785-97.

ROBERTS, A. B., SPORN, M. B., ASSOIAN, R. K., SMITH, J. M., ROCHE, N. S., WAKEFIELD, L. M., HEINE, U. I., LIOTTA, L. A., FALANGA, V., KEHRL, J. H. & ET AL. 1986. Transforming growth factor type beta: rapid induction of fibrosis and angiogenesis in vivo and stimulation of collagen formation in vitro. *Proc Natl Acad Sci U S A,* 83**,** 4167-71.

ROHRL, J., YANG, D., OPPENHEIM, J. J. & HEHLGANS, T. 2010. Human beta-defensin 2 and 3 and their mouse orthologs induce chemotaxis through interaction with CCR2. *J Immunol,* 184**,** 6688-94.

ROSZER, T. 2015. Understanding the Mysterious M2 Macrophage through Activation Markers and Effector Mechanisms. *Mediators Inflamm,* 2015**,** 816460.

ROTHMAN, B. L., MERROW, M., DESPINS, A., KENNEDY, T. & KREUTZER, D. L. 1989. Effect of lipopolysaccharide on C3 and C5 production by human lung cells. *J Immunol,* 143**,** 196-202.

ROTTINO, A. 1957. Therapeutic results in treatment of Hodgkin's disease with CB 1348 and R-48. *Blood,* 12**,** 755-65.

ROTTINO, A. & LEVY, A. L. 1957. Serum-properdin levels in patients with Hodgkin's disease and carcinoma. *Cancer,* 10**,** 877-83.

ROTTINO, A., LEVY, A. L. & CONTE, A. 1958. A study of the serum properdin levels of patients with malignant tumors. *Cancer,* 11**,** 351-6.

RUDY, W., GUCKEL, B., SIEBELS, M., LINDAUER, M., MEUER, S. C. & MOEBIUS, U. 1997. Differential function of CD80- and CD86-transfected human melanoma cells in the presence of IL-12 and IFN-gamma. *Int Immunol,* 9**,** 853-60.

RUNAU, F., ARSHAD, A., ISHERWOOD, J., NORRIS, L., HOWELLS, L., METCALFE, M. & DENNISON, A. 2015. Potential for proteomic approaches in determining efficacy biomarkers following administration of fish oils rich in omega-3 fatty acids: application in pancreatic cancers. *Nutr Clin Pract,* 30**,** 363-70.

RUTKOWSKI, M. J., SUGHRUE, M. E., KANE, A. J., MILLS, S. A. & PARSA, A. T. 2010. Cancer and the complement cascade. *Mol Cancer Res,* 8**,** 1453-65.

SAHOO, N. C., RAO, K. V. & NATARAJAN, K. 2002. CD80 expression is induced on activated B cells following stimulation by CD86. *Scand J Immunol,* 55**,** 577-84.

SAMATAR, A. A. & POULIKAKOS, P. I. 2014. Targeting RAS-ERK signalling in cancer: promises and challenges. *Nat Rev Drug Discov,* 13**,** 928-42.

SAWANOBORI, Y., UEHA, S., KURACHI, M., SHIMAOKA, T., TALMADGE, J. E., ABE, J., SHONO, Y., KITABATAKE, M., KAKIMI, K., MUKAIDA, N. & MATSUSHIMA, K. 2008. Chemokine-mediated rapid turnover of myeloid-derived suppressor cells in tumor-bearing mice. *Blood,* 111**,** 5457-66.

SCHREIBER, R. D., OLD, L. J. & SMYTH, M. J. 2011. Cancer immunoediting: integrating immunity's roles in cancer suppression and promotion. *Science,* 331**,** 1565-70.

SEO, N., HAYAKAWA, S., TAKIGAWA, M. & TOKURA, Y. 2001. Interleukin-10 expressed at early tumour sites induces subsequent generation of CD4(+) T-regulatory cells and systemic collapse of antitumour immunity. *Immunology,* 103**,** 449-57.

SERAFINI, P., BORRELLO, I. & BRONTE, V. 2006. Myeloid suppressor cells in cancer: recruitment, phenotype, properties, and mechanisms of immune suppression. *Semin Cancer Biol,* 16**,** 53-65.

SERAFINI, P., MGEBROFF, S., NOONAN, K. & BORRELLO, I. 2008. Myeloid-derived suppressor cells promote cross-tolerance in B-cell lymphoma by expanding regulatory T cells. *Cancer Res,* 68**,** 5439-49.

SERGENTANIS, T. N., ANTONIADIS, A. G., GOGAS, H. J., ANTONOPOULOS, C. N., ADAMI, H. O., EKBOM, A. & PETRIDOU, E. T. 2013. Obesity and risk of malignant melanoma: a meta-analysis of cohort and case-control studies. *Eur J Cancer,* 49**,** 642-57.

SHOAG, J., HAQ, R., ZHANG, M., LIU, L., ROWE, G. C., JIANG, A., KOULISIS, N., FARREL, C., AMOS, C. I., WEI, Q., LEE, J. E., ZHANG, J., KUPPER, T. S., QURESHI, A. A., CUI, R., HAN, J., FISHER, D. E. & ARANY, Z. 2013. PGC-1 coactivators regulate MITF and the tanning response. *Mol Cell,* 49**,** 145-57.

SICA, A. & BRONTE, V. 2007. Altered macrophage differentiation and immune dysfunction in tumor development. *J Clin Invest,* 117**,** 1155-66.

SICA, A., PORTA, C., RIBOLDI, E., ERRENIM. & ALLAVENAP. 2011. Functions of Diverse Myeloid Cells in the Tumor Micro-Environment *In:* BISWAS, D. S. (ed.) *Tumor Microenvironment*

USA: John wiley and Sons, Ltd.

SIEZENGA, M. A., CHANDIE SHAW, P. K., VAN DER GEEST, R. N., MOLLNES, T. E., DAHA, M. R., RABELINK, T. J. & BERGER, S. P. 2009. Enhanced complement activation is part of the unfavourable cardiovascular risk profile in South Asians. *Clin Exp Immunol,* 157**,** 98-103.

SILVA-SANTOS, B., SERRE, K. & NORELL, H. 2015. gammadelta T cells in cancer. *Nat Rev Immunol,* 15**,** 683-91.

SOMANI, R., GRANT, P. J., KAIN, K., CATTO, A. J. & CARTER, A. M. 2006. Complement C3 and C-reactive protein are elevated in South Asians independent of a family history of stroke. *Stroke,* 37**,** 2001-6.

SOMANI, R., RICHARDSON, V. R., STANDEVEN, K. F., GRANT, P. J. & CARTER, A. M. 2012. Elevated properdin and enhanced complement activation in first-degree relatives of South Asian subjects with type 2 diabetes. *Diabetes Care,* 35**,** 894-9.

SPITZER, D., MITCHELL, L. M., ATKINSON, J. P. & HOURCADE, D. E. 2007. Properdin can initiate complement activation by binding specific target

surfaces and providing a platform for de novo convertase assembly. *J Immunol,* 179**,** 2600-8.

SRIVASTAVA, M. K., SINHA, P., CLEMENTS, V. K., RODRIGUEZ, P. & OSTRAND-ROSENBERG, S. 2010. Myeloid-derived suppressor cells inhibit T-cell activation by depleting cystine and cysteine. *Cancer Res,* 70**,** 68-77.

STEINER, T., FRANCESCUT, L., BYRNE, S., HUGHES, T., JAYANTHI, A., GUSCHINA, I., HARWOOD, J., CIANFLONE, K., STOVER, C. & FRANCIS, S. 2014. Protective role for properdin in progression of experimental murine atherosclerosis. *PLoS One,* 9**,** e92404.

STEPHANIE, G., BERNARD, L., MARTIN, M., HELMER, S. K. & MARC, A. 2012. Soil respiration in forest ecosystems: combination of a multilayer approach and an isotopic signal analysis. *Commun Agric Appl Biol Sci,* 77**,** 139-43.

STOVER, C. 2010. Dual role of complement in tumour growth and metastasis (Review). *Int J Mol Med,* 25**,** 307-13.

STOVER, C. M., LUCKETT, J. C., ECHTENACHER, B., DUPONT, A., FIGGITT, S. E., BROWN, J., MANNEL, D. N. & SCHWAEBLE, W. J. 2008. Properdin plays a protective role in polymicrobial septic peritonitis. *J Immunol,* 180**,** 3313-8.

STOVER, C. M., MCDONALD, J., BYRNE, S., LAMBERT, D. G. & THOMPSON, J. P. 2015. Properdin levels in human sepsis. *Front Immunol,* 6**,** 24.

STRUNK, R. C., EIDLEN, D. M. & MASON, R. J. 1988. Pulmonary alveolar type II epithelial cells synthesize and secrete proteins of the classical and alternative complement pathways. *J Clin Invest,* 81**,** 1419-26.

SUAREZ-CARMONA, M., HUBERT, P., DELVENNE, P. & HERFS, M. 2015. Defensins: "Simple" antimicrobial peptides or broad-spectrum molecules? *Cytokine Growth Factor Rev,* 26**,** 361-70.

SUMIYOSHI, M., SAKANAKA, M., TANIGUCHI, M., BABA, K. & KIMURA, Y. 2014. Anti-tumor effects of various furocoumarins isolated from the roots, seeds and fruits of Angelica and Cnidium species under ultraviolet A irradiation. *J Nat Med,* 68**,** 83-94.

SUN, H. L., ZHOU, X., XUE, Y. F., WANG, K., SHEN, Y. F., MAO, J. J., GUO, H. F. & MIAO, Z. N. 2012. Increased frequency and clinical significance of myeloid-derived suppressor cells in human colorectal carcinoma. *World J Gastroenterol,* 18**,** 3303-9.

SUN, Y. & LODISH, H. F. 2010. Adiponectin deficiency promotes tumor growth in mice by reducing macrophage infiltration. *PLoS One,* 5**,** e11987.

SWANN, J. B. & SMYTH, M. J. 2007. Immune surveillance of tumors. *J Clin Invest,* 117**,** 1137-46.

TAKEDA, Y., LI, Q., KAZAROV, A. R., EPARDAUD, M., ELPEK, K., TURLEY, S. J. & HEMLER, M. E. 2011. Diminished metastasis in tetraspanin CD151-knockout mice. *Blood,* 118**,** 464-72.

TALMADGE, J. E. & FIDLER, I. J. 2010. AACR centennial series: the biology of cancer metastasis: historical perspective. *Cancer Res,* 70**,** 5649-69.

TERANO, T., SHIINA, T. & TAMURA, Y. 1996. Eicosapentaenoic acid suppressed the proliferation of vascular smooth muscle cells through modulation of various steps of growth signals. *Lipids,* 31 Suppl**,** S301-4.

THOMAS, D. A. & MASSAGUE, J. 2005. TGF-beta directly targets cytotoxic T cell functions during tumor evasion of immune surveillance. *Cancer Cell,* 8**,** 369-80.

THURMAN, J. M. & HOLERS, V. M. 2006. The central role of the alternative complement pathway in human disease. *J Immunol,* 176**,** 1305-10.

TIRAPU, I., HUARTE, E., GUIDUCCI, C., ARINA, A., ZARATIEGUI, M., MURILLO, O., GONZALEZ, A., BERASAIN, C., BERRAONDO, P., FORTES, P., PRIETO, J., COLOMBO, M. P., CHEN, L. & MELERO, I. 2006. Low surface expression of B7-1 (CD80) is an immunoescape mechanism of colon carcinoma. *Cancer Res,* 66**,** 2442-50.

TSOU, C. L., PETERS, W., SI, Y., SLAYMAKER, S., ASLANIAN, A. M., WEISBERG, S. P., MACK, M. & CHARO, I. F. 2007. Critical roles for CCR2 and MCP-3 in monocyte mobilization from bone marrow and recruitment to inflammatory sites. *J Clin Invest,* 117**,** 902-9.

TSUJI-TAKAYAMA, K., SUZUKI, M., YAMAMOTO, M., HARASHIMA, A., OKOCHI, A., OTANI, T., INOUE, T., SUGIMOTO, A., TORAYA, T., TAKEUCHI, M., YAMASAKI, F., NAKAMURA, S. & KIBATA, M. 2008. The production of IL-10 by human regulatory T cells is enhanced by IL-2 through a STAT5-responsive intronic enhancer in the IL-10 locus. *J Immunol,* 181**,** 3897-905.

TSUJI, M., MUROTA, S. I. & MORITA, I. 2003. Docosapentaenoic acid (22:5, n-3) suppressed tube-forming activity in endothelial cells induced by vascular endothelial growth factor. *Prostaglandins Leukot Essent Fatty Acids,* 68**,** 337-42.

UMANSKY, V., SEVKO, A., GEBHARDT, C. & UTIKAL, J. 2014. Myeloid-derived suppressor cells in malignant melanoma. *J Dtsch Dermatol Ges,* 12**,** 1021-7.

VADREVU, S. K., CHINTALA, N. K., SHARMA, S. K., SHARMA, P., CLEVELAND, C., RIEDIGER, L., MANNE, S., FAIRLIE, D. P., GORCZYCA, W., ALMANZA, O., KARBOWNICZEK, M. & MARKIEWSKI, M. M. 2014. Complement c5a receptor facilitates cancer metastasis by altering T-cell responses in the metastatic niche. *Cancer Res,* 74**,** 3454-65.

VALKOVIC, T., DOBRILA, F., MELATO, M., SASSO, F., RIZZARDI, C. & JONJIC, N. 2002. Correlation between vascular endothelial growth factor, angiogenesis, and tumor-associated macrophages in invasive ductal breast carcinoma. *Virchows Arch,* 440**,** 583-8.

VALZASINA, B., PICONESE, S., GUIDUCCI, C. & COLOMBO, M. P. 2006. Tumor-induced expansion of regulatory T cells by conversion of CD4+CD25- lymphocytes is thymus and proliferation independent. *Cancer Res,* 66**,** 4488-95.

VAN DEN BERG, C. W., TAMBOURGI, D. V., CLARK, H. W., HOONG, S. J., SPILLER, O. B. & MCGREAL, E. P. 2014. Mechanism of neutrophil dysfunction: neutrophil serine proteases cleave and inactivate the C5a receptor. *J Immunol,* 192**,** 1787-95.

VAN RAAMSDONK, C. D., GRIEWANK, K. G., CROSBY, M. B., GARRIDO, M. C., VEMULA, S., WIESNER, T., OBENAUF, A. C., WACKERNAGEL, W., GREEN, G., BOUVIER, N., SOZEN, M. M., BAIMUKANOVA, G., ROY, R., HEGUY, A., DOLGALEV, I., KHANIN, R., BUSAM, K., SPEICHER, M. R., O'BRIEN, J. & BASTIAN, B. C. 2010. Mutations in GNA11 in uveal melanoma. *N Engl J Med,* 363**,** 2191-9.

VATNER, R. E. & FORMENTI, S. C. 2015. Myeloid-derived cells in tumors: effects of radiation. *Semin Radiat Oncol,* 25**,** 18-27.

VENCE, L., PALUCKA, A. K., FAY, J. W., ITO, T., LIU, Y. J., BANCHEREAU, J. & UENO, H. 2007. Circulating tumor antigen-specific regulatory T cells in patients with metastatic melanoma. *Proc Natl Acad Sci U S A,* 104**,** 20884-9.

VIGNESH, P., RAWAT, A., SHARMA, M. & SINGH, S. 2017. Complement in autoimmune diseases. *Clin Chim Acta,* 465**,** 123-130.

VOISEY, J. & VAN DAAL, A. 2002. Agouti: from mouse to man, from skin to fat. *Pigment Cell Res,* 15**,** 10-8.

WEISCHENFELDT, J. & PORSE, B. 2008. Bone Marrow-Derived Macrophages (BMM): Isolation and Applications. *CSH Protoc,* 2008**,** pdb.prot5080.

WEISS, J. M., SUBLESKI, J. J., BACK, T., CHEN, X., WATKINS, S. K., YAGITA, H., SAYERS, T. J., MURPHY, W. J. & WILTROUT, R. H. 2014. Regulatory T cells and myeloid-derived suppressor cells in the tumor microenvironment undergo Fas-dependent cell death during IL-2/alphaCD40 therapy. *J Immunol,* 192**,** 5821-9.

WEISSER, S. B., MCLARREN, K. W., KURODA, E. & SLY, L. M. 2013. Generation and characterization of murine alternatively activated macrophages. *Methods Mol Biol,* 946**,** 225-39.

WESTCOTT, M. M., HENRY, C. J., COOK, A. S., GRANT, K. W. & HILTBOLD, E. M. 2007. Differential susceptibility of bone marrow-derived dendritic cells and macrophages to productive infection with Listeria monocytogenes. *Cell Microbiol,* 9**,** 1397-411.

WETSEL, R. A. & KOLB, W. P. 1983. Expression of C5a-like biological activities by the fifth component of human complement (C5) upon limited digestion with noncomplement enzymes without release of polypeptide fragments. *J Exp Med,* 157**,** 2029-48.

WHO 2017. Cancer; Fact sheet.

WILSON, H. M. 2014. SOCS Proteins in Macrophage Polarization and Function. *Front Immunol,* 5**,** 357.

WOJTOWICZ-PRAGA, S. M., DICKSON, R. B. & HAWKINS, M. J. 1997. Matrix metalloproteinase inhibitors. *Invest New Drugs,* 15**,** 61-75.

WOLIN, K. Y., CARSON, K. & COLDITZ, G. A. 2010. Obesity and cancer. *Oncologist,* 15**,** 556-65.

WOUTERS, K., VAN GORP, P. J., BIEGHS, V., GIJBELS, M. J., DUIMEL, H., LUTJOHANN, D., KERKSIEK, A., VAN KRUCHTEN, R., MAEDA, N., STAELS, B., VAN BILSEN, M., SHIRI-SVERDLOV, R. & HOFKER, M. H. 2008. Dietary cholesterol, rather than liver steatosis, leads to hepatic inflammation in hyperlipidemic mouse models of nonalcoholic steatohepatitis. *Hepatology,* 48**,** 474-86.

WU, W. K., SUNG, J. J., CHENG, A. S., CHAN, F. K., NG, S. S., TO, K. F., WANG, X. J., ZHANG, L., WONG, S. H., YU, J. & CHO, C. H. 2014. The Janus face of cathelicidin in tumorigenesis. *Curr Med Chem,* 21**,** 2392-400.

XU, M., XING, Y., ZHOU, L., YANG, X., YAO, W., XIAO, W., GE, C., MA, Y., YANG, J., WU, J., CAO, R., LI, T. & LIU, J. 2013. Improved efficacy of therapeutic vaccination with viable human umbilical vein endothelial cells against murine melanoma by introduction of OK432 as adjuvant. *Tumour Biol,* 34**,** 1399-408.

YAMAGUCHI, T., FUSHIDA, S., YAMAMOTO, Y., TSUKADA, T., KINOSHITA, J., OYAMA, K., MIYASHITA, T., TAJIMA, H., NINOMIYA, I., MUNESUE, S., HARASHIMA, A., HARADA, S., YAMAMOTO, H. & OHTA, T. 2016. Tumor-associated macrophages of the M2 phenotype contribute to progression in gastric cancer with peritoneal dissemination. *Gastric Cancer,* 19**,** 1052-65.

YAMAZAKI, S., DUDZIAK, D., HEIDKAMP, G. F., FIORESE, C., BONITO, A. J., INABA, K., NUSSENZWEIG, M. C. & STEINMAN, R. M. 2008. CD8+ CD205+ splenic dendritic cells are specialized to induce Foxp3+ regulatory T cells. *J Immunol,* 181**,** 6923-33.

YANG, R., CAI, Z., ZHANG, Y., YUTZY, W. H. T., ROBY, K. F. & RODEN, R. B. 2006. CD80 in immune suppression by mouse ovarian carcinoma-associated Gr-1+CD11b+ myeloid cells. *Cancer Res,* 66**,** 6807-15.

YANG, S. P., MORITA, I. & MUROTA, S. I. 1998. Eicosapentaenoic acid attenuates vascular endothelial growth factor-induced proliferation via inhibiting Flk-1 receptor expression in bovine carotid artery endothelial cells. *J Cell Physiol,* 176**,** 342-9.

YANG, X., SUN, J., GAO, Y., TAN, A., ZHANG, H., HU, Y., FENG, J., QIN, X., TAO, S., CHEN, Z., KIM, S. T., PENG, T., LIAO, M., LIN, X., ZHANG, Z., TANG, M., LI, L., MO, L., LIANG, Z., SHI, D., HUANG, Z., HUANG, X., LIU, M., LIU, Q., ZHANG, S., TRENT, J. M., ZHENG, S. L., XU, J. & MO, Z. 2012. Genome-wide association study for serum complement C3 and C4 levels in healthy Chinese subjects. *PLoS Genet,* 8**,** e1002916.

YING, W., CHERUKU, P. S., BAZER, F. W., SAFE, S. H. & ZHOU, B. 2013. Investigation of macrophage polarization using bone marrow derived macrophages. *J Vis Exp*.

YOUN, J. I., KUMAR, V., COLLAZO, M., NEFEDOVA, Y., CONDAMINE, T., CHENG, P., VILLAGRA, A., ANTONIA, S., MCCAFFREY, J. C., FISHMAN, M., SARNAIK, A., HORNA, P., SOTOMAYOR, E. & GABRILOVICH, D. I. 2013. Epigenetic silencing of retinoblastoma gene regulates pathologic differentiation of myeloid cells in cancer. *Nat Immunol,* 14**,** 211-20.

YOUN, J. I., NAGARAJ, S., COLLAZO, M. & GABRILOVICH, D. I. 2008. Subsets of myeloid-derived suppressor cells in tumor-bearing mice. *J Immunol,* 181**,** 5791-802.

ZHANG, B., WANG, Z., WU, L., ZHANG, M., LI, W., DING, J., ZHU, J., WEI, H. & ZHAO, K. 2013. Circulating and tumor-infiltrating myeloid-derived suppressor cells in patients with colorectal carcinoma. *PLoS One,* 8**,** e57114.

ZHANG, W., LONG, Y., ZHANG, J. & WANG, C. 2007. Modulatory effects of EPA and DHA on proliferation and apoptosis of pancreatic cancer cells. *J Huazhong Univ Sci Technolog Med Sci,* 27**,** 547-50.

ZHAO, E., XU, H., WANG, L., KRYCZEK, I., WU, K., HU, Y., WANG, G. & ZOU, W. 2012. Bone marrow and the control of immunity. *Cell Mol Immunol,* 9**,** 11-9.

ZHAO, L., LIM, S. Y., GORDON-WEEKS, A. N., TAPMEIER, T. T., IM, J. H., CAO, Y., BEECH, J., ALLEN, D., SMART, S. & MUSCHEL, R. J. 2013. Recruitment of a myeloid cell subset (CD11b/Gr1 mid) via CCL2/CCR2 promotes the development of colorectal cancer liver metastasis. *Hepatology,* 57**,** 829-39.

ZHENG, G., TEUMER, J., COLMENARES, C., RICHMOND, C. & STAVNEZER, E. 1997. Identification of a core functional and structural domain of the v-Ski oncoprotein responsible for both transformation and myogenesis. *Oncogene,* 15**,** 459-71.

ZHENG, X. F., HONG, Y. X., FENG, G. J., ZHANG, G. F., ROGERS, H., LEWIS, M. A., WILLIAMS, D. W., XIA, Z. F., SONG, B. & WEI, X. Q. 2013. Lipopolysaccharide-induced M2 to M1 macrophage transformation for IL-12p70 production is blocked by Candida albicans mediated up-regulation of EBI3 expression. *PLoS One,* 8**,** e63967.

ZHOU, G. & LEVITSKY, H. I. 2007. Natural regulatory T cells and de novo-induced regulatory T cells contribute independently to tumor-specific tolerance. *J Immunol,* 178**,** 2155-62.

ZHU, Z., LIU, W. & GOTLIEB, V. 2016. The rapidly evolving therapies for advanced melanoma--Towards immunotherapy, molecular targeted therapy, and beyond. *Crit Rev Oncol Hematol,* 99**,** 91-9.

ZIEGLER-HEITBROCK, L., ANCUTA, P., CROWE, S., DALOD, M., GRAU, V., HART, D. N., LEENEN, P. J., LIU, Y. J., MACPHERSON, G., RANDOLPH, G. J., SCHERBERICH, J., SCHMITZ, J., SHORTMAN, K., SOZZANI, S., STROBL, H., ZEMBALA, M., AUSTYN, J. M. & LUTZ, M. B. 2010. Nomenclature of monocytes and dendritic cells in blood. *Blood,* 116**,** e74-80.

ZOU, W. 2006. Regulatory T cells, tumour immunity and immunotherapy. *Nat Rev Immunol,* 6**,** 295-307.